# DOCTOR OF PHILOSOPHY

## Impact of Artificial UV Light Sources on the Skin

Tierney, Patrick Joseph

*Award date:*
2015

*Awarding institution:*
University of Dundee

# Impact of Artificial UV Light Sources on the Skin.

**Patrick Joseph Tierney**


A thesis presented for the degree of Doctor of Philosophy

University of Dundee

June 2015

# Declaration

I declare that the work presented within this thesis is, unless other wise acknowledged, entirely my own; that all references cited herein have been consulted by me; and that this work has not been previously accepted for a higher degree.

Patrick Joseph Tierney

Signature _____ Date _____

I certify that Patrick Joseph Tierney has carried out research under my supervision, and has fulfilled the conditions of the relevant ordinance and regulation for the completion of a PhD degree.

Professor Harry Moseley

Signature _____ Date _____

# Preface

The work presented in this thesis was originally carried out in conjunction with Cancer Research UK (CRUK), which financially supported the data collated from artificial tanning units through out England. The project took place at the Photobiology Unit, Ninewells Hospital Dundee, during 2010-2015. The research topic concerns the emissions from sunbeds and the impact of artificial tanning units on human skin. The research was done done under the guidance of Professor Harry Moseley and Doctor Sally Ibbotson.

# Abstract

UV radiation has the ability to cause erythema, photoaging and photo-cancer. In 2010 Westminster wanted information on sources of artificial UV radiation in particular sunbeds. The objective of this study was to measure the spectral outputs from artificial tanning units throughout England and to compare the outputs to European and British compliance levels.

The emissions from the collated data allowed the calculation of exposure doses of each sunbed. By applying plausible sunbed exposure habits (no of sunbed sessions per year) it was possible to use this data in a skin cancer mathematical model. The time-dose model is based on cumulative lifetime exposure dose and age. The first step was to apply plausible sunbed habit scenarios using the collated emission data which was used in a mathematical model to estimate the risk of developing non-melanoma skin cancer.

Another objective of this study was to determine the optical properties of skin tissue that govern the transport of light through tissue and secondly to develop a model for light transport in tissue that makes it possible to investigate the number of photons absorbed beneath the skin. Different skin types of various pigmentation levels were investigated.

To this end, the absorption and scattering properties of tissue as a function of wavelength were derived. The effect of photo-lesion formation from DNA damage was investigated. To study light transport in tissue, a Monte Carlo model has was developed. This model gives a full 3-D simulation of light transport, and takes into account specular reflection and refraction at the tissue boundaries. To validate the model, predictions have been tested against reliable analytical data. Monte Carlo simulations are implemented to investigate the propagation of UV photons in skin tissue. In this thesis, a data driven semi-empirical model is presented that used spectra obtained from sunbed emissions in the Monte Carlo Radiative Transfer (MCRT) code. A number of applications of the model, together with results from experiments are presented such as skin type photo-shielding and quantification of DNA damage.

UV radiation can affect the appearance and the sensitivity of human skin by triggering a biophysical response such as eythema (redness). A pilot study is presented that investigates if multiple sub-erythemal doses can induce erythema in the skin. The study involved healthy volunteers and photosensitive patients. It is demonstrated that the multiple sub-erythemal doses have an additive mechanism.

# Acknowledgements

I would to thank everybody in the Photobiology Unit who made it possible to produce this thesis. First of all I would like to thank my supervisor Professor Harry Moseley for his patience and putting up with this eternal thesis writing for such a long time. Harry has been especially important in creating networks of interdisciplinary researchers and for helpful suggestions throughout the PhD. process.

I am also grateful to Doctor Sally Ibbotson for valuable clinical advice and support. I would like to extend my thanks to Dr. Frank de Gruijl of Leiden University Medical Center for general enthusiasm and scientific advice.

I owe my thanks to Dr. Ronan Valentine and Dr. Ewan Eadie who were both instrumental at different stages of my PhD.

Special thanks to Lynn Fullerton and all the technicians for their practical help with equipment and guidance in the clinic.

I want to extend my thanks to June Gardner for help with ethics approval and clinical study. I would like to thank Dr. Julie Woods for all invaluable biological advice and knowledge throughout.

I am also very grateful to Dr. Kenny Wood for provision of original Monte Carlo code and support. I would like to extend my gratitude to Dr. Tom Brown for excellent suggestions and advice. I also would like to thank Louise Campbell for her support with Monte Carlo coding.

I am also very grateful to all my friends and family for their support throughout the PhD. process.

# List of Publications

**Refereed Journal Publications**

Tierney P, Ferguson J, Ibbotson S, Moseley H, Nine out of ten sunbeds in England emit UV radiation levels that exceed current safety limits. British Journal of Dermatology. Volume 168, Issue 3, pages 602–608, March 2013. DOI: 10.1111/bjd.12181

Tierney P, de Gruijl F.R., Ibbotson S, Moseley H, Predicted increased risk of squamous cell skin cancer induction associated with sunbed exposure habits. British Journal of Dermatology. Volume 173, Issue 1, pages 201–208, July 2015. DOI: 10.1111/bjd.13714

**Conference Presentations and Posters**

The contribution of Solar and Sunbed exposure to skin cancer risk. It all adds up! Tierney P, de Gruil FR, Ibbotson S, Moseley H. Poster European Society Photobiology, Liege, Belgium 2013.

A Monte Carlo Radiative Transfer approach to UV skin modelling. Patrick J. Tierney, A Dinkova-Kostova, SH Ibbotson, H Moseley Photobiology Unit, Ninewells Hospital  Medical School, University of Dundee, Scotland, UK. 91st Scottish Skin Biology Club Meeting. Glasgow 2014

Predicted increased risk of skin cancer induction associated with sunbed use. Tierney P, de Gruil FR, Ibbotson S, Moseley H. XV World Congress on Cancers of the Skin 3 – 6 Edinburgh. September 2014.

The College of Medicine, Dentistry and Nursing,Student Symposium June 2014, Monte Carlo Radiative Transfer UV Sunbed, Talk and Poster

Web Interview.http://ecancer.org/video/3073/risk-of-common-skin-cancer-increased-by-as-much-as-90-per-cent-with-sunbeds–study-finds.php

**Manuscript in Preparation**

P Tierney, C Campbell, R M Valentine, J Woods, CTA Brown, K Wood, S L. Jacques, H Moseley, A Monte Carlo Radiative Transfer approach to determine DNA damage from UV exposure of sunbeds.

# List of Figures

# List of Tables

# List of Abbreviations

**3-D** ..... Three Dimensional

**8-OHdG** ..... 8-Oxo-deoxyguanosine

**A/D** ..... Analog-to-digital

**AK** ..... Actinic Keratosis

**ASR** ..... Age Standarised Rate

**AUC** ..... Area Under the curve

**BCC** ..... Basal Cell Carcinoma

**BS EN** ..... British and European Standard

**CAD** ..... Chronic Actinic Dermatitis

**CC-3** ..... Cosine Corrector

**CCD** ..... Charge-coupled Device

**CDF** ..... Cumulative Distribution Function

**CPS** ..... Counts per second

**CIE** ..... Commission Internationale de l'éclairage

**CF** ..... Correction Factor

**CPD** ..... Cyclobutane Pyrimidine Dimer

**CRUK** ..... Cancer Research UK

**DOF** ..... degrees of freedom

**DNA** ..... Deoxyribonucleic acid

**dsDNA** ..... Double Stranded DNA

**EWI** ..... Erythemal weighted irradiance

**IR** ..... Infra-red

**kbp** ..... kilo base pair

**MC** ..... Monte Carlo

**MCRT** ..... Monte Carlo Radiative Transfer

**MS** ..... Melanin Score

**MED** ..... Minimum erythema dose

**MFP** ..... Mean free path

**NPL** ..... National Physical Laboratory

**NMSC** ..... Non-melanoma skin cancer

**NER** ..... Nucleotide Excision Repair

**OFLV** ..... Variable Longpass Order-sorting Filters

**OD** ..... Optical Density

**ONS** ..... Office of National Statistics

**PBU** ..... Photobiology unit

**PDT** ..... Photodynamic Therapy

**PDF** ..... Probability Distribution Function

**PHE** ..... Public Health England

**PUVA** ..... Psoralen + UVA Radiation

**RCI** ..... Relative Cumulative Incidence

**RGN** ..... Random generated number

**ROS** ..... Reactive oxygen species

**RTE** ..... Radiative Transfer Equation

**RR** ..... Relative Risk

**SCC** ..... Squamous Cell Carcinoma

**SCCP** ..... Scientific Committee on Consumer Products

**SCUP-h** ..... Skin Cancer Utrecht Philadelphia-human

**SCUP-m** ..... Skin Cancer Utrecht Philadelphia-murine

**SED** ..... Standard Erythema Dose

**SNR** ..... Signal-to-noise ratio

**ssDNA** ..... Single Stranded DNA

**SMA** ..... SubMiniature version A

**UKIACR** ..... United Kingdom and Ireland Association of Cancer Registries

**UKAS** ..... United Kingdom Accreditation Service

**UT** ..... Universal time

**UV** ..... Ultraviolet

**UVA** ..... Ultraviolet A

**UVB** ..... Ultraviolet B

**UVC** ..... Ultraviolet C

**UVR** ..... Ultraviolet Radiation

**Vm** ..... Volume fraction of melanosomes

**XP** ..... Xeroderma pigmentosum

# Glossary

$\mathbf{A}(\lambda)$ ..... Biological action spectrum

$\boldsymbol{\alpha}$ ..... Age power independent of dose

$\boldsymbol{\beta}$ ..... Biological amplification factor, power of dose

$\mathbf{a}_o$ ..... Reference age, 65 years

$\mathbf{a}$ ..... Age

$\mathbf{a}$ ..... Albedo

$\mathbf{A}$ ..... Absorbance

$\mathbf{A}_{el}$ ..... % of body exposed for hands, 4%

$\mathbf{A}_{eU}$ ..... % of body exposed for posterior neck and face, 6%

$\mathbf{A}_e$ ..... total % of body exposed day-to-day, 10%

$\mathbf{a}_h$ ..... Age holiday sunbathing begins, assume 5 years

$\mathbf{a}_s$ ..... Age when sunbed use begins, assume 20 years

$\mathbf{A}_U$ ..... % of body exposed excluding trunks or bathing suit, 85%

$\mathbf{c}$ ..... Speed of light ($\mathrm{ms}^{-1}$)

**CL2** ..... Quartz halogen lamp

**CL3** ..... Deuterium lamp

$\mathbf{C}_{eu}(\lambda)$ ..... Eumelanin concentration $\mathrm{gL}^{-1}$

$\mathbf{C}_{hb}(\lambda)$ ..... Haemoglobin concentration $\mathrm{gL}^{-1}$

$\mathbf{C}_{mel}(\lambda)$ ..... Melanin concentration $\mathrm{gL}^{-1}$

$\mathbf{C}_{ph}(\lambda)$ ..... Pheomelanin concentration $\mathrm{gL}^{-1}$

$\mathbf{t}_{do}$ ..... Cumulative median UVR dose at 65 years ($\mathrm{a}_o$)

$\mathbf{D}_d$ ..... Day-to-day UVR dose (SEDs per year)

$\mathbf{D}_H$ ..... Holiday dose, assuming 10.5 days (SEDs per year)

$\mathbf{H_2O}$ ..... Water

**$H_2O_2$** ..... Hydrogen Peroxide

**OH·** ..... Hydroxyl Radicals

**$D_s$** ..... Annual UVR sunbed dose(in SEDs)

**$\mathcal{E}$** ..... Energy of a photon(J)

**E** ..... Irradiance ($Wm^{-2}$)

**E'** ..... Fluence Rate ($Wm^{-2}$)

**$E(\lambda)$** ..... Spectral irradiance ($W\ m^{-2}\ nm^{-1}$)

**$\Delta E^*$** ..... colour difference parameter

**$\epsilon$** ..... molar extinction coefficient

**$\varepsilon_{a,eu}$** ..... Eumelanin absorption coefficient

**$\varepsilon_{a,ph}$** ..... Pheomelanin absorption coefficient

**$\varepsilon_{eu}(\lambda)$** ..... Eumelanin extinction coefficient

**$\varepsilon_{ph}(\lambda)$** ..... Pheomelanin extinction coefficient

**$f_2$** ..... diffuse cosine error

**g** ..... anistropy factor

**h** ..... Planck's constant (J s)

**H** ..... Fluence ($Jcm^{-2}$)

**$HbO_2$** ..... Oxyhaemoglobin

**Hb** ..... Deoxyhaemoglobin

**$I_v$** ..... Specific intensity

**l** ..... pathlength (cm)

**$\lambda$** ..... wavelength (nm)

**L** ..... Luminosity

**L*a*b** ..... Chromameter measurement parameters

**MFP** ..... Mean free path

**n** ..... Refractive Index

**N** ..... Number of Photons

**$N_A$** ..... total number of absorbed photons

**$N_B$** ..... number of absorbed photons causing biological effect

**Q** ..... Absorbed energy (J $cm^{-3}.sec^{-1}$)

**Φ** ..... Quantum Yield

**Ψ** ..... Fluence rate ($Wcm^{-2}$)

**R($\lambda$)** ..... Reflectance

**Sequence I** ... (UVB, UVAII, UVAI)

**Sequence II** .. (UVAI, UVAII, UVB)

**$^1O_2$** ..... Singlet Oxygen

**$O_2^{-\cdot}$** ..... Superoxide

**$R(\theta_i, \theta_t)$** ..... Fresnel Reflection

$\sum_L$ ..... Sum over dose level for each person at risk

$\sum_S$ ..... Sum over body sites

**$SO_2$** ..... Oxygen saturation %

**TD** ..... Total dose

**wL** ..... Site dose-weighting factor

**YLD(a)** ..... Tumour yield at age a

**S** ..... physical distance

$\tau$ ..... optical depth

$\theta_c$ ..... critical angle

**Type H** ..... Horizontal sunbed

**Type HP** ..... High Pressure sunbed

**Type V** ..... Vertical sunbed

**UVAI** ..... Ultraviolet AI (340-400nm)

**UVAII** ..... Ultraviolet AII (315-340nm)

**UVB** ..... Ultraviolet B (280-315nm)

$\mu_a$ ..... absorption coefficient

$\mu_{a,base}$ ..... baseline absorption coefficient

$\mu_{a,dhb}$ ..... deoxyhaemoglobin absorption coefficient

$\mu_{a,DNA}$ ..... DNA absorption coefficient

$\mu_{a,epi}$ ..... epidermis absorption coefficient

$\boldsymbol{\mu_{a,ohb}}$ ..... oxyhaemoglobin absorption coefficient

$\boldsymbol{\mu_{a,mel}}$ ..... melanin absorption coefficient

$\boldsymbol{\mu_s}$ ..... scattering coefficient

$\boldsymbol{\mu_t}$ ..... attenuation coefficient

$\boldsymbol{V}$ ..... frequency (Hz)

**Vm** ..... Volume fraction of melanosomes

**Vp** ..... Volume fraction of blood in papillary dermis

$\boldsymbol{\xi}$ ..... Random number

# Contents

# Chapter 1

# Introduction

## 1.1 Overview and Motivation

Sunlight represents the primary source of life and energy on Earth, yet excessive exposure to solar ultraviolet radiation (UVR) is deleterious to biologic systems. For *Homo sapiens* the correct balance of radiation exposure necessary for health maintenance varies dramatically between individuals depending on skin phenotype, presence of pathologic photosensitivity, and genetic factors. For normal healthy, individuals, sunlight is necessary for promoting a psychological sense of well being as well as providing the energy for endogenous vitamin D(3) synthesis [122]. On the other hand, excessive sunlight leads to photoaging, immunosuppression, and photocarcinogenesis [116, 233].

Ultraviolet (UV) irradiation present in sunlight is an environmental human carcinogen. The toxic effects of UV from natural sunlight and therapeutic artificial lamps are a major concern for human health. The major acute effects of UV irradiation on normal human skin comprise sunburn inflammation (erythema), tanning, and local or systemic immunosuppression. At the molecular level, UV irradiation causes DNA(Deoxyribonucleic acid) damage such as cyclobutane pyrimidine dimers (CPDs) and (6-4) photoproducts, which are usually repaired by nucleotide excision repair (NER). Chronic exposure to UVR leads to photoaging, immunosuppression, and ultimately photocarcinogenesis. Photocarcinogenesis involves the accumulation

of genetic changes, as well as immune system modulation, and ultimately leads to the development of skin cancers. In the clinic, artificial lamps emitting Ultraviolet B(UVB) and Ultraviolet A(UVA) radiation in combination with drugs are used in the therapy of many skin diseases, including psoriasis and vitiligo. Although such therapy is beneficial, it is accompanied with undesirable side effects. Thus, UV radiation is like two sides of the same coin: on one side, it has detrimental effects, and on the other side, it has beneficial effects.

Solar radiation reaching the earth's surface includes UV, visible, and IR radiation between 290 and 4000 nm. Upon reaching earth, wavelengths greater than 2500 nm are absorbed by the Earth's atmosphere by water vapor and carbon dioxide, whereas wavelengths less than 290 nm are absorbed in the atmosphere by nitrogen and oxygen via the ozone layer. Thus, the solar radiation finally reaching us at the Earth's surface usually has wavelengths between 290 to 2500 nm, as seen in Figure 1.1.

Terrestrial sunlight fluctuates dramatically not only in terms of overall intensity but also in its spectral composition by time of day, elevation, and latitude. These effects on spectral irradiance predominantly affect the UV component of the solar spectrum. The quality and quantity of solar radiation vary depending on geography and time. Skin cancers are associated with the increased exposure to UVR from the sun [154]. Modern sunbeds emit approximately 95% – 99.9% UVA and 0.1% – 5% for UVB [267].

Clinical, epidemiological and molecular evidence has demonstrated that DNA damage and the subsequent mutations induced by the UV component of sunlight are critical events in the incidence of skin tumours [99, 147, 248]. While the sun, a natural UV source, is known to cause DNA damage and skin cancer, another artificial source of UV radiation are tanning units or sunbeds. The motivation for this work was to collate a comprehensive dataset for sunbed emissions throughout England. Second, the aim was to incorporate this data in various plausible scenarios and models to predict skin cancer risk.

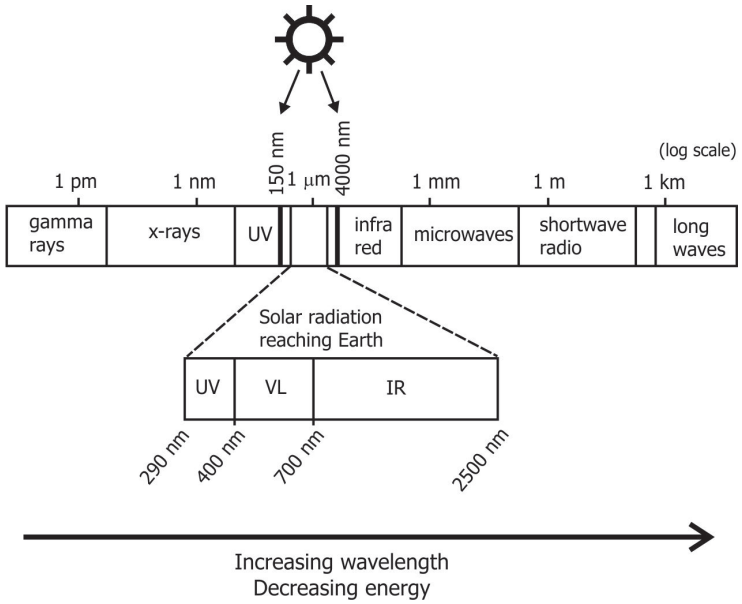


Figure 1.1: Schematic of electromagnetic spectrum with Solar radiation wavelengths.

The increased use of sunbeds, emitting significant amounts of UVA, is of concern, especially since a substantial proportion of young people use sunbeds [301]. There is evidence to suggest the the risks of melanoma are associated with sunbed use [32]. In the past, studies on the risk of sunlamp use for the development of skin cancer have suffered from various methodological and practical problems, such as strong confounding factors of sunbed use with sun exposure. However, even in studies that reported a positive association, adjustment for these potential confounder factors and the dose response were not always carried out, which casts uncertainties on the interpretation of the results. Even though there has been a previous sunbed assessment carried out in Scotland [211] there were a lack of objective measurements for sunbed exposure in England. There was also a shortage of quantitative data on the emissions from the new "high power" sunbeds with definitive traceable calibration and measurement techniques.

In the past, there has been recall bias in recalling lifetime sun and sunbed exposure in cases and controls [17, 26, 71, 280, 286]. In the work reported in this thesis, the sun dose is calculated from lifetime cumulative day-to-day and holiday exposure. In addition, there was also no reliable information on the frequency and duration of sunbed use. This issue was addressed in this study, whereby the sunbed dose was

calculated from sunbed exposure times and number of sessions. This data with various plausible scenarios allowed the modelling of skin cancer risk. A computational skin model was also developed that used the measured emission spectra from the sunbeds to provided a data-driven semi-empirical simulation of photon penetration with a biological endpoint to quantify DNA damage.

Taken together, the available data support the idea that CPDs rather than photooxidative damage may be responsible for the genotoxic effect of UVA in mammalian cells, a notion which is confirmed by the mutational specificity of UVA. In addition, the induction of CPDs at biologically relevant doses of UVA radiation lead us to suggest that UVA radiation may be involved in solar mutagenesis.

In the $20^{\text{th}}$ century, people associated skin damage only with the inductions of burns, with only the UVB component causing harm. Therefore, sunscreens were developed only to block the UVB radiation. Thanks to these sunscreens, people felt protected and could then spend several hours in the sun without seeing the appearance of sunburn.

### 1.1.1 History of Tanning

The ancient Egyptians, Greeks and Romans first discovered the healthy benefits of sunbathing, known as "heliotherapy"(sun therapy).

Prior the Industrial Revolution, it was the high society who had a pale skin, as they worked or stayed indoors, while the lower classes were mainly outdoors and were sun exposed. During the industrialisation of society in the $19^{\text{th}}$ century, with introduction of machines, the working classes started working indoors in the factories. In the $20^{\text{th}}$ century only the wealthy had the time and money to afford recreational outdoor life, such as going to the beach, sports, walking in the mountains, skiing and sailing, and having a tan became the symbol of the moneyed class and being healthy. By the early 1920s, daily exposure to sunlight was also advised as a cure for many diseases such as acne, rickets and tuberculosis, especially for children. By the 1930s, a suntan had become a symbol for health and wealth. During

the 1960s, swimwear fashion changed with the introduction of the bikini, allowing women's bodies to receive nearly total UV exposure. Since the 1950s, holidays to sunny destinations and charter flights initially to Mediterranean regions and later to the subtropical countries became popular, and could be afforded by an increasing number of people.

In the 1940s, suntan lotion was originally developed to promote the tanning process and not to protect against the sun. During this period, people associated skin damage only with the induction of burns, with only the UVB component causing harm. Therefore, sunscreens were designed only to block the UVB radiation. Thanks to these sunscreens, people felt protected and could then spend several hours in the sun without seeing the appearance of sunburn. In the 1950s, the first wariness that sunlight could cause melanoma emerged [161]. In the 1960s, indoor tanning became possible through the use of sunlamps. These artificial tanning lamps were used at home and emitted a broad spectrum of radiation from Ultraviolet C (UVC) to infrared (IR). In the late 1970s to early 1980s, it was suggested that an UVA induced tan was safer than one caused by UVB and UV lamps were then produced with minimal or no UVB radiation [250,286]. Thus, for decades, people have been exposed to high doses of UVA.

Throughout the 1970s and 1980s, reports of the increasing incidence and mortality rates of melanoma were reported [15, 53, 164], while fashion suggested that suntans make you look and feel healthier. The use of sunbeds became increasingly popular during the 1980s. Tanning salons flourished and sunbeds became available for use at home. Tanning became increasingly popular, despite a growing body of scientific evidence indicating that it not only leads to premature aging of the skin, but also causes skin cancer [161, 174]. Awareness of the association between UV exposure and skin cancer gained more ground. One of the reasons for this was when people became concerned about the damage to the ozone layer in the early 1980s. To some individuals, a tanned skin is socially desirable. Thus, the 'suntanning industry' has expanded, particularly in northern Europe and North America, in which

artificial sources of UVR supplement exposure to sunlight. In the early days many people were exposed to UVR from a mercury or carbon arc lamp for treatment [186].

## 1.2 Ultraviolet Radiation

The term ultraviolet means "beyond violet", violet being the colour of the shortest wavelengths of the visible spectrum. In 1801, the German physicist Johann Wilhelm Ritter studied radiation at wavelengths shorter than this violet region and observed a type of invisible light beyond violet [97]. At that time, many scientists including Ritter, concluded that light was composed of three separate components: an infra-red, a visible-light and an ultraviolet. Different parts of the spectrum were understood through contributions from Macedonio Melloni [24], Alexandre-Edmond Becquerel [56] and others in 1900s. UV light is an electromagnetic radiation with a wavelength from 100 nm to 400 nm, shorter than that of visible light but longer than X-rays depicted in Figure 1.2. UVR is officially divided into UVC ($100-280$ nm), UVB ($280-315$ nm) and UVA ($315-400$ nm), with UVA being sub-classified into UVAII ($315-340$ nm) and UVAI ($340-400$ nm).

UVC and short-wavelength UVB ($280-290$ nm) are totally blocked by the atmosphere and thus are not considered as a hazard for human health. The long-wavelength UVB ($290-315$ nm), the most energetic terrestrial wavelengths, represents $0.4-5.5\%$ of the solar UV spectrum at the surface of Earth. Exposure to solar UVR is a major risk factor in the induction of skin cancer. UVB radiation is, however, most efficient at producing DNA damage, essentially bipyrimidine photoproducts, which lead to the mutagenic events at the origin of tumours [248]. In contrast, lower-energy UVA photons ($315-400$ nm) constitute the large majority of terrestrial UV radiation but are less cytotoxic than UVB radiation.

However, the recent widespread use of artificial tanning units accompanied by prolonged periods of sunbathing with UVB-blocking sunscreens, has led to a large increase in the level of human exposure to UVA which can potentially cause mutations [239]. This trend is also emphasised by the popular use of high-intensity

UVA-tanning sunbeds [296].

Recent work concerning the interaction of UVA radiation with cultured cells has revealed the mutagenic effect on eukaryotic cells [272]. At present, the premutagenic DNA lesions induced by UVA have not been identified.

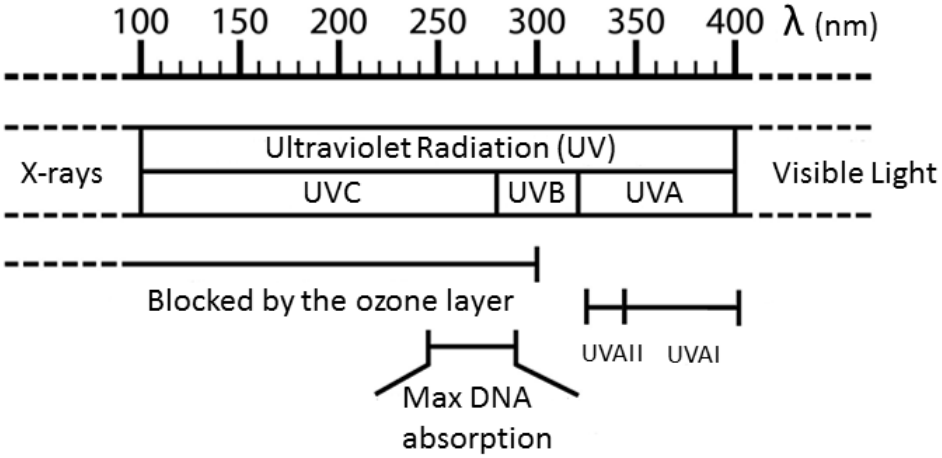


Figure 1.2: Schematic of UV wavelengths and DNA absorption range.

UV radiation is a toxic agent with genotoxic effects. It has been discovered to be associated with chromosome aberrations caused by breaks in the DNA strands. Various mechanisms exist to repair DNA if damaged by UVR, for example, the nucleotide excision repair (NER) mechanisms [265]. In NER, a small region of the strand surrounding the damage is removed from the DNA helix as an oligonucleotide. Oligonucleotides are short nucleic acid polymers usually consisting of $13 - 25$ nucleotides. The term oligonucleotide is derived from the Greek "oligo," which means "few" or "small". The length of the oligonucleotide is usually denoted by the term "mer", which is Greek for "part." The small gap remaining in the DNA helix is filled in by the sequential action of DNA polymerase and DNA ligase. NER recognises a wide range of damage, including damage caused by UV irradiation and chemicals.

UV induced damage is involved in the initiation of melanoma; melanin is involved in the formation of free radicals [21]. UVB exposure is considered to be responsible for non-melanoma skin cancer, as it generates CPDs in skin cells, which in turn can develop into cutaneous squamous cell or basal cell carcinomas [203]. Through the increasing usage of UVA tanning beds and the parallel rise in the development of

melanomas, the adverse effects of UVA exposure was also suggested [203]. Like UVB, UVA can cause non-melanoma skin cancers, but tumours take longer to develop and require much higher doses. UVA-induced skin cancers have been thought to derive from indirect damage to DNA caused primarily by the generation of reactive oxygen intermediates [204].

### 1.2.1 DNA Damage

DNA is a large, high molecular weight macromolecule composed of subunits called nucleotides. Genomic DNA, located in the nucleus of cells, is the basis of our genetic identity, controlling cellular functions. This identity is coded by four nitrogenous bases represented by letter's: A for adenine, T for thymine, G for guanine and C for cytosine. A and G are purines. C and T are pyrimidines. These four bases are organised in a precise structure: the genome, which is shared by all cells within a given organism. DNA has a double helix structure, as shown in Figure 1.3, in which two complementary strands of nucleotides coil around each other. The two outside helices of DNA form a sugar phosphate backbone.

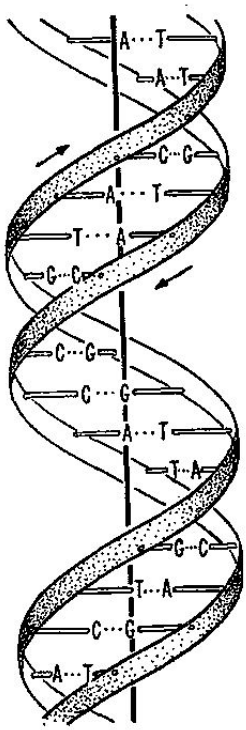


Figure 1.3: A schematic of DNA double helix adapted from Double Helix [281].

DNA repair refers to an assembly of mechanisms by which a cell singles out and corrects damage to the DNA molecules that encode its genome. UV radiation is an exogenous environmental factor that can cause DNA damage and excessive exposure from sunlight or sunbeds can lead to skin cancer [166, 190]. It has been estimated that DNA can undergo 1 million alterations in a day [172], which results in less than 0.0002% of the $6 \times 10^9$ bases [$3 \times 10^9$ base pairs (bp)] of the human genome. DNA damage to the genome is constantly been corrected by repair processes in the system. The chances of tumour formation increases when lesions in integral tumour suppressor genes like the *TP53* gene are unrepaired, thus affecting the cell's ability to repair. Abnormalities in the *TP53* gene, which codes for the *p53* protein, have been discovered in more than 50% of human cancers [137].

One frequent damage occurs when adjacent bases, which usually bond across the "ladder", bond with each other instead. As a result a bulge is formed and the distorted DNA molecule does not operate correctly.

A cell with DNA damage can have three possible fates: 1) the repair succeeds and the cell becomes healthy, 2) the repair fails and the cell dies, or 3) the repair remains faulty, but the cell survives the fault characteristics and may become carcinogenic. The chances of DNA repair error increases after excessive exogenous UV exposure when the body's ability to repair is saturated [10].

UV photons affect the DNA molecules of living organisms in different ways. There are two main types of DNA damage: endogenous and exogenous. Exogenous sources of DNA damage are caused by external agents such as UV radiation from the sun or sunbeds, while endogenous damage occurs from reactive oxygen species (ROS) produced from normal metabolic byproducts. In living cells ROS are formed continuously as a consequence of metabolic and other biochemical reactions. These ROS include superoxide ($O_2{-}\cdot$), hydrogen peroxide ($H_2O_2$), hydroxyl radicals ($OH\cdot$) and singlet oxygen ($^1O_2$). The induction of 8-Oxoguanine (8-oxo) is one of the most common DNA lesions resulting from ROS and can result in a mismatched pairing with adenine resulting in G to T and C to A substitutions in the genome [179].

ROS free radicals are generally considered to develop primarily from UVA exposure causing oxidative damage of the bases.

UV radiation, present in sunlight and sunbeds, can cause damage to the genetic information in the cell's DNA molecules. This occurs from UVR absorbed by the nucleic acid bases, and the resulting energy from a photon can induce strand changes leading to photo-products. The most frequent photo-products are the consequences of bond formation between adjacent pyrimidines within one strand, and, of these, the most frequent are CPDs. Pyrimidine dimers are the most representative DNA lesion [183].

### 1.2.2 Cyclobutane Pyrimidine Dimers

The absorption of UV can result in the formation of intra-strand CPDs in DNA, which can lead to mutations or cell death [117, 150, 158]. Pyrimidines are molecular components in the biosynthesis process and include thymine and cytosine as seen in Figure 1.4. Thymine and cytosine are two of the base-pair components of DNA, the others being adenine and guanine. UV radiation has been experimentally demonstrated to cause DNA damage, mostly by the formation of dimeric photoproducts between adjacent pyrimidine bases on the same strand. Two forms of pyrimidine dimers have been well described: CPDs and (6-4) photo-products (pyrimidine pyrimidinone adducts). These are the two predominant DNA lesions caused by absorption of photons and are considered to be responsible for the mutations observed in skin tumours [42].

CPDs are formed by the covalent binding of carbon atoms at the C5 and C6 positions of two adjacent pyrimidines (thymine and/or cytosine), whereas (6-4) photo-products result from the covalent binding between the C6 and C4 positions [47, 269].

CPDs were at least 20 — 40 times more prevalent than any other DNA photo-product when DNA or cells were irradiated with simulated sunlight [299]. A recent *in vivo* study has demonstrated that UVAI has the ability to produce CPDs which was considered to just be a UVB mechanism in the past [194]. Therefore, sunbeds,

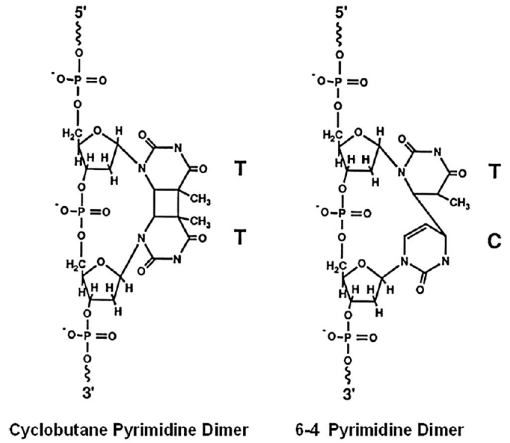


Figure 1.4: Chemical structures for pyrimidine dimers [180].

a high UVA source, have the ability to generate CPDs. This is further bolstered in a study where short-term tanning salon exposure (10 sessions in 2 weeks) resulted in the formation of CPDs [289].

Cyclobutane dimers can be removed from the DNA of eukaryotic cells by the powerful excision repair mechanism that is deficient in cells from most sun-sensitive, skin cancer-prone patients with the hereditary disease, xeroderma pigmentosum [98,153]. There is increasing evidence that UVA generates pyrimidine dimers in DNA directly [135]. Previous studies that determined the frequency of CPDs in human engineered skin for solar UVA and solar simulator UV sources showed similar CPD formation [237,260]. A quantifiable CPD yield was calculated from a dose equivalent to 2 hours at noon time [260]. Despite the fact that the formation of pyrimidine dimers has been demonstrated in the UVA range [234], it requires between 3 and 6 orders of magnitude more energy at 365 nm than that required by UVB. Recently, Mouret *et al.* [203] showed that thymine dimers were induced in human cells and human skin by UVA. These authors even suggested that the yield of UVA-induced thymine dimers could be higher than the yield of 8-oxo-deoxyguanosine (8 oxo-dG) oxidative damage. So far, the nature of the photosensitizer involved in such a process is unknown. In fact, UVA toxicity mainly depends on indirect mechanisms in which ROS are generated through photo-activation of endogenous photosensitizers such as porphyrins, riboflavin and quinones.

### Photon Energy

One way to describe electromagnetic radiation other than as wave motion is to consider the radiation as a stream of particles. These are called photons. Each operating photon represents a certain amount of energy. It can be useful to consider UV energy incident upon an area in terms of the number of photons, or the photon density. Each photon carries an amount of energy called a quantum, $\mathcal{E}$ (J), determined from quantum mechanics as [197]:

$$\mathcal{E} = \mathrm{h}v = \mathrm{h}\frac{\mathrm{c}}{\lambda} \tag{1.1}$$

where:

$\mathrm{h}$ = Planck's constant, $6.626 \times 10^{-34}$ (JS)

$v$ = frequency, (Hz)

$\mathrm{c}$ = the speed of light, $3 \times 10^{8}$ $(\mathrm{ms}^{-1})$

$\lambda$ = wavelength(nm)

Since hc is constant, we see that the photon energy increases with decreasing wavelength. For a certain dose it is possible to calculate the number of photons. For example the frequency of an UVA wavelength at 365nm corresponds to $8.21 \times 10^{14}$Hz and the energy is calculated to be $5.44 \times 10^{-19}$J/photon. Inverting this value gives $1.83 \times 10^{18}$ photons/Joule. So for a typical sunbed session of 2 – 3 standard erythemal dose (SED), where 1 SED = 100 $\mathrm{Jm}^{-2}$, a 2 SED exposure produces $1.83 \times 10^{20}$ photons per $\mathrm{m}^2$.

### Radiometric Quantities

Radiometry can be applied to all optical sources and to all exposures to optical radiation (including solar radiation and UVR). In radiometry, radiant energy is the energy of electromagnetic radiation. The SI unit of radiant energy is the joule (J). Power is the rate at which energy is delivered, and is measured in watts ($\mathrm{Js}^{-1}$). The quantity of radiant energy may be calculated by integrating power with respect to time.

$$\text{Energy(J)} = \text{Power(W)} \times \text{time(s)} \tag{1.2}$$

Irradiance, E, is the radiation power incident on a flat surface of unit area ($\text{Wm}^{-2}$). The term 'spectral' placed before any of the quantities implies restriction to a unit wavelength band, for example spectral irradiance (watts per square metre per nanometre) [199].

A surface exposed to irradiance, E, over a given time (s) results in a dose, ($\text{Jm}^{-2}$). The relationship is shown in the equation below:

$$\text{dose}(\text{Jm}^{-2}) = \text{E}\ (\text{Wm}^{-2}) \times \text{time(s)} \tag{1.3}$$

Fluence, H, is often confused with dose as it is also measured in energy per unit area, $\text{Jm}^{-2}$. The difference is that dose refers to light incidence at the surface while fluence is the total amount of radiant energy from all directions incident on an infinitesimally small sphere of surface area divided by the cross sectional area of that sphere.

The term fluence rate was introduced by Rupert in 1974 [240]. For the purposes of this work, a clear distinction needs to be made between "irradiance" and "fluence rate". The quantities have the same units ($\text{W m}^{-2}$) but are conceptually quite different. Note that the definitions given here apply for any wavelength range. The fluence rate (symbol $\text{E}'$; units ($\text{W m}^{-2}$)) is defined as the total radiant power incident from all directions onto an infinitesimally small sphere of surface area divided by the cross sectional area of that sphere. Note fluence rate can be thought of as spherical irradiance, as defined by the International Commission on Illumination (CIE) [3].

## 1.3 Methods of Measuring Ultraviolet Radiation

UVR can be measured by chemical or physical detectors, often in conjunction with a monochromator or band-pass filter for wavelength selection. Physical detectors

include radiometric devices, which depend for their response on the heating effect of the radiation, and photoelectric devices, in which incident photons are detected by a quantum effect such as the production of electrons. Chemical detectors include photographic emulsions, actinometric solutions and UV-sensitive plastic films.

**Spectroradiometry**

The fundamental way of characterising a source of UVR is on the basis of its spectral emission distribution, which indicates the spectral irradiance as a function of wavelength. The data is obtained by an instrument called a spectroradiometer which measures radiometric quantities in narrow wavelength intervals over a given spectral region.

A spectroradiometer comprises three essential components [108]:

1. input optics, such as an integrating sphere or Teflon diffuser, which collects the incident radiation and conducts it to the entrance slit.

2. a monochromator, which disperses the radiation by means of one or two wavelength dispersive devices (either diffraction grating or prism). The monochromator incorporates an entrance slit, mirrors to guide the radiation from the entrance slit to the dispersion device and on to the exit slit, where it is incident on radiation detector.

3. a radiation detector, normally a photodiode or, for higher sensitivity, a photomultiplier tube.

Spectroradiometry is generally considered to be the best way of specifying UV sources, although the accuracy of spectroradiometry, particularly with respect to the UVB waveband of terrestrial radiation, is affected by a number of parameters including wavelength calibration, band width, stray radiation, polarization, angular dependence, linearity and calibration sources. It is therefore essential to employ a double monochromator for accurate characterisation of terrestrial UVR [20].

The Photobiology Unit in Ninewells Hospital (Dundee) provides a radiometer calibration traceable to National Physical Laboratory (NPL, Teddington, UK) and accredited by United Kingdom Accreditation Service (UKAS). This traceability was achieved by exposing UV radiometers to an appropitate phototherapy source and comparing against a calibrated spectroradiometer (DM 150, Bentham Instruments Ltd Reading, UK). The spectroradiometer is calibrated using two NPL transfer lamp standards: a deuterium lamp (CL3, Bentham Instruments Ltd) and a Quartz halogen lamp (CL2, Bentham Instruments Ltd). The standard lamps are measured by the Bentham spectroradiometer and compared at each wavelength to their known irradiance as given by the NPL.

## 1.4 UV Radiation Effects On The skin

The skin is the organ most exposed to environmental UVR. Exposure to UVR may result in erythema and sunburn, tanning, skin aging, photosensitivity, and carcinogenesis in the form of non-melanoma skin cancer (NMSC) and cutaneous malignant melanoma.

The acute and long-term normal clinical effects of solar ultraviolet radiation (UVR) on the skin are well established. These include erythema (sunburn), pigmentation (tanning), skin cancer and photoaging [293].

The acute clinical effects of exposure to sunlight or artificial tanning units UVR consist of erythema and pigmentation, as well as thickening of the epidermis, in particular the upper stratum corneum layer. Erythema is an acute cutaneous inflammatory reaction that follows excessive exposure of the skin to UVR due to increased blood volume. It is the most prominent and well-known acute response to UV radiation, and is associated with the classic signs of inflammation, such as redness, warmth, tenderness and oedema (fluid retention).

There are also other biological reactions, such as immunosuppression and the photosynthesis of vitamin D(3), which will not be discussed here. Most human UV radiation exposure is from sunlight, but other sources such as phototherapy lamps,

sunbeds, arc-welding apparatus and unshielded fluorescent and metal halide lamps can cause similar effects. The individual erythema and tanning responses of human skin are primarily genetically predetermined.

Skin colour is an important factor in offering photo-protection from UVR and thus determines the likelihood that an individual will develop erythema [18]. While fair-skinned type I individuals only require 15 – 30 mins in noontime Summer sunlight to induce an erythemal reaction, people with moderately pigmented skin may take 1 – 2 hours of exposure and dark skin type III and greater will normally not burn. Other phenotype traits that may influence susceptibility to sunburn are eye colour, hair colour and freckles. The erythema biological reaction to ultraviolet radiation depends on the waveband range, which we investigate in the next chapter. Table 1.1 represents the different skin types (I – VI) and the characteristic tanning history responses. A typical individual with skin type I would be of Celtic origin with red hair, blue eyes and freckles. This skin type has a high propensity to burn.

Table 1.1: Fitzpatrick skin type adapted from [90].

| **Skin type** | **Tanning history** | **Description** |
|---|---|---|
| I | Always burns, never tans | White skin colour |
| II | Usually burns, minimal tanning | White skin colour |
| III | Sometimes burns, average tanning | White skin colour |
| IV | Slightly burns, above average tanning | Light Brown skin colour |
| V | Rarely burns, strong tanning | Brown skin colour |
| VI | Never burns, deeply pigmented | Black skin colour |

A chromophore (chromo = colour, phore = carrier) is a chemical molecule that absorbs a specific wavelength of the electromagnetic spectrum. One of the major chromophores in skin tissue is melanin, the complex molecule largely responsible for the colour of skin and hair. Most melanin is stored in microscopic subcellular structures called melanosomes.

Another major skin chromophore is haemoglobin in the red blood cells that are abundant within blood vessels and that are in close proximity to the walls of the vessels.

Melanin pigments represent the most important UVR protecting factor of human

skin. Two subtypes of melanin have been identified, occurring in various volumes in skin. The black to brown eumelanin is found predominantly in dark hair and eyes as well as in the skin of dark-haired subjects. The yellow-reddish pheomelanin mainly occurs in the hair and skin of blond-and red-haired individuals. Noticeable amounts of pheomelanin were detected in melanocytic especially dysplastic lesions, and the highest degrees of pheomelanin were found in melanoma cells [243].

Melanin absorbs highly in the ultraviolet region of the spectrum as displayed in Figure 1.5, thus acting as a photo-shield protecting cellular structures in the lower layers of the skin [212]. Melanin is not a good scavenger of free radicals in light-skinned phototypes I-II. Moreover, melanin can produce free radicals, namely reactive oxygen species (ROS), and damage cellular material including DNA.

The role of the two subtypes eumelanin and pheomelanin during the interaction with UVR is not fully clear. Eumelanin appears to be more photoprotective melanin of human skin,whereas pheomelanin is associated with phototoxic effects [136].

UVR increases the risks of developing skin cancer, mainly in susceptible people (skin types I–II and tendency to freckle, with many naevi). For all skin cancers, skin photo-type is an important determinant of risk; people who are prone to sunburn have a higher risk of developing skin cancer compared with those who tan easily and do not burn [90, 173].

Haemoglobin is carried in red blood cells, or erythrocytes, and comprises approximately $40 - 45\%$ of whole blood. It is responsible for delivering oxygen from the lungs to the body tissues and returning waste gases, such as carbon dioxide, to the lungs to be exhaled. Haemoglobin consists of the protein globin bound to four haem groups. Each haem group contains an iron atom at the centre of a ring-like structure. An iron atom in the ferrous ($Fe^{2+}$) form will bind physically to an oxygen molecule to become oxygenated, as opposed to oxidised which would involve a chemical bond. Therefore, one haemoglobin molecule with its four iron centres can carry a total of four molecules of oxygen, in which case it is said to be 100% saturated. In the oxygenated state haemoglobin is known as oxyhaemoglobin ($HbO_2$). The deoxy-

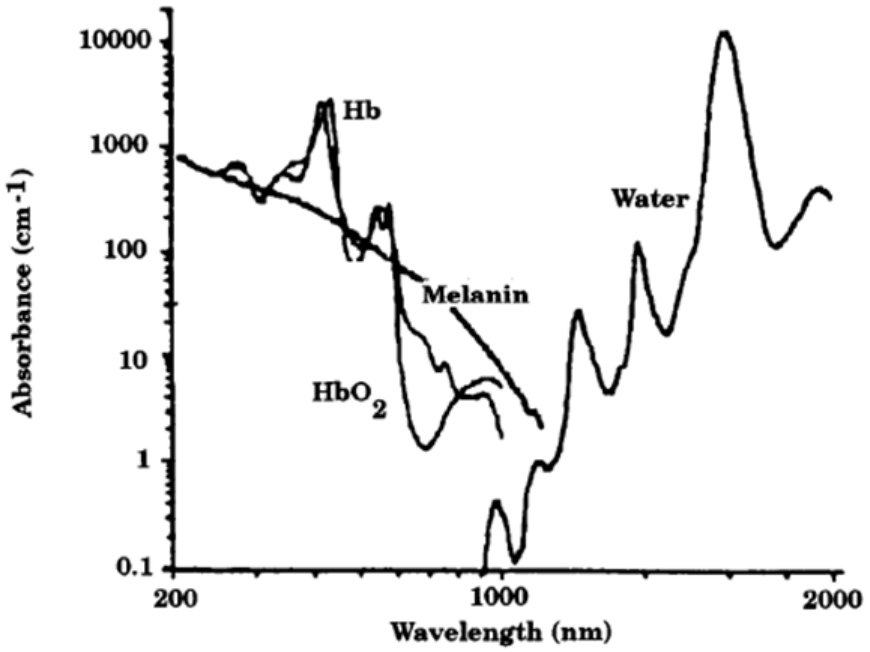


Figure 1.5: Chromophore absorbance in human tissue reproduced from [231].

genated form, with no oxygen molecules attached, is known as deoxyhaemoglobin (Hb).

Water ($H_2O$) is the most abundant molecule in the human body, accounting for 60–80% of total body mass [178]. The water content varies with tissue type and is age and gender-dependent. Owing to its high concentration in most biological tissue, water is considered to be one of the most important chromophores in tissue spectroscopy measurements. However, between 200 and 900 nm there exists a region of low absorption. Hence, the water is not a major chromophore in the UV region.

## 1.5 Skin Cancer

Human skin cancers are closely associated with exposure to UV [30, 84, 273]. The frequency of precancerous lesions depends, among other things, on the frequency of damage induced by carcinogenic agents such as UV photons. The work presented in this thesis quantifies the DNA photon absorption and the formation of CPDs. Skin cancers are predominantly caused by the CPD lesions in DNA produced by the UV component from the sun. Therefore, sunbeds, also a UV source, have the capability

to induce skin cancers.

Skin cancer occurs when there is an abnormal growth of cells, and leads to uncontrolled cellular proliferation, which in turn develops into a tumour and cancer. The main types of skin cancer are non-melanoma (basal and squamous cell carcinoma) skin cancers and melanoma skin cancer shown in Figure 1.6. The non-melanoma skin tumours originate from keratinocytes that have undergone malignant transformation, while melanoma results from transformed melanocytes in the skin. The availability of epidemiological evidence indicates clearly that solar UV radiation is associated with skin cancer. Thus, UV radiation is the main etiological agent producing human skin cancer. By investigating UV DNA damage the initialisation of photolesion induction, tumourgenesis and carcinogenesis can be dissected.

Secondary effects from DNA damage in stem cells or extracellular structures are elastosis, premature aging of the skin, wrinkling and intra-ocular cataracts [258].

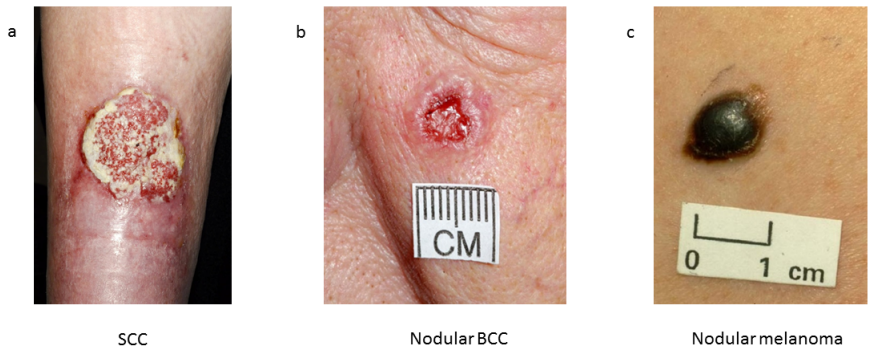


Figure 1.6: Skin cancers a) SCC, b) BCC and c) melanoma from left to right provided by Dr.Sally Ibbotson, PBU, Dundee, Ninewells Hospital.

### 1.5.1 Non-melanoma skin cancer

Non-melanoma skin cancer (NMSC), consisting of basal cell carcinoma (BCC) and squamous cell carcinoma (SCC), is the most common cancer in Caucasians. Caucasian stems from the Caucasus mountain region that describes white people of

European ancestry. This type of skin type is rated as skin type I and II on the Fitzpatrick scale and is usually related to individuals of Celtic origin with pale complexion that freckle easily. However, the precise relationship between UVR and the risk of NMSC is complex, and the relationship may differ by skin cancer type. Predominantly, NMSC occurs in maximally sun-exposed anatomical sites of fair-skinned people. NMSC is uncommon in individuals of skin type V and VI with naturally high pigmentation. The head and neck region is the most common site for BCC and SCC; 80% – 90% of cases occur in this area in the general population. NMSC is more common in people older than 50 years, and the incidence in this age group is increasing rapidly [102]. People with immune suppression, including organ transplant recipients, also are at higher risk. Genetic conditions, such as basal cell nevus syndrome, xeroderma pigmentosum (a condition in which there is a genetically determined defect in the repair of DNA damaged by UVR) [219] and albinism, are risk factors for the accelerated development of NMSC. Treatment with UVR for psoriasis also increases risk [170].

UVR is the most important aetiological factor for induction of SCC and BCC [60, 165,196]. For SCC, the cumulative total exposure is the main risk factor [253], while for BCC, both total exposure and the exposure pattern may play roles [165, 195]. Patterns of solar UV exposure are continuous (i.e. individuals working outdoors or living in a geographic region with a high annual UV index) or intermittent (i.e. individuals working indoors and experiencing most of their sunlight exposure on the weekends or while holidaying to regions with a higher UV index than their place of residence). An intermittent exposure pattern is relatively more associated with BCC compared to an overall total dose [101, 155].

UV irradiation of albino mice has demonstrated the development of skin cancer in laboratory conditions with SCC been the most prevalent. Studies of time-dose realtionships have shown the link between exposure and the incidence of skin cancers [64]. These studies have provided time-dose-response expressions which can be implemented in the analysis of epidemiological data and form the foundation for the

risk model in Chapter 3. The cumulative UV dose over a life time appears to be the main risk factor for SCC skin cancer. Recently UV exposure has been shown to induce melanoma in transgenic mice and opposums [167]. Melanoma is more associated with UV exposure earlier in life in comparison to SCC which is more related to a lifelong cumulative UV dose [288]. Furthermore, the time-dose relationship in murine studies have provided valuable data on the wavelength dependency of UVR to induce skin cancer. The most complete SCC skin cancer action spectrum was developed by De Gruijl et al. [62] from albino hairless mice, called SCUP–m (Skin Cancer Utrecht Philadelphia-murine) discussed later in Chapter 2.

This SCUP-m action spectrum was adapted by de Gruijl and van der Leun [59] for humans by including the differences in skin transmission between murine and human skin. This led to the development of the human action spectrum for SCC, called the SCUP–h (Skin Cancer Utrecht Philadelphia-human) action spectrum which is plotted in Figure 2.16. The SCUP–h action spectrum closely resembles an action spectrum for CPD formation in DNA following an adjustment for transmission of the epidermis [95].

### 1.5.2 Melanoma

Cutaneous malignant melanoma is less common than the familiar NMSC, basal and squamous cell tumours of the skin, but has a much higher probability of fatality. It is mainly a disease associated more with fair skin type individuals, but people with a more pigmented skin can also develop melanomas. Melanoma results from transformed melanocytes in the skin. Melanomas represent less than 10% of all skin cancers, yet they account for the vast majority of skin related deaths due to the high metastatic potential. Melanoma incidence rates continue to rise in Europe over the last few decades [66]. Previously published data estimated that around 86% of malignant melanomas in the UK in 2010 were linked to exposure to UVR from the sun and sunbeds [103, 213].

Intermittent exposure to UVR is the main environmental risk factor for melanoma,

especially in combination with endogenous factors such as skin types I, II, immune-deficient status and genetic predisposition [13]. Patients with genetic UV repair abnormalities like xeroderma pigmentosum are at a 1000-fold increased risk of developing melanoma [112]. This indicates that UV can cause skin cancer but in most people it is repaired. However, some people can have a genetic predisposition to skin cancer. If there is a family history of melanoma, the relative risk of developing another skin cancer is $2-3$ fold [121].

Melanoma is uncommon in black (skin type VI) people probably due to a better photo-protection of the skin by a larger amount of pigment in the skin. UVR is considered a less substantial risk factor for skin cancer in individuals of this skin type. In addition, melanomas appear more often on the non-pigmented regions of the skin [113] for this phenotype. However, it is usually the non-tanned (higher risk) individual that seeks a tan and uses a sunbed.

The increased use of sunbeds, emitting high amounts of UVA, is of concern, especially since a substantial proportion of young people use sunbeds [301]. This could have grave implications down the line as there is a lag time in developing skin cancer. Although there has not been a definitive link with sunbed use and risk of melanoma, it is likely that the effects on the skin are equal for all sources of UVR. Previous studies on the risk of sunlamp use for the development of skin cancer, have suffered from various methodological and practical problems.

UV radiation is specifically carcinogenic to the skin because it does not penetrate the body any deeper than the skin. A 2007 meta-analysis by the International Agency for Research on Cancer(IARC) reported positive associations of ever use of tanning beds with increased risk of melanoma and SCC [110]. In 2009, the IARC classified UV radiation from tanning beds as “carcinogenic to humans” (group 1 carcinogen) on the basis of its meta-analysis [92]. Since the individuals with poor ability to tan are more likely to use indoor tanning beds more often but are also more sensitive to UV damage [80], some have argued that these individuals are more susceptible to skin cancer after indoor tanning [26].

A meta-analysis that found a 75% increase in the risk of melanoma when indoor tanning started during adolescence or young adulthood [32]. An update of this meta-analysis has now revised this figure upwards to an 87% increased risk of melanoma with first use of sunbeds before the age of 35 years, with the risk increasing with the number of sunbed sessions. Colantonio et al. reconfirmed the association between sunbeds and melanoma, and also suggested that newer tanning beds were not safer than older models [51]. A 2014 study estimated that more than 400,000 cases of skin cancer may be attributable to sunbeds in the United States each year causing 245,000 basal cell carcinomas, 168,000 squamous cell carcinomas, and 6,000 melanomas [282]. Another study by Lazovich *et al.* found that the risk of getting melanoma increased the more years, hours, or sessions spent indoor tanning [162].

## 1.6 Monte Carlo Radiative Transfer Method

The Monte Carlo Radiative Transfer (MCRT) method was first implemented in astrophysics to model the distribution of cosmic dust distribution which is three dimensions (3-D). Modelling dust grain absorption and scattering requires 3-D radiative transfer calculations. However, the 3-D radiative transfer problem suffers from non-local coupling due to scattering where a photon created at one location can affect a very distant region through scattering. Nevertheless, Woods *et al.* [294, 295] has provided a code that is capable of solving these 3-D radiative transfer problems which has been adapted for a 3-D skin tissue model.

How UVR behaves beneath the surface of the skin is the key to understanding the absorption of a photon by DNA. One technique to ascertain a photon's behaviour is the Monte Carlo (MC) method, as applied to the transport of light radiation which is based on the radiative transport equation (RTE) described in Equation 1.5. This RTE involves computer-simulated calculations of photon propagation in scattering turbid media.

In the simplest form, Monte Carlo simulations are where photons are injected into a medium individually and their paths traced until they are either absorbed or

permanently scattered out of the region of interest [216]. The rules of photon propagation are expressed as probability distributions (hence the name 'Monte Carlo'), which are based on the geometry and optical properties of the tissue media. Monte Carlo is an integration method that allows to solve multidimensional integrals by sampling from a suitable stochastic distribution. The accuracy of Monte Carlo estimator depends on the number of samples (N) obeying Poisson statistics:

$$\sigma = \frac{1}{\sqrt{N}} \tag{1.4}$$

### 1.6.1 Tissue turbid media

Absorption and scattering coefficients of *in-vivo* human skin provides critical information on non-invasive skin diagnoses for aesthetic and clinical purposes. To date, very few *in-vivo* skin optical properties have been reported. In past studies, reported absorption and scattering properties of *in-vivo* skin in the wavelength range from 650 to 1000 nm [270]. Tissue medium is highly scattering with photons effectively bouncing off structures in the skin (mainly collagen fibre bundles).

Scattering of the photon continues until it either exits from the skin (back scattering) or is absorbed by a chromophore. Human skin, especially the epidermis, contains several major solar UVR absorbing endogenous chromophores including DNA, urocanic acid, amino acids and melanin [300]. The overall effect of scattering and absorption means that the penetration of photons decreases with depth in the skin. Shorter UVB wavelengths are more easily scattered and do not penetrate very far, however longer UVA wavelengths are less easily scattered and penetrate more deeply in skin tissue. In this work, we present a MC approach to model the path of a photon using *in-vivo* optical properties.

The MC technique describes the fate of a photon that expressed, in the simplest case, as probability distributions that describe the step size of a photon's movement between sites of photon-tissue interaction, and the angles of deflection in a photon's trajectory when scattering events occur.

The MC method permits the usage of complex and detailed models, while retaining simple implementation. The disadvantages of the Monte Carlo method are noise introduced by the stochasticity and long simulation time when high accuracy is needed. Hence, large numbers of photons are launched to build up a realistic model of photon propagation. Thus, the MC method is computationally intensive, as millions of photons are simulated.

## 1.7 The Radiative Transfer Equation (RTE)

The propagation of electromagnetic radiation is often described by Maxwell equations [275]. However, it must be noted that the skin may be too complicated a medium for a Maxwell solution, due to the inhomogeneity and complex micro structures [216, 292].

In the last few decades, RTE has been more popular in tissue optics than the Maxwell equations. The RTE model assumes that the light purely follows the particle model. There is no interaction between photons, nor interference. The motivation in RTE modelling is to predict the energy transport in turbid media.

As a result of non-locality effects and multi-dimensionality, the RTE Equation 1.5 is too complicated to be solved analytically for a 3-D skin medium. Therefore, the RTE is usually approximated in order to obtain a more tangible model. Although various numerical approximations [33, 125, 157, 226] are used to solve RTE, 3-D RTE is commonly solved using the Monte Carlo (MC) technique. This numerical stochastic approach is adopted for MC simulations in this thesis [225].

As light passes through a small volume of space there are two possibilities:

1. the intensity is either reduced by absorption or scattering of radiation out of the beam.

2. the intensity is increased by the emission of photons by matter in the volume or scattering of photons originally headed in other directions into the same direction as the beam is pointed towards.

The two possibilities are governed by the absorption coefficient $\mu_a$ , the scattering coefficient $\mu_s$ and the emissivity $j_v$. The absorption $\mu_a$ and scattering $\mu_s$ coefficients which, are both wavelength dependent given in units $\mathrm{cm}^{-1}$, are discussed in Chapter 4 and are related to the optical properties for different skin layers and chromophores. The emissivity is a local source of photons.

The RTE models the time and spatial change of specific intensity $I_v(r, \hat{s}, t)$ in the tissue defined in Section 5.4. For now consider the change in specific intensity $I_v(r, \hat{s}, t)$ equal to the loss in energy due to absorption and scattering out of $\hat{s}$, plus the gains in energy from light scattered into the $\hat{s}$-directed packet from other directions and from any local source of light at location$r$ for time point $t$. The light transport in tissue can be modelled by examining how the specific intensity $I_v(r, \hat{s}, t)$ changes when it passes through an infinitely small volume, dV. The RTE is shown in Equation 1.5 [44].

This energy balance is represented by terms in the RTE as follows:

$$\begin{aligned}\frac{1}{c}\frac{\partial I_v(r,\hat{s},t)}{\partial t} + \hat{S} \bullet \nabla I_v(r,\hat{s},t) = &- \underbrace{(\mu_a + \mu_s) I_v(r,\hat{s},t)}_{\text{aborption and scattering}} \\ &+ \underbrace{\mu_s \int_{4\pi} p(\hat{s},\hat{s}') I_v(r,\hat{s}',t)\, d\Omega'}_{\text{scattering}} + \underbrace{j_v(r,\hat{s},t)}_{\text{source}}\end{aligned} \tag{1.5}$$

where $I_v$ is the specific intensity at spatial location $r$ moving towards $\hat{S}$ in units $(Wcm^{-2}sr^{-1}Hz^{-1})$ (Figure 5.2 ). In volume element in position, $r$, the radiation is scattered to a new direction, $\hat{S}'$. The scattering angle is determined by the scattering phase function, $p(\hat{s}, \hat{s}')$, representing the probability of light with propagation direction $\hat{s}'$ being scattered into solid angle $d\Omega$ around $\hat{s}$ depicted in Figure 5.2. The phase function depends only on the angle between the scattered $\hat{s}'$ and incident $\hat{s}$ directions. The phase function describes the anisotropic scattering behaviour of photons in biological tissue and is further discussed in section 5.3.

The left hand side of RTE is the time derivative of $I_v$ divided by the speed of light, c, to represent the change of specific intensity per distance travelled. This

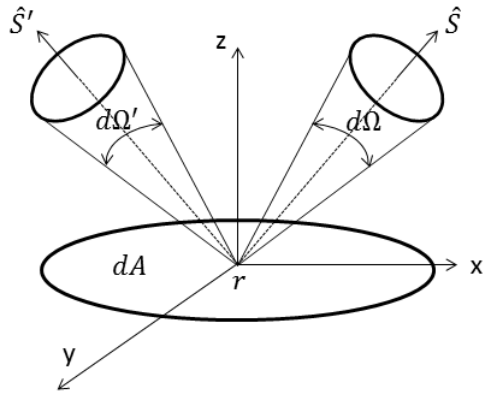


Figure 1.7: The phase function describes the change of photon direction from $\hat{s}'$ to $\hat{s}$ for a scattering event scattering at point r within a solid angle.

change is equal to the four additive terms on the right hand side of Equation 1.5.

Each term in Equation 1.5 is represented below:

$$\frac{1}{c}\frac{\partial I_v\left(r,\hat{s},t\right)}{\partial t}+\hat{S}\bullet\nabla I_v\left(r,\hat{s},t\right)$$

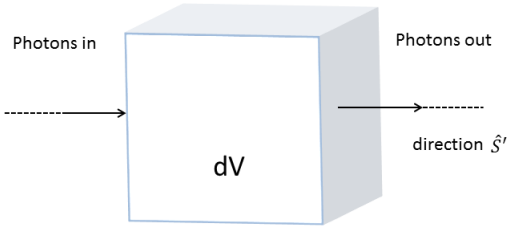


Difference between the flow of energy entering and exiting the volume as a function of time, i.e the net flow.

$$\left(\mu_a+\mu_s\right)I_v\left(r,\hat{s},t\right)$$

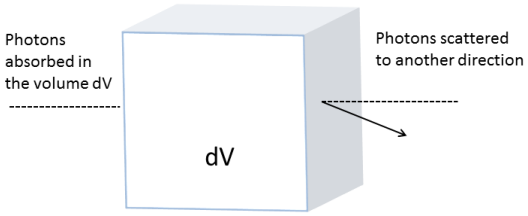


Loss of energy due to absorption and scattering.

$$\mu_s\int_{4\pi}p\left(\hat{s},\hat{s}'\right)I_v\left(r,\hat{s}',t\right)d\Omega'$$

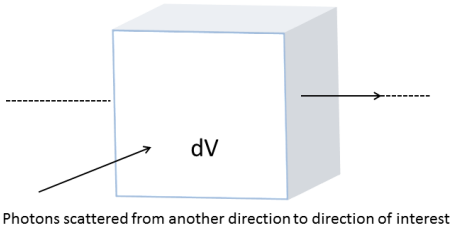


Gain in energy due to scattering in all directions $\hat{s}'$ into direction $\hat{s}$

$$j_v\left(r,\hat{s},t\right)$$

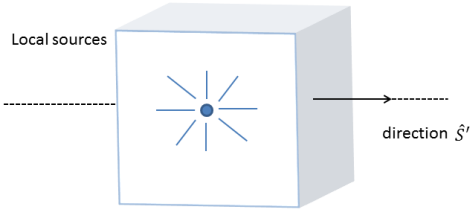


Local Sources: The emission component $j_v\left(r,\hat{s},t\right)$ is the local source of photons otherwise known as volume emissivity $(Wcm^{-3}sr^{-1})$ and represents the power injected

into a solid angle centred on $\Omega$ in a unit volume at $r$ inside a scattering medium.

Once the optical properties of the tissue are established in Chapter 4, the RTE can be implemented to calculate the fluence rate, $\Psi(r,t)$ in units ($\mathrm{Wcm}^{-2}$) at any position for a given source specification. The fluence rate is an important to model the distribution of UVR as it passes through biological media [278] and can therefore predict how the UV will reach certain skin layers, such as the basal layer.

The fluence rate, $\Psi(r,t)$, is defined as the energy flow per unit area per unit time irrespective of flow direction and is obtained by integrating the specific intensity over the entire $4\pi$ solid angle at a location $r$.

$$\Psi\left(r,t\right)=\int_{4\pi}I_{v}\left(r,\hat{s},t\right)d\Omega dv \tag{1.6}$$

The MC method offers a stochastic approach to model light propagation based on radiative transfer theory. The MCRT technique is further discussed in Chapter 5.

## 1.8 Thesis Overview

Having introduced the main objective of the project, this section will give an overview of the thesis from characterisation, SCC risk modelling, optical properties, MC modelling, DNA damage and skin UV effects.

Chapter 2 introduces the artificial tanning units and the development of the calibration methods. The various types of sunbeds are described with corresponding spectral emissions. Also discussed are the measuring techniques employed when collating the sunbed emissions in the field. The application of biological weighting factors to the obtained sunbed data is also reported.

In Chapter 3, the application of plausible scenarios from the sunbed outputs yields a dose. The various doses are implemented in a simple power law equation with age and dose parameters to yield a relative risk. The relative risk compares a baseline sun exposure to a sunbed user for various sunbed use regimes.

Chapter 4 discusses the derivation of optical properties for tissue media in the UV range. The main skin layer absorption and scattering coefficients are described. Published data on optical properties is reviewed. The main UV chromophores are also postulated from first principals.

Chapter 5 elucidates the MCRT method from distribution functions and skin attenuation coefficients. The phase function is described in more detail along with scattering governance. The model for photon transport in multi-layered tissues has been coded in Fortran 77 programming language. The model represents a semi-empirical 3-D simulation of human tissue data driven by sunbed and solar spectra. Monte Carlo simulations offer a rigorous, yet flexible approach to photon transport in turbid tissue media. The skin model is verified with published data on fluence for tissue media. A comparative test demonstrates the number of absorbed photons for noontime sun and a sunbed session. One of the goals in this work was to quantify DNA damage in terms of pyrimidine dimer lesion formation from sunbeds. MCRT offers a tool to evaluate the number of absorbed photons to develop CPD lesions. By knowing the number CPD lesions formed from the photon yield for the sun one can indirectly measure the absorbed photons from a sunbed. Simulations also considered different skin types and compare photo-shielding of each.

Chapter 6 describes the investigation into sub-erythemal dose for healthy and photosensitive patients. Also described, is the melanin skin type characterisation from readings.

Chapter 7 gives an overall review of the techniques developed in this thesis and their ability to predict skin cancer risk and lesion formation. Suggestions for additional work are also discussed, highlighting the direction from here towards the main aim of the project: to predict the potential photo-carcinogenesis from sunbeds.

# Chapter 2

# Artificial Tanning Units

## 2.1 Introduction

Sunbeds are an artificial source of UV radiation emitting primarily in the wavelength range 280 – 400nm. UVA is the primary component of sunbeds and accounts for 95 – 99% of the total UV. The International Agency for Research on Cancer (IARC), an agency of the World Health Organization, has classified sunbeds as a Group 1 carcinogen, which is the highest risk category [81, 91].

Despite the unequivocal evidence for the dangers of sunbeds mentioned in the previous Chapter 2, before this study there was a shortage of objective data on the levels of UV radiation received and the detailed spectrum to which sunbed users were exposed. Previous preliminary studies carried out in Scotland revealed high levels of UVB found in new high-power sunbeds [200, 201, 211]. These studies also revealed that the estimated cancer risk from sunbeds had increased by a factor of three in the last 10 years due to the use of high-power sunlamps.

A British and European Standard, introduced in 2003 [8], set limits on the UV emission of sunbeds. However, no study had been performed to investigate compliance with the standard in England. The standard did not oblige sunbed operators in England to provide advice on health risks to customers. Conversely, operators in Scotland come under the Public Health Scotland Act 2008. During the study English operators could operate unmanned premises, equipped with coin-

operated sunbeds available to anyone of any age. Indeed, there have been reports of under age sunbed use in the North of England at the time of this study in 2010 [266].

Since the 2003 British Standard was published there has been the introduction of the Sunbed (Regulation) Act 2010 to ban under 18s using sunbeds. However, unmanned sunbed premises still exist in England. In various regions of England, tanning outlets are required to operate under licence from their local authority, but UV emission levels are not compared against regulatory limits due to the cost and complexity of obtaining reliable data.

In this study all the sunbeds were compared to a compliance level of 0.3 $Wm^{-2}$ erythemal-weighted irradiance. This is the maximum irradiance limit for UV tanning equipment and is based on the opinion of the EU's Scientific Committee on Consumer Products (SCCP) [1]. As a comparison it represents the intensity of the midday sun in the summer in the Mediterranean. Strictly speaking the safe limit is intended to match sunbed output to the maximum that human Caucasians have biologically evolved to deal with. It is important to assess whether the artificial tanning unit was operating within the specification and guidelines in the British and European Standard (BS EN 60335-2-27:2003) [8].

The BS-EN standard classifies UVR emitters into four 'types' depending on the wavelength of the UVR emitted and the levels of irradiance in $Wm^{-2}$ displayed in Table 2.1. This classification will also dictate to the operator the circumstances under which the appliance can be used. It should be noted that a fundamental weakness of this system is that an operator of a sunbed can undertake a complete re-fit of the lamps, which could essentially change the 'UV type', unknown to the users and perhaps even the operator.

The main purpose of the standard is to impose a classification labelling of UVR emitting devices. It also ensures that safety information and instructions for use are produced by the sunbed manufacturer. Type 3 sunbeds are intended for general use and it is expected that sunbeds in beauty parlours will compare to the limits shown in Table 2.1.

Table 2.1: Erythemal Irradiance UV appliance Limits and Classification of use (Source: BS-EN 60335-2-27:2003).

| UV Type | UVB ($\lambda : 280 - 320$nm) ($\mathrm{Wm}^{-2}$) | UVA ($\lambda : 320 - 400$nm) ($\mathrm{Wm}^{-2}$) | USE |
|---|---|---|---|
| Type 1 | <0.0005 | >0.15 | Supervised |
| Type 2 | 0.0005 -0.15 | >0.15 | Supervised |
| Type 3 | <0.15 | <0.15 | Unskilled |
| Type 4 | >0.15 | <0.15 | Medical |

The aim of this work was to measure the sunbed spectra emissions for sunbeds across England including North Tyneside, Cheltenham, Coleford, Newton Abbot, Derbyshire, Nottinghamshire and boroughs of London. A biological action spectrum (explained later in this chapter) was applied to the resulting data. The weighted data was then compared with the British and European standard on sunbed emissions compliance levels.

### 2.1.1 History of Tanning Lamps

In 1906 a German company called Heraeus developed a high pressure mercury-vapour, quartz glass lamp that produced high levels of UVR. These lamps offered medical treatment of calcium deficiency and bone disorders until the 1930s, with tanning as a welcomed side effect.

In 1960s, Friedrich Wolf decided to use UV lamps for non medical benefits in commercial tanning. He asked Philips to make him the world's first tubular UV lamp, from which the original wooden sun benches were made.

Before the mid 1970s, the source of UVR was usually an unfiltered, medium or high pressure mercury arc lamp which emitted a broad spectrum of radiation, from UVC to visible and Infra-red (IR) radiation [73]. The units often incorporated one or more IR heaters and were commonly called "sunlamps". By incorporating several mercury arc lamps into a "solarium", whole body exposure was achieved. Tanning devices based on mercury arc lamps emit relatively large quantities of UVB and UVC radiation, resulting in a significant risk of burning and acute eye damage. Solaria

that incorporate unfiltered mercury arc lamps are therefore now less popular [70].

Sunbeds, incorporating high-intensity UVA fluorescent lamps, were developed in the 1970s. These devices consisted of a bed and/or canopy incorporating 6 – 30 fluorescent lamps. Later, canopies were added and recognisable sunbeds appeared in the late 1970s consisting of high-intensity UVA fluorescent lamps. Vertical sunbeds were invented in the late 1980s. The first high-pressure tanning beds incorporating more than a single high-pressure lamp were manufactured in the mid to late seventies by companies such as Ultrabronz and JK Ergoline. These units required special filter glass to remove the UVC and the majority of the UVB that was emitted. These were generally large units, with a padded area to lie on and consisted of 6 to 36 lamps in a canopy or canopy and bench configuration 150 – 180 cm in length as seen in Figure 2.1. The earliest type of UVA lamp used in sunbeds is represented by the Philips TL09, Wotan LI00/79 and Wolff Solarium lamps [74].

Figure 2.1: Horizontal Unit UWE ibed XTT® Lamps(×57) : Cosmedico 200W.

Specially designed fluorescent lamps are used in solaria for artificial tanning units [109]. The emission spectrum from these lamps comprises the fluorescence continuum, extending from about 315 to 400 nm and peaking at 360 – 370nm. These lamps have spikes in the spectrum which are the emission lines of mercury atoms; the most dominant ones are at 313, 365, 405, 408, and 436 nm [107]. The UVA

irradiance at the skin surface from a typical sunbed or suncanopy containing these lamps is between 50 and 150Wm$^{-2}$ [34, 40].

In the late 1990s a new generation of advanced, stylish fully enclosed artificial tanning units emerged. At first, sunbed tanning consisted of lying on a flat acrylic sheet for 30 minutes or more. Then there was the 'stand-up' or vertical units often seen in gyms. With the introduction of 'high power' (180 – 250W) output lamps, session times reduced. Body cooling was introduced as lamps got hotter, and then air conditioning.

### 2.1.2 Artificial Tanning Units

Tanning lamps are the part of a tanning bed, booth or other tanning device that actually produce the artificial ultraviolet radiation. While there are literally hundreds of different tanning lamps, they can usually be classified into basic groups: low pressure and high pressure.

The fundamental purpose of the tanning lamp is to develop a suntan by means other than exposure from the sun. This is accomplished in a tanning bed, tanning booth, tanning canopy or free standing tanning unit. The quality of the tan (or how similar it is to a tan from the natural sun) depends upon the spectrum of the light that is generated from the lamps. Most tanning lamps produce much more UV than the sun on a typical day. This gives the sunbed user a faster base tan, but one that fades faster and offers less protection from the sun than a natural tan.

High pressure lamps are 3 to 5 inches long and typically powered by a ballast with 250 to 2000 watts. The most common is the 400 watt variety that is used as an added face tanner in the traditional tanning sunbed. High pressure lamps use quartz glass, and as such do not filter UVC. Because UVC can be particularly harmful, a special filter glass (usually purple) is required that will filter out the UVC and UVB. The purpose with high pressure tanning lamps is to produce an ultra high amount of UVA only. Using a tanning sunbed or other device with high pressure lamps but no filter glass is extremely dangerous and should never be done. UVC is used in

germicidal lamps and for water purification [254] but damages human skin. The contents of a high pressure lamp are inert gas (such as argon) and mercury [77]. There are no phosphors used, and the mercury is clearly visible if it is not in a gaseous state.

Low pressure lamps more closely resemble the common fluorescent lamp used in offices. Like all fluorescent lamps, low pressure tanning lamps work when the ballast directs enough energy to the lamp that a plasma is generated inside the lamp. The lamps are coated on the inside with special phosphors and contain a small amount of mercury (20mg typical).

Unlike high pressure lamps, the glass that is used in low pressure lamps filters out the UVC. Once the plasma is fully flowing in the lamp (less than one second), it strips away the outer electrons from the mercury, which emits short wavelength photons that are absorbed in the phosphor coating causing emission of longer wavelengths suitable for tanning. Typical lifespans for low pressure lamps are from 300 to 1600 hours of actual use although they may actually light (and produce very little UV) for as much as 5000 hours.

Three types of artificial tanning units were included in this research, which are referred to as 'vertical', 'horizontal' and 'high pressure' sunbeds. Many establishments use the horizontal 'lie down sunbeds' which consist of an upper canopy and lower base bench arrayed with a total of 40 to 50 lamps of power range $80 - 250$ watts an example of this type seen in Figure 2.1. The upper canopy might have a built in 'facial' tanner with high pressure xenon lamps and the lower bench could have integrated shoulder lamps either eight low power (25 watts) or two high pressure lamps. It should be noted that there also may be booster 'spaghetti' lamps ($15 - 25$W) arranged in between the larger upper canopy lamps. Hence forth this type of sunbed will be referred to as Type H.

The vertical sunbeds (Type V) are usually known as 'stand up beds' or 'sunshowers' whereby a person stands inside a cabin and is irradiated from $48 - 60$ lamps in either a circumference or split up into equal banks e.g. (4 banks x 13 lamps) seen


Figure 2.2: Vertical Unit: megaSun® T230W Tower by KBL Lamps 230W (×52).

in Figure 2.2. The lamps are guarded either by a metal cage or UV grade Perspex Acrylic sheeting.

The 'high pressure' or Type HP sunbeds are either a Type H combination, where the canopy consists of the high pressure metal halide lamps from 300 – 1000W and the lower unit has the regular low pressure lamps, or a type V combination with high pressure lamps. The goal of high pressure lamps is to provide high UVA output. Vertical tanning units can also contain just high pressure lamps.

## 2.2 Materials and Methods

### 2.2.1 Sunbed Spectra

The measurements of vertical sunbeds were taken without the cabin being occupied. In order to mimic an occupied cabin for a type V sunbed folding plastic crates were stacked upon each other as in Figure 2.3. This had the effect of placing a barrier behind the collecting optics to absorb UV radiation in a similar manner to a client

Figure 2.3: Vertical Unit Sunvision® Alisun 180XXL Lamps(×48): Cosmedico Cosmolux 180W.

standing within the cabin. The diffuser and optical fibre were placed in a custom holder and mounted on top of a camera tripod at a height of 160 cm. The holder was clamped in place and the face was directed parallel to a bank of lamps positioned 22 cm away using a spacer. This distance approximated to the position of someone standing in the cabin. The door was closed and the optical fibre transmitted the UV radiation to the spectrometer, which was placed outside the cabin to avoid heating.

For horizontal sunbeds, measurements were taken of the canopy and lower lamps separately. To measure the UV from the lower lamps, a bespoke designed holder was used to hold the front end of the collecting optics in close proximity to the lamps. The design of the holder prevented light entering from the upper canopy, which would normally be blocked by the client's body. The mean of three readings was calculated from a central 15 cm zone. The holder was then flipped over to measure the UV from the canopy (mean of three readings). Used this way, the collecting optics were raised 20 cm above the perspex acrylic surface at a similar position to that occupied by someone lying on the sunbed. A black cloth was used to cover the lower lamps in order to block both light from the lower lamps and also reflections

that would not be present in an occupied sunbed. The outputs from the canopy and lower lamps were usually similar. However, the higher of the two readings was used, as clients do not generally turn over during treatment and so one side will receive the higher dose. Figure 2.4 shows that there are three different types of sunbed spectra measured on-site. The most common type of sunbed spectrum with characteristic mercury spikes occuring at 313mnm and 365nm, is depicted in red.

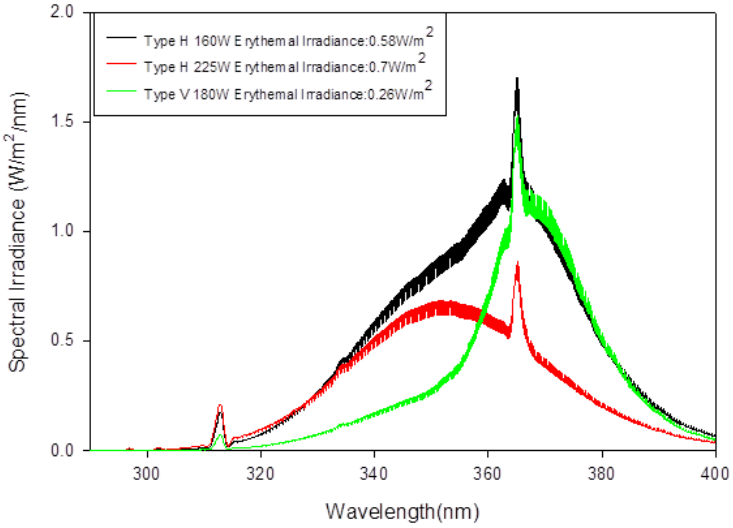


Figure 2.4: Three typical spectral emission for artificial tanning units.

The next sections describe the calibration techniques used to ensure accurate measurements for the sunbed emission spectra.

### 2.2.2 Calibration

All calibration was carried out in the photophysics laboratory of the Photobiology Unit (PBU), Ninewells Hospital, University of Dundee, Dundee.

#### Spectrometry

Spectroradiometry covers the measurement of spectral radiance and spectral irradiance. Spectral irradiance, for example, is the spectral distribution of the radiation incident on a surface, per unit area of that surface. A spectradiometer normally

consists of input optics, a device for splitting the radiation beam into its constituent wavelengths and a suitable detector system.

For in field sunbed measurements a portable spectroradiometer was used. A schematic of the array-based spectroradiometer Maya 2000Pro Ocean Optics Spectrometer (Ocean Optics, Dunedin, FL, U.S.A.) is shown in Figure 2.5.

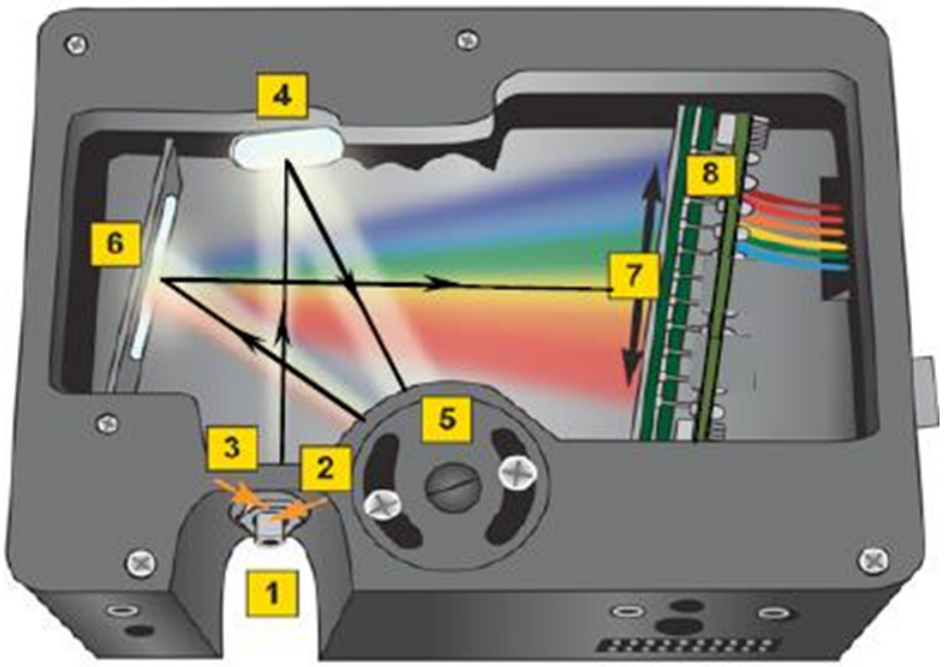


Figure 2.5: Maya Pro 2000 spectradiometer (Oceanoptics.com) [4].

1. SMA Connector - Secures the input fibre to the spectroradiometer. Light from the input fibre enters the optical spectroradiometer through this connector.

2. Slit - A dark piece of material containing a rectangular aperture, which is mounted directly behind the SMA Connector. The size of the aperture regulates the amount of light that enters the spectroradiometer and controls spectral resolution.

3. Filter - Restricts optical radiation to pre-determined wavelength regions. Light passes through the filter before entering the optical bench. Both bandpass and

longpass filters are available to restrict radiation to certain wavelength regions.

4. Collimating mirror - Focuses light entering the optical bench towards the Grating of the spectrometer.

5. Grating - Diffracts light from the collimating mirror and directs the diffracted light onto the focusing mirror.

6. Focusing Mirror - Receives light reflected from the grating and focuses the light onto the CCD (charge-coupled device).

7. Detector with OFLV Filter - Variable Longpass Order-sorting Filters are applied to the detector's window to eliminate second and third order effects.

8. Back-thinned Area Detector - 75% quantum efficiency and bins pixels in a vertical column to acquire from the entire height of the spectroradiometer's slit image. This improves light collection and signal-to-noise significantly. This 2-D area detector is back-thinned (back-illuminated).

The array spectroradiometer's main advantages over a double grating scanning spectroradiometer are:

1. Portability

2. Lightweight

3. Fast acquisition times

However, the instrument does have some disadvantages:

1. Stray Light

2. Dark noise

3. Dynamic Range

On site measurements of sunbeds were made using a Maya 2000Pro Spectrometer with the diffraction grating tuned to $230 - 440$nm for optimum UV measurement.

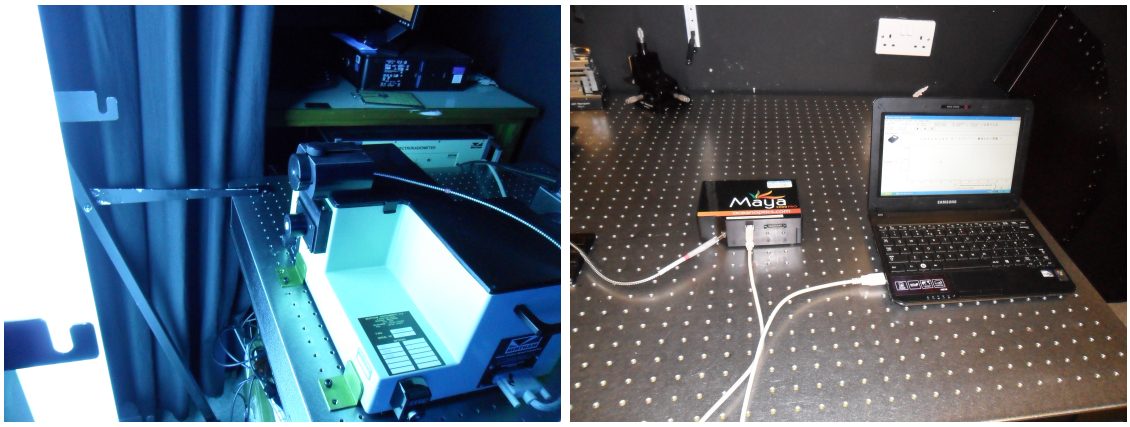


(a) Bentham calibration with 6 bank of Philips 100W UVA lamps 30cm from Bentham.

(b) Maya Pro 2000 connected to laptop with SpectraSuite and optical fibre 600$\mu$m diameter to cosine detector.

Figure 2.6: Calibration of spectroradiometer.

The input optics consisted of an optical fibre and cosine corrector with Spectralon diffusing material (CC-3-UV-S). The spectrometer was calibrated to UVA fluorescent lamps with a similar spectral distribution to that found in cosmetic tanning units.

A double grating scanning spectroradiometer was used for the characterisation and calibration techniques shown in Figure 2.6a. The calibration was performed by taking simultaneous measurements, at a distances of 30cm, from a bank of six Philips Cleo Performance 100W–R lamps with the Maya 2000Pro and a bench based double grating monochromator (Bentham DM150). The calibration of the monochromator is traceable to the NPL.

For consistency, during the calibration the CC-3 cosine diffuser end of the optical fibre probe was mounted in the same holder that was used during sunbed measurements. This was then placed 10cm above the diffuse input sensor of the Bentham monochromator. The Bentham was given at least 2 hours warm up prior to calibration while the UV lamps were given 5 minutes to warm up.

The output from the Bentham is multiplied by the Bentham calibration file, which is derived from calibrated lamps and traceable to NPL. This gives the spectral irradiance of the source. Spectral Irradiance =

measured Bentham signal(nA) x Bentham calibration file ($mWm^{-2}.nm^{-1}.nA^{-1}$).

The spectral irradiance ($mWm^{-2}.nm^{-1}$) data from the Bentham is then divided by the output from the Maya to give a calibration file. This calibration file is then multiplied by the Maya output anytime a measurement of a sunbed was performed. A calibration factor at each wavelength increment was derived for the spectrometer thus:

$$CF_\lambda = EB_\lambda / ES_\lambda \tag{2.1}$$

where $CF_\lambda$ is the correction factor at wavelength $\lambda$,

$EB_\lambda$ is the irradiance as measured by the Bentham at wavelength $\lambda$, and

$ES_\lambda$ is the output from the spectrometer at wavelength $\lambda$.

### 2.2.3 Dark Light Correction

With all spectrometers some signal is recorded even when the instrument is in darkness, due to thermal dark current generation. A dark current occurs in a CCD device such as the spectrometer whether the sensor is being exposed to light or not. Therefore a dark light correction had to be applied to the reading. A dark current was recorded when the spectroradiometer was in true darkness with the lights switched off. The CC-3 cosine diffuser end of the optical fibre probe was covered with black cloth during the dark reading as a secondary precaution. Figure 2.7 shows a dark reading for integration time 500ms and acquired for 3 averages.

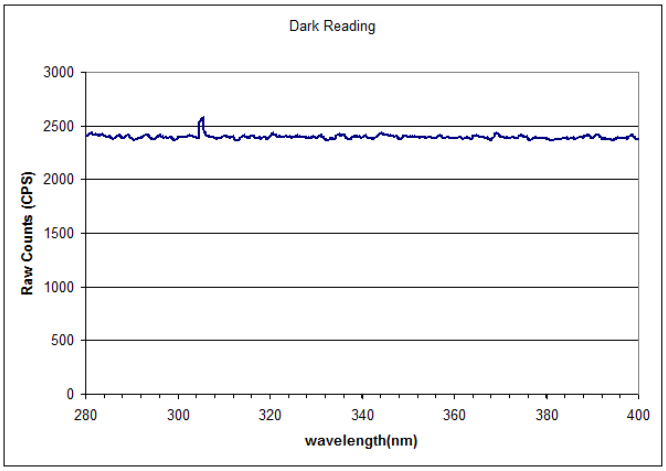


Figure 2.7: Dark reading in counts per second (CPS).

Here the wavelengths from 279.93 – 400.06 nm with raw counts were averaged depending on the number of measurements taken. A typical dark reading in Figure 2.7 shows a defective pixel occurring at 305nm. A pixel is defective when the the responsiveness differs compared to the mean values of all neighbouring pixels. Here the defective pixel differs by $\pm$ 4%.

Please note, that all the light measurements were dark light corrected with the same acquisition times.

### 2.2.4 Stray Light Correction

Stray light is one of the most problematic issues when measuring optical radiation. Stray light is defined as light detected by the measurement system when or where it should not exist [249]. The stray light recordings for $S_o$ and $S_{filter}$ have been dark light corrected with the same integration times.

There are two basic types of stray light :

1. External stray light - due to scattering from outside e.g. scattering around the edges of a filter or reflections off walls;

2. Internal stray light - due to scattering and reflections within the spectrometer.

External stray light is a potential problem in all optical radiation measurements regardless of the measuring equipment. External stray light was reduced in this study with the use of black cloth to cover reflective surfaces and areas of the sunbed not being measured. It should be noted during calibration that the photophysics lab is painted black to further reduce the effects of stray light. Internal stray light is an inherent problem in many array systems because of their small size. It is much more difficult to remove internal stray light in a physically small system where there is a restriction on the use of baffles .

If the stray light can not be physically removed then the artefact needs to be removed through calculation. The most common approach to compensate for in-system stray light is to use a series of cut-off filters. A cut-off filter transmits radiation only above a certain wavelength. The important feature of these filters is that for a certain wavelength range the transmission is near zero. The levels of stray light in the Maya were assessed as follows:

(a) A broadband source similar to that likely to be encountered in sunbeds, was measured with no filter ($S_0$) for the entire wavelength range of interest (280 – 400nm).

(b) The measurement was then repeated with the cut-off filter placed against the input optics ($S_{filter}$).

(c) The ratio between the two measurements was determined and multiplied by 100 to get the percentage (%) of stray light seen in Equation 2.2.

$$\%Straylight = \left(\frac{S_{filter}}{S_o} \times 100\right) \tag{2.2}$$

where $S_{filter}$ is the signal with filter
$S_o$ is the signal transmission without filter.

(d) For a cut-off filter, stray light % should be zero for wavelengths below the the cut-off mark. Any non zero signal in these regions is likely to indicate the presence of in-system stray-light.

(e) The measurements were repeated for a sufficient number of filters to enable an assessment of stray light performance across the whole region of interest to be made-performance at one particular wavelength cannot be taken as representative of the whole thing.

(f) Once the stray light percentage is calculated for the wavelength range, the average % is applied to the measurements. It is important to note that the quantity of stray light will depend upon the light source being measured.

As a result of the known stray light artefact, a correction was introduced across all measurements using the filter method as described above.

A broadband xenon arc source and filters with cut off wavelengths 305nm, 345nm, 375nm and 420nm were used to asses stray light. A dark reading was subtracted from both filtered and non filtered reading. The ratio of signal with filter to signal without filter (i.e. transmission) was plotted against wavelength. A visual representation of the internal stray light can be seen in Figure 2.8. There is also noise present in the signal as the light levels are close to the limitations of the device.

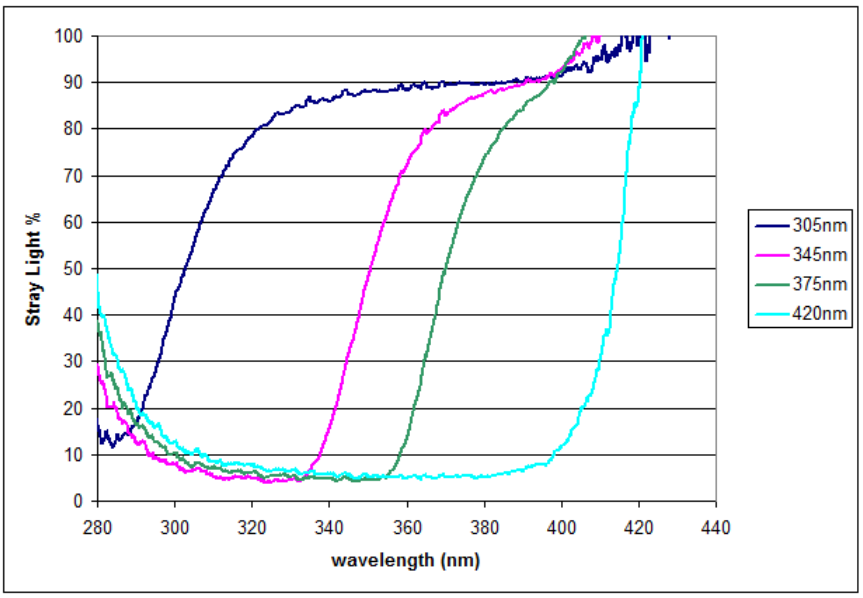


Figure 2.8: Percentage of straylight for series of cut-off filters with ≈ 5% stray light for 310 nm – 390 nm.

### 2.2.5 Cosine Response

UV radiation that reaches the surface of the skin comes from different angles from the the lamp source. Diffuser heads with angular response proportional to the cosine of the zenith angle are needed for the sunbed irradiance measurements.

The CC-3 cosine-corrected irradiance probes are optics designed to collect radiation from a wide field of view, thus eliminating light collection interface problems inherent in other sampling devices. The probe used for the measurements was the CC-3-UV-S with Spectralon$^{TM}$ diffuser screwed onto the end of an optical fibre, making an irradiance probe. The probe couples to a spectrometer to measure the intensity of light normal to the probe surface. When coupled to a spectrometer, these irradiance probes can be used to measure UVA and UVB radiation from artificial tanning units.

The radiant power incident on a flat surface is proportional to the cosine of the angle between the direction of the incident radiation and the surface normal. As the skin is an approximation for a flat surface, the dose will depend on the angle of the radiation. [257]. Thus, a spectroradiometer used for measurement irradiance ($Wm^{-2}$) or counts per sec should have an angular response that matches the cosine

as closely as possible.

$$E = \frac{I_e cos\theta}{r^2} \tag{2.3}$$

where E= irradiance

$I_e$ = radiant intensity

$\theta$ = angle of illumination to normal of irradiated area

$r$ = distance of point source from irradiated area.

Measurements were performed using a xenon arc lamp to calculate the angular response of the MayaPro 2000. The detector was positioned at a distance of 60 cm on the sling arm jig seen in Figure 2.9. Measurements were performed at 0° with incremental angles of 10° reaching both clockwise and anticlockwise as far as ± 60°. Due to the bulk of the xenon arc lamp the light source could not be positioned at further angles.

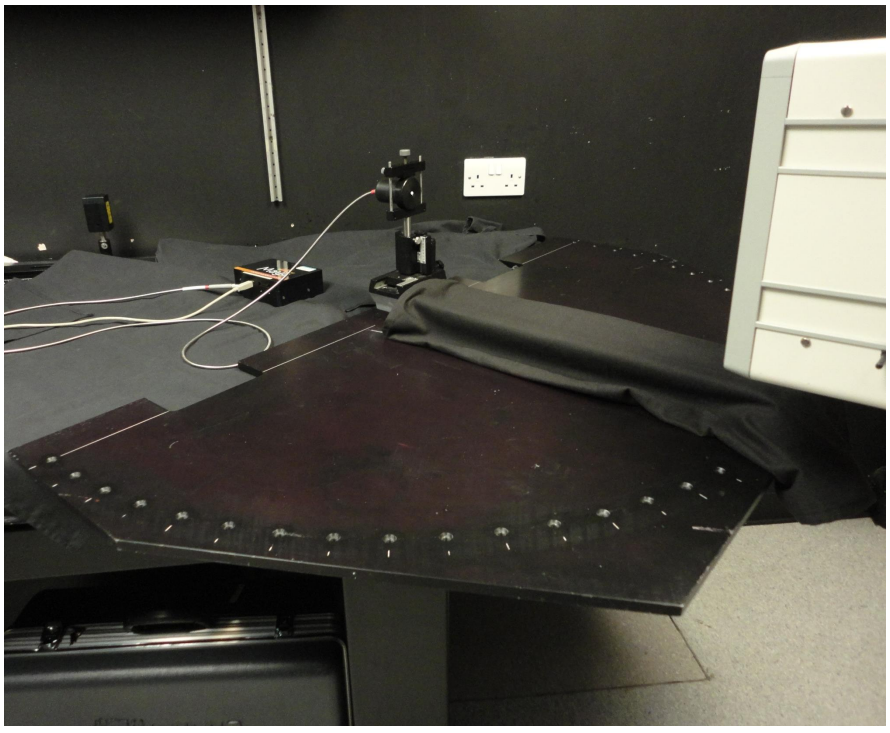

Figure 2.9: Spectroradiometer, xenon-arc lamp and jig used to measure angular responses.

### 2.2.6 Diffuser Quality

The quality of the diffuser is defined by the diffuse cosine error $f_2$ which is defined as:

$$f_2(\theta) = \left( \frac{S(\theta)}{S(0^\circ)\cos(\theta)} - 1 \right) \times 100\% \tag{2.4}$$

where $S(\theta)$ is the measured signal at the zenith angle $\theta$. This formula assumes the angular response to be independent of the azimuth angle. The integrated cosine error, as defined in CIE technical report [65], can be calculated as

$$f_2 = \int_{0^\circ}^{60^\circ} |f_2(\theta)| \sin(2\theta)\, d\theta \tag{2.5}$$

The weighting term $\sin(2\theta) = 2\cos(\theta)\sin(\theta)$ ensures that the contribution of the integrand goes to zero at large zenith angles, where the effective area of the diffuser approaches zero, as well as at small zenith angles, where the cone of angles of the spherical coordinate system approaches zero. Parameter $f_2$ gives the fractional error caused by the non-ideal angular response of the diffuser head under the assumption that the radiance is constant [65].

#### Measurements for Cosine response

The angular response of the UV probe was determined by rotating the broadband light source at 10° intervals from $-60^\circ$ to 60° with respect to the stationary detector source centred on the jig. The measured angular responses and the ideal cosine response function are displayed in Figure 2.10.

The first step was to normalize the signal at $\theta = 0^\circ$. The counts per second were multiplied by integration steps and then summed. By integrating equation 2.4 between $-60^\circ$ to 60° the error can be represented by the value $f_2$ Equation 2.5. The f2 value was measured as $f_2 = 6.69\%$ , which is below the 10% maximum recommended for commercial UV radiometers [228].

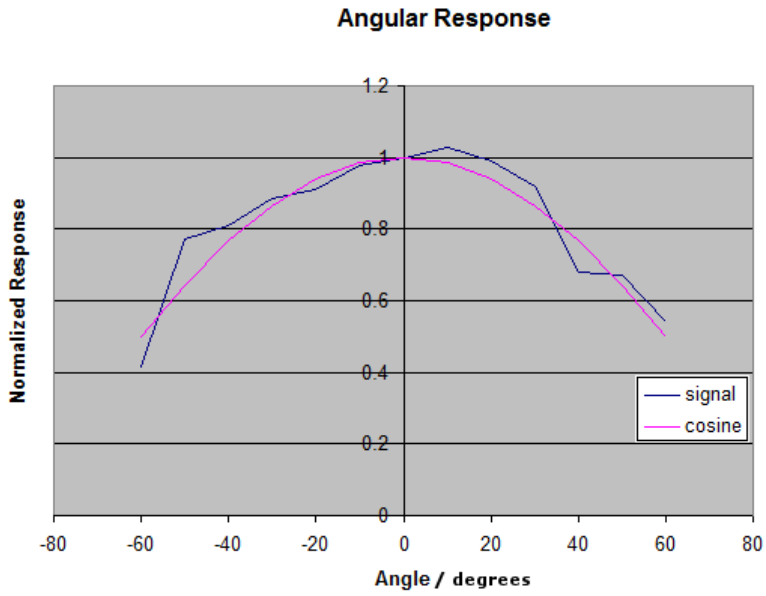


Figure 2.10: Measured angular responses and the ideal cosine response function.

### 2.2.7 Dynamic Range

The term 'dynamic range' can be used to describe the range of signal levels over which the system will operate reliably. It is usually limited at the lower end by noise and dark current, and at the upper end by system non-linearity and saturation effects. Thus in order to specify the dynamic range of a system it is necessary to investigate its dark current characteristics and its linearity. Manufacturers usually state the dynamic range of their systems in terms of number of bits for example a '16 bit dynamic range'. This relates to the performance of the analog-to-digital (A/D) converter alone. The Maya2000Pro contains a Hamamatsu S10420 CCD which is a two dimensional CCD. The sensor has 2048 x 64 active pixels and acquisition times from 6ms to 5 seconds. Since the dynamic range signal of the 16 bit CCD did not measure details at the lower and upper ranges in one acquisition, a method to increase dynamic range was required.

One method of increasing dynamic range is to use multiple integration times A long integration time is likely to give a saturation at the upper region of the spectral output but more information at the lower sector seen in Figure 2.11. A short integration time reveals the upper sector of the spectral output but there was a loss of detail at the lower sector.

The dynamic range can be increased by merging the two spectra together in a technique called 'splicing' [100]. The spectrum is acquired twice, each time with a different integration time. The UVA peak is measured with a short integration time, while a large integration time allows for an accurate measurement of the lower signals, ignoring the saturated response of the UVA peak. Dark readings obtained at corresponding short and long integration times were subtracted from the spectral measurements. The sensitivity of the spectrometer depends on the count rate, so a 2048 arrays element recording a high number of counts for a long integration time must be corrected relative to elements providing a low number of raw counts for short integration time. The spectrum correction is implemented by measuring the spectrum of a reference source with known relative spectral irradiance. The known normalized counts-per-second (CPS) spectrum is divided or multiplied by the normalised measured reference spectrum to obtain the relative spectral response correction.

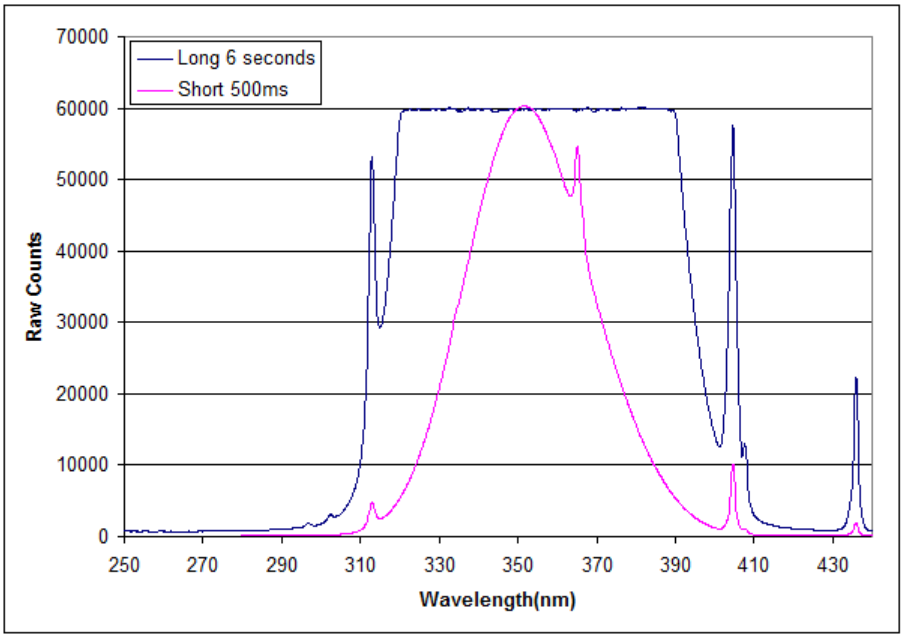


Figure 2.11: Graph showing long integration time (t = 6secs) reaching saturation and short integration time (t = 500ms) revealing upper peak.

Afterwards, both measured spectrum data are combined to generate a spectrum with a larger dynamic range. This is achieved by getting each spectrum in CPS by multiplying the short integration time 500ms × 2 and dividing 6 sec counts by 6.

The merging occurs at wavelength section of greatest overlap and least deviation in raw counts. For example if the longer integration time has a count of 6937.55 at 317.75nm and the least gap in raw counts is at the next wavelength of the short integration time then the counts will take over with 7054.4 counts at 317.86. The raw counts are taken above the longer integration time as there is less noise so there is a greater signal-to-noise ratio (SNR). Typically the merging took place from bottom to peak at wavelengths from 316.12nm to 319.27nm and then from peak to bottom at wavelengths 390.95 to 398.53. A spectrometer with a CCD array

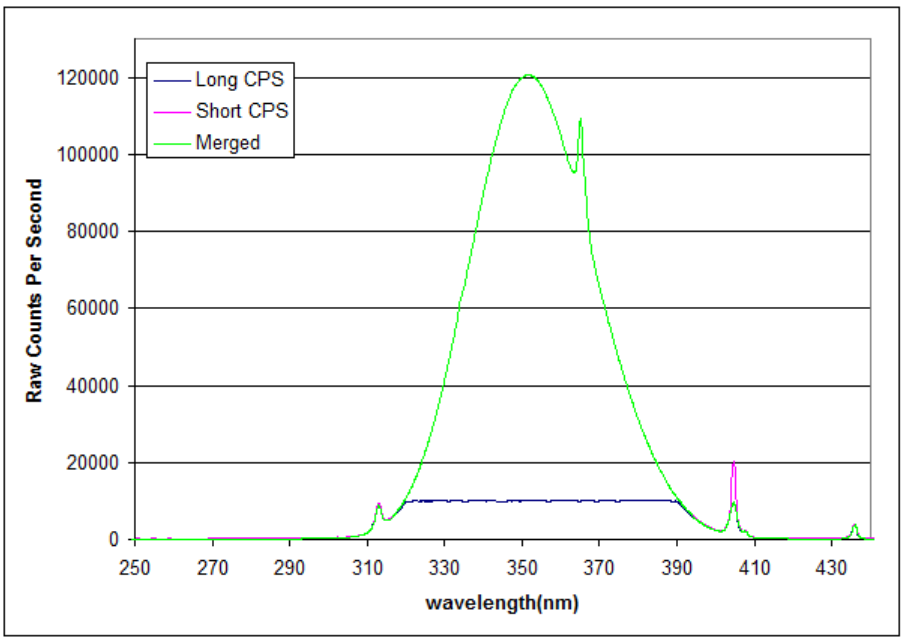


Figure 2.12: Merged Spectra.

detector acquires a spectrum over an extended wavelength range by accumulating two spectra at different integration times. Comparison of the measured wavelengths and the known wavelengths suggests that artefacts exposed by splicing do not play a critical role in the wavelength calibration. Figure 2.12 displays the long, short and merged spectral sunbed shaped normalised. The merged spectra has a greater dynamic range.

### 2.2.8 Linearity

A system is linear if the output varies in direct proportion to the input, for example, if the responsiveness of the system is constant as the input is varied. If there is no straight line relationship between the measured signal and the input quantity relationship a system is non-linear. Non-linearities may arise due to the characteristics of individual pixels in the array or because of imperfections in the amplifiers or other electronics. In most cases the system will be linear within a certain range of operating conditions, but will become non-linear if these conditions are exceeded.

Manufacturers frequently state that their systems are "linear" without further qualification of this statement and usually any linearity checks that are performed relate only to one element, such as the electronics, rather than the complete system. For example, a known electrical signal may be applied to the detector electronics and a record made of the number of counts generated. The deviation from a straight fit of this data is then quoted as the linearity of the system; in fact, it is the linearity of the detector electronics alone and the system itself may show very different linearity characteristics.

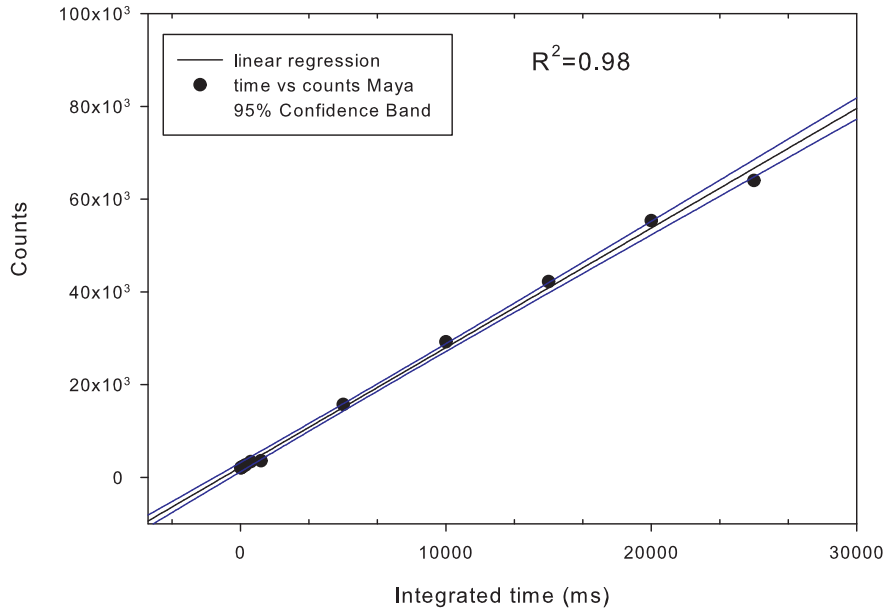


Figure 2.13: Linear regression fit and 95% confidence levels bands (dark blue).

Therefore, it was necessary to assess the linearity of the spectrometer as a whole

system. With most spectrometers the signal is integrated over a period of time and the "raw" (unprocessed) data is presented as the actual measured signal levels. The linearity test involved recording the raw counts for a range of integration without reaching saturation (a fall-off in response) at the high integration times. The integration times ranged from 15.625 ms seconds to 25,000 ms and the counts were recorded at wavelength $\lambda = 330.5$nm using the same incident power and distance from the source.

The results show the system is linear with linear regression $R^2 = 0.98$ goodness of fit for integration times up to 25,000 ms and further examination of the data reveals that the saturation plateau beyond this point is due to saturation at about 65,000 counts for the spectrometer. Note also that the noise on the signal $\leqq$ 500ms integration time appears as "noise" on the measured non-linearity. The regression fit in Figure 2.13 ignores the saturation point at the longer integration time of 30,000 ms which is never encountered during during sunbed acquisition times. Here the spectroradiometer has been evaluated for short, medium and long integration times at the same distance from the source. Care needs to be taken that the out signal is not significantly affected by noise at low integration times. Any change in the measured linearity with integration time is likely to indicate saturation of the detector array, and can be used to set an upper limit to time-integrated signal which can be measured reliably.

### 2.2.9 Biologically Effective Weighting Spectra

An action spectrum is a weighted wavelength range that describes the relative effectiveness of photon energy in producing a particular biological response. "Biological response" may refer to effects at a molecular level, such as DNA damage, or inflammatory response like erythema. An action spectrum is used as a weighting factor for the UV spectrum to find the actual biologically effective irradiance for a given effect. This relation is described in the Equation 2.6 below for erythemal weighted irradiance, EWI ($\lambda$):

$$EWI(\lambda) = \int_{280\text{nm}}^{400\text{nm}} \mathrm{E}(\lambda)\,\mathrm{A}(\lambda)\,\mathrm{d}\lambda \tag{2.6}$$

where

E($\lambda$) (J.m$^{-2}$)) is the spectral irradiance

A($\lambda$) is the biological action spectrum for erythemal damage (described below)

d($\lambda$) is the integration step.

A photo induced biological response begins with the absorption of a photon by a chromophore. These chromophores can initiate a photochemical reaction for example DNA demonstrates a peak absorption at 260nm with a significant tail into the UVB, and proteins such as tryptophan and tyrsosine have a peak absorption around 280nm with a tail into the UVB. A wavelength dependent spectrum to quantify the biological effectiveness by weighting the UVB and UVA component is called the action spectrum.

However, not every photon absorbed necessarily produces a photochemical reaction. The number of defined events occurring per photon absorbed by the system is called the quantum yield $\Phi(\lambda)$:

$$\Phi(\lambda) = \frac{\text{number of events}}{\text{number of absorbed photons}} \tag{2.7}$$

It is not possible to carry out measurements of UV absorption by chromophores in vivo. What is usually studied in photobiology is the relationship between surface

exposure and the biological response under investigation. A wavelength dependence can be deduced by measuring the exposure, E($\lambda$), required at different wavelengths to evoke the same level of response. Artificial UV tanning units have the potential to cause premature ageing, erythema and carcinoma in human skin. Several studies indicate that there is a wavelength dependency with more emphasis on wavelengths $\leq$ 320nm.

Studies of the wavelength dependence of tumour induction in mouse skin and of erythema induction in human skin indicate the efficiency of damage induction by UV photons in the wavelength range 280 – 400nm [62, 185].

**Erythemal Weighting**

The biological weighting function used to approximate the wavelength-dependent sensitivity of Caucasian skin to erythema inducing radiation is the model proposed by McKinlay and Diffey [185], and adopted as a standard by the Commission Internationale de l'Éclairage (CIE) [3]. This model is given by the equations (wavelengths $\lambda$ in nm):

$$A(\lambda) = \begin{cases} 1, & \text{if } \lambda < 298. \\ 10^{-0.094(\lambda - 298)}, & \text{if } 298 \leq \lambda < 328. \\ 10^{-0.015(\lambda - 139)}, & \text{if } 328 \leq \lambda. \end{cases} \tag{2.8}$$

The normalisation of the McKinlay and Diffey action spectrum for erythema is chosen to be such that the function is equal to unity at 298 nm. Because the normalisation of A ($\lambda$) is arbitrary, the units of exposure should also be considered to be arbitrary.

The biological effectiveness of the UV radiation is represented by the plot in Figure 2.14, the skin is 1000 times more sensitive to radiation at 285 nm than to that at 320 nm. The effect of applying an erythemal weighting factor [62, 185] is demonstrated in Figure 2.15. Although the emission from the sunbed is mainly in the UVA region, when it is weighted by the erythemal action spectrum, the significance

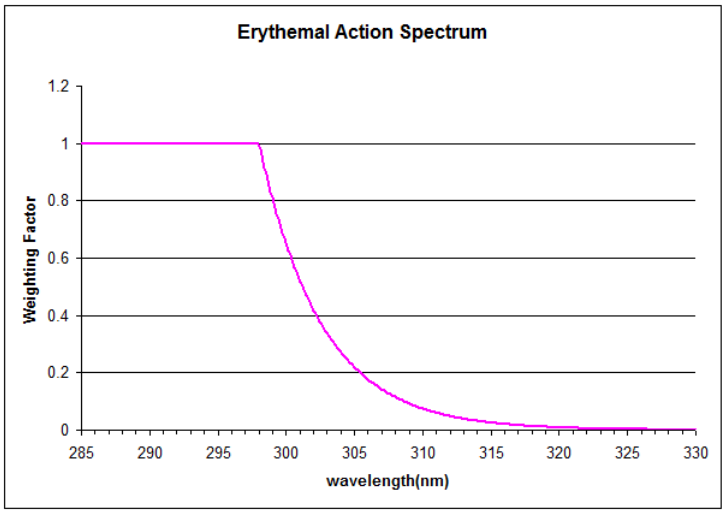


Figure 2.14: Erythema action spectrum.

of the short wavelength UVB becomes apparent. It is the convolution of this action spectrum and the spectral irradiance that gives the erythemal weight irradiance for a sunbed. The summation value is then the sunbed output level in $\mathrm{Wm}^{-2}$ and this number should not exceed 0.3 $\mathrm{Wm}^{-2}$ plotted in Figure 2.15.

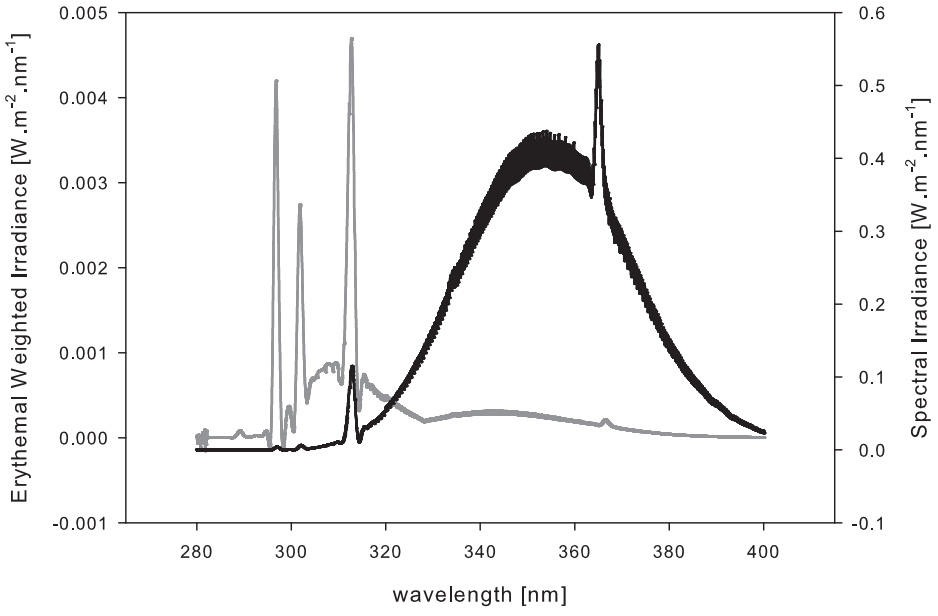


Figure 2.15: Data from an UWE® Starflight sunbed Lamps: Newtechnology 100W (17 top; 17 bottom) showing the spectral irradiance (black) and the erythema-weighted spectrum (grey). The total UV erythema-weighted irradiance is 0.36 $\mathrm{Wm}^{-2}$.

### Skin Cancer Utrecht Philadelphia Human (SCUP-h) Weighting

Another method of estimating the wavelength dependence of carcinogenesis by UV radiation is the application of the Skin Cancer Utrecht Philadelphia action spectrum. The original collaboration was on the SCUP-m (murine) action spectrum based on the induction of tumours by UV exposure on albino SKH:HR1 mice. The SCUP-h (human) action spectrum was developed by transforming the SCUP-m to include the transmittance spectrum of human epidermis [62]. The SCUP-h shifts relative effectiveness emphasis to 299nm. While the relative effectiveness occurring at mercury emission line 313nm is reduced by a magnitude of ten.

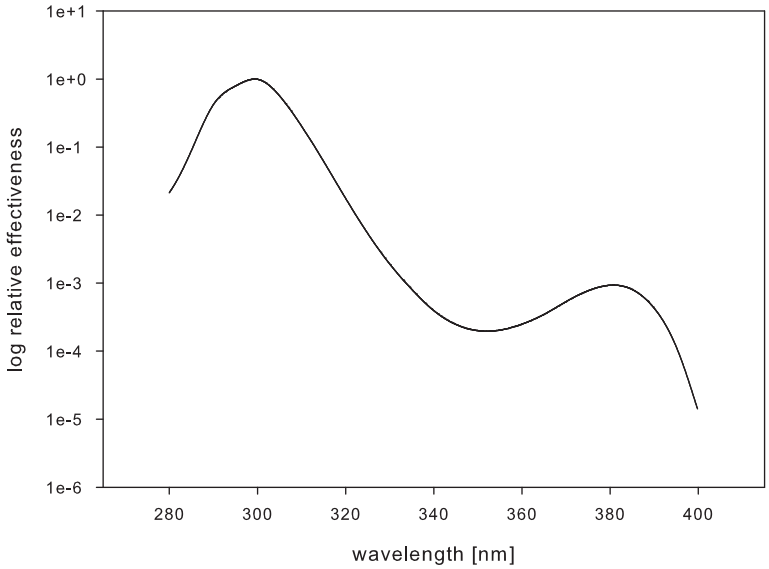


Figure 2.16: Logarithmic scale of SCUP-h action Spectrum with spline curve fit.

As there is no formula for the SCUP-h action spectrum a spline curve was fitted to match the integration steps of the Maya spectrometer which increments in steps of 0.10 or 0.11nm. The spline curve fit is a polynomial interpolation avoiding Runge's phenomenon. In mathematics, a spline is a numeric function that is piecewise-defined by polynomial functions, and which possesses a sufficiently high degree of smoothness at the places where the polynomial pieces connect. The log relative effectiveness is displayed Figure 2.16, and a typical sunbed spectrum weighted by the SCUP-h action spectrum is shown in Figure 2.17.

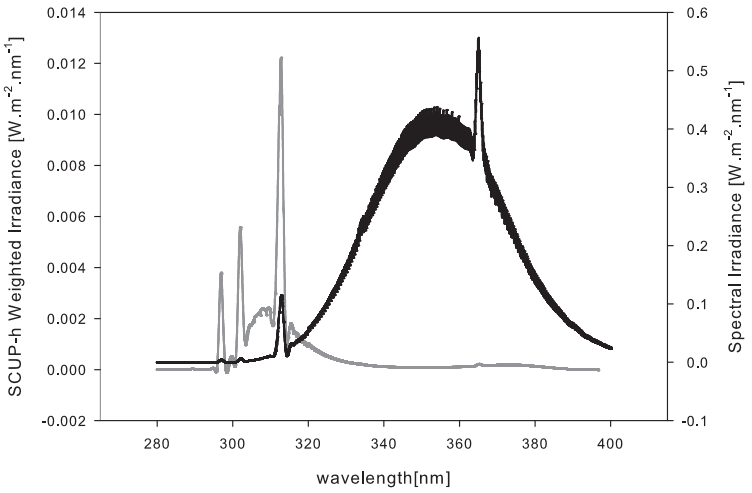


Figure 2.17: Type H: UltraSun® Sunrise 3500 Lamp: 120W Sunfit Pro+ Top(×17) Bottom(×16) Weighted SCUP-h: 0.63 $\mathrm{Wm}^{-2}$.

According to measurements by Freeman *et al.* [96] the action spectrum for the induction of CPDs in human skin resembles the SCUP-h action spectrum, especially in the UVB region as seen in Figure 2.18. A similar plot up to 310nm can be produced for mouse skin with data on CPD from Johnson [138] and Ley *et al.* [168]. This indicates that pyrimidine dimers are a dominant cause of the UV-induced squamous cell carcinomas.

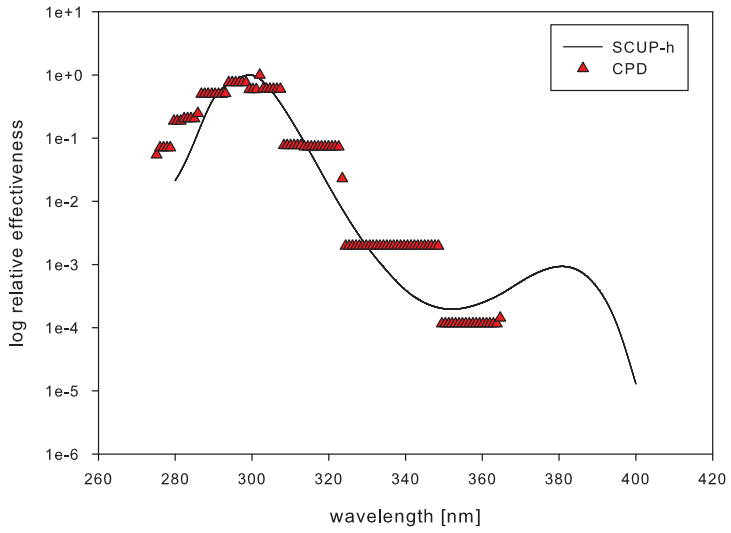


Figure 2.18: Comparison of the estimated action spectrum for squamous cell carcinoma in humans, SCUP-h (curve) [59] and the measured action spectrum for induction of CPDs in human skin (red triangles) [96].

Although the erythemal action spectrum can also vary, it bears a close resemblance to the SCUP-h action spectrum [29,58]. Young *et al.* reported that there was a similarity for the thymine dimer action spectra in human epidermis and erythema suggesting that DNA is the chromophore for erythema [302]. While there is still an uncertainty in the UVA range from 340 to 400nm the dip is closely related to findings by Tyrell *et al.* [159]. The spectrum of yield for induction of oxidative DNA base 8-oxo-dG in human skin fibroblasts damage closely resembles the SCUP-h action spectrum.

**ROS action spectra**

UV radiation activates a series of cascading biological reactions in human skin. Continuous exposure to UV radiation stimulates inflammatory processes that contribute to the accumulation of free radicals. The reactions of over-exposure of the skin to sunlight are well documented. While UVB is the dominant wavelength to induce erythema, UVA has been associated with the generation of free radicals especially by reactive oxygen species (ROS) [303]. The production of ROS is one of the key components of photodamage. Increased ROS load has been implicated in photoaging [223] and photocarcinogenesis [245]. Biological effects induced by UVA are mainly related to the generation of reactive oxygen species (ROS) [268].

At longer UVA wavelengths, indirect effects mediated by active oxygen species become more important and induce various damages including DNA breaks and oxidative modifications of nucleic acid bases. However, DNA absorbs in the UVA and UVB region of the spectrum. While absorption of UVB is mainly attributed to the formation of CPDs, it has been shown that CPDs have the potential to be induced also by UVA [79, 203]. Considering that UVA acts mainly through the generation of ROS it made sense to apply the ROS action spectrum to the UVA dominant lamp spectra.

ROS are chemically reactive molecules containing oxygen. Examples include oxygen ions and peroxides. ROS are formed as a natural byproduct of the normal

metabolism of oxygen and have important roles in cell signalling and homeostasis. However, during times of environmental stress such as exposure to UV, ROS levels can increase dramatically. This may result in significant damage to cell structures. Cumulatively, this is known as oxidative stress. One major contributor to oxidative damage is hydrogen peroxide ($H_2O_2$), which is converted from super oxide.

These free radicals are at the beginning of a cascade of molecular biological events with potentially destructive effects and potential photo-carcinogenesis. The action spectrum shown in Figure 2.19 is derived from [304]. Convolution of the action spectrum with sunlight spectral irradiance showed that 50% of the total skin oxidative burden was generated by the UVA component.

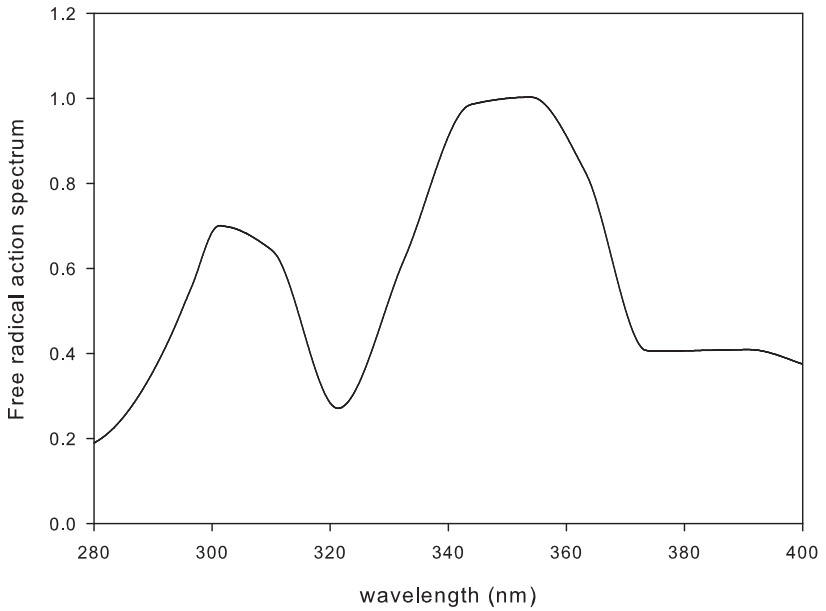


Figure 2.19: Free radical action spectrum in the UV range. The spectrum is normalised to 1 at 355 nm [303].

## 2.3 Results

### 2.3.1 Irradiance of Artificial Tanning Units compared to Natural Sun

The erythemal irradiance of the natural sun at midday was compared to the erythemal irradiance to Type H, V and HP tanning units observed during inspections. The spectral irradiance for the sun was recorded by Laboratory of Atmospheric Physics, University of Aristotle, Thessaloniki, Greece 40°39′N, 22°58′E for 18$^{th}$ July 2009 at 10.36 Universal Time (UT) , which is solar noon when the irradiance is maximum seen below in Figure 2.20. The erythemal and SCUP-h action spectra were applied to the solar spectra the results of which are seen in Figure 2.21. The erythemal irradiance was calculated from the spectral irradiance to be 0.19Wm$^{-2}$ while the SCUP-h weighting resulted in value of 0.43Wm$^{-2}$. These results were used as a comparative test for the sunbed outputs.

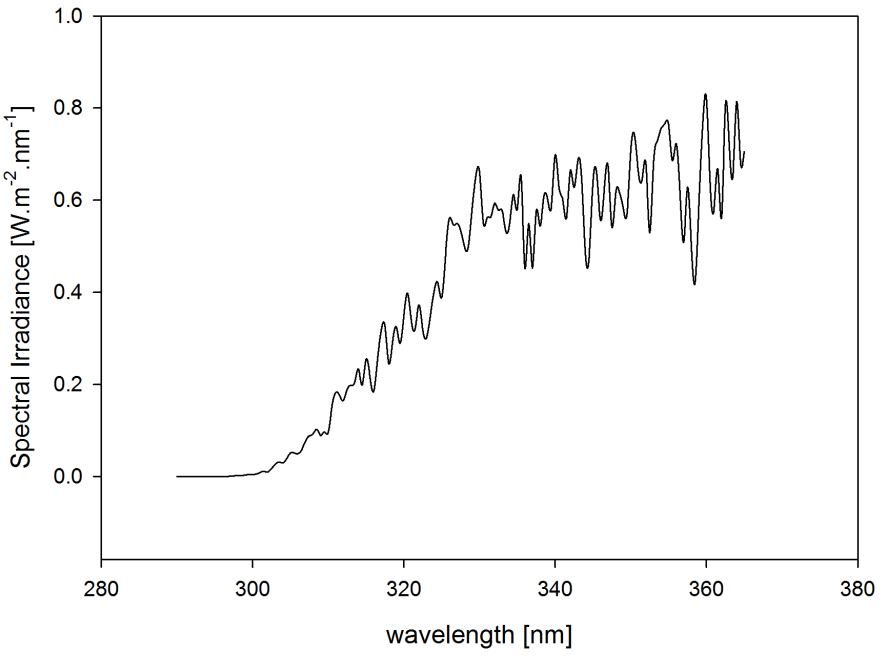


Figure 2.20: Solar spectrum Thessaloniki 40°39′N, 22°58′E Zenith Angle = 24.06° noon time.

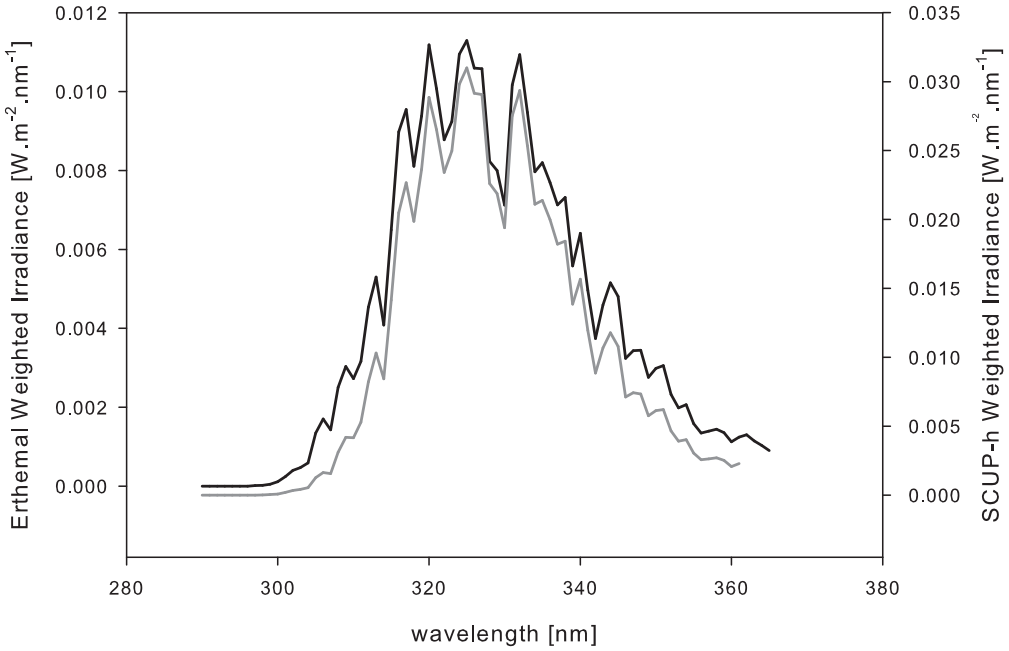


Figure 2.21: Erythemal (black line) and SCUP-h (grey line) weighted irradiance for solar spectrum Thessaloniki 40°39′N, 22°58′E Zenith Angle = 24.06° noon time.

### 2.3.2 Shoulder and Facial Tanning Output

The majority of sunbeds used UVA fluorescent tubes for irradiating the body and shoulders, while filtered metal halide lamps, which have a higher proportion of UVA1, irradiated the face. Only five high pressure quartz units were encountered during the survey. This type of exposure was primarily in the UVA. The essential difference between standard tanning sunbeds and high-pressure sunbeds like the Sunquest X6 in Figure 2.22 is the type of lamps they use. Instead of the fluorescent tubular lamps used in standard sunbed units, high-pressure sunbeds use quartz lamps to vary their UV output. In addition, the X6 high-pressure tanning stand has a series of filters that block out most of the (UVB) rays while allowing UVA rays to penetrate deeper into skin.

High-pressure lamps range from 600 – 2000 watts and are virtually all UVA exposure. Comparatively, power of standard tanning lamps ranges from 100 – 180 watts. Eighty three of the horizontal tanning units had facial lamps incorporated in them. But two of the sunbeds had non functioning facial lamps. A typical facial

and shoulder lamp for type H sunbed are depicted in Figure 2.23.

Figure 2.22: High Pressure Unit: Sunquest UV Intensiv X6® (6 lamps × 4 columns) 500-1000W.

Figure 2.23: Ergoline® Excellence 700 Face Lamps(×4): Ultra VIT 2.4 520W shoulder lamps(×12): Ergoline SD 25W.

The use of filtered high pressure metal halide lamps for irradiating the body or face delivers less of the UVB erythemal irradiance and hence less erythemal burning.

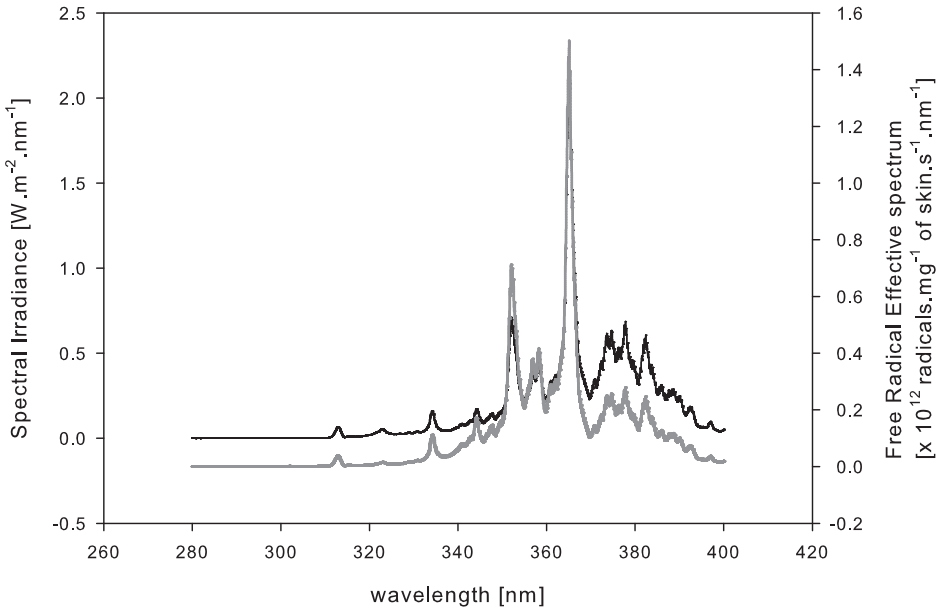


Figure 2.24: Free radical effectiveness spectrum (grey curve) calculated for High Pressure Face Ergoline Ultra VIT 2.3 500W (black curve).

However the UVA exposure may be higher potentially leading to the induction of malignant melanomas. UVA radiation is only slightly less effective than UVB with regards the induction of melanocyte hyperplasia a precursor to melanoma in shaved opossums [167].

UVA irradiation has been shown to induce free radicals, including reactive oxygen species in melanocytes which cause oxidative DNA damage [160] and thus may cause DNA mutations contributing to melanoma genesis.

Figure 2.24 shows a typical spectrum from a HP and facial quartz lamp at 1000W and 500W. Total UVA outputs have a tendency to be higher than for fluorescent lamps. Since the quartz lamps have emissions mainly in the UVA spectrum we applied the ROS action spectrum to investigate the wavelength dependency for free radicals.

### Sunbed Providers

The majority of the inspections occurred at fitness centres, gyms, beauty salons, hairdressers and tanning centres. However the tanning centres were at the core of the survey with 65 establishments visited. This was followed by beauty salons and hairdressers see Figure 2.25. The places offering tanning in the category of 'Other' included swimming pools, post office and company sport facilities where tanning is offered as an auxiliary service.

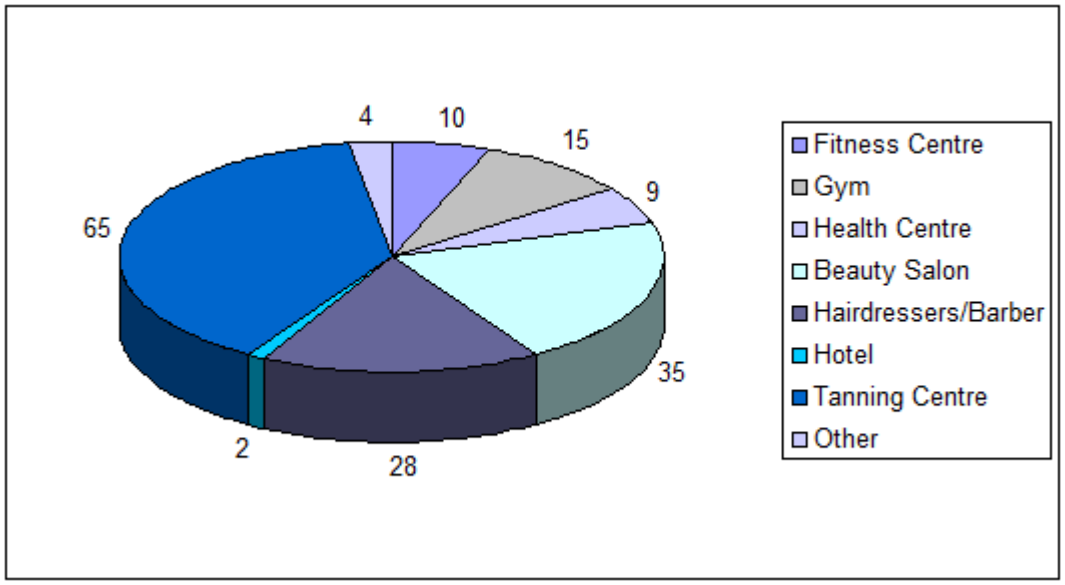


Figure 2.25: Distribution of tanning establishments.

The quantity of tanning units available at the sites ranged between 1 and 8 units with 63% of the tanning units been type V and 36% being type H. The remaining 1% consisted of the HP type. In general the vertical beds were marketed as having the stronger 'fast tan' lamps with the highest power detected at 250W. Although the higher end of power existed at 235W, 200W and 180W there were also lamps found at 100W and 80W. There is no guarantee that replacement lamps are the same as those originally supplied by the manufacturer of the sunbed. Furthermore when a lamp is replaced it will have a much higher output. The UV levels decrease by approximately 20 – 30% after 600 hours of use [285]. All this equates to confusion amongst the consumers who may not know how powerful the tanning unit is if the cabin says 180W but the lamps are 250W. One example was a tanning cabinet with

a mixture of lamps which were replaced individually as they degraded. This then left new powerful lamps and old lamps operating at 70% of their original output. The percentage of sunbed types encountered on the study shown in Figure 2.26 with over two-thirds of the stand-up variety.

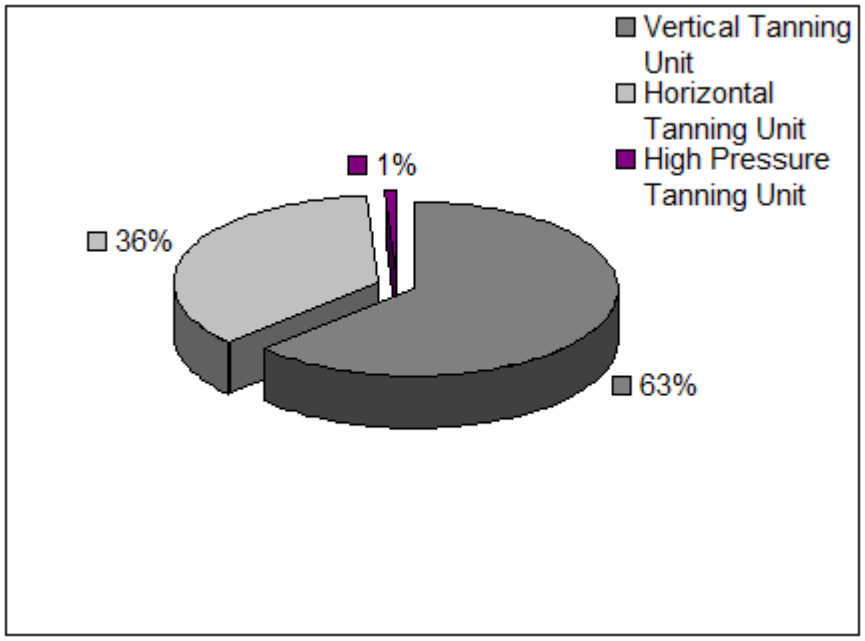


Figure 2.26: Percentage of tanning unit categories.

**Results**

The effective erythemal UVB, UVA and total irradiance from each tanning unit was calculated. This is the summed total for the convoluted spectral irradiance and the erythemal action spectrum for UVB, UVA and total UV range. Comparing the magnitude of the UVB region with the UVA region allows the tanning units to be classified by the BS-EN standards. The results from this study has shown that 90% of the sunbeds tested were emitting UV radiation above the permitted level allowed. The European Standard (see BS EN standard referenced above) in which safe limits for UV radiance are stated, specifies a limit of 0.3 $Wm^{-2}$.

The significance of the total erythemal irradiance, UVB irradiance and UVA Irradiance was assessed performing a SigmaPlot t-Test with Shapiro-Wilk normality method. The mean erythemal irradiance is almost double the compliance level. In

relation to the total UV irradiance it was found that only 10% can be categorised as type 3. Consequently the remaining 90% of the tanning units fall under the category as type 4 requiring medical advice.

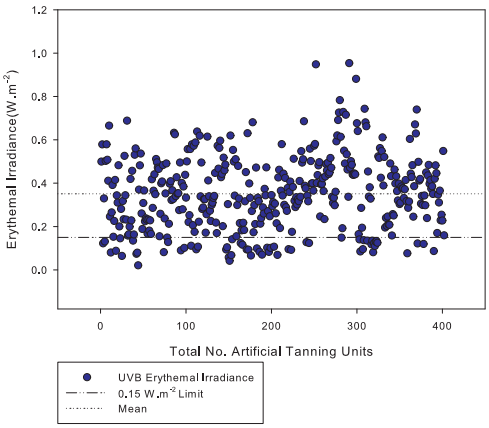


Figure 2.27: UVB Irradiance.

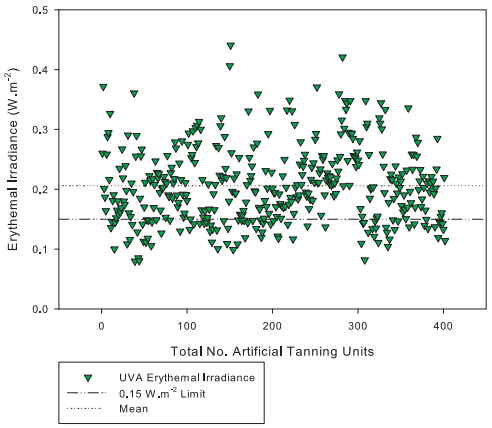


Figure 2.28: UVA Irradiance.

The UVB weighted erythemal irradiance of 0.35 $\pm$ 0.17Wm$^{-2}$ (n=402) shown in Figure 2.27. This mean value is more than double the compliance limit of 0.15 Wm$^{-2}$. Further examination reveals that only 15% of the results are below this compliance value. Moreover two tanning units were outputting UVB irradiance at the 1.0 Wm$^{-2}$ mark with a maximum of 1.06 Wm$^{-2}$. Significant spectral irradiance in the UVB range at 313nm can contribute to 20 – 25% of erythema effectiveness.

The UVA weighted erythemal irradiance average was 0.21 $\pm$ 0.06Wm$^{-2}$ (n=402) shown in Figure 2.28, which is above the compliance limit of 0.15 Wm$^{-2}$. Further examination reveals that only 26% of the total artificial tanning units are below the compliance value of 0.15Wm$^{-2}$. The maximum UVA erythemal irradiance was 0.44 Wm$^{-2}$.

Total erythemal irradiance ranged between 0.10 Wm$^{-2}$ and 1.32 Wm$^{-2}$ with a mean 0.56 $\pm$ 0.21Wm$^{-2}$ (n=402) shown in Figure 2.29. Only 10% of the sunbeds were below the compliance level 0.3Wm$^{-2}$.

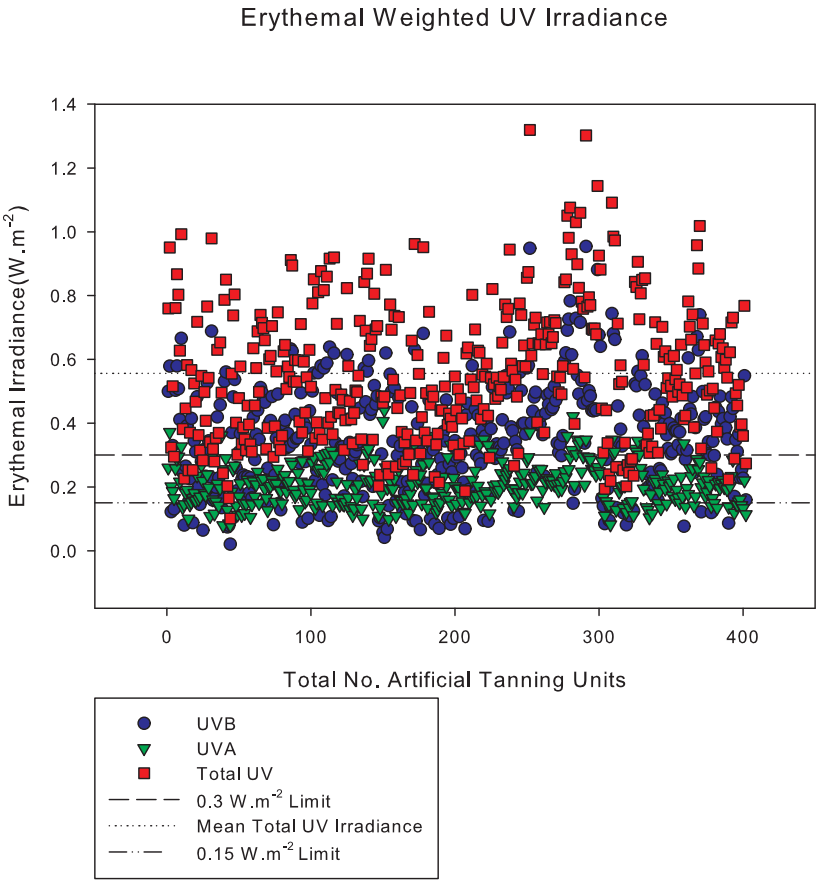


Figure 2.29: Total UV, UVB and UVA Irradiance.

### Facial and Shoulder Erythemal Irradiance

A total of 80 facial lamps were measured from horizontal sunbeds and the erythema irradiance was calculated for each displayed in Figure 2.30. UVB values ranged from 0.01 $Wm^{-2}$ to 0.31 $Wm^{-2}$ with a mean of 0.12 $\pm$ 0.05W $m^{-2}$ (n=80). The UVB mean is below the 0.15 $Wm^{-2}$ compliance level. The UVA values ranged from 0.06 $Wm^{-2}$ to 0.41 $Wm^{-2}$. As expected with UVA Irradiance the value of the mean is higher at 0.19 $\pm$ 0.09W $m^{-2}$ (n=80).

In contrast to the UVB mean the UVA mean is above the 0.15 $Wm^{-2}$ limit value. In fact 52 of the sunbeds can be classified as type 3 with under UVB wavelength range. While only 27 of the tanning units can be in the same classification under the UVA wavelength. The total erythemal irradiance for the facial lamps had a maximum value of 0.64$Wm^{-2}$. The average total erythemal irradiance was 0.32 $\pm$ 0.11W $m^{-2}$ (n=80) which is slightly above 0.3 $Wm^{-2}$ compliance. Only 29 of the tanning

units were overall classified as type 3 totalling both UVB and UVB irradiance.

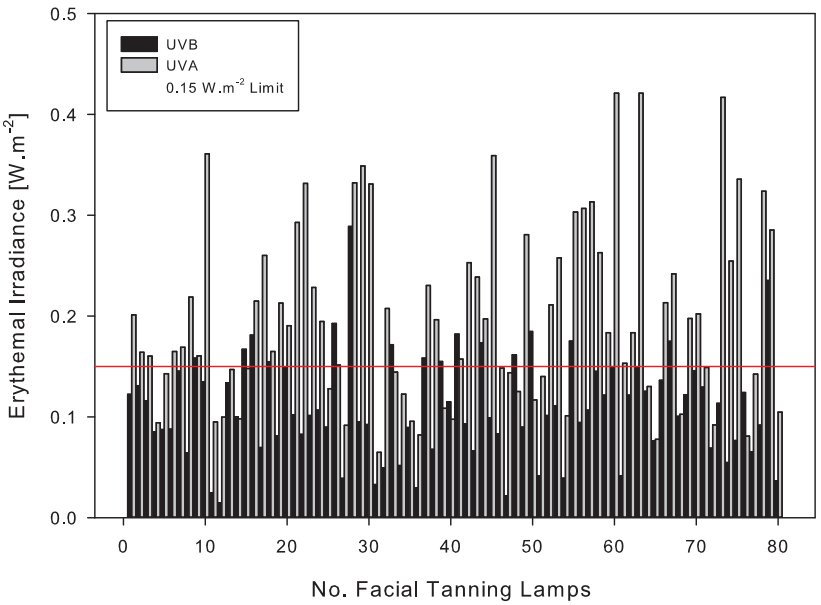


Figure 2.30: Total UV, UVB and UVA Irradiance.

A total of forty measurements were taken from shoulder lamps in sunbeds, all of which were fluorescent lamps at 25W except one which was a quartz lamp at 240W and had an erythemal irradiance of 0.97 $Wm^{-2}$ and SCUP-h 1.75 $Wm^{-2}$. These were HD lamps on Ergoline Prestige 990 Dynamic Power unit. Only one of this type was encountered during the measurements and so was omitted from the shoulder total erythemal irradiance shown in Figure 2.31.

The mean total erythemal irradiance for the 25W shoulder lamps was (0.30± 0.14W $m^{-2}$ (n=39) which is just above the 0.3 $Wm^{-2}$ compliance level. The majority of shoulder lamps were below the irradiance limit with 61 % compliant. The mean UVB erythemal irradiance of 0.20±0.10W $m^{-2}$ (n=39) was above the 0.15$Wm^{-2}$ compliance. The mean UVA erythemal irradiance of 0.10 ± 0.04W $m^{-2}$ (n=39) was below the 0.15$Wm^{-2}$ compliance level.

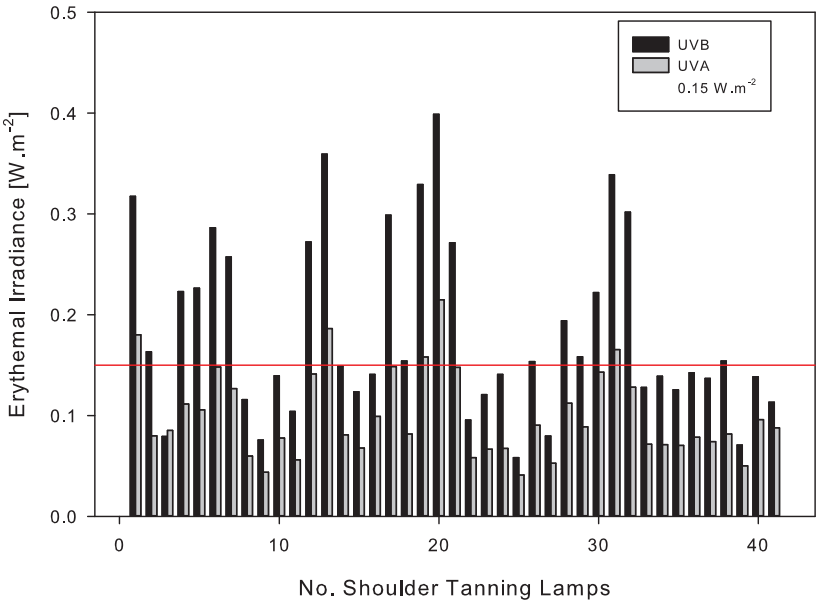


Figure 2.31: Total UV, UVB and UVA irradiance.

**SCUP-h**

The total SCUP-h weighting is also analysed with a one way t-test. A two sample t-test was implemented to compare the irradiance between licensed and unlicensed areas. The statistical significance was taken as $p < 0.05$.

The SCUP-h weighted effective irradiance for the tanning units varied between 0.17 $Wm^{-2}$ and 2.52 $Wm^{-2}$ with a mean of 0.99 $\pm$ 0.41W $m^{-2}$ (n=402) shown in Figure 2.32. The effective SCUP-h for Mediterranean noon sun was calculated at 0.43$Wm^{-2}$. Hence, comparing this value to the mean total SCUP-h it can be said that the average artificial tanning unit is nearly 2.5 times more carcinogenic per minute exposure than that of midday Mediterranean sun. The maximum SCUP-h value was 2.52 $Wm^{-2}$ and this was measured from a Vertical unit using 250W lamps. Using this strongest tanning unit measured in this current work, the comparison factor was over six times that of Mediterranean sun.

The mean total SCUP-h for the quartz facial lamps was 0.52 $\pm$ 0.22W $m^{-2}$ (n=80) which was above the midday Mediterranean sun SCUP-h calculation of 0.43$Wm^{-2}$. Based on measurements attained in this study the SCUP-h equivalent to 0.3$Wm^{-2}$ erythemal irradiance turns out to be 0.48$Wm^{-2}$. Over 33% of facial

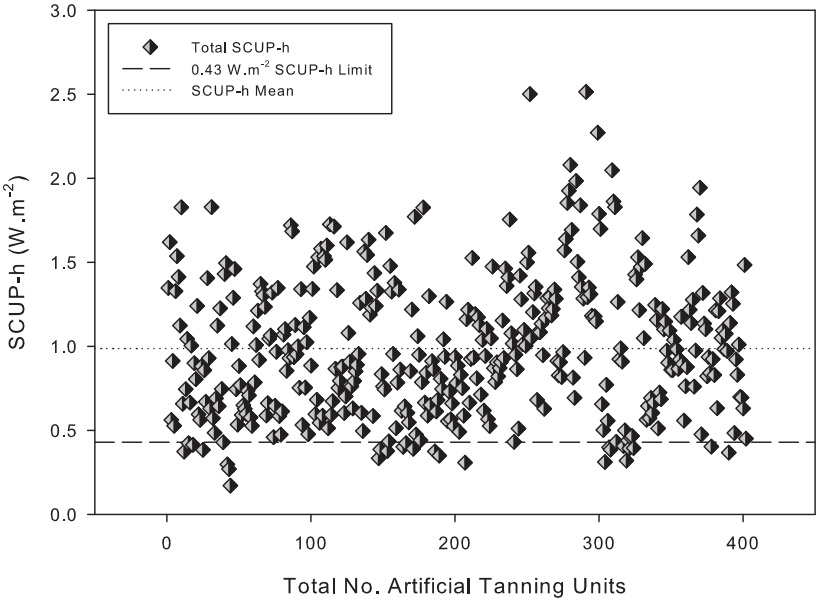


Figure 2.32: SCUP-h total.

tanners(27 facial tanners) have SCUP-h values that are lower than 0.43Wm$^{-2}$, but two facial tanners were about three times the value for midday Mediterranean sun of 0.43Wm$^{-2}$. The mean SCUP-h for the shoulder lamps was also calculated at 0.54 $\pm$ 0.25W m$^{-2}$ (n=39) which is above 0.43Wm$^{-2}$ value.

## Regional Variation

Results from sunbeds surveyed around England are shown in Table 2.2. There were 76 sunbeds surveyed in the metropolitan borough of North Tyneside and Newcastle-upon-Tyne in North-East England. This area includes the unlicensed areas of Wallsend, North Shields, Whitley Bay, Forest Hall, Camperdown, Dudely, West Allotment and Gosforth. In total 56 tanning units were measured across Nottinghamshire and Derbyshire. These included the licensed areas of Chesterfield, Mansfield, Ashfield and Ripley, and Amber Valley.

Six London boroughs were visited during the survey. These were the licensed boroughs of Barnet (n = 48), Bromley (n = 32), Islington(n = 47) and Sutton (n = 33), and the unlicensed Newham (n = 24) and Bexley (n = 41). In the South West of England measurements were conducted in Cheltenham, Coleford and Newton

Abbot in the Teignbridge district of Devon. These were all licensed regions.

Table 2.2: Erythemal Irradiance levels for UVB, UVA and Total UV(combined).

| Location | n | Total erythemal irradiance $Wm^{-2}$(SD) | UVB erythemal irradiance $Wm^{-2}$(SD) | UVA erythemal irradiance $Wm^{-2}$(SD) | SCUP-h* irradiance $Wm^{-2}$(SD) |
|---|---|---|---|---|---|
| London Barnet | 48 | 0.48(0.24) | 0.29(0.19) | 0.19(0.07) | 0.85(0.45) |
| London Bromley | 32 | 0.48(0.23) | 0.29(0.18) | 0.19(0.08) | 0.89(0.45) |
| London Islington | 47 | 0.47(0.20) | 0.27(0.17) | 0.20(0.07) | 0.83(0.39) |
| London Sutton | 33 | 0.49(0.13) | 0.29(0.13) | 0.20(0.06) | 0.85(0.28) |
| London Newham | 24 | 0.57(0.20) | 0.38(0.14) | 0.19(0.06) | 1.03(0.36) |
| London Bexley | 41 | 0.50(0.17) | 0.31(0.14) | 0.19(0.05) | 0.88(0.34) |
| North Tyneside | 76 | 0.70(0.21) | 0.46(0.17) | 0.24(0.05) | 1.25(0.42) |
| South-West | 45 | 0.45(0.25) | 0.27(0.18) | 0.18(0.08) | 0.79(0.46) |
| Derbyshire | 56 | 0.53(0.19) | 0.33(0.15) | 0.20(0.07) | 0.93(0.37) |
| All sunbeds | 402 | 0.56(0.21) | 0.35(0.17) | 0.21(0.06) | 0.99(0.41) |

* SCUP-h, skin cancer Utrecht Philadelphia-human (skin-cancer weighting factor).

At the time of the study, North Tyneside and the London boroughs of Bexley and Newham were unlicensed. A two group t-test was implemented between the licensed and unlicensed London boroughs. The difference between the mean values of sunbed irradiance for the two groups was not statistically significant ($p = 0.237$). When the two-group t-test was performed between the unlicensed North East and the licensed South West, there was a statistically significant difference in the mean values of the two regions ($p < 0.001$).

An average erythema-effective irradiance of 0.56 $Wm^{-2}$ was determined for sunbeds. This corresponds to a UV index of 22.4, which is significantly higher than the UV index of 8.5 of the high summer sun at noon at intermediate latitudes [107]. The index is equal to the EWI (in $Wm^{-2}$) multiplied by 40. An Index of 12 is equivalent to an EWI of $0.3Wm^{-2}$.

## 2.4 Discussion

In this work, considerable care was taken to ensure that UV measurements were accurate. The array spectrometer used in this study has a CCD detector. One of the major technical limitations of CCD arrays is the high level of stray light. For this reason, stray light corrections were carried out. Another error can arise when measurements are being taken in an unoccupied sunbed. A person standing in or lying on a sunbed absorbs incident UV radiation; when the sunbed is unoccupied, radiation from one bank of lamps strikes the opposite lamps and reflectors, and reflects on to the detector. The methodology adopted ensured that this error did not occur. These two measurement artefacts would both lead to an inappropriately high radiation output value, and so considerable care was exercised to ensure that the data collected were reliable.

To date there have been only a small number of sunbed studies carried out in which full spectral measurements were performed on site. Spectral data are required to give accurate information on the UVA and UVB content of sunbeds and to allow the use of weighting factors in the analysis. The importance of measuring on site is that the spectrum and intensity of UV radiation depend on the type, condition, age, stacking density and temperature of the lamps, the design and condition of the reflectors, and the material and condition of the perspex lamp protector.

A hazard assessment of 38 artificial tanning units carried out in Scotland in 1998 found that SCUP-h irradiances were comparable with U.K. summer sunlight [200]. These results were confirmed in a similar study published shortly afterwards [184]. A follow-up study of 133 sunbeds in Scotland in 2007 found that the median of the SCUP-h irradiance of all lamps was then equivalent to Mediterranean sunlight [211]. This was due to the widespread use of 'fast tan' lamps. Although the new British and European standard was in place, 83% of sunbeds exceeded the UVB limit set out in the new standard.

Since 1983, all tanning models in Norway have needed approval before being sold, and type-3 limits were applied from late 1992 onwards [208,209]. However, on-

site inspections in 1998–99 revealed that only 28% of tanning devices were equipped with the correct lamps (i.e. the same type of sunlamps as approved), though this had increased to 59% in 2003. This highlights another problem, which is ensuring that replacements lamps are the same as or similar to the original.

In a recent similar study on sunbed emissions by Public Health England found that 85% of the 197 sunbeds were over the limits of a type-3 sunbed [146].

In this work, on-site spectral measurements were performed on 402 sunbeds in England. The mean erythema weighted UVB and UVA irradiances were $0.35 \pm 0.17\mathrm{Wm}^{-2}$ and $0.21 \pm 0.06\mathrm{Wm}^{-2}$, respectively, and the mean erythemal total UV irradiance was $0.56 \pm 0.21\mathrm{Wm}^{-2}$. Only 10% of sunbeds tested complied with the type-3 limit.

There is a trend that may be identified from reviewing the reports on recent measurements of sunbeds. UV emissions are increasing with the development of new high-power sunlamps. Moreover, the publication of a European Standard in 2003 does not seem to have arrested this development. Sunbeds with erythema-weighted UVB irradiance exceeding $0.15\mathrm{Wm}^{-2}$ should be used only following medical advice,according to BS EN 60335. Yet 85% of sunbeds tested exceeded this level. It is interesting to note that for wavelengths less than 320 nm, the erythema action spectrum resembles the absorption curve for DNA [235]. This will be discussed in greater detail in Chapter 4. The SCUP-h action spectrum indicates the relative effectiveness for induction of nonmelanoma skin cancer [62]. Its merit is in facilitating a quantitative comparison between artificial tanning units and sunlight. In the present study, the mean SCUP-h irradiance was 2.3 times that of Mediterranean sunlight. The maximum value recorded was six times higher than Mediterranean sunlight. The CPD action spectrum follows a similar pattern to the SCUP-h. What is important here is that UVR has the capability to form CPDs. This will be further investigated in Chapter 5.

The ROS action spectrum is heavily weighted in the UVA so facial emission spectra from the sunbed was an obvious choice for the convolution to display the

number of ROS species generated.

Sunbeds tested in North-East England had significantly higher UV emissions than those in the South West $0.7 \pm 0.21 \mathrm{Wm}^{-2}$ versus $0.45 \pm 0.25 \mathrm{Wm}^{-2}$. Sunbeds are licensed in the South West but not in the North East. It may be that licensing was a contributory factor in the difference observed, although there may be other influences such as competition in the market place. In this respect, there was no significant difference between the London boroughs that had licensing and those that did not, and so in this more closely comparable area, licensing per se did not appear to influence compliance with the European standard. This is not surprising, as the local authorities do not have the capability for making the necessary UV spectral measurements. A possible solution would be if only type-3 sunbeds were permitted to be sold and used within the U.K., and units were inspected to show that only the correct lamps were fitted.

Five of the tanning centres visited were unmanned and operated on a coin or credit card system. Anyone of any age or skin type can turn up and use them, and can have as many treatments as they wish. Until recently, these were in widespread use, but they are now banned in Scotland. Individual studies examining the association between sunbeds and skin cancer may have contradictory findings. Although Elliot *et al.* [82] did not show a link between melanoma and sunbed use, Lazovich *et al.* [162] found a dose–response relationship for years during which sunbeds were used. A meta analysis combines results from all investigations, taking due account of the strength of evidence in each study. In a recent meta-analysis, results from 25 studies were combined [32]. This revealed that use of sunbeds increased the risk of melanoma by 20%. The risk of melanoma was almost doubled when use started before the age of 35 years [32]. It was estimated that 3438 cases (5.4%) of melanomas in Western Europe were related to sunbed use. Calculations showed that 99 deaths each year in the U.K. were attributable to sunbed use.

Most people use sunbeds for purely aesthetic reasons. If the sunbed were a cosmetic product it would have been withdrawn years ago. However, legislation has

been very slow in coming within the U.K. The bill regulating sunbeds in Scotland was passed in 2008 and came into force in 2009. This banned unmanned salons and prevented the use of sunbeds by those under the age of 18 years. It also required prescribed information on the health risks to be supplied to users. The other governments in the U.K. followed Scotland's example,and now England, Wales and Northern Ireland all have legislation in place prohibiting the use of sunbeds by people under the age of 18 years. Supporting measures still need to be introduced in the legislation in England, which is the only nation in the U.K. to allow the use of unmanned tanning salons.

The present study, covering 402 sunbeds spread throughout England, indicates clearly that the current situation is very unsatisfactory, and much more needs to be done in England to discourage the use of sunbeds. This investigation clearly shows that 90% of sunbeds emit levels of UV radiation that exceed the limits allowed by the British and European standard. The standard is intended to safeguard the public but it is being largely ignored by the sunbed industry. Stricter control measures must be put in place along with continued programmes of education. Otherwise, the melanoma burden will continue to increase.

In the next chapter we incorporate our readings into plausible scenarios with sunbed exposure sessions giving certain doses. From that we use a model to predict the risk of squamous cell carcinoma developing later in life.

# Chapter 3

# Squamous Cell Carcinoma Model

## 3.1 Squamous Cell Carcinoma

### 3.1.1 Introduction

Nonmelanoma skin cancers (NMSCs), predominantly squamous cell carcinoma (SCC) and basal cell carcinoma (BCC), are the most common cancers in fair-skinned populations throughout the world [252] with increasing incidence in recent years. The use of indoor artificial tanning devices increases the risk of cutaneous malignant melanoma [26], but the association with risk of squamous cell carcinoma of the skin is unclear.

Chronic exposure to the sun generate regions of Actinic Keratoses (AK) containing keratinocytes which differentiate and proliferate [61]. AKs are characterised by cutaneous lesions on sun exposed sites of skin types I–II [242]. The majority of these keratoses will regress but approximately one in a thousand will progress to SSC [50]. Even though SCC is fully treatable some lesions may become locally invasive and destructive, potentially leading to metastasis or death.

SCC and BCC appear especially in advanced age (70 years and up) mainly due to cumulative lifetime UV exposure. They are found predominantly in the areas exposed to the sun, either on the face, neck and hands. If they are detected early enough, the majority of the NMSCs can be treated. While primary cutaneous

SCC has a low rate of metastasis of approximately 5%, after it has metastasised to distant locations the prognosis is generally poor [238]. The risk of metastasis increases significantly in patients with high risk of SCC [38]. SCC is a preventable cancer as UV radiation is the main environmental risk factor. In spite of this, levels of SCC continue to rise throughout the population yearly.

Exposure to UV radiation (UVR) is the primary cause of NMSC, although the pattern of exposure that gives rise to different types of NMSC appears to vary. Squamous cell carcinoma is predominantly caused by long-term sun exposure. SCC is the second most common type of skin cancer and affects at least 10,000 people in the UK each year [251]. Although SCC has a high cure rate it can cause death if it is neglected and allowed to spread. The average age standardised incidence rate for 2010 was 24.7 new SCC cases for every 100,000 in the U.K. [139].

This slow-growing disease affects individuals who have regular exposure to sunlight. Until recently, this cancer was most common in older people, particularly men who worked outdoors. Now, however, more women and younger individuals are being diagnosed with squamous cell skin carcinoma, especially those who spend leisure time in the sun [83] and increased use of sunbeds [141]. Individuals with fair skin; blonde or red hair; or blue, green or gray eyes have higher than average risk.

SCC occurs most frequently on areas of the body frequently exposed to the sun such as the face, ears, neck, scalp, shoulders, and back. The rim of the ear and lower lip are especially vulnerable to these cancers. Tumours sometimes develop on areas where the skin has suffered injury: sun damage, burns, scars, sores, or sites exposed to x-rays or chemicals. Chronic skin inflammation also may encourage the development of squamous cell skin carcinoma.

The characteristics of a person susceptible to developing SCC are:

(1) advanced age

(2) significant cumulative exposure to life in the sun

### 3.1.2 SCC Model

Solar UV radiation is recognised as the principal environmental cause of skin cancer. In particular, the risk of induction of squamous cell carcinoma (SCC) has been shown to increase with cumulative exposure to UV radiation. Models of risk of SCC induction have been developed but these do not include the use of sunbeds and this was the purpose of the present study. To this end, the values of published on-site UV levels emitted from sunbeds were used to provide real measured sunbed exposure levels to inform the model. The model incorporated three conditions of exposure: day-to-day, holiday and sunbed exposure. The risks associated with different exposure scenarios were implemented in the model. Baseline exposure comprised day-to-day and holiday exposure. Relative risk was defined as the risk of SCC induction from (sunbed + baseline dose) / baseline dose. The algorithm was implemented in Matlab programming package [182]. The purpose of this work is to estimate the additional carcinogenic risk from the use of sunbeds using the actual on-site UV measurements from sunbeds. To this end, several exposure scenarios are considered in terms of use of sunbeds and type of sunbed used. The additional risk factor is determined compared to sunlight exposure using a model developed for SCC induction [63].

Fears *et al.* demonstrated for a given genetic susceptibility, that age and UVR exposure are the most important determinants for relative risk [87].

Risk of SCC induction has been shown to follow a simple power-law relation in

accordance with the following basic equation 3.1

$$Risk \propto (annual\ UV\ dose)^{\beta}(age)^{\alpha+\beta} \tag{3.1}$$

The biological amplification factor '$\beta$' reflects the fact that any percentage increase of the annual UV dose results in a greater percentage increase in the incidence of SCC. This is attributable to the steepness of the power relationship between the doses of UV radiation and the incidence of skin cancer. The parameter '$\alpha$' reflects an age dependent factor. The exponent values from $\alpha$ and $\beta$ were derived from values published in a review of epidemiological data [210]. In the present study, we use the power parameters $\beta = 2.3$ and $\alpha = 3.8$. This equation is applicable to conditions where the annual exposed dose received by people remains unaltered throughout life. However, in most cases changes in lifestyle with age indicate that annual UVR exposure does not remain constant throughout life. This situation occurs when one uses artificial tanning units for a limited period in a life span.

The situation of abrupt change in annual UV exposure was examined in a series of time-dose experiments in mice by de Gruijl and resulted in an adapted version of the equation to estimate the risk of NMSC [64]. The relative risk from total body tanning using sunbeds will depend on the sunbed emission spectra output (erythemal irradiance $\mathrm{Wm}^{-2}$), the length of time of each session, the number of sessions per year and the number of years of use. Typical sunbed sessions were noted during the original study to range from 2 minutes to 20 minutes. In our analysis, we consider sunbed sessions lasting 3 minutes, 9 minutes and 12 minutes. In general, lower output horizontal sunbed units had longer sunbed session times compared to 'fast tan' vertical and horizontal units.

**Sunbed Dose**

We used the erythemal-weighted UV irradiance data from our published large scale survey of sunbeds [267]. In this study, on-site UV spectra were measured from 402 artificial tanning units distributed across England. Instrumentation calibration was

traceable to the NPL in order to ensure the reliability of the data. Sunbed exposure was considered as an additional component in addition to day-to-day exposure and holiday exposure. Erythemal irradiance is commonly expressed in terms of the Standard Erythemal Dose (SED), where 1 SED is equivalent to an erythemal effective radiant exposure of 100 $Jm^{-2}$ [185].

### Baseline Dose

For day-to-day exposure, we used the median value of 166 SED which is taken from a Danish epidemiological study [262]. Holiday exposure was also taken into consideration in the model. The dose from one week holiday in the Mediterranean sun has been shown to be equivalent to 57 SED [221]. In this study it was assumed a whole-body holiday dose lasting for 10.5 days the national average time abroad a proxy to holiday exposure [5]. The model also made the assumption that the holiday exposure for a child did not begin until five years of age and there was no difference in annual dose between teenagers and adults.

### Body Site Weighting

We additionally examined the effect of exposure of various body-sites, from those normally exposed such as face, posterior neck and arms to more usually unexposed sites. The latter include the trunk and legs which account for approximately 80% of body surface area. The normally exposed areas from day to day consist of the face, posterior neck and hand. There is a significant difference between the dose to the face and neck compared to the dose to the hand. Thus, a weighting factor 'wLu' = 2 was added to the upper regions which receive twice the dose compared to lower 'wLL' =1 regions [261].

The percentage of body-site area for daily exposure is approximately 10% depicted in Figure 3.1. This is split into 6% for face 'AeU' and posterior neck and 4% for dorsal hands 'AeL'. Ae is the total percentage area exposed day-to-day, 10%. The fractional area for whole body exposure sunbathing or on a sunbed is approx-

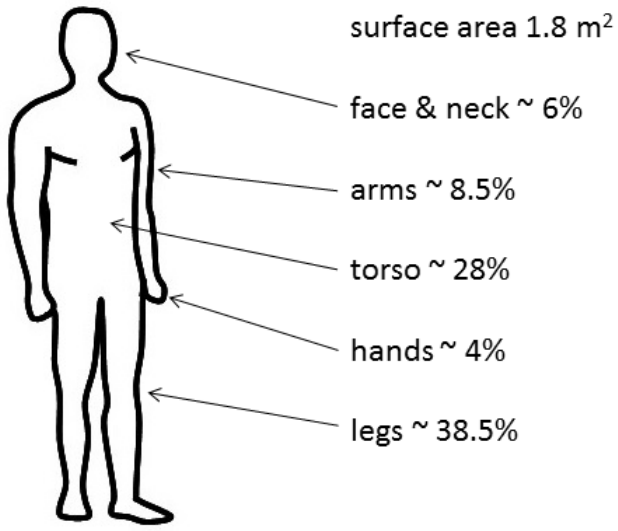


Figure 3.1: Body surface percentage areas: day-to-day exposure (face,neck and hands) 10% and max exposure area 85% [16].

imately 85% 'Au' excluding volar hands and feet and parts covered by trunks or bathing suit [16, 104]. Sunbed exposure was set for the years between 20 and 35 years with the age of first sunbed use being 20 years, and no sunbed use after age 35 years. By summating the dose contributions from day-to-day $D_d$ holiday and sunbed exposure we formulate subsequent equation of total dose $TD_e$ of normally exposed body-sites (face, neck and hand):

$$TD_e = a.D_d + (a - a_h).D_H + (a - a_s).D_s \tag{3.2}$$

for $a > a_h$ (holiday exposure), $a_s < a < 35$ (sunbed exposure);
where $D_d = wL_u.D_d$ or $wL_L.D_d$

Similarly for

$$TD_u = (a - a_h).D_H + (a - a_s).D_s \tag{3.3}$$

where

$TD_u$ is the dose for the routinely unexposed sites (legs, trunk, arms, etc.).

### 3.1.3 Tumour Yield

The assumptions outlined above are incorporated into the equation to calculate tumour yield for discrete age intervals of five years up to eighty years of age. For this model we modified the equation to include the fraction of usually unexposed and exposed areas and also a weighting factor for the face and wrist. This is due to the fact that the Danish study found the correlation between the SED at the head and wrist was statistically significant [261]. The dosimeter readings at the forehead were double that of the wrist. Therefore the dose received was multiplied by two to give a comparable UV facial exposure dose [262]. The average number of tumours accumulated per individual at risk in a birth cohort of age "a" in absence of death was referred to as the tumour yield. The following equation gives the tumour yield YLD(a) at age 'a' and considers the areas of the body that are normally exposed in day-to-day outdoor activities (subscript 'e') and the areas that are normally unexposed (subscript 'u') but receive additional exposure on a sunbed and on holidays. The equation is composed of a purely UV dose-dependent factor and a purely time-dependent factor and includes explicitly two terms representing the fractional area exposed (i.e. normally sun-exposed and unexposed).

$$YLD(a) = \sum_L \left( \sum_S \left( A_e \left( \frac{TD_{eU}}{t_{do}} \right)^{\beta} . \left( \frac{a}{a_o} \right)^{\alpha} \right) + \sum_S \left( A_u \left( \frac{TD_u}{t_{do}} \right)^{\beta} . \left( \frac{a}{a_o} \right)^{\alpha} \right) \right) \quad (3.4)$$

where

$t_{do}$ , reference total dose up to $a_o$ to match actual YLD(65)

$\sum_L$, sum over dose level for each person at risk

$\sum_S$, sum over body sites.

Expanding this further to include upper and lower areas of normally exposed sites we deduced the following equation:

$$YLD(a) = \sum_L \sum_S \left( A_{eU} \left( \frac{TD_{eU}}{t_{do}} \right)^{\beta} . \left( \frac{a}{a_o} \right)^{\alpha} + A_{eL} \left( \frac{TD_{eL}}{t_{do}} \right)^{\beta} . \left( \frac{a}{a_o} \right)^{\alpha} + A_u \left( \frac{TD_u}{t_{do}} \right)^{\beta} . \left( \frac{a}{a_o} \right)^{\alpha} \right) \quad (3.5)$$

For baseline calculation of just day-to-day and holiday dose the sunbed contribution was omitted from the total dose calculation. The number of cases of SCC per year was described as the age-specific incidence I(a) (the number of new cases per year per individual at risk at age 'a') defined by:

$$I(a) = \frac{\Delta(Yield(a))}{\Delta(a)} \quad (3.6)$$

The first derivative of Yield with respect to 'a', which is estimated by the increase in the yield, $\Delta$ Yield, over a 5-year age interval, $\Delta$ a. The baseline age-specific incidence estimated from the Yield is scaled to the 2010 SCC incidence rate provided by Public Health England (PHE) [7]. From the data we can establish the incidence per $10^5$ persons for each 5-year age group. Initially, the yield difference was normalised for each 5-year age group to the one at 65 years and then used a scaling factor to fit the delta yield output across all ages to match the PHE data. The scaling factor 'm' is used to match incidence of SCC per 5-year age group (PHE data) to the number of cases of SCC from our yield equation.

$$m = \frac{Incidence(a)}{\Delta Yield(a)} \quad (3.7)$$

The initial yield from the model is a good approximation of the exponential rise of SCC cases with age; further scaling allows us to match our model to PHE data. The exponential curves for PHE SCC cases and our model as a function of age are in good correlation for baseline doses. The curve for incidence of SCC across all age groups in the U.K. population is taken as the baseline without sunbeds (neglecting a possible small contribution to the PHE data). Once the matching factor was established it was applied to all the other scenarios where extra dose from sunbeds yields more SCC tumours. By calculating the ratio of the area under the curve

(AUC) between baseline 'no sunbed' and sunbed use it was possible to establish the relative cumulative incidence (RCI), which should equal the relative risk (RR) (as established by the ratio of yields).

$$RR = \frac{\text{incidence of SCC among persons exposed to sunbeds}}{\text{incidence of SCC among persons not exposed to sunbeds}}$$

### 3.1.4 Incidence

#### Increased Risk

The lifetime risk of developing cutaneous SCC was estimated for normal day-to-day solar exposure and 10.5 days abroad in a Mediterranean resort with additional sunbed exposure from ages 20 to 35 years. We investigated various exposure doses using the UV outputs measured during our previous survey [267]. In order to consider the effects of sunbed exposure over a wide range of sunbed outputs and exposure times, we decided to examine the 5th, 50th and 95th percentile doses for sunbeds. The dose from each sunbed scenario was added to the personal annual dose, as reported in the Danish cohort study taking the 25th, 50th and 75th percentile of the reported day-to-day population exposure. This allowed us to compare situations of low day-to-day dose from an office worker who uses sunbeds extensively to an outdoor worker who uses sunbeds infrequently. The relative contribution of sunbeds to SCC incidence was calculated by dividing incidence per age group among sunbed users by the baseline incidence without sunbed exposure. The worst case scenario of approximately two 12-minute sessions per week (90 sessions) with the maximum sunbed output amounted to an extra dose of over 850 SED per year.

Figure 3.2 provides a summary of all the annual doses encountered for a sunbed session time of 12 minutes for different sunbed regimes of 15, 45, 60 and 90 sessions per year shown as a boxplot graph. In some situations there will be an overlap in doses from different scenarios. The average sunbed session time of 12 mins was established in European study by Bock *et al.* [31]. Other sunbed times of 3, 6, 9 and 18 mins were also encountered during the original study. For example, if we calculated the cumulative dose for a 9 minute session for a median sunbed output twice weekly regime (90 sessions per year) the resultant dose was 262 SED. There can be also an overlap of total dose from a sunbed depending on different exposure times and overall sessions. This scenario is encountered if we calculate the cumulative dose for a 9 minute session for median sunbed output for a weekly regime (60 sessions per year) and compare the dose to a 12 minute session 45 times per annum. This

would correspond to a cumulative dose of 176 SED for both scenarios or 2.9 SED and 3.9 SED per sunbed session respectively.

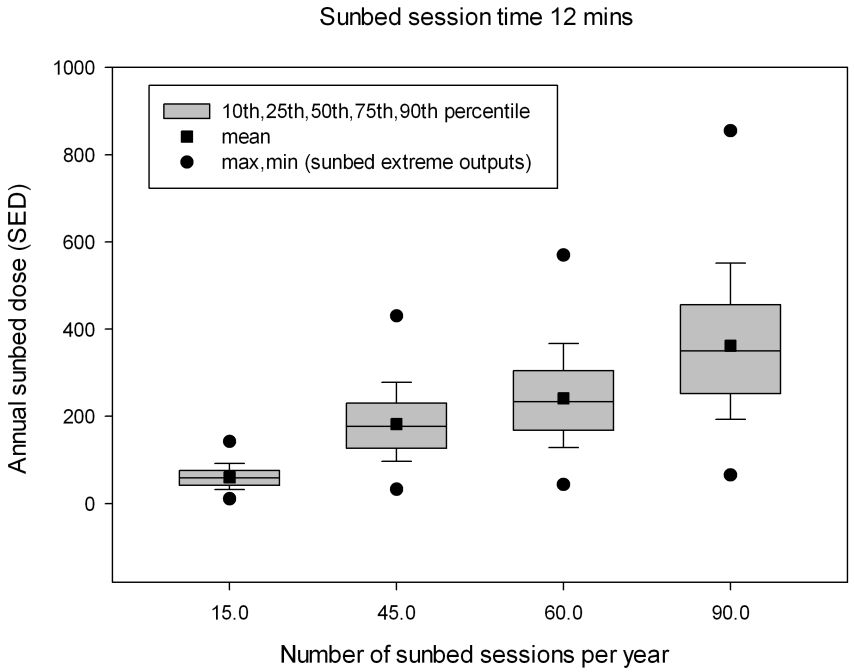


Figure 3.2: Annual dose received due to sunbed use showing the effect of a 12 minute session and number of sessions per year based on the UV perecentile spread of sunbed emission levels measured in the large-scale UK survey. [267] ■ mean level output from a sunbed value of 0.54 $Wm^{-2}$. ● represent the extreme outputs of sunbeds.

The same European study of nearly 5000 individuals aged 14–45 years revealed a median sunbed exposure time of 180 min per year [31]. Further analysis of the data showed that the 75th percentile annual sunbed exposure was 544 minutes which is equivalent to 45 sunbed sessions for 12 mins. The sunbed dose is calculated as the product of time (secs) by sunbed irradiance output. For example the median irradiance results in a dose of 176 SED. During the previous study in which we measured UV irradiance levels in England, it was noted that the horizontal units predominantly had the highest session times of up to 20 mins which corresponded with findings in an earlier Swiss study [181]. We can compare the various sunbed doses calculated from our on-site sunbed irradiance study with the day-to-day dose range calculated by Thieden *et al.* [263]. Once we established absolute sunbed doses the next step was to put them in terms of risk by also including different day-to-

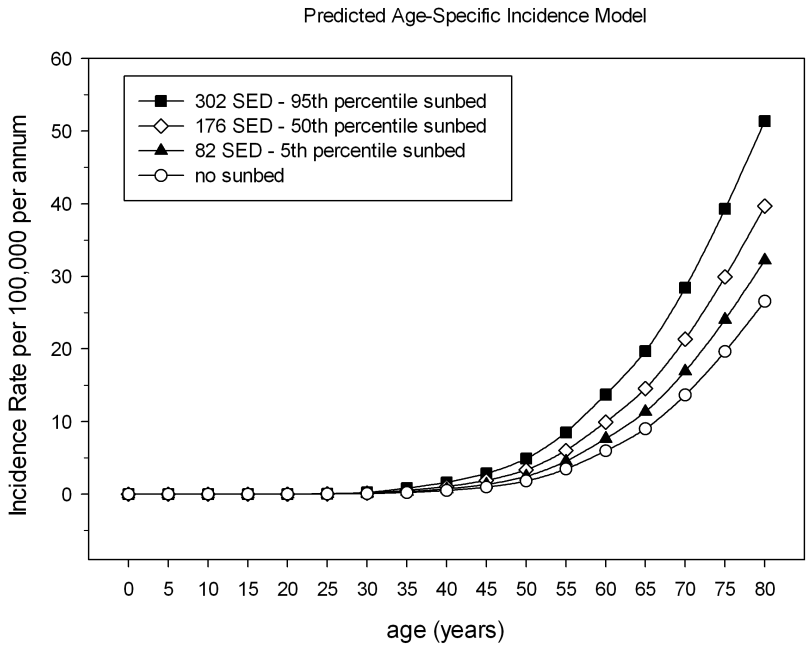


Figure 3.3: Modelled age-specific incidence curves for rate of SCC induction model with a day-to-day baseline dose 166 SED, plus a 10.5 holiday exposure of 85.5 SED and a range of sunbed outputs. Rates are scaled according to age specific incidences in the 2010 U.K. population per 100,000 persons (Source: PHE [7]).

day exposures which we have derived from the Danish study. The day-to-day dose followed a log-normal distribution. The rationale was to obtain a risk estimate for say an indoor worker with low solar exposure who might use a sunbed. Also we investigated the other higher end of day-to-day exposure. The age specific incidence was thereby derived from the median day-to-day exposure of 166 SED with holiday dose 85.5 SED. This was known as the "baseline" dose. Any additional exposure from sunbed dose was entered in the model to estimate the extra risk involved.

In Figure 3.3 above we illustrate the fitted age incidence curves with additional UV sunbed dose for SCC pooled together for both sexes. The curves deviate from the baseline after the last sunbed use at 35 years for higher sunbed doses. At the higher sunbed doses we notice a much higher rate of incidence of SCC.

The model was setup for a less extreme sunbed use by changing the sunbed use parameter for 10 years. The resulting incidence graph is represented in Figure 3.4.

While the previous two models with sunbed use might be still considered high but still plausible it was decided to run the predicted incidence for a just sunbed use

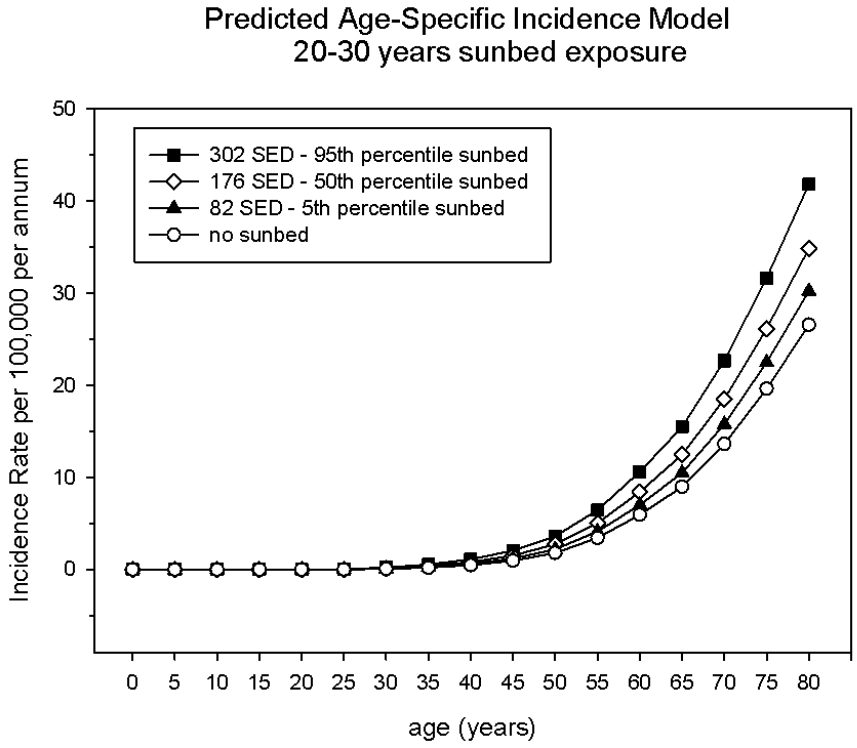


Figure 3.4: Modelled age-specific incidence rate for sunbed exposure from ages 20–30 years).

for 5 years. Figure 3.5 displays the predicted increased incidence for a low sunbed use period. There is still a significant increase in incidence for just 5 years of sunbed use.

Another estimate of the cancer risk can be put in terms of age standardised rate (ASR). This is calculated by multiplying the age-specific incidence from our model in 5-year intervals by European age standarised rates per 100,000 people. The ASR is a summation over all age groups of age-specific incidences weighted by number of people of that age group per 100,000 in the (European standardised) population. Summed up to 80 years of age the age standarised rate is 26.6 per 100,000 persons for a baseline 166 SED exposure and 10.5 holidays with no sunbed use. For a sunbed use of median scenario output the incidence increases to 39.7 per 100,000 people at 80 years of age, i.e. 50 % increase.

We made the simplifying assumption that everybody is exposed to the base line day-to-day exposure and holiday exposure. However, the daily dose varies over the population and so we addressed this by using the distribution of day-to-day

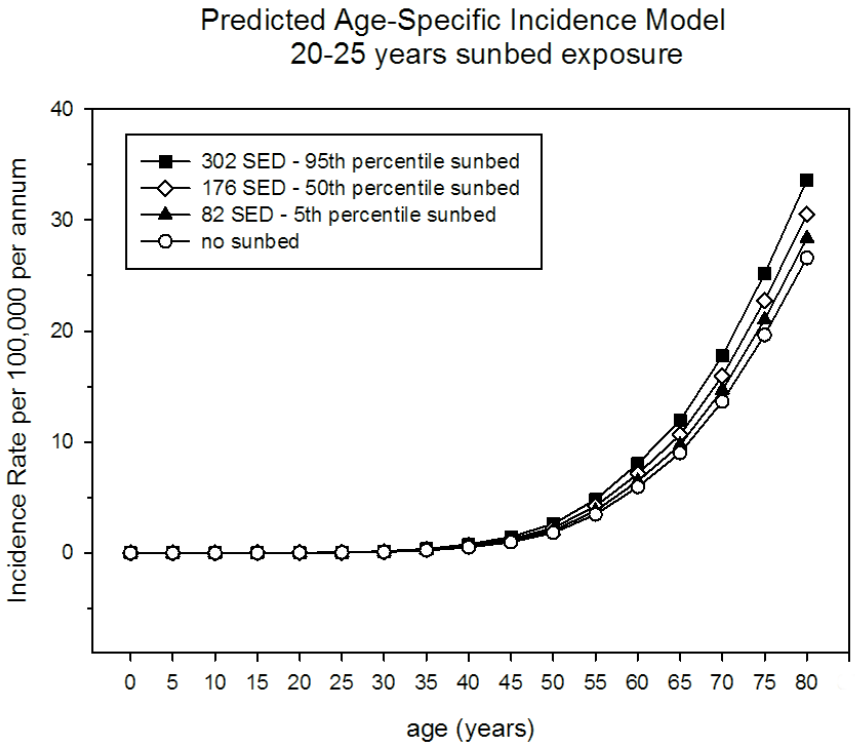


Figure 3.5: Modelled age-specific incidence rate for sunbed exposure from ages 20–25 years).

exposures from the Danish cohort study. Therein we also investigated the risk for a range of sunbed outputs with a low day-to-day dose (110 SED), lower quartile from Danish study, for baseline which would be analogous to an indoor office worker with reduced day-to-day sunlight exposure. This scenario gives an ASR of 27.6 at age 80 years for the median sunbed output. If we omit the sunbed contribution for this day-to-day does we yield ASR 16.6. Also examined was a high day-to-day dose (251 SED), upper quartile form Danish study, for the baseline which would occur in people who work and spend lengthy spells outdoors such as builders, keen gardeners and golfers. The baseline for this scenario resulted in ASR 48.4 when not including sunbeds. The resultant ASR was 64.9 at age 80 years when including the median sunbed use scenario as the relative day-to-day dose dominated over the extra UV exposure from sunbeds.

### 3.1.5 Relative Cumulative Incidence

In these calculations, based on various sunbed exposure scenarios, the additional risk was estimated with escalation in annual UV dose from sunbeds. Age-specific incidence curves were mathematically modelled for rate of SCC induction model with a day-to-day baseline dose 166 SED, plus a 10.5 holiday exposure of 85.5 SED and a range of sunbed outputs. Rates were scaled according to age specific incidences in the 2010 U.K. population per 100,000 persons [7]. The RCI is defined as cumulative incidence of skin cancer up to a given age in sunbed users divided by the cumulative incidence at the same age in non-sunbed users [69]. The cumulative risk was estimated from scenarios used in Figures 3.3-3.5. RCIs (AUC) of SCC are represented in Tables 3.1-3.3.

Table 3.1: RCI of sunbed user to non-sunbed user for a baseline day-to-day dose 166 SED, 10.5 holiday and additional sunbed dose based on a 12 min session 45 times per year (equivalent to 6 min 90 sessions or 9 min 60 sessions).

| Age (years) | RCI for 5th Percentile Sunbed Dose 82 SED | RCI for Median Sunbed Dose 176 SED | RCI for 95th Percentile Sunbed Dose 302 SED |
|---|---|---|---|
| 55 | 1.4 | 1.9 | 2.8 |
| 80 | 1.2 | 1.6 | 2.1 |

In Table 3.1 there is a 90% increase for sunbed exposure for 15 years with a median level output by mid-age 55. For the higher end sunbed outputs this can significantly increase with a risk of three fold compared to a non sunbed user.

Table 3.2: Relative Cumulative Incidence (RCI) for exposure years 20–30 years.

| Age (years) | RCI for 5th Percentile Sunbed Dose 82 SED | RCI for Median Sunbed Dose 176 SED | RCI for 95th Percentile Sunbed Dose 302 SED |
|---|---|---|---|
| 55 | 1.23 | 1.55 | 2.05 |
| 80 | 1.16 | 1.37 | 1.68 |

Table 3.2 represents the RCI for a 10 year sunbed exposure period. There is still quite a high increased risk of 55% for median level sunbed output and a two fold increase for the higher sunbed emissions.

Table 3.3: RCI for exposure years 20 -25 years.

| Age (years) | RCI for 5th Percentile Sunbed Dose 82 SED | RCI for Median Sunbed Dose 176 SED | RCI for 95th Percentile Sunbed Dose 302 SED |
|---|---|---|---|
| 55 | 1.11 | 1.25 | 1.46 |
| 80 | 1.08 | 1.17 | 1.31 |

Table 3.3 displays the RCI for a 5 year period. While the RCI is lower than the two previous regimes there still is a considerable risk. At 55 years old a median sunbed output for 5 years would give a RCI of 25% and nearly 50% for the higher end sunbeds.

### 3.1.6 Conclusion

In this study we used on-site measurements of UV irradiance from sunbeds reported previously in Chapter 2 [267] and applied a skin cancer risk model to these data. We have considered the effects of using different sunbeds and a variety of plausible exposure scenarios. The model used data from a Danish case-control study which revealed an increased risk of SCC with lifetime sun exposure [236]. A risk model was derived to include age at first sunbed exposure, annual sunbed exposure time and annual holiday patterns. We calculated typical dose from different sunbed scenarios such as the practice of pre-holiday 'base' tanning, moderate (15 sessions per year) to higher over once a week exposure throughout the year. The percentile range included: 5th percentile, median and 95th percentile sunbed doses. The RCI was calculated by dividing the incidence of SCC for sunbed users with a 10.5 holiday divided by that of a non-sunbed user with a 10.5 holiday. It is well established that the anatomical site distribution of lesions is heavily weighted towards sun-exposed sites, such as head, neck and face [94, 175]. Due to the fact the distribution of SCC tumours occur predominantly on chronically sun exposed sites we assumed equal sensitivities for all anatomical sites. However, in this model we did include the percentage area for normally exposed (face, neck and hand) and unexposed areas. A weighting factor was applied between these regions as the head receives twice as much dose as the hand.

The increased risk of SCC induction was calculated from the ratio of area under the curve for baseline sunbed to non-sunbed user. For example, looking at the median sunbed output (176 SED) with the median annual day-to-day dose (166SED) and a 10.5 holiday (85.5 SED) we can estimate the increase in RR. The risk at age 55 years would have increased '1.9' fold for sunbed users who partake in a 12 min session 45 times per year (or 6 min session 90 times per year) over a 15 year period from age 20 to 35. SCC is a preventable cancer as UV radiation is the main environmental risk factor. In spite of this, levels of SCC are increasing throughout the population. However, there may be an under-estimate of SCC incidence in that only

the first SCC per person is recorded on the cancer registries as per United Kingdom and Ireland Association of Cancer Registries (UKIACR) rules [206]. Sunbeds are now classified as Group I carcinogens [81,91]. The additional sunbed dose combined with sunlight increases the the risk of non-melanoma skin cancer. As SCC is closely associated with cumulative UV-exposure, sunbed users are not restricted by seasons and accumulate unnecessary extra UV exposure throughout the year. Previous studies in which multivariate analysis was used have demonstrated exposed anatomical sites such as the head and neck to have a higher susceptibility to developing SCC [94]. In our model we retain sensitivities across all body-sites equal.

Campaigns have been launched through popular media warning of the dangers of sunbeds. It is important that the public understands the risks of UV exposure. In addition, there is considerable variation in the output of artificial tanning units. The results of the model indicate that the additional UV dose from sunbed use compared to normal day-to-day solar exposure potentially adds a significantly increased risk for development of SCC. These findings are consistent with previous meta-analyses of sunbed use and NMSC risk, which found a significant increase in risk for the development of squamous cell carcinoma [78, 111, 283]. Previous studies have revealed strong links between sunbed use and the risk of SCC, with a dose-response relationship [142,305]. While SCC occurs more frequently with older people mainly due to the amount of UV exposure over a lifetime, young people are also at risk of developing SCC, especially those who expose themselves to artificial tanning sources such as sunbeds. As this is an unnecessary and avoidable risk, the data presented here strongly support public health campaigns aiming to significantly reduce sunbed exposure. The mathematical dose-time model predicts the increased risk of developing SCC later in life with sunbed use for a certain number of years. The sunbed irradiance established in Chapter 2 permits us to apply plausible sunbed exposure times to give a dose. This increased dose for an average sunbed of 176 SED per year over a 15 year period can cause a 90% increase of developing SCC by mid 50s.

# Chapter 4

# Optical Properties

## 4.1 Optical Properties of Skin

Accurate understanding of the optical properties of human skin remains a challenge to biomedical optics, and theoretical modelling of light propagation in skin tissues continues to be active [12, 277]. The radiative transfer theory has served as a framework for modelling light propagation and distribution within which various numerical approaches have been pursued because analytical solutions are rarely attainable [126].

One stochastic approach, the Monte Carlo method, in which a model of independent photons undergoing random walk is used, has acquired extensive preference above others owing to its strong capability to provide solutions with simple algorithms in spite of the intense computing requirement [144]. However, the tissue model is only as accurate as the optical properties entered into the MCRT code. Thus, it is important to have accurate data for the various layers and light absorbing chromophores.

The structure of the skin plays a role in the distribution of light, for the model we assume optically smooth interfaces at the surface and between the layers. Optical properties which determine a photon's migration in the skin may be summarised through the process interaction between UVR and the skin layers - absorption, reflection and scattering.

Light energy interacts with the skin by: absorption (chromophores absorb photon energy and transform it into heat), elastic scattering (light changes its path due to differences in refraction index within the skin.

### 4.1.1 Introduction

The four important optical parameters that influence the propagation of light through tissue are the absorption coefficient ($\mu_a$), the scattering coefficient ($\mu_s$), the anisotropy factor (g) and the refractive index (n). Human skin tissue can be considered as a turbid media where both scattering and absorption of UV radiation occurs. As a photon migrates through a turbid media it can be attenuated. The total attenuation $\mu_t$ of the turbid media can be expressed by:

$$\mu_t = \mu_a + \mu_s \tag{4.1}$$

Where $\mu_a$ and $\mu_s$ are absorption and scattering coefficients respectively and are typically measured in inverse centimetres. The average distance traversed by a moving photon between successive absorption and scattering events is known as the mean free path (MFP) displayed in Figure 4.1 . Hence the MFP of photons in the turbid media is the inverse of total attenuation coefficient $\mu_t^{-1}$.

$$\text{MFP} = \frac{1}{\mu_a + \mu_s} \tag{4.2}$$

The values of $\mu_a$ and $\mu_s$ are determined from published data on skin absorbing and scattering optical properties in different skin layers.

The refractive index value, n, remained constant over the wavelength range while the anisotropy factor, g, was wavelength dependent [277]. In the model the optical properties for each layer are specified separately, but assumed uniform throughout a specific layer. The skin model was divided into 101 layers and each layer into $101 \times 101$ segments to form a small 3-dimensional (3-D) volumes or voxels in the grid. The photons absorbed in each of the voxels were registered to give the total

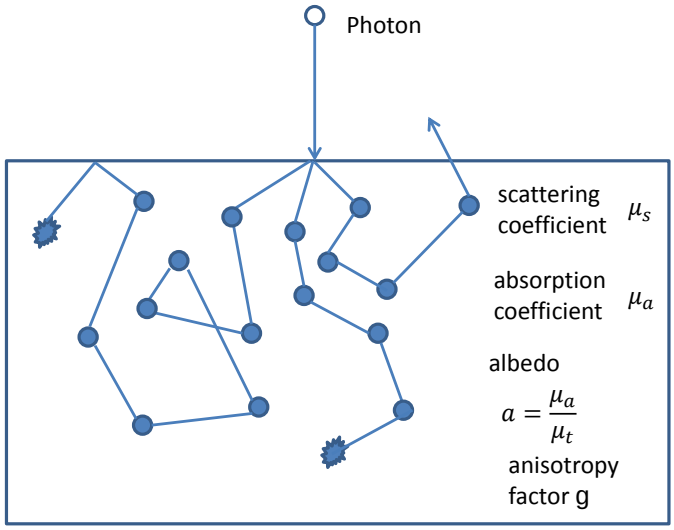


Figure 4.1: One-dimensional representation of distance travelled by a photon between scattering and absorbing events in turbid medium.

absorption in each layer.

## 4.2 Absorption and Scattering Theory

The Beer-Lambert law describes the exponential attenuation of light as it passes through an absorbing medium:

$$I(z) = I_0 e^{-\mu_a z} \tag{4.3}$$

$I_o$ is the initial intensity of the light and I is the intensity after passing through a distance $z$ of material with an absorption coefficient $\mu_a$ (note that this is the manner in which the absorption coefficient is defined). The experimentally measured absorbance of a material will typically be reported as one of the following two quantities:

1. the absorbance, A (also called the optical density, OD):

$$A = \log_{10}\left(\frac{I_o}{I}\right) \quad \text{(unitless)} \tag{4.4}$$

2. the absorption coefficient $\mu_a$,

$$\mu_a(\lambda) = \mathrm{C}\,\epsilon\,(\lambda) \quad (\mathrm{cm}^{-1}) \tag{4.5}$$

which is the molar extinction coefficient of a chromophore, $\epsilon$ ($\mathrm{M}^{-1}\,\mathrm{cm}^{-1}$), multiplied by the concentration of the chromophore, C (Molar). The molar extinction coefficient of a substance is wavelength ($\lambda$) dependent. C is the concentration of the absorbing species (this can be measured in a variety of units, and care must be taken to ensure that the dimensionality of the above expressions is maintained). In biological tissues there are many different chromophores of varying concentrations depending on location. In this chapter the derivation of the absorption optical properties is presented for the different skin layers and chromophores.

When a photon interacts with a turbid medium such as skin, one of the possible outcomes is that the direction of the propagation can change. This type of interaction is called scattering. There are two types of scattering: inelastic and elastic. The latter, is where there is no energy transfer between the incident photon and the scattering molecule, while inelastic scattering is where the energy of the scattered photon differs from the incident photon [124]. Scattering in biological tissue can be modelled using the Mie and Rayleigh scattering conditions [241]. Mie scattering occurs from large tissue structures, such as collagen fibers. Mie scattering in tissue is anisotropic, biased towards forward scattering. The scattering interactions from particles smaller than wavelengths, such as from various small skin organelles, can be modelled as Rayleigh scattering, which leads to scattering oriented almost equally in all directions: isotropic scattering described in Figure 5.2. However, the scattering angle is stochastic and the tendency for a photon to be forward or backward scattered is governed in this work by the Henyey-Greenstein phase function described in section 5.3. Monte Carlo simulations (see Chapter 5) serve as a method to model the scattering of photons in a turbid medium based on the knowledge of wavelength dependent scattering coefficient $\mu_s$ ($\mathrm{cm}^{-1}$). Scattering coefficients have

been derived from published data and reviews of skin layer optical properties and discussed in the following sections [25, 39, 45, 128].

## 4.3 Skin Structure

Human skin is is a partial translucent, multi-layered and heterogeneous medium and is comprised of lipid cross-linked with proteins which form the essential barrier that maintains tissue integrity [256]. Skin can be divided into three main sections: stratum corneum, epidermis and dermis depicted in Figure 4.2. The stratum corneum, a stratified structure composed mainly of dead cells, called corneocytes, is the first and outermost section of human skin. Light absorption is low in this tissue, which is considered by some authors to be part of the epidermis [271].

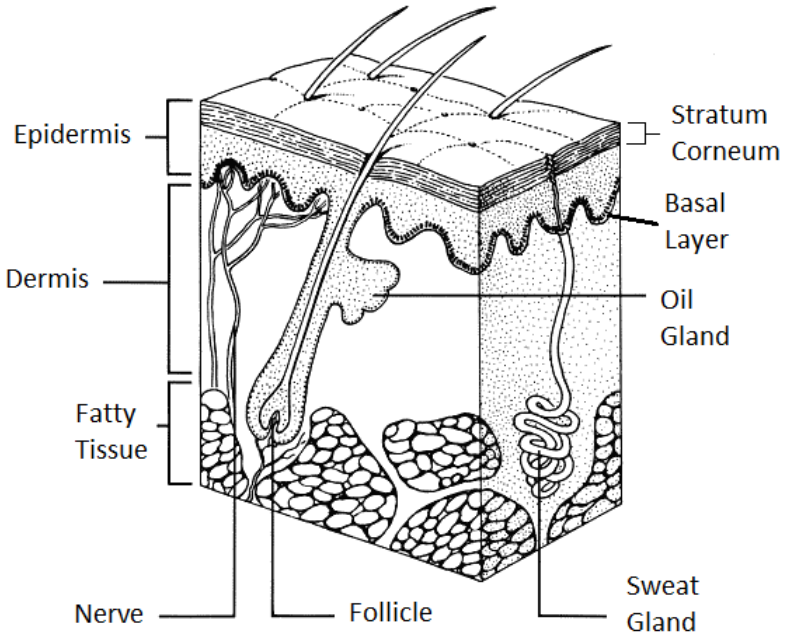


Figure 4.2: The skin has two layers: the epidermis and the dermis, below which lies subcutaneous tissue. (Source: Adapted from the National Cancer Institute) [6].

The epidermal layer thickness can vary based on anatomical location and ranges between 20 $\mu$m and 150 $\mu$m [12, 128, 220]. The epidermis consists of layers of keratinocyte cells that progressively become cornified to develop a resilient tough exte-

rior [163]. The basal epidermal layer is comprised of melanocytes that produce the pigment melanin and transported by melansomes [171].

The dermis is situated directly underneath the epidermis. It is much thicker than the epidermis, approximately 1 – 3mm [11, 12]. The dermis also propagates and absorbs light, and it is mostly comprised of dense, irregular connective tissue with nerves and blood vessels. The main absorber in the dermis is haemoglobin. Absorption of both oxyhaemoglobin and deoxyhaemoglobin have absorption peaks in blue (400 – 420nm), and green-yellow range (540 – 577 nm), and decrease gradually for longer wavelengths. Deoxyhaemoglobin has its highest absorption peak at 420nm, and a second peak at 580nm. Oxyhaemoglobin shows its highest absorption peak at 410nm, and two secondary peaks at 550 – 600nm range. The intensity of absorption directly depends on the volume fraction of tissue occupied by haemoglobin 0.2 – 7% [128]. The blood volume fraction in the cutaneous blood content (in the dermal papillae about 100 – 200 $\mu$m from the surface) is about 2 – 5%, while in other parts of the dermis the volume fraction is much lower [12]. A simplified schematic used in the MCRT model is shown in Figure 4.3.

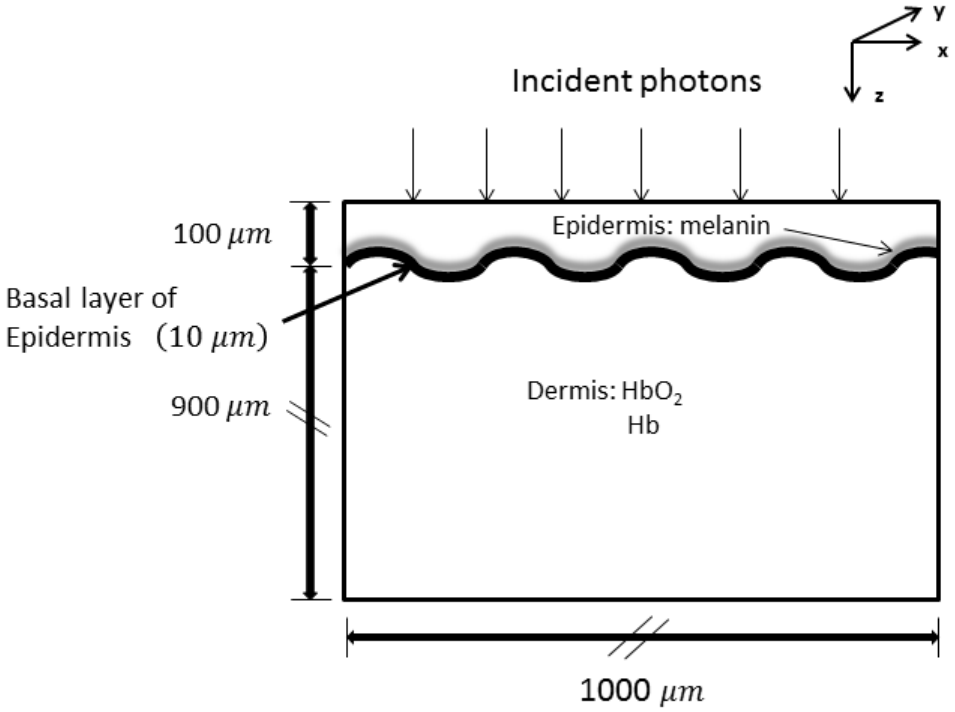


Figure 4.3: Skin layer schematic with chromophores.

Other blood derived pigments, bilirubin and carotenoids, are responsible for the yellowish and olive hue in basic skin tan. Beta-carotene and lycopene have absorption peaks at 488 and 515nm, respectively, and bilirubin at 460nm. However, the contribution of these blood chromophores are negligible in the UV range [55]. Further light absorption by other tissue chromophores that may contribute to the the range of sunbed UV absorption include: epidermal nucleic acids (peak at 260nm) and urocanic acid (peak at 277 nm) [115]. However, these epidermal chromophores are usually surpassed by the absorption of melanin and weakly absorb in the UVA region.

Melanin is produced by cells called melanocytes embedded in one of the epidermis constituent layers and it is found in organelle particles called melanosomes. According to Pathak and Fitzpatrick (1976) [215], melanin and the distribution of melanosomes in the epidermis are the most important factors in the protection of human skin from the effects of UVR. The epidermal absorption coefficient directly depends on the volume fraction of epidermis that is occupied by melanosomes (1.3 – 43%) [129].

### 4.3.1 Epidermis

The dominant chromophore in this layer when dealing with UV is melanin. New cells are generated in the stratum basale. These cells gradually migrate up into the stratum spinosum and into the stratum granulosum. The stratum granulosum contains granules of keratohyalin, which are involved in the keratin formation. In this layer the nuclei and other cell components including melanin start breaking down. The epidermis without the stratum corneum upper layer has scattering and absorption coefficients that are lower than those for the stratum corneum but still appreciably higher than for most other tissues.

As mentioned absorption in the epidermis is primarily due to the UV absorbing chromophore melanin and flesh. Thus, the absorption coefficient, $\mu_{a,epi}$, in the epidermal layer can be expressed as the following [128]:

$$\mu_{a,epi}(\lambda) = \mu_{a,mel}(\lambda)V_m + \mu_{a,base}(\lambda)(1 - V_m) \tag{4.6}$$

where $V_m$ is the volume fraction of melanosomes and $\mu_{a,base}(\lambda)$ is the background human non-melanised tissue give by:

$$\mu_{a,base}(\lambda) = 7.84 \times 10^8 \lambda^{-3.255} \tag{4.7}$$

The scattering on the epidermis is caused by inhomogeneities such as collagen fibres and intracellular structures. The scattering optical properties are derived from published data [25,39,217]. The results for the absorption and scattering coefficients for the UVB and UVA range are displayed in Figure 4.4 .

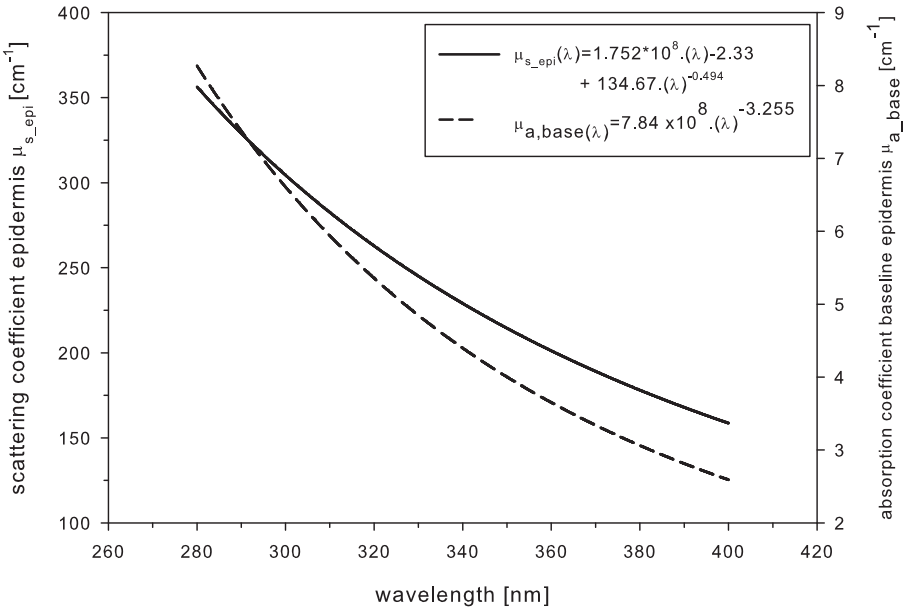


Figure 4.4: Epidermis scattering coefficient and baseline absorption coefficient without melanin.

While the epidermal layer absorption coefficient can be derived from the above equations. Another method of obtaining the epidermal optical properties *in vivo* is by a techniques called photoacoustics. This method uses a pulsed laser light, which is then scattered within the skin tissue. Owing to local expansion "heat" the pressure wave can be detected by a transducer similar to ultrasound. Meinhardt

*et al.* obtained absorption coefficients for different skin phenotypes: I – IV [189]. However, the absorption coefficients were measured only in the range from 290 – 331 nm. So an extrapolation technique was employed using a Weibull curve fit following the shape profile from Diffey *et al.* used to mathematically model photon absorption in the skin [68]. The rationale for using the Weibull curve fit is that for low melanised skin below 290nm it is uronaic acid that is the dominant chromophore of UVR which follows a dipping peak shape at UVB-UVC border.

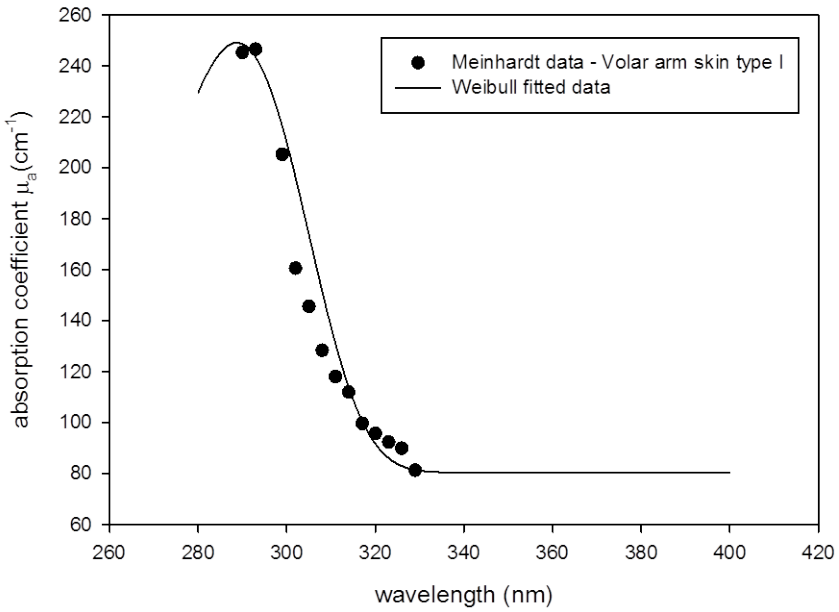


Figure 4.5: Epidermis absorption coefficient.

Skin that is regularly exposed to UV radiation display optical properties different from those located in low exposure areas such as the volar arm. In our model we used low pigmented site of the arm with skin types I – II from the Meinhardt study. The data points for the unpigmented volar arm skin type were extrapolated with Weibull curve fit to include wavelengths 280 – 400nm. The reasoning here is that the Jacques [128] baseline solution only offered a totally non melanised eipdermis which is not the true representation of skin as pigmentation is distributed through. Thus, we use a low pigmented absorption coefficient for epidermis and can control the skin type with the additional melanin layer with the melanosome volume fraction discussed later in this chapter.

The value for the mean scattering cosine, anisotropy factor $g$, is $g \approxeq 0.72$ where $g$ increases with increasing wavelength is published by Van Gemert *et al.* [277]. The equation is established from goniometer measurements and displays good agreement with Bruls *et al.* [39]. The dermal and epidermis $g$ values are considered identical. The experimental $g$ value presented in Figure 4.6 suggest that skin layers are strongly forward scattering media for wavelengths between 280 and 400 nm given by:

$$g_{epidermis \sim dermis} = 0.62 + 0.29\lambda \times 10^{-3} \tag{4.8}$$

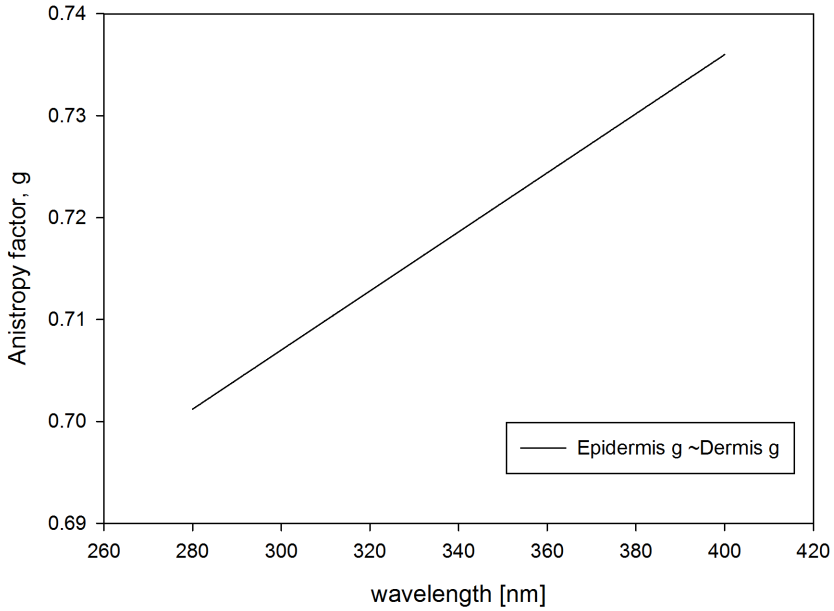


Figure 4.6: Wavelength dependent anisotropy factor $g$ for epidermis and dermis.

### 4.3.2 Dermis

The dermis, located beneath the epidermis, is responsible for the skin's pliability, temperature control and mechanical resistance. The dermis is primarily composed of collagen fibres, nerves, capillaries, and blood vessels, but also contains elastin and fibroblasts. The dermis consists of 70% of collagen fibres, giving it strength and toughness. Elastin maintains normal elasticity and flexibility. The dermis is composed of the papillary and reticular dermal layers. The papillary dermis connects

the lower epidermis tissue layer.

Approximately half of the blood volume is occupied by red blood cells that are responsible for oxygen transfer from the lungs throughout the body. Red blood cells are composed mainly of haemoglobin molecules which reversibly bind to oxygen molecules in the lungs to form oxyhaemoglobin. Haemoglobin is known as deoxyhaemoglobin once it has released its oxygen molecules. Haemoglobin absorption dominates the total absorption in the dermis in the visible range and near-infrared (IR) compared to UV absorption. Since haemoglobin can be either in the form of oxyhaemoglobin or deoxyhaemoglobin, their concentrations can be estimated using the known molar extinction coefficients of biological tissues at different wavelengths [224]. The extinction coefficients for oxyhaemoglobin and deoxyhaemoglobin are displayed in Figure 4.7. Both show peaks around 440nm with deoxyhaemoglobin showing more pronounced peaks at longer wavelengths. The absorption coefficient of the dermis is dominated by blood absorption and the papillary dermis total absorption coefficient was defined as:

$$\mu_{a,dermpap}(\lambda) = (\mu_{a,ohb}(\lambda) + \mu_{a,dhb}(\lambda))V_p + \mu_{a,base}(\lambda)(1 - V_p) \tag{4.9}$$

where:

$\mu_{a,ohb}(\lambda)$ = oxyhaemoglobin absorption coefficient,

$\mu_{a,dhb}(\lambda)$ = deoxyhaemoglobin absorption coefficient,

$V_p$ = volume fraction (%) of the papillary dermis occupied by whole blood $\div$ 100.

The absorption coefficient for oxyhaemoglobin is given by:

$$\mu_{a,ohb}(\lambda) = \frac{(\varepsilon_{ohb}(\lambda))}{66500} c_{hb} \times \mathrm{SO}_2 \tag{4.10}$$

where:

66500 = molecular weight of haemoglobin (g mole$^{-1}$) ,

$c_{hb}(\lambda)$ = haemoglobin concentration (g $L^{-1}$),

$SO_2$ = Oxygen saturation %.

Similarly, the absorption coefficient for deoxyhaemoglobin $\mu_{a,dhb}(\lambda)$ was calculated using molar extinction coefficient $\varepsilon_{dhb}(\lambda)$ and replacing $SO_2$ with $1 - SO_2$ in Equation 4.10.

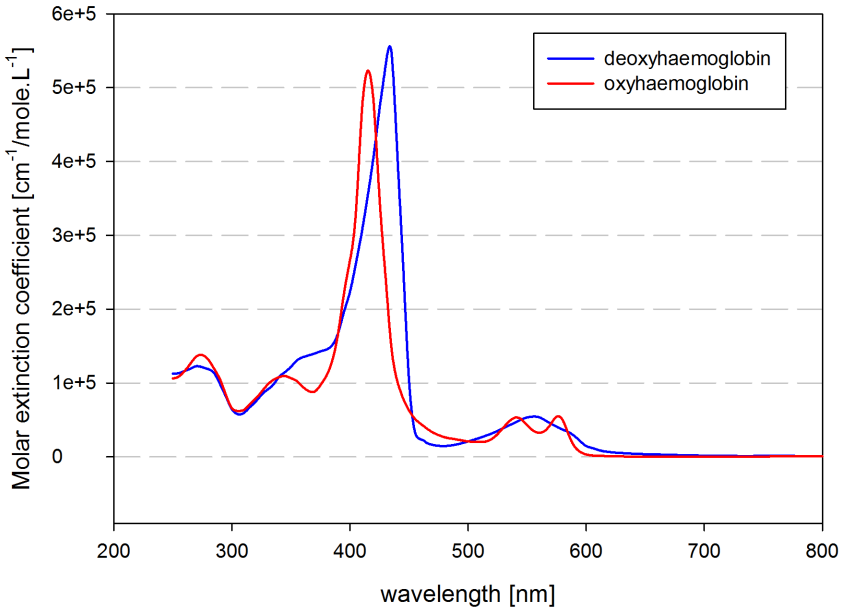


Figure 4.7: Molar extinction coefficient for oxyhaemoglobin and deoxyhaemoglobin reproduced Prahl *et al.* data [224].

According to the literature, oxygen saturation $SO_2$ can range from 20% to 100 % for the dermal layers. In Figure 4.8 the dermis absorption coefficient for two different saturation levels of 50% and 75% are determined [156, 222]. The blood volume percent can also vary in the dermis depending on the location. The papillary absorption coefficients were calculated for different volume percentages [128, 271]. The final papillary dermis parameters used were $Vp$=2% and $SO_2$ = 75% highlighted in red in Figure 4.8.

The dermis scattering coefficients are assumed to be identical [277] to the epidermis and both skin layers adopt the anisotropy derived from $g$ from Equation 4.8.

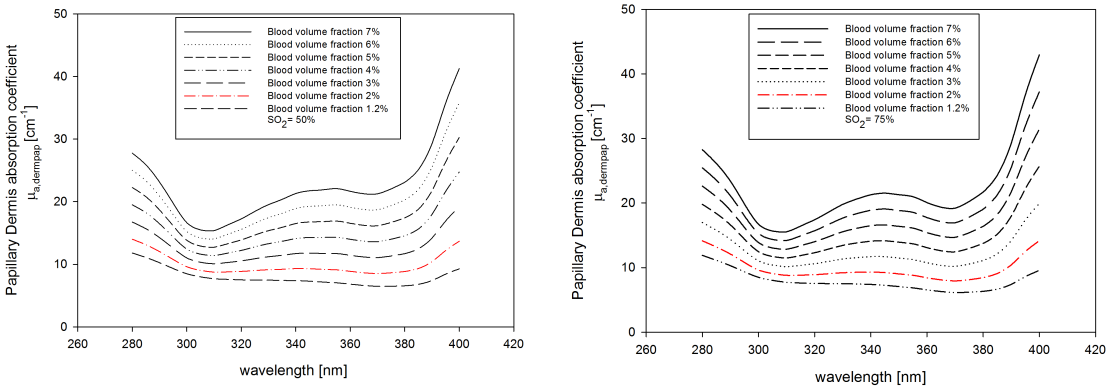


(a) Oxygen saturation 50%

(b) Oxygen saturation 75%

Figure 4.8: Dermis absorption coefficient.

## 4.4 Skin Chromophores

UVR may be transmitted, reflected, scattered or absorbed by chromophores in any skin layer. Absorption is wavelength dependent and is derived from the optical properties of the responsible chromophore. Absorption of UV radiation by a tissue chromophore is a prerequisite for any photochemical or photobiological effect; however, absorption does not necessarily have a biological consequence. The optical properties of a skin layer are affected by the volume content of an acting chromophore. The skin responds to UVR exposure by developing two defensive barriers: thickening of the stratum corneum and the distribution of a melanin filter in cells of the epidermis. The palms and soles are the regions with the thickest stratum corneum, and they are exceptionally resistant to UV damage. The keratins and proteins within the stratum corneum act mainly by scattering and absorbing the UV. The melanocytes containing the melanosomes responsible for the biosynthesis and storing of the melanin are located in the basal layer of the epidermis [54, 67]. In recent studies on skin colour it was established that the number of melanocytes in the epidermal layer was independent of racial skin type [37, 259].

The amount of melanosomes may differ between individuals of the same skin type and even from one anatomical region to the next in the same individual. Differences in skin type are dependent on variations in the size, number and aggregation of

the melanosomes, both inside the melanocytes and keratinocytes, as well as on the distribution throughout the epidermis. Previous histological detections have confirmed the position and distribution of melanin residing around the basal layer [37, 49]. In Figure 4.9 the melanin content in the basal layers of the epidermis is substantially higher in black skin compared to Asian or white skin, although the number of melanocytes is virtually identical in skins of different ethnicity.

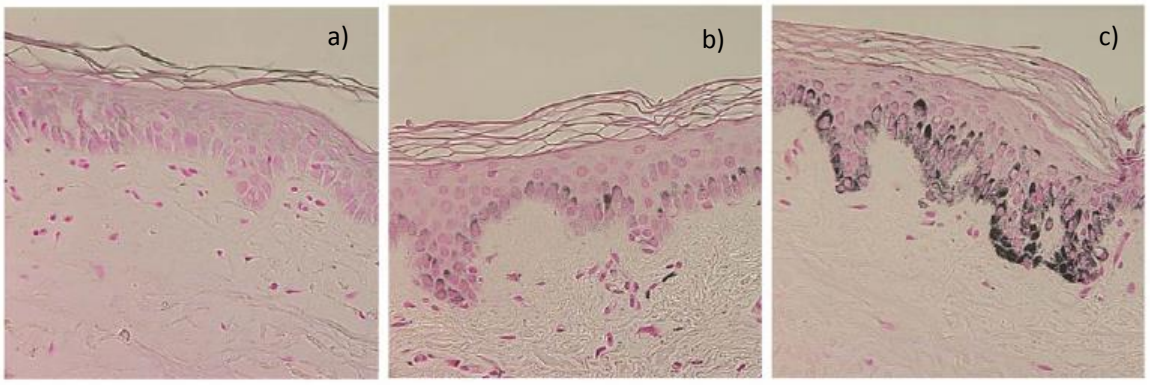


Figure 4.9: Melanin content in the basal layers of the epidermis for different skin types a) Caucasian, b) Asian and c) black [37].

### 4.4.1 Melanin

Melanin is a highly effective UVR absorbing chromophore and occurs in skin and hair. It is a biological polymer and is derived from the oxidation of the amino acid tyrosine [232]. The name 'melanin' originates from the ancient Greek *melanos*, meaning 'dark'. Human skin exists in a wide range of different pigmentation, ranging from white to brown to black, which is due to the presence of melanin, which is produced by melanocytes that branch up from the basal layer.

Melanin plays an essential role in shielding the body against harmful UV radiation from environmental sources and sunbed exposure. We have to consider melanin in our optical properties as it is the dominating chromophore in the UV region. Melanin resides mostly around the basal layer of the epidermis for skin types I – III and the suprabasal layer for skin types III – VI.

There are two types of melanin: the red/yellow phaeomelanin and a brown/back

eumelanin. Their absorption spectra are high in the UV wavelengths and tails off in the visible wavelengths, with higher values for shorter wavelengths in the UV range as seen in Figure 4.10. The ratio between the concentration of phaeomelanin and eumelanin present in human skin varies from between individual's, with much overlap between skin types. Upon UV irradiation pheomelanin exhibits higher pro-oxidative effects [13], whereas eumelanin is suggested to possess no phototoxic potential [14].

The primary and most vital function of eumelanin in the human epidermis is protection against damage caused by UV radiation [37]. Eumelanin absorbs and scatters UV photons, thus reducing the amount of damage caused to important biomolecules and structures within and below the dermis [149, 192, 196, 207, 297]. The greatest evidence in support of the photoprotective role of eumelanin stems from studies examining the regulation of its production and its location within the skin, in supranuclear melanin caps within keratinocytes that are located in the supra basal layer. Exposure to UVR upregulates production of eumelanin through the immediate and delayed tanning responses, which results in darkening of the skin and enhanced photoprotection [229].

Paradoxically, although melanin is a photo-protective it has also been associated in the chain of events that lead to malignant melanoma [76, 191], although this link is very poorly understood. Highly pigmented skin is more protected from carcinogenesis than unpigmented skin [171], but it has been suggested that pheomelanin may actually function as a photosensitizer [145], and has been shown to actually enhance DNA damage in cells in response to UVR [246, 284]. The skin is the most common location of cancer in humans [171], and although melanoma is one of the rarer types of skin cancer, it causes the majority of skin cancer related deaths [35].

The first possible link between pheomelanin and carcinogenesis involves pheomelan in generating ROS. Pheomelanin is known to generate ROS when irradiated with UVA [177]. Although the mechanism of pheomelanin mediated ROS generation is not thoroughly understood, pheomelanin seems to be unique in its ROS generation ability when compared with eumelanin.

The variation in skin colour among different races and ethnicities is determined mainly by the number, melanin content, and distribution of melanosomes produced and transferred by each melanocyte to a cluster of keratinocytes surrounding it. The melanin absorption level depends on how many melanosomes per unit volume are in the epidermis. Typically, the volume fraction of the epidermis occupied by melanosomes varies from 2.55 – 13.5% (lightly to highly pigmented skin types) as noted in Table 4.1 [128].

The total absorption coefficient for each layer is the sum of the absorption coefficient for each pigment present in the layer, which is obtained by multiplying the pigment's spectral molar extinction coefficient by its estimated concentration in the layer. The spectral molar extinction coefficients for these pigments, denoted $\varepsilon_{eu}(\lambda)$ and $\varepsilon_{ph}(\lambda)$ respectively, are obtained from the curves shown in Figure 4.10.

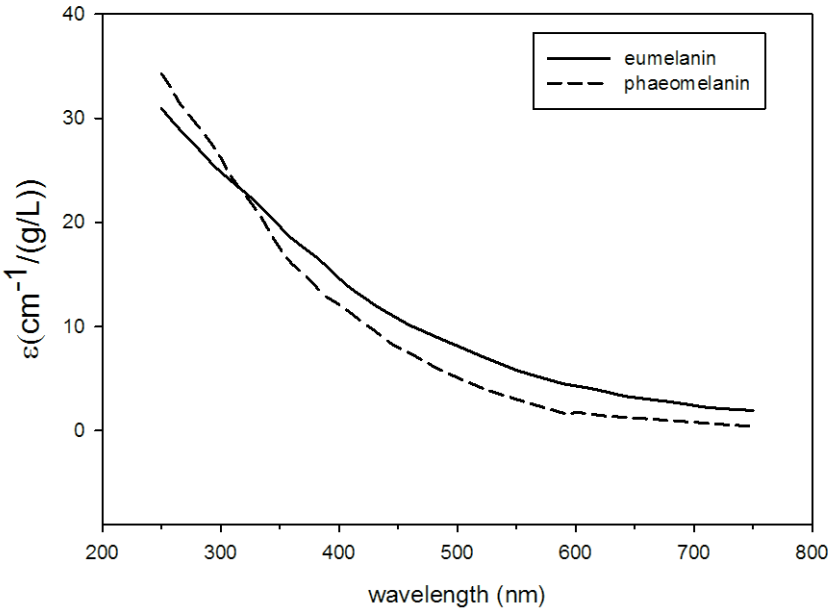


Figure 4.10: Spectral molar extinction coefficient $\epsilon$ curves for the melanin chromophores present in skin tissues. Courtesy of S. Prahl and the Oregon Medical Laser Center (OMLC) [224].

The total melanin absorption coefficient is expressed in Equation 4.11:

$$\mu_{a,mel}(\lambda) = (\mu_{a,eu}(\lambda) + \mu_{a,ph}(\lambda))V_m \tag{4.11}$$

where:

$\mu_{a,ph}(\lambda)$ = phaeomelanin absorption coefficient, ($\mathrm{cm}^{-1}$)

$\mathrm{V}_m$ = volume fraction (%) of the epidermis occupied by melanosomes $\div$ 100.

The absorption coefficient for eumelanin is given by:

$$\mu_{a,eu}(\lambda) = (\varepsilon_{eu}(\lambda)c_{eu}(\lambda)) \tag{4.12}$$

where:

$c_{eu}(\lambda)$ = eumelanin concentration ($\mathrm{gL}^{-1}$).

Similarly, the absorption coefficient for phaeomelanin $a_{ph}(\lambda)$ is calculated by multiplying its spectral molar extinction coefficient $\varepsilon_{eu}(\lambda)$ by its concentration $c_{eu}$.

The model parameters for eumelanin and pheomelanin concentrations in the epidermis are $80\mathrm{gL}^{-1}$ and $12\mathrm{gL}^{-1}$, respectively [143]. The eumelanin and pheomelanin concentrations were retained at the above values for all skin types, while the value volume fraction of the melanosomes was varied according to skin type. Thus, the melanin ($\mathrm{mg\,mL}^{-1}$) in the epidermal layer was calculated by multiplying the total melanin $92\mathrm{gL}^{-1}$ concentration by the the volume fractions. $C_{mel}$ is the total melanin concentration in the epidermis calculated by total of $c_{eu}$ and $c_{ph}$ and multiplying the result by the volume fraction Vm.

According to the data reported by Jacques [129], the volume fractions of melanosomes based on the whole skin epidermis are 1.3 – 6.3%, 11 – 16% and 18 – 43% for lightly,

Table 4.1: Volume fraction of melanosomes for different skin types and corresponding melanin concentrations.

| Fitzpatrick (estimate) skin type | Volume fraction % melanosomes | Melanin concentration (mg $mL^{-1}$) | Reference |
|---|---|---|---|
| I | 2.55 | 2.34 | [143] |
| I-II | 3.8 | 3.49 | [129] |
| II-III | 5.2 | 4.77 | [156] |
| III | 8.45 | 7.76 | [129] |
| IV | 13.5 | 12.4 | [129] |

moderately and heavily pigmented skin, respectively. As a result, the corresponding average values are 3.8%, 13.5% and 30.5%. However, these values were initially overestimated and a true value corresponds to a melanosome volume fraction Vm range 1.3 – 16% [127,143]. For this work it was considered that the epidermal melanin only filled the basal layer of epidermis, and the remaining areas of epidermis were without melanin. The skin geometry used here included a 10$\mu$m melanin layer, 10$\mu$m thick basal layer of epidermis and an 80$\mu m$ thick low pigmented layer of epidermis, the volume fractions of melanosomes in the basal layer of epidermis were initially setup for skin type I. Figure 4.11 shows the melanin absorption coefficients are displayed for different melanin concentrations, volume fractions and corresponding skin types.

### 4.4.2 DNA Absorption

DNA absorbs highly in the UV and has a maximum wavelength absorbance around 260nm. This is due to the presence of the nitrogenous bases (A,G,C and T). Specifically, DNA absorbs wavelengths of between 245 and 290 nm [269], i.e. the UVC and, to a lesser extent, UVB. This UV absorption by DNA provides the energy needed for covalent binding of adjacent pyrimidines.

#### DNA Thymine-Adenine

Since DNA is the region where carcinoma originates knowledge of the photon absorption in this location is important in order to quantify lesion formation more

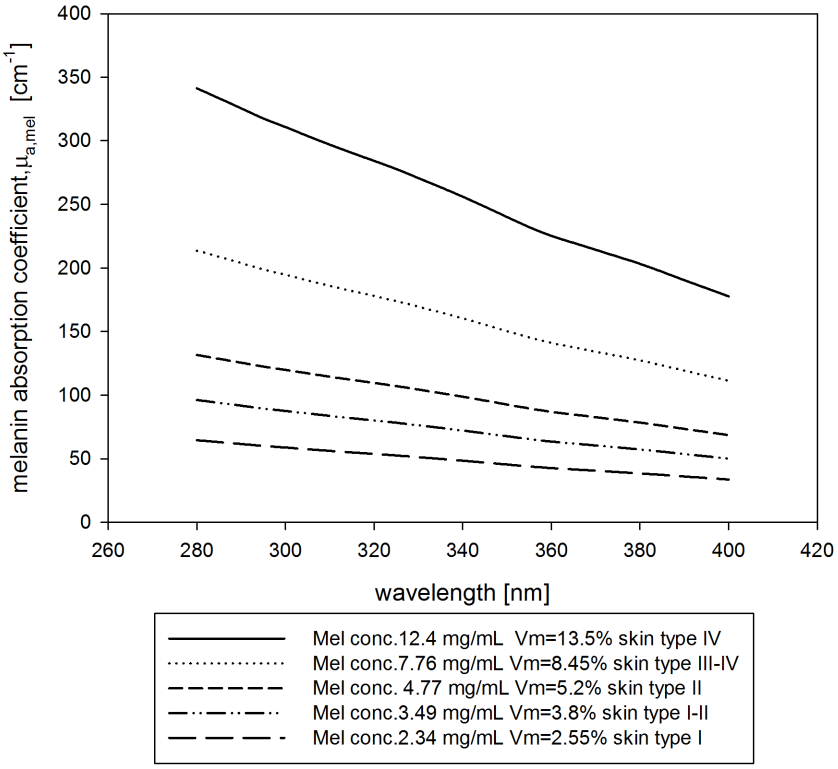


Figure 4.11: Melanin absorption coefficient for various melanin concentration and corresponding volume fraction of melanosomes.

specifically CPDs. Thus, the amount of absorbed photons in the DNA layer needs to be determined. One of the challenges in determining the DNA absorption coefficient, $\mu_{a,DNA}$, is that most published literature focused on 260nm or 280nm wavelengths, the peak DNA absorption for single strand DNA (ssDNA) and double stranded DNA (dsDNA) DNA, for cuvette absorbance (OD) for certain DNA concentrations [43]. Direct measurements of nucleic acid samples at OD260 or protein samples at OD280 can be converted to concentration using the Beer-Lambert law, which relates absorbance to concentration using the pathlength of the measurement and an extinction coefficient. Generally, these standard coefficients are used in place of the extinction coefficient for dsDNA, single stranded RNA, and ssDNA. However, the purpose of this model was to investigate the UV absorption coefficient from all bases in human genome.

One solution for this was to employ the extinction coefficient for an oligomeric duplex $dA_{20} : dT_{20}$, which has been used to determine photo-damage in DNA [41].

The photochemical properties of the DNA duplex $dA_{20} : dT_{20}$ are comparable to those of the DNA single strands. It has been demonstrated that base pairing increases the probability of absorbing UVA photons [23].

Thus, it was possible to use the wavelength dependent molar extinction coefficient of the duplex $dA_{20} : dT_{20}$ with DNA concentration to determine the DNA absorption for our model. To calculate the DNA absorption coefficient we incorporate the Beer-Lambert's Law from Equation 4.4:

$$\mu_{a,DNA}(\lambda) = \epsilon\, C \tag{4.13}$$

where $\epsilon$ is the molar extinction coefficient provided by Mouret *et al.* [204] and C is the concentration of DNA. The DNA concentration is derived from the method employed by Mohlenhoff *et al.* using $6.6 \times 10^9$ bases for human DNA [198].

In order to calculate the the DNA concentration from first principals a good understanding of genome is required. The genome is all the genetic material in the chromosomes of a particular organism. In eukaryotic cells (diploid cells), the term "nuclear genome" is sometimes used to refer to the genetic information in the nucleus (this is to distinguish the genes in the nucleus from those in eukaryotic organelles, like mitochondria). The amount of DNA which corresponds to the size of one diploid genome (C value). The genome size is generally given as the total number of base pairs. For humans, that number is about 3 billion base pairs per haploid genome, that is, in a sperm or egg. In somatic cells, which are diploid, the number of basepairs is doubled. For calculating the number of bases for the equation we multiply the number of basepairs $6.6 \times 10^9$ by 2. The average size of nucleus is approximately $10\mu$m in diameter where all the DNA information is compacted as seen in Figure 4.12 [86].

By using the volume of a sphere and the average radius for a diploid cell it is possible estimate the total volume occupied by human genomic DNA.

$$V = \frac{4}{3}\pi r^3 \tag{4.14}$$

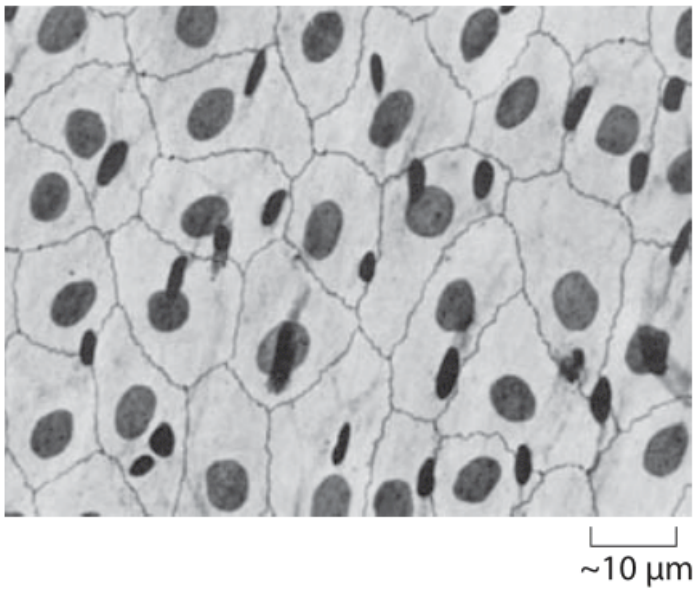


Figure 4.12: Light microscopy image of a human epithelial sheet. The dark ovals are the cell nuclei stained with silver. Adapted from electron micrograph from D. W. Fawcett, The Cell, Its Organelles and lnclusions: An Atlas of Fine Structure [86].

$$V_{nucleus} = \frac{4}{3}\pi(5 \times 10^{-6})^3$$

$$V_{nucleus} \approx 10^{-13}\,\mathrm{L}$$

Thus, assuming the above nuclear volume and using human DNA length of $1.32 \times 10^{10}$ bases based on average diploid cell the concentration C of DNA can be derived from Equation 4.15

$$C = \left(1.32 \times 10^{10} \,/\, 6.023 \times 10^{23} mol^{-1}\right) / \, 10^{-13}\,\mathrm{L} \tag{4.15}$$

$$\approx 0.22M$$

using a C = 0.22 M in Equation 4.13 and the molar extinction coefficient $\epsilon$ for oligonucleotide [204], it is possible to calculate the absorption coefficient of DNA. The DNA absorption coefficient for the UV wavelength range 280 – 400nm is displayed below in Figure 4.13 for C = 0.22 M.

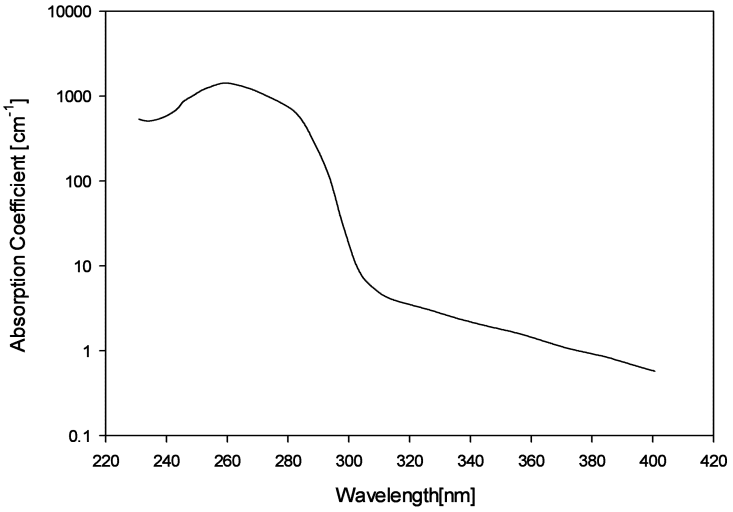


Figure 4.13: Chromophore absorption coefficient spectrum of oligonucleotide DNA complex $dA_{20} : dT_{20}$ for concentration C=0.22 M derived from *Mouret et al.* [204].

The DNA concentration per nucleotide determined by absorption spectroscopy using the molar absorption coefficient at 260nm as 6600 $M^{-1}cm^{-1}$ [230] is in good agreement with oligonucleotide DNA complex $dA_{20} : dT_{20}$ extinction coefficient at 260nm. The absorption spectrum of the $dA_{20} : dT_{20}$ duplex as shown in Figure.4.13 exhibits a long-wavelength tail over the UVA range.

Most investigations in the past have focused on UVB, but the longer UVA wavelengths have had less emphasis. This may be due to the fact that individual bases do not absorb UVA radiation.

However, there have been studies that demonstrate that this is not the case for oligonucleotide duplexes, which show a weak absorption tail above 300nm [204, 255]. Furthermore, it has been revealed that absorption of UVA radiation by natural isolated, genomic and oligonucleotide DNA leads to the production of mutagenic CPDs [79, 95]. This is an important issue because UVA photons are much more abundant than those of UVB when considering a solar or sunbed radiation [75].
Also please note the diploid DNA absorption coefficient is assumed to be a monolayer

just below melanin layer at the basal layer shown in Figure 4.3.

In the next section we see how we can incorporate these optical properties in the MCRT model to simulate the fate of a photon as it propagates through the tissue turbid media. We then can see how many photons are scattered and absorbed with different chromophores including DNA.

## 4.5 Reflection and Refraction

When light traverses a boundary with differing refractive indices, the light is partly reflected back from the surface. This reflection is called specular or Fresnel reflection.

On entry into, and exit from, the grid a photon will undergo specular reflection and refraction at the air tissue boundary. The refraction of light traversing from one medium to another can be calculated from Snell's law:

$$n_i \sin\theta_i = n_t \sin\theta_t \tag{4.16}$$

where $\mathrm{n_i}$ and $\mathrm{n_t}$ are the refractive indexes of medium one and two, respectively, $\theta_i$ is the angle of incidence and $\theta_t$ is the angle of transmission.

In traversing from a medium with a high refractive index to one with a lower refractive index, total internal reflection occurs for angles larger than the critical angle, $\theta_c = \arcsin\left(\frac{n_i}{n_t}\right)$. Therefore, any light radiated on the tissue–air boundary greater than 46.43° will be reflected back into the tissue.

To account for specular reflection at the surface we can adopt the formula for for Fresnel reflection, expressed as:

$$R\left(\theta_i, \theta_t\right) = \frac{1}{2}\left[\frac{\sin^2(\theta_i - \theta_t)}{\sin^2(\theta_i + \theta_t)} + \frac{\tan^2(\theta_i - \theta_t)}{\tan^2(\theta_i + \theta_t)}\right] \tag{4.17}$$

The probability of whether a photon is internal reflected or transmitted is determined by a random generated number (RGN) in the code. If $\xi < R\left(\theta_i, \theta_t\right)$ the photon is internally reflected, otherwise the photon is transmitted, where $\xi$ is RGN. This permits the MCRT model to account for photons that escape the tissue–air

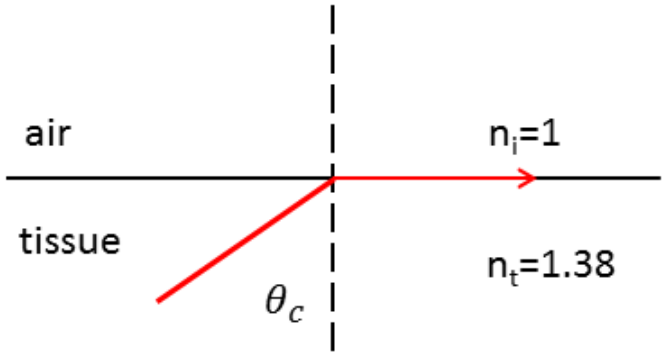


Figure 4.14: Refractive index of air tissue boundary.

interface or are reflected back and continue on random path-length with updated position and direction. This will be discussed more in Chapter 5.

Reflection of light on the skin surface occurs on the account of differences in refraction indices between the air (1.0) and the corneal layer (1.38) displayed in Figure 4.14. Equation 4.17 illustrates the proportion of light that is reflected and refracted (transmitted towards deeper layers) on the air–skin interface, as functions of incident angle of light and refractive index of the medium from which the light beam approaches the skin (air usually) and the medium that further transmits the light (incident and transmissive medium). When the incident angle is close to normal ($\geqslant 40°$) about 5% of light is directly reflected from the corneal layer surface, and the remaining 95% enters the epidermis [12]. The reflected light does not interact with the deeper tissue layers and is not colour-modified by skin chromophores.

The skin model maintains a single refractive index value for all skin layers because there is negligible difference between layers, also we do not compensate for the sebum effect at the surface. The presence of sebum smooths the roughness of the skin surface and leads to a higher refractive index (1.5) increasing the amount of light reflected off the air-sebum interface, and accentuates the appearance of shine [169].

In the next chapter we implement the established optical properties in multilayer skin structure using the Monte Carlo technique.

# Chapter 5

# Monte Carlo Radiative Transfer Model

## 5.1 Introduction

The Monte Carlo method was first used for what are essentially experiments on random numbers (random sampling) in 1944. However, long before then Monte Carlo type techniques were sporadically applied. One of the first applications in the second half of the nineteenth century can be considered to be 'Buffon's needle problem', where a needle is thrown a large number of times onto a set of equally spaced lines on a board to find the value of Pi [114].

In the 1940s random sampling became a widely used technique. The technique was applied to work on the atomic bomb, where the random diffusion of neutrons in fissile material was modelled. This was also the time the phrase 'Monte Carlo' originated. This statistical approach is credited to Ulam and Metropolis, who refined the original direct simulations with various variance reduction techniques [193]. The first use of Monte Carlo techniques for the modelling of light transport in tissue was reported in 1983 by Wilson and Adams [291].

Light propagation can be considered as a stream of particles, each with a localised quantum of energy (photons). Photon transport through turbid media can

be mathematically expressed by the RTE (Equation 1.5). RTE is derived by considering the energy balance of incoming, outgoing, absorbed and emitted photons of an infinitesimal volume element in the medium described in Chapter 1.

The Monte Carlo method, as applied to the transport of light radiation is based on the RTE and involves computer-simulated calculations of photon propagation in scattering media. The MCRT model was programmed in Fortran 77 and simulations were performed on a computer with a processor Intel quad core i7 3632QM speed of 2.2 GHz, with each simulation taking approximately 5 minutes to complete 8 million photon simulations.

The MCRT model used throughout this research was based on a three dimensional (3-D) cube shaped geometry [294, 295] and removed the assumption of an optically semi-infinite tissue volume. Simulations were performed on a 3-D Cartesian grid divided up into 101 x 101 x 101 grid cells. Each grid cell was represented by a 3-D array location (i, j, k) and could be assigned varying wavelength-dependent optical properties. The optical properties are characterised by $\mu_a$, $\mu_s$, g and n , as described Chapter 4.

The Monte Carlo method permits the usage of complex and detailed models, while retaining simple implementation. The disadvantages of the Monte Carlo method are noise introduced by the stochasticity and long simulation time when high accuracy is needed.

## 5.2 Probability distributions

Probability distributions are the core of the MCRT modelling. The "random walk" of photons as they propagate down through turbid medium may be determined by pseudo-random computer generated number. In order to sample quantities of scattering angles and photon lengths it is possible to incorporate the use of probability distribution functions (PDFs).

By randomly sampling from PDFs using cumulative distribution functions (CDFs), variables such as optical depths (described in next section) and photon scattering

directions may be randomly chosen at interaction sites, enabling the position, direction and path of a photon to be determined. To ascertain the random walk of a photon, certain random variables such as the path length between two scattering events or the scattering angle, must be assigned at every interaction site. Therefore, variables are sampled randomly from the probability distribution function P(x), which defines the distribution of the variable x over the interval [a $\leq x \leq$ b], where

$$\int_a^b P(x)dx = 1 \tag{5.1}$$

Then the sampled, $x_i$, where i = 1,2,3...n is randomly generated numerous times based on a pseudo-random generator, which generates a random number $\xi_i$,

$$\int_a^{x_i} P(x)dx = \xi_i \tag{5.2}$$

where $\xi_i$ is generally uniformly distributed over the interval [0,1].

By inverting the CDF it is possible to solve for $x_i$. The values on the x-axis can be obtained from taking the inverse of the function $x = F^{-1}(\xi)$ seen in Figure 5.1.

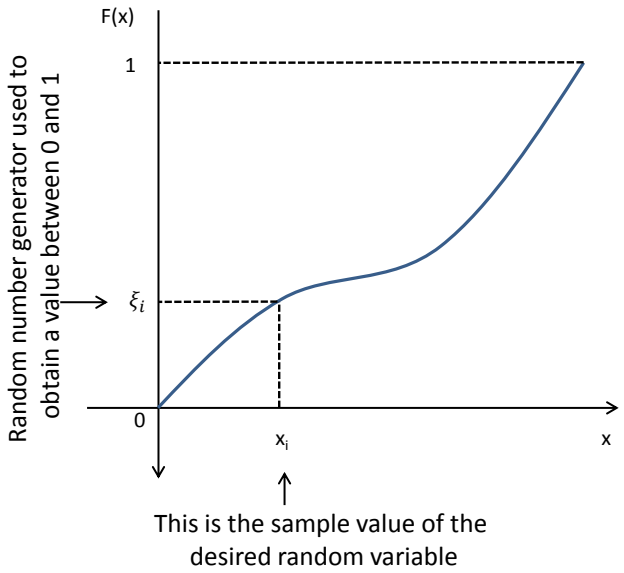


Figure 5.1: Illustration of the inverse method.

These are the fundamental equations for the MCRT method, which depends on pseudo-random numbers. By implementing these equations it is possible to

randomly sample the optical depth, $\tau$, the albedo, a, and the scattering angles - cosine of the deflection angle, $\theta$ and the azimuthal angle, $\psi$.

### 5.2.1 Turbid Media

The manner in which skin reflects and transmits radiation of different wavelengths is determined by the inherent optical properties of the skin layers derived in Chapter 4. Each of these layers has different inherent optical properties, primarily due to differences in the concentration of melanin and blood. In an event driven simulation the trajectory of a photon moving in a turbid medium has the probability of travelling a distance S without interaction according to $\exp(-\tau)$, where $\tau = \mu_t \mathrm{S}$ and $\mu_t^{-1}$ is the total mfp described in Equation 4.2.

The optical depth $\tau$ of a layer is the integrated attenuation coefficient of a beam going perpendicularly through that layer. Light can be attenuated either by absorption or by scattering into another direction. Physically, the optical depth $\tau$ over a distance S in a given direction is the number of photon mean free paths (mfps) over that distance. In general the optical depth is expressed as

$$\tau = \int_0^{\mathrm{S}} \mu_t d\mathrm{s} \tag{5.3}$$

where $\mu_t$ is the total attenuation coefficient and S is the physical distance to an interaction site.

To randomly sample an optical depth, $\tau$ the following applies

$$P(\tau) = e^{-\tau} \tag{5.4}$$

By randomly sampling many $\tau$, it is possible to deduce $e^{-\tau}$

$$\xi = \int_0^{\tau} e^{-\tau} d\tau = 1 - e^{-\tau} \tag{5.5}$$

By solving for Equation 5.5 yields

$$\tau = -ln(1 - \xi)$$

Substituting $\xi$ for $(1 - \xi)$ for range [0,1] gives

$$\tau = -ln\,\xi \tag{5.6}$$

where $\tau$ is the optical depth and $\xi$ is a random number between [0,1]

Therefore, having sampled a random optical depth in the model it is possible to derive the total physical distance $S$ that the photon travels from Equation 5.3. The step size of the photon is calculated based on sampling the probability for the photon's MFP. The photon is moved a propagation distance $\Delta$s which is calculated by RNG $\xi$. Thus, Equation 5.6 can be rearranged to provide a means of selecting step size:

$$\Delta s = \frac{-ln(\xi_i)}{\mu_t} \tag{5.7}$$

After a photon has traversed a random optical depth , $\tau$, it can be either scattered or absorbed. This eventuality occurs depends on the albedo, a, which is simply the probability that a photon is scattered (and not absorbed):

$$a = \frac{\mu_s}{\mu_t} \tag{5.8}$$

where $\mu_t = \mu_a + \mu_s$ is the total attenuation coefficient and $\mu_s$ is the scattering coefficient coefficient. Thus, for $\xi <$a the photon is scattered. Otherwise, the photon is absorbed.

## 5.3 Phase Function

One of the imperative aspects in Monte Carlo simulations is to define the new photon direction after each scattering event. The phase function is the probability that a photon will be scattered from one direction to another. The name is misleading since the scattering has no connection with the phase of the incident light waves and would be more appropriately called a scattering function.

The phase function first mentioned in Equation 1.5 describes the angular distribution for a single scattering event and is usually assumed to be a function only of the angle between the incident $\hat{s}$ and scattered $\hat{s}'$ directions (Figure 5.2). If the integral(over all angles) of the phase function is normalised to equal one, then $p(\hat{s}, \hat{s}')$ is the PDF for scattering from direction $\hat{s}'$ to direction s seen in Figure 5.2.

$$\int_{4\pi} (\hat{s}, \hat{s}') d\Omega' = 1 \tag{5.9}$$

where $4\pi$ steradians in a complete sphere.

The phase function will differ from photon to photon. For simplicity an average phase function which adequately describes the most important features of the scattering process can be used.

Hence, a parameter called the average cosine of the phase function is used to describe the degree of anisotropy of the phase function. This parameter is often denoted by $g$ and is defined below in Equation 5.10

$$g = \langle \cos\theta \rangle = \int_{4\pi} (\hat{s}' \cdot \hat{s}) P(\hat{s}' \cdot \hat{s}) d\Omega \tag{5.10}$$

Many estimates of the tissue phase function are used. But one of the most common is the Henyey-Greenstein phase function [105,132]. The Henyey-Greenstein phase function was first used for describing scattering of starlight off dust grains in interstellar medium, but it is shown to be suitable also for describing scattering in skin and other biological tissues.

The probability distribution for the cosine of the deflection angle, $\cos\theta$, is de-

scribed by the Henyey-Greenstein phase function in Equation 5.11:

$$p(\theta) = \frac{1}{4\pi} \frac{1 - \mathrm{g}^2}{(1 + \mathrm{g}^2 - 2\mathrm{g}\cos\theta)^{3/2}} \tag{5.11}$$

where the parameter g is defined as the integral over all angles of the phase function multiplied by the cosine of the angle $\theta$.

The anisotropy factor g varies in the range from 0 to 1: $g = 0$ relates to isotropic scattering. In pure forward scattering media, $g = 1$ and $g = -1$ in the case of pure backward scatter. All three cases are depicted in Figure 5.2. The anisotropy range for human skin is often: $g \in [0.7 - 0.95]$ [105, 271]. The anisotropy factor for skin tissue is wavelength dependent with a typical value of $g \approx 0.7$ [277].

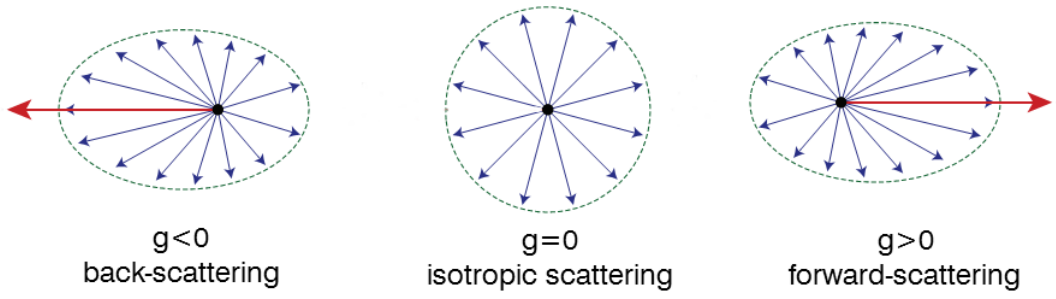


Figure 5.2: The anisotropy factor, $g$, describes the angular distribution of light scattering at any point x within turbid media. In the simplest case, light is scattered equally in all directions (centre). Light is preferentially scattered in the backward (left) or forward (right) direction.

### 5.3.1 Photon Scattering

The PDF for the scattered cosine of the deflection angle $\cos\theta$ in tissue is characterised by the Henyey-Greenstein phase function. The first order of function of the Henyey-Greenstein function in Equation 5.11 is a good approximation of scattering in skin. Hence we can sample the angle directly from Equation 5.11 which is an exact distribution of the incident radiation:

$$\cos\theta = \frac{1}{2g}\left\{1 + g^2 - \left[\frac{1-g^2}{1-g+2g\xi}\right]^2\right\} \text{ if } g \neq 0 \tag{5.12}$$

The scattering of a photon is represented by two angles; the deflection angle $\theta$ and the azimuthal angle, $\psi$ depicted in Figure 5.3. For isotropic scattering, $\cos\theta$ is sampled over the interval range : [0,$\pi$].

$$\cos\theta = 2\xi - 1; \qquad \text{if } g = 0 \tag{5.13}$$

Next the azimuthal angle, $\psi$, is sampled over the interval : [0, $2\pi$] and may be generated by multiplying a random number $\xi$: [0–1] by $2\pi$.

$$\psi = 2\pi\xi \tag{5.14}$$

Thus, a photon is scattered at angle $\cos(\theta,\ \psi)$. Note phase function has no azimuth dependence.

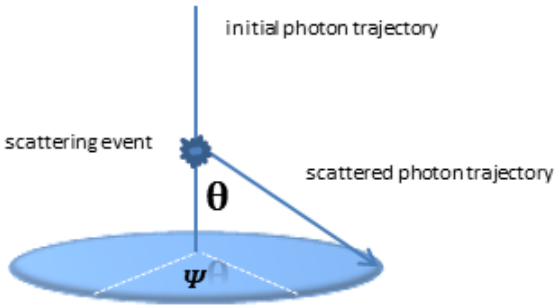


Figure 5.3: The deflection angle, $\theta$ and the azimuthal angle, $\psi$.

Once the deflection angle is chosen, the new direction and the x and y coordinates of the photon can be updated for the next event as in Equation 5.15. To specify the spatial position of a photon in the grid, a Cartesian system is implemented with coordinates (x, y, z). The direction of incident photons is initially specified by the polar angle $\theta$ and the azimuthal angle $\psi$. To facilitate the coordinate transformations that are required, the angles are converted into their corresponding direction cosines $(n_x, n_y, n_z)$. These direction cosines form the components of a vector **n** of unit length

pointing in the direction of the photon. Photons are launched into the grid with initial photon Cartesian coordinates at the origin (x, y, z) and the direction of the cosines of the photon are:

$$n_x = \sin\theta\cos\psi \tag{5.15}$$

$$n_y = \sin\theta\sin\psi$$

$$n_z = \cos\theta$$

Once the deflection $\theta$ and azimuthal angles $\psi$ are chosen, the new direction and the new (x, y,z) coordinates of the photon can be updated. Thus,

$$\mathrm{x} = \Delta\mathrm{x} + \mathrm{n_x ds}, \quad \mathrm{y} = \Delta\mathrm{y} + \mathrm{n_y ds}, \quad \mathrm{z} = \Delta\mathrm{z} + \mathrm{n_z ds}. \tag{5.16}$$

Once the positions are updated the photon continues on it's random walk until another event and may be scattered, absorbed or escape from the grid.

## 5.4 Monte Carlo Radiative Transfer Model

The purpose of MCRT is to provide a numerical solution to the radiative transfer equation (RTE) using the probabilistic nature of photon interactions. The MCRT handles the photons as particles and does not account for the interference or other phenomena associated with the wave nature of light.

The first step is to split the total energy equally amongst the photon packets. Each packet, which has a direction of travel, then carries a fraction of the total energy and these packets are related to the specific intensity $I_v\left(r, \hat{s}, t\right)$ first introduced in chapter 1, section Equation 1.5.

The specific intensity, $I_v$, is defined as the amount of energy $\Delta E_v$ flowing through a unit surface area dA at angle $\theta$ normal to surface area per unit solid angle d$\Omega$ in frequency range $dv$ per unit time dt in units $Wcm^{-2}sr^{-1}Hz^{-1}$.

The total energy rate (power) is also known as luminosity, L, in astronomy may

be divided equally among MCRT photons:packet of energy. Each energy packet, $E_i$ is related to the specific intensity, $I_v$ by the following equation

$$I_v\left(r,\hat{s},t\right)=\frac{\Delta E_i}{\cos\theta dAd\Omega dvdt} \tag{5.17}$$

An energy parcel, $E_i$ may be expressed in units Joules, J, as

$$\Delta E_i=\frac{L\Delta t}{N} \tag{5.18}$$

where L is the luminosity -energy per second ($Js^{-1}$) Watts, $\Delta t$ is the time in seconds and N is the number of MCRT photons.

MCRT photon energy parcels are related to actual number of physical photons, $N_\gamma$, through the subsequent equation

$$N_\gamma=\frac{E_i}{hv_i} \tag{5.19}$$

where $h$ is Plank's constant and $v_i$ is the frequency of the MCRT photon energy packets.

The fluence rate, $\psi(r,t)$ ($\mathrm{Wcm}^{-2}$) first described in Equation 1.6 is related to the voxel photon power( Luminosity) (W) as follows

$$\psi=\frac{L}{N\Delta V}\sum_i S_i \tag{5.20}$$

where N is the total number of photons launched, $\Delta V$ is the volume of the cell and $\sum_i S_i$ is summation of the photon path-lengths in a cell.

When a photon is absorbed it deposits energy in the tissue. Energy deposition is calculated by including the Fluence rate with absorption coefficient component expressed as:

$$Q=\frac{L}{N\Delta V}\sum_i \mu_a S_i \tag{5.21}$$

where Q is the energy absorbed per cubic centimetre per second, L is the energy

per second (Watts), $\Delta V$ is the volume of the cell, $\mu_a$ is the absorption coefficient and $\sum_i S_i$ is summation of the photon path-lengths in a cell.

## 5.5 The MCRT Simulation

As we have seen, it is difficult to know how a single photon will behave in a medium. What is easier to constrain is how an ensemble of N photons behave in terms of their statistical properties. This is ideally suited for Monte Carlo methods. The basic procedure is as follows:

1. Emit N photon packets (hereafter referred to simply as photons)

2. Track the progress of each photon, one-by-one, through the medium. The locations of interaction are found by sampling optical depth $\tau$ from the distribution described in Equation 5.4. The scattering and absorption of the photons are determined by sampling from the albedo and phase functions.

3. Photons are placed into a "bin" array depending on the position in the grid cell. By generating many photons and capturing them in bins it is possible to build up an image (analogous to photons captured on a CCD).

A 3-D grid array is used to describe the four-layer skin model. The model used voxels of $10\mu m$ in each dimension representing the different tissue media types. Each voxel is assigned a voxel type corresponding to the optical properties of that tissue type. For example, in a four-layer skin model , the media types could be epidermis, melanin, DNA or dermis depending on the depth in the grid.

A program schematic illustrates the movement of a photon depicted in Figure 5.4. Each excitation photon packet is launched from the source and migrates through the cubic grid, whilst undergoing scattering or absorption.

The photons were launched down into the grid with defined optical properties and propagate until it reaches its first interaction site, as given by Equation 5.6. As a result, the photon is either scattered or absorbed, the probability of which is

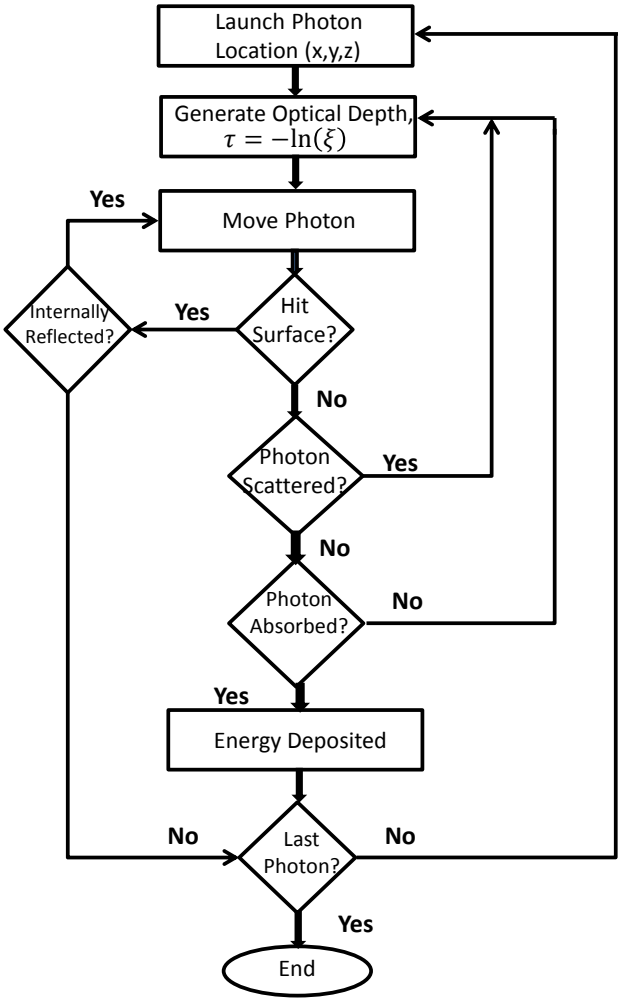


Figure 5.4: MCRT programme flow chart.

determined by the albedo a, where a high albedo value, corresponds to a more highly scattering environment. If the photon is scattered in the grid, it will therefore scatter into a new direction governed by the Henyey-Greenstein scattering phase function. Scattering will continue until the photon is eventually absorbed or exits the grid. The process continues in a loop until the number of simulated photons is reached. The model includes photon reflection at the exterior boundary of the tissue domain. The "repeating boundaries" are where photons may be internally reflected at the exterior boundary undergoing further scattering or absorption. If absorption occurs, the photon contributes to the amount of energy deposited in the corresponding cell.

To obtain images, photons are binned according to x, y, z positions depending on the plane of interest. It is possible to to collect all photons and bin by their wavelength $\lambda$ to obtain spectra as a function of depth. So essentially any plane

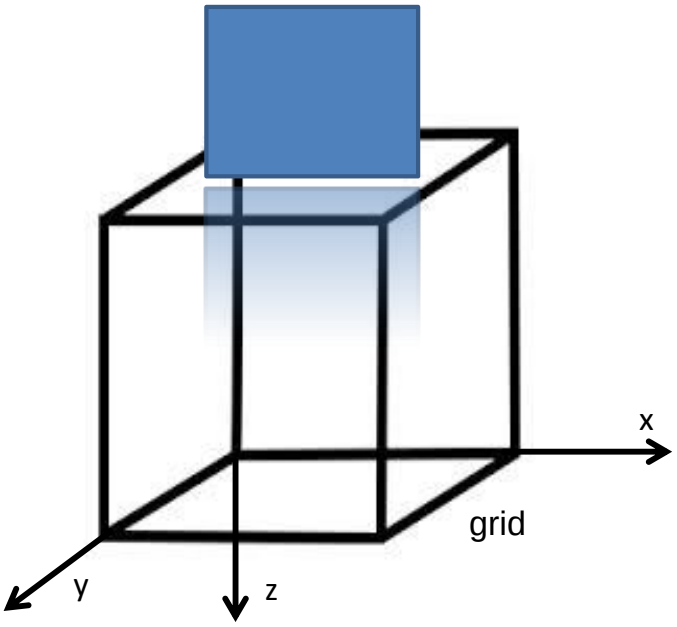


Figure 5.5: Schematic of midway slice for X-Z plane in grid (101 $\times$101 $\times$ 101).

"slice" can be extracted from the 3-D matrix cube. The code generates a fluence rate output file where we can extract a midway slice as seen in Figure 5.5, then by averaging across all the columns it is possible to obtain a plot for fluence rate.

The code also generates an output file with the number of absorbed photons. In Figure 5.6 is the sunbed spectra for the binned absorbed photons as a function of wavelength. The spectral irradiance is attenuated in the upper 100 $\mu$m epidermal layer by the optical properties. The photons are attenuated due to scattering and absorption events. The longer UVA wavelengths penetrate further down into the tissue compared to the shorter UVB wavelengths. However, the UVB component is reaching the the critical basal layer, this drops of significantly with further depth. By averaging all the slices in the X-Z plane for fluence rate it is possible to plot the fluence rate as a function of depth in the skin seen in results Figure 5.11. It is possible to investigate the optical depth penetration of UV photons as they propagate through turbid media which is the intensity dropped to 1/e (37%) of the incident value [227].

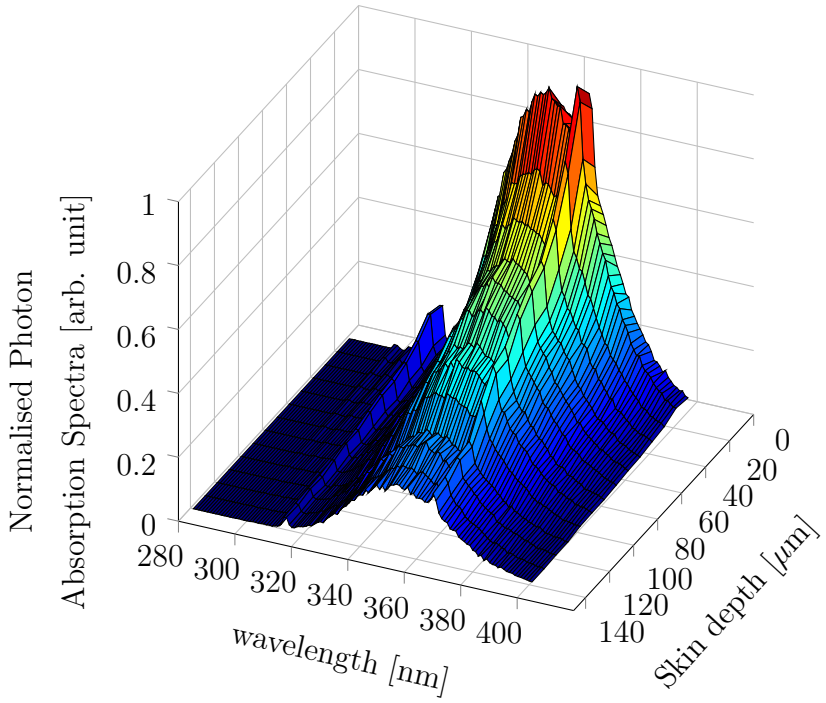


Figure 5.6: Absorption spectra as a function of depth. Colourmap: jet

Simulations were performed to investigate the impact of UV sources on the skin. These included the sun (solar spectra) and artificial tanning units(sunbed spectra). From these simulations the photon penetration and absorption can be deduced. The results from these models indicated that light penetration can indeed reach the deeper layers and cancer-prone basal layer at 100$\mu$m. We can even notice some of the shorter UVB component reaching as far as 140$\mu$m which could be a thicker site on the body.

In order to represent the observed histological structure of real skin seen in Chapter 4 Figure 4.2, the boundary of the layers were modelled as periodic surfaces seen in Figure 5.7. These boundaries are closer to the structure of observed histological sections than plane boundaries. This can be important as the statistics of a photon reflections at the boundary will be affected [188]. Another reason for the sinusoidal basal layer is that the amplitude of undulations are known to range $\pm$30% of basal cell layer average depth which could affect the radiation protective properties of the layer [152].

The surface plot of sinusoidal form in Figure 5.7 describes the junction between skin layers in the model, corresponding to a cross-section of a real image of the epidermal boundary. The distribution and scale correspond to published data from confocal micrographs for basal layer in human skin [134].

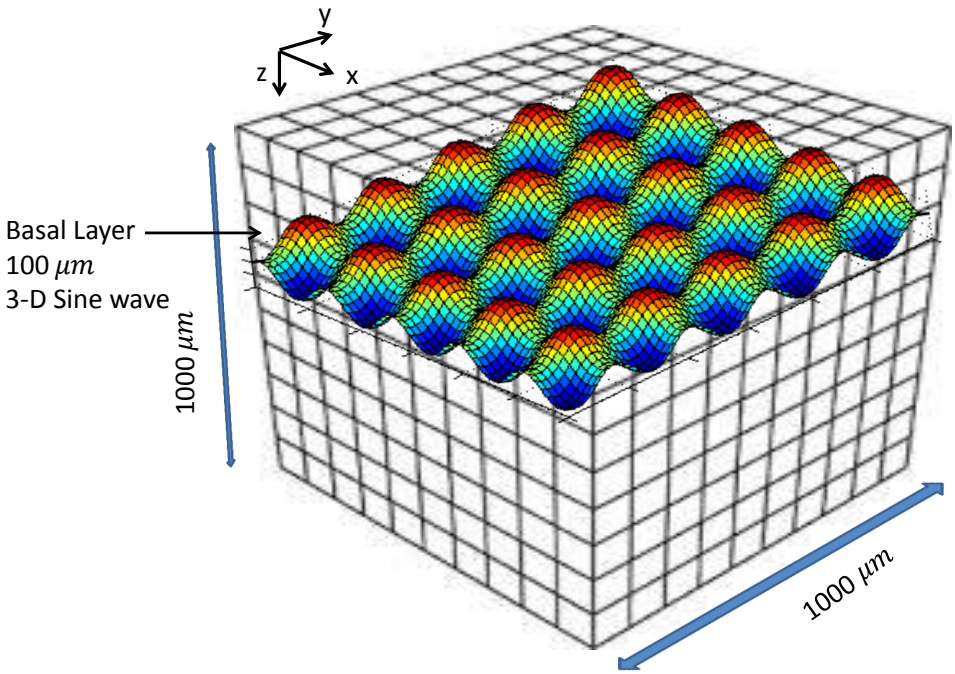


Figure 5.7: 3-D Cube ($101 \times 101 \times 101$) with sinusoidal wave for papillae representation.

The light distribution down through the layers can be viewed by imaging the fluence in the turbid media. Therefore, the structure of the model can be viewed more specifically the papillae layer. This confirms the histological structure resembles real skin tissue for layer boundaries. By extracting the X-Y plane from the fluence rate 3-D cube array it possible to simulate the dermal papillae in at depth $\approx 100\mu m$, as seen in Figure 5.8. Both the tissue architecture and size of the dermal papilla (round patches) were consistent with observations by Jensen *et al.* on confocal micrographs of epidermis foreskin [134].

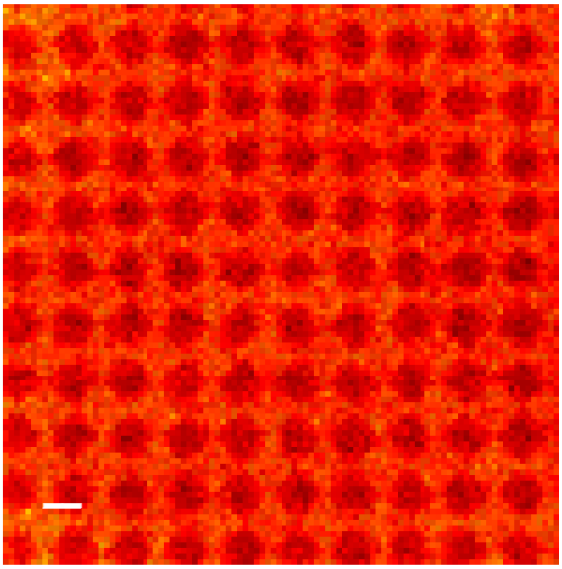

Figure 5.8: Simulated fluence rate image of sub-surface $\approx 100\mu$m X-Y plane Scale bar 60 $\mu$m. Colourmap: Eos (Earth observing system)

### 5.5.1 Validation of the Simulation

Once the skin models optical properties and structure were developed the code required validation. The first step in validating the Monte Carlo code was to compare the results for the remitted flux of photons from a semi-infinite homogeneous medium with an analytic solution of the diffusion equation as has been done in the past by several others [274].

Initially the code had to be validated to ensure that the simulation was producing the same fluence rate achieved by Jacques *et al.* [133]. The specified parameters were for single wavelength of 630nm, $\mu_a = 1.8$ , $\mu_s = 21$, $n = 1.38$, $g = 0.88$. The cube size was 1cm $\times$ 1cm $\times$ 1cm in size. One million photons were launched for each simulation. The results were compared to penetration of light as function of depth obtained by Jacques *et al.* and were found to be in close agreement demonstrated in Figure 5.9 [133].

Previously published data indicates that the formation of cyclobutane pyrimidine dimers follows a linear regression with absorbed photons on the scale of approximately $6 \times 10^{14}$ [22, 203]. Kulunsics *et al.* present a yield for CPDs per kilo base pair(kbp) caused by natural light on a clear Summer's day at noontime [158]. They state that in their comparison they only consider the UV components in dosimetry

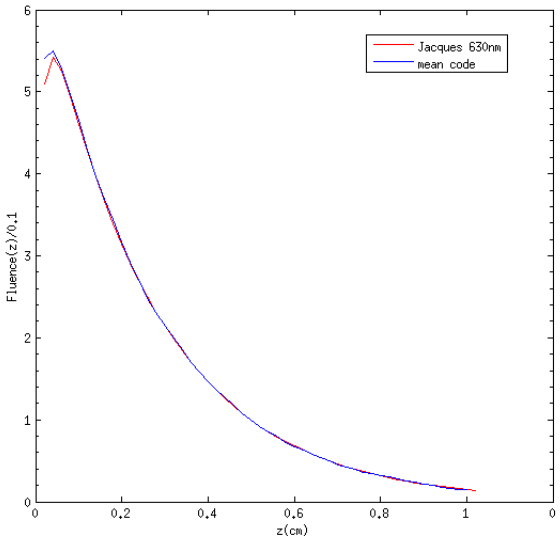


Figure 5.9: Mean of simulated fluence rate from MCRT and the fluence rate reproduced from Jacques [133].

which is ideal for our solar spectra investigation. By using the Thessaloniki spectra in Figure 2.20 and calculating the UV dose it is possible to deduce the CPD formation. In the code we have adapted the code to compensate for the direct and diffuse component of sunlight [27]. A sunbed is considered to be purely a diffuse light source.

Once validated the MCRT code is now in a position to be adapted for UV light source such as the spectra obtained from collated 402 sunbed data set. The next step was to change the light source from a collimated laser beam to a diffuse UV lamp source. By applying this there will be photons entering the surface at all angles isotropically. There is high fluence at the surface and falls off as function of depth. Fluence is calculated by summing path lengths as photons are passing through the cells therefore a higher fluence rate is experienced at the surface. As expected the UV radiation is already diffuse from its starting point and falls off more rapidly going down through the grid layers.

Next the optical properties for the UV range $280 - 400$nm were added to the model along with real sunbed spectra. Initially the model incorporated absorption and scattering coefficients for the stratum corneum from previously published data

[68].

A collated UV sunbed spectrum was inputted into the MCRT code to give an informed simulation of penetration depth of UV into the epidermis. Individual photons can be tracked as they exit the system, and bin them in x and y to make images (given a specification of the image plane); we can simply collect all photons and bin by their wavelength $\lambda$ to obtain spectra. Photons are absorbed at certain wavelengths, thus the position and number of the photons in a certain layer can be recorded. Each grid layer in code is set up for 10 $\mu$m for each grid so by the tenth layer it as at 100$\mu$m i.e. the basal layer. The recorded spectrum is then subtracted from original sunbed spectra to give spectra shape as function of depth.

### Comparison of anisotropy factor

The simulation can be further verified by testing for anisotropy. A $g$ value close to zero was coded into the simulation (here 0.1) so that the biological tissue was assumed to be nearly isotropic. By implementing the absorption and scattering coefficients of all four layers the forward propagation of photons is examined.

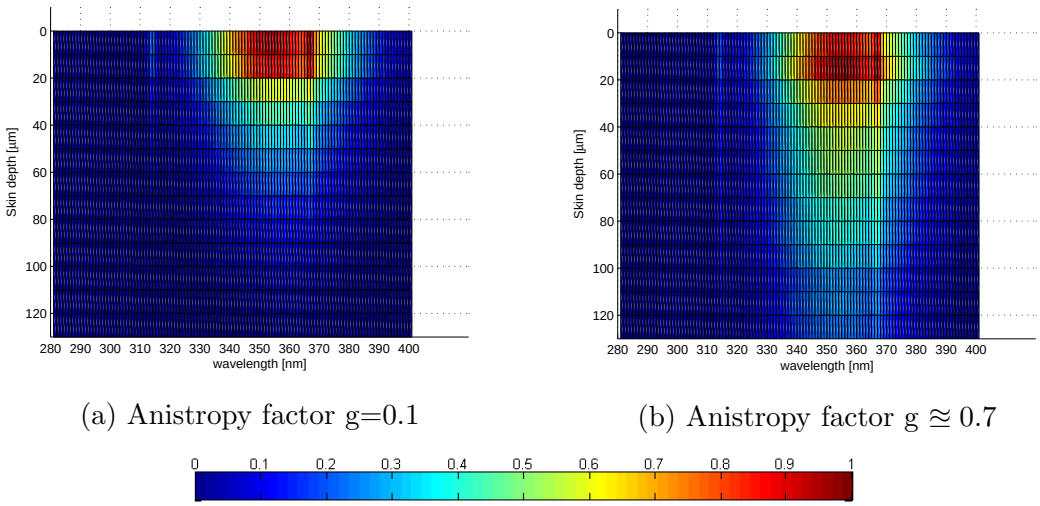


(a) Anistropy factor g=0.1 (b) Anistropy factor g $\approxeq$ 0.7

Figure 5.10: Photon forward-biased scattering in tissue media. Colourmap: jet

Figure 5.10 displays the forward propagation of photons in the Z-X plane. As the medium in Figure 5.10a is more isotropic than Figure 5.10b the transmittance of photons is less. The higher g $\approxeq$ 0.7 factor gives a more forward biased photon

penetrating deeper into the dermis [277]. This test indicates that our model is behaving in a fashion that we would expect from photons migrating through tissue media [176]. Once the MCRT code was validated and functioning correctly the simulations were executed.

### 5.5.2 MCRT Simulation Results

The computational results for our tissue media incorporating the established optical properties in Chapter 4 are described in this section. The MCRT model simulates the number of absorbed photons in each layer along with the fluence rate. The number of absorbed photons for the solar and sunbed UV sources are evaluated and compared.

The main objective for the biophysical model was to investigate the potential DNA damage from artificial tanning units. While this was an unknown quantity, there was published literature highlighting the UVA formation of pyrimide dimer lesions, more specially cyclobutane dimers from sun exposure. It is believed these lesions are the primary precursor of tumourgenesis and photo carcinoma.

The first simulations determined the amount of actual absorbed photons in the DNA layer of the model and compare the solar and sunbed UV exposures. A melanin level for skin type I was set for the MCRT code. Various exposure times were investigated for both UV sources to establish a time when the number of absorbed photons was matched.

The next stage was to investigate different skin types to evaluate the natural chromophore photo protection.

As the model simulates a UV spectral range and not just one single wavelength a conversion factor is required in the code. Hence, the code converts from photon energy to number of absorbed photons.cm$^{-3}$ from Equation 5.17 by multiplying by $5 \times 10^{15}\lambda$ [$\lambda \times (10^{-9})$ / hc] as we are investigating purely the number of absorbed photons in the DNA species.

In order to better understand the relative contribution of the different UV compo-

nents to solar and sunbed mutagenesis we wanted to investigate how many photons are actually getting absorbed in the cancer prone region of the basal layer where the DNA resides.

Once the optical properties for skin tissue were established we did a comparative test using the solar spectra in the model to give us a value of absorbed photons. The next stage was to replace the UV source in the code with the sunbed spectra and adjusting the irradiance levels accordingly. The aim was to compare the number of absorbed photons per UV source.

### Quantum Yield

For a given photo biological process, for instance, CPD formation, one may express its efficiency in terms of a quantum requirement where the number of photons needed for each CPD produced or, more commonly, in terms of its reciprocal. The "quantum yield" is the the number of CPDs formed per photon absorbed. Thus, a quantum yield is a ratio of absorbed photons that cause a biological change to the total absorbed photons, expressed as:

$$\phi = \frac{N_B}{N_A} \tag{5.22}$$

where

$N_B$ = number of photons causing biological effect,

$N_A$ =total number of absorbed photons.

When quantum yield is measured as a function of the wavelength of light used, then one obtains the so-called "action spectrum" for CPD formation as mentioned in Chapter 2. If the dimer quantum yield is 1.0, every absorbed photon results in a dimer formation. However, this is not the case as not every absorbed photon leads to a CPD lesion. Until recently the quantum yields for CPD formation in the UVA region has been unavailable [23]. Below in Table 5.1 yield fro UVB and UVA component of UV spectra.

Table 5.1: Quantum Yield for CPD formation.

| | UVB | UVA | Ref. |
|---|---|---|---|
| CPD $\Phi$ | 0.05 | 0.0005 | [22, 23] |

### 5.5.3 Results

#### Fluence Rate

The rate of photon fluence as described in Chapter 1 and defined in Equation 5.20 can be deduced from the simulation revealing information about the photon attenuation down through tissue media. The fluence rate in a homogeneous turbid medium tends to attenuate exponentially with tissue depth [278]. The layer specific absorptions are bulk quantities that can be used to determine the amount of radiative energy deposited in a layer. However, estimation of the fluence rate ($\Psi$) is necessary to determine parameters such as penetration depth of photons in a multi-layered turbid medium. The fluence rate ($\Psi$) is closely related numerically to the photon absorption albeit with the omission of the local absorption coefficient, $\mu_a\,(cm^{-1})$ of the layer.

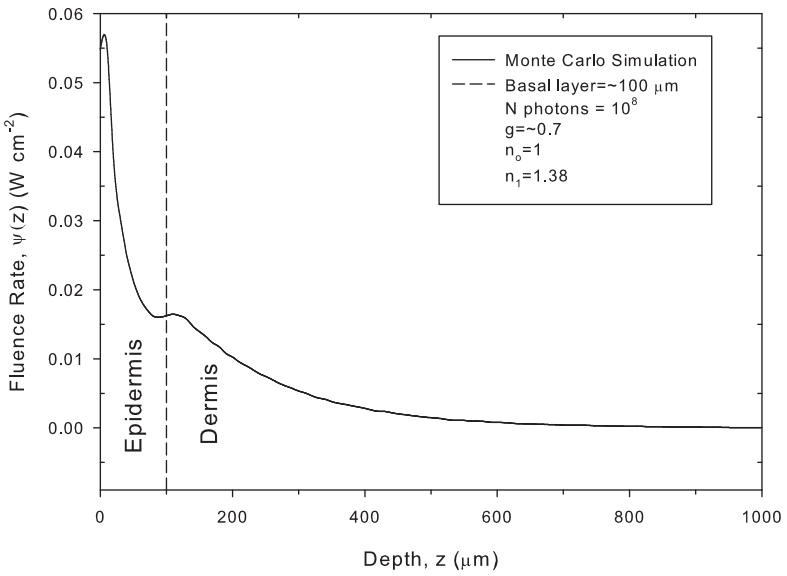


Figure 5.11: The sunbed fluence rate $\mathrm{Wcm}^{-2}$ versus depth from skin surface (cm) for skin model. Refractive index matching with $n_1 = 1.38$ is assumed for all layers. Epidermis thickness 100 $\mu m$. Dermis thickness 900 $\mu m$. Anistropy factor $g \approxeq 0.7$.

Therefore, the fluence rate ($\Psi$) dictates how absorption occurs in the multilayered MCRT model for a certain luminosity delivered over the grid size. Figure 5.11 illustrates the fluence rate with depth, $\Psi(z)$, estimated by MCRT simulations. The fluence rate exhibits the characteristic subsurface maximum near the tissue surface due to the total internal reflection caused by refractive index mismatch. Conversely photons that would have escaped from the boundary of a medium may be reflected back down and have an increased chance of being absorbed. Furthermore, the fluence near the surface is larger because the back-scattered light augments the fluence. Figure 5.11 reveals a rapid fall off of photons as they migrate down then trail off at the epidermis - dermis boundary. The fluence rate in the tissue decreases exponentially with increasing depth.

The MCRT allows us to investigate the absorption of photons in terms J.cm$^{-3}$.sec$^{-1}$ for each species layer in our model, which can be converted to number of absorbed photons photons.cm$^{-3}$.sec$^{-1}$ . The simulations were executed for solar and sunbed spectrum and the absorbed energy for each layer was determined, as represented in Figures 5.12, 5.13.

The first simulation incorporated the sunbed spectra for a skin type I phenotype and the number of absorbed photons are depicted in Figure 5.12. By taking the midway X-Y plane from the 3-D cube for each of the four layers it is possible to image the number of absorbed photons per unit volume per sec. Each of the four layer simulation outputs were concatenated and imaged in Matlab (R2011b, The MathWorks Inc., Natick, MA, 2011) [182]. The addition of a colourmap, jet, scales the intensity of the absorbed photons.

The next stage was to run a simulation with the solar spectra in order to compare the number of photons absorbed in each DNA layer seen in Figure 5.14. The simulations are implemented for incrementing times for solar UV spectra. Since the number of absorbed photons is always a linear response for CPD formation the number of CPDs per kbp can be deduced from the solar dose. Once this is established we can they run the MCRT model with the sunbed spectra. This resulted

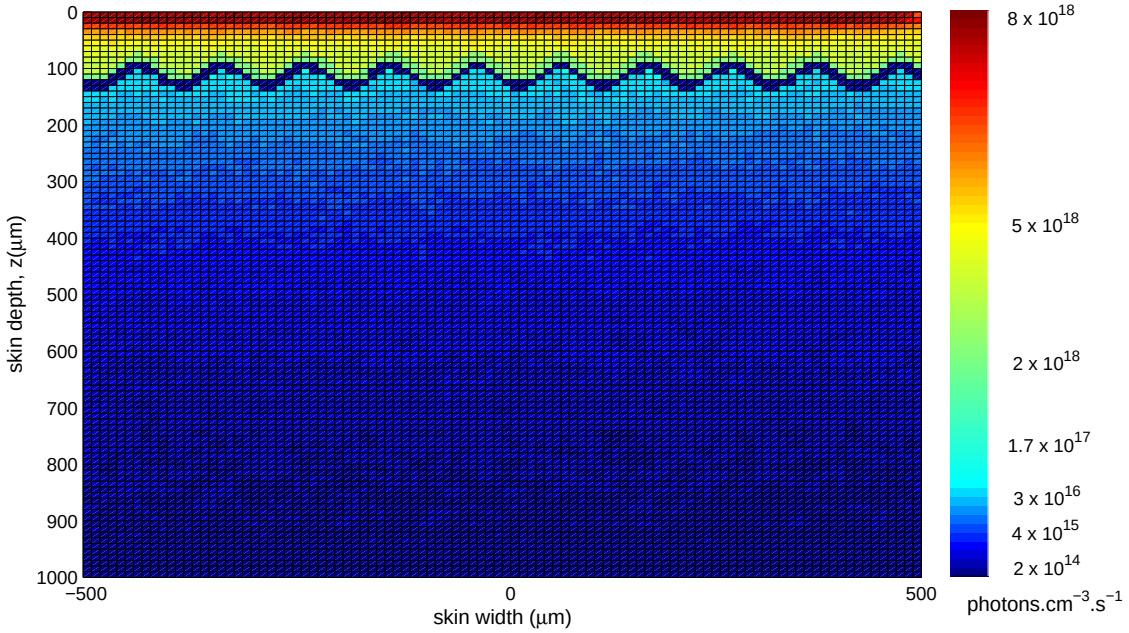


Figure 5.12: Sunbed absorbed photons for multilayer skin model.

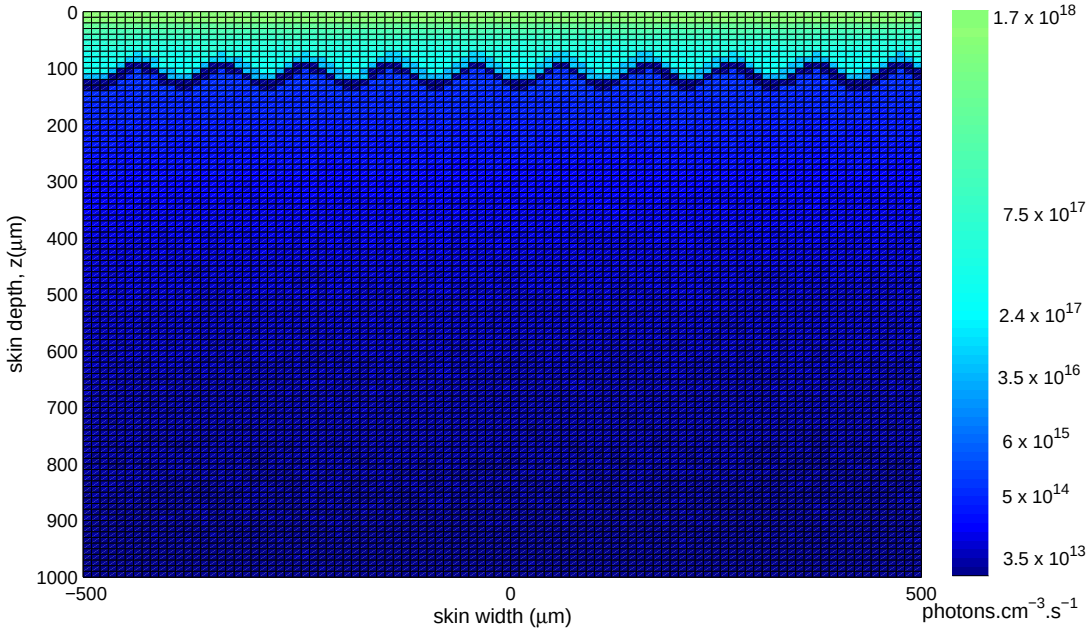


Figure 5.13: Sun absorbed photons for multilayer skin model.

in a higher number of photons absorbed in the DNA, hence a higher number of CPD formation. The measurement of CPD provides a highly relevant biological endpoint with respect to photocarcinogenesis. DNA is the target for UV induced carcinogenesis. The amount of absorbing DNA depends on the spectral irradiance

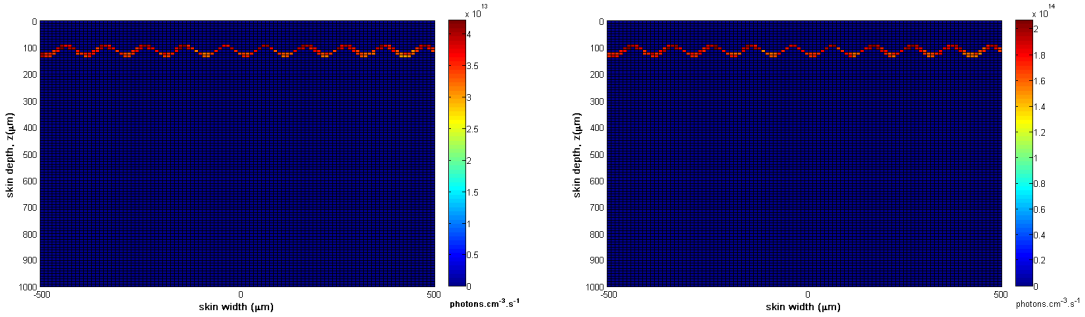


(a) Solar Spectra, 60 $Wm^{-2}$ (b) Sunbed Spectra, 280 $Wm^{-2}$

Figure 5.14: Absorbed photons for Oligonucleotide DNA complex $dA_{20} : dT_{20}$.

and the transmission through the skin. As the germinating basal layer is the most cancer prone it is the region of interest for absorbing photons. Thus, this layer is extracted from the overall concatenated matrix and isolated. The graphs depicted the DNA absorbing basal layer for the sun and sunbed spectral irradiance number of absorbed photons.

Although we know that CPDs are formed almost exclusively via direct absorption by UVB with a higher quantum yield of production, this work demonstrates that the absorption of UVA photons can lead to CPDs which in turn play a role in skin cancer development.

Table 5.2: Mean absorbed photons for peaks and troughs.

| | Solar | Sunbed |
|---|---|---|
| mean of peaks | $3.68\times10^{13}$ | $1.90\times10^{14}$ |
| mean of troughs | $3.36\times10^{13}$ | $1.68\times10^{14}$ |
| total mean | $3.5\times10^{13}$ | $1.78\times10^{14}$ |

Since the model had a sinusoidal basal layer it was possible to investigate the difference in absorbed photons at the varying amplitude. The peaks are the upper crest of amplitudes for the epidermis boundary layers. While the troughs are the lower end of amplitude. The total mean value for the DNA absorption was $1.78\times10^{14}$ photons for a sunbed and $3.5\times10^{13}$ for the sun for exposures on 1 second, as described in Table 5.2.

Since not all photons are forming a CPD on a one-to-one basis we consider the

quantum yield efficiency of 0.05% for UVA in Table 5.1, the effective number of photons producing CPDs. By calculating the mean absorbed photons for the DNA species we can investigate the exposure of the sun for 30 minutes which has an effective absorbed photons number of $0.31 \times 10^{14}$ which is in line with published data [22].

In order to quantify the formation of CPDs by the sun in comparison to the sunbed we used the number of absorbed photons as a comparative value. The yields of formation of lesions (CPDs/kbp/Jm$^{-2}$) were governed by the equation $(1.4 \pm 0.2) \times 10^{-2}$ for UVA irradiation [158]. As the sun and sunbeds are emitting 95% UVA and 5% UVB we only consider the UVA yield ignoring the direct UVB damage as method described by Kuluncsics *et al.* [158]. As a result we consider only the the UVA component in the formation of CPD formation and not the UVB. While it ignores the UVB damage it is useful for comparative purposes.

The dose for various times was calculated using solar total UV irradiance value of 60Wm$^{-2}$. Table 5.3 highlights the number of absorbed photons and CPDs for incremental exposure times [158]. The effective absorbed photons is the application of the UVA quantum yield described in Table 5.5.

Table 5.3: Time in noon sun, dose , CPD yield and absorbed photons.

| time (mins) | dose (kJ m$^{-2}$) | CPDs (kbp$^{-1}$) | total absorbed photons | effective absorbed photons |
|---|---|---|---|---|
| 30 | 108 | 0.015 | $6.38\times10^{16}$ | $0.31\times10^{14}$ |
| 60 | 216 | 0.032 | $1.27\times10^{17}$ | $0.63\times10^{14}$ |
| 120 | 432 | 0.0604 | $2.55\times10^{17}$ | $1.28\times10^{14}$ |

The MCRT model simulated the sunbed spectra with UV irradiance of 280Wm$^{-2}$, a typical sunbed irradiance, with similar exposure times as above. It was discovered that there was a higher magnitude of photon absorption occurring at the DNA region when compared to simulations with the solar spectra. As a result, it was decided to find a sunbed exposure time that yielded the same number of photons absorbed for 60 minutes of sun exposure. By knowing the absorbed photons for the sun it is

possible to obtain the number of CPDs likely to form as a proxy for a sunbed. Table 5.5 displays the number of absorbed photons for noon sun and the CPD values with corresponding sunbed exposure time to yield a similar number of absorbed photons.

Table 5.4: Number of CPDs per kbp caused by natural light on clear summer day at noon and equivalent sunbed session time.

| UV Source | Solar | Sunbed |
|---|---|---|
| Absorbed photons | $\times 10^{17}$ | $\times 10^{17}$ |
| CPDs(kbp$^{-1}$) | 0.032 | 0.032 |
| Exposure time | (60mins) | (6mins) |

The simulations return the same yield on photons reaching the DNA basal layer. This indicates that 6 mins sunbed exposure causes the same amount of DNA damage as with 60 mins of sunlight. Since we can look up the UVA formation CPDs from literature for the solar source, we can equate the same number absorbed photons to yield an equivalent amount of DNA damage. The UV irradiance of a sunbed for value 280Wm$^{-2}$ for 6 minutes gives the same amount if DNA absorption as 60 minutes sun exposure at 60Wm$^{-2}$. While there is a factor of ten difference in the times, there is only a factor of 4.6 difference in irradiance.

### Skin Type Simulations

As there are many different skin phenotypes it is possible to investigate the different photo-protective characteristics of each using the optical properties derived in Chapter 4. The first stage was to run the simulations for skin types I to IV for the solar spectra with exposure times 30–120 mins. Figure 5.15 indicates that higher pigmented skin protection is only really significant from skin type III onwards.

As skin there is a lower skin skin cancer risk associated with skin types IV and above, it was decided to investigate a medium pigmented skin cancer skin phenotype III and compare the number of DNA absorbed photons to low pigmented skin type I for a sunbed UV source.

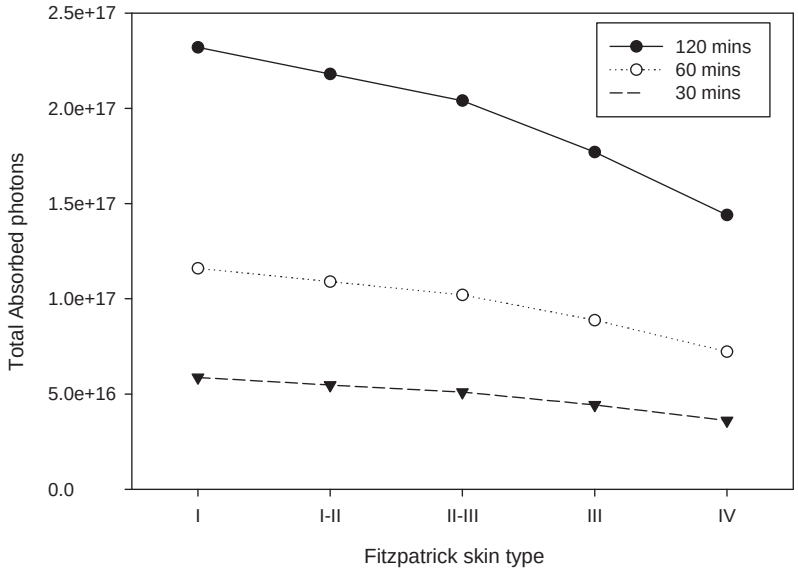


Figure 5.15: Total absorbed photons by DNA layer for different skin types at sun exposure times 30, 60 and 120 mins.

The next step was to use the sunbed spectrum in the simulations and compare the susceptibility of different skin types for typical sunbed exposure times.

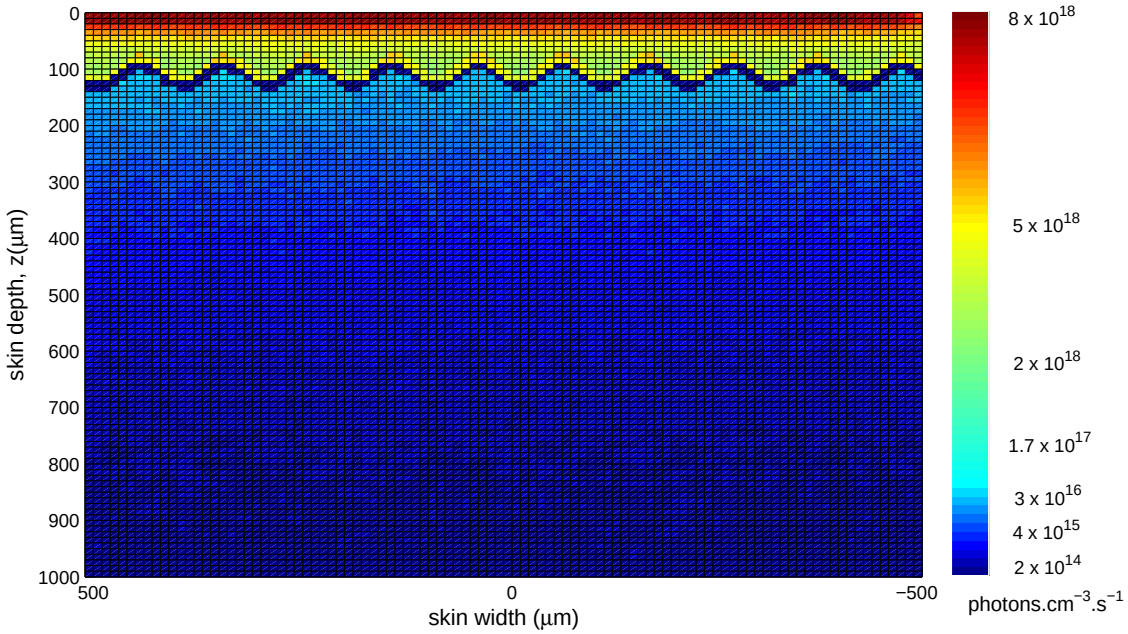


Figure 5.16: Total absorbed photons by DNA layer for skin type III for sunbed exposure.

In Table 5.5 the UV melanin shielding is demonstrated for two typical sunbed

exposure times. The higher skin type III has fewer absorbed photons in the cancer prone basal layer when compared to skin types I and II. Skin type IV shows slightly greater photo-protection but we are not modelling this skin type. In Figure 5.16 there is a high colourmap intensity for absorbed photons in the melanin layer for skin type III. Note no time exposure as per second. When the melanin layers are compared for the two skin types it becomes apparent that the higher skin type offers the greater absorbed photons. This indicates a higher natural DNA shield for higher skin types. Skin type I reveals a higher number of absorbed photons for typical sunbed exposure times compared to skin type III.

Table 5.5: Comparison of the number of DNA absorbed photons for different skin types.

| time mins | Skin type I Absorbed photons | Skin type III Absorbed photons | Ratio* |
|---|---|---|---|
| 6 | $6.68\times10^{16}$ | $4.94\times10^{16}$ | 0.74 |
| 12 | $1.33\times10^{17}$ | $9.88\times10^{16}$ | 0.74 |

*Ratio's denotes skin type III to skin type I.

In Table 5.5 comparing these skin types has highlighted that skin type I has a higher amount of DNA photon absorption than skin type III. In agreement with literature, it is demonstrated that skin type III has a greater photo-shielding effect. Consequently, as expected, skin type III is more effective at protecting DNA. Skin type I had on average approximately 35% more absorbed photons at the basal layer for higher skin type III. There is still a high number of photons reaching DNA layer for skin type III. The exposure times are standard for sunbed sessions. Skin type I demonstrates a higher amount of absorbed photons for typical sunbed session times of 6 and 12 mins giving a ratio of 0.74.

### Discussion and Conclusion

The MCRT simulations determined the photon absorption in the turbid media for the different skin layers. The simulations incorporated the optical properties for the

various skin phenotypes established in Chapter 4. The DNA (basal layer) was the layer of interest for cancer induction. The importance of the location of melanin for DNA protection is described [207, 297]. In untanned skin types I–II melanin pigments only reside in the basal layer of the epidermis acting as a protective cap above DNA. In contrast, skin type VI individual's have pigmentation is distributed throughout the epidermis in the supra basal layer as seen in Chapter 4 Figure 4.9. The MCRT model for the first time provides a method to investigate the amount of UVR that reaches the cells in the epidermis, and thus can damage the DNA in the cells. In addition, it is possible to examine the photo-protective properties of melanin for the DNA. Photocarcinogenesis was assumed to occur in the basal layer of the epidermis (z $\approx 100\mu$m).

The first simulations validated the MCRT code by comparing the output to the results generated by Jacques *et al.* [133] for single wavelength light distribution in skin. The next set of simulations verified that the MCRT was behaving in the correct manner by altering the anisotropy factor $g$ and observing the the forward scattering response. Once both these requirements were satisfied the experimental simulations began. Two different UV spectra,the solar and sunbed, were implemented in the simulations described in Chapter 2. The UV irradiance of each spectrum was calculated and entered into the code accordingly. The number of absorbed photons for each UV source were ascertained and compared. The simulations revealed a magnitude of higher absorbed photons for the sunbed source. This corresponds to the higher irradiance for the UV range of the spectrum compared with the solar UV irradiance.

By introducing a time component we can investigate the number of absorbed photons for the multilayer semi-empirical model at various times for midday sun exposure. By extracting the DNA layer we get a quantifiable number reaching the basal layer (cancer susceptible region). From our solar spectra we can calculate the irradiance for our UV component only which translates to a number of CPDs seen in Table 5.3. Data from previous studies inform us that above $10^{14}$ absorbed photons

is enough to generate CPDs [22]. So we know there are enough absorbed photons above this threshold to produce the photo lesions. More of the UV radiation from solar and sunbeds is in the UVA region and thus we consider just the UVA region for CPD formation. From literature we can use the linear relationship between UVA dose and CPD generation [158].

While there is a factor of ten difference in the times, but only a factor of 4.6 difference in irradiance can be explained by the different characteristics of the inputted spectra for sampling and the wavelength dependency of the optical properties. The sunbed spectrum displayed in Figure 2.4 shows a peak at approximately 355nm, while the sun spectra in Figure 2.20 has a more more broader shaper across the UV range. So the sunbed spectrum gives a more focused absorption for the overlapping integration wavelengths.

This comparative analysis using different UV spectra in conjunction with the MCRT model, has permitted a direct evaluation of the UV shielding capacity of the melanin layer. The capacity of melanin to protect against UV damage of the skin has been previously described [106]. The MCRT simulations demonstrates a comparative photo-protection efficiency against the formation of CPDs in basal layer with respect to reduced absorbed photons. The lack of photo-protection afforded by the UV for skin type I has been ascribed to the lower melanin content predominantly located at the basal layer above the DNA.

The simulation's results reveal that melanin does not provide adequate protection in untanned skin type I, therefore providing an indication of potential carcinoma. In Figure 5.16 there is a high colour map intensity for absorbed photons in the melanin layer for skin type III in comparison to Figure 5.12 for skin type I. This would indicate a greater level of photo-protection for higher skin types which agrees with published literature [106]. It follows that the higher pigmentation for the higher skin types offer a greater photo-protection for the DNA basal layer. DNA damage can lead to oncongenic alterations that play important roles in the induction of cancers. To evaluate the role of sunbeds the number of absorbed photons in the DNA layer

was determined. CPDs are considered to be one of the most significant UV induced DNA lesions as precursor for cancer. To establish this CPD yield a spectrum of sunlight was first simulated. Published data yield a corresponding CPD formation for a certain dose which was calculated from the UV irradiance and the exposure times. By finding an equivalent sunbed session for a 60 min midday sunlight exposure that yielded the same number of absorbed photons, it was possible to quantify the number of CPDs for a sunbed. This is displayed in Table 5.5 the number of DNA absorbed photons for a sunbed time of 6 minutes corresponds to a midday solar exposure of 60 minutes. This is the fist time an attempt has been made to quantify sunbed hazard in terms of DNA damage and potential CPD formation.[§]

[§]P Tierney, C Campbell, R M Valentine, J Woods, CTA Brown, K Wood, S L. Jacques, H Moseley, "A Monte Carlo Radiative Transfer approach to determine DNA damage from UV exposure of sunbeds", Manuscript in Preparation.

# Chapter 6

# Multiple Sub-erythema Exposure Pilot Study

## 6.1 Introduction

For certain dermatology patients, UVR from sunlight can be an exogeneous agent that precipitates a dermatosis (e.g. solar urticaria or chronic actinic dermatitis) or the means by which a skin condition can be ameliorated or treated (e.g., psoriasis). Furthermore, as exemplified by polymorphous light eruption, sunlight can also, paradoxically, serve as the both inciting factor and means of relief by natural hardening with repeated sunlight exposure.

A range of different biologic effects of ultraviolet exposure on normal human skin commence immediately after absorption of UV photons within the tissue. These include skin reddening or erythema. A minimum erythema dose (MED) is defined as the lowest actinic dose that produces a just noticeable erythema on normal, non exposed skin. This quantity corresponds to a radiant exposure of monochromatic radiation at the maximum spectral efficiency $\lambda = 295$nm of roughly $100\,\mathrm{Jm}^{-2}$ in skin type I.

Generally the skin's response to UV exposure is a protective and reparative reaction. Sunburn is an example of inflammation, a photoreparative response of skin.

Thickening of the epidermis is predominantly a protective response often associated with inflammation. Delayed tanning of the skin may also result from UV exposure. This protective response is due to the increased amount of melanin produced by melanocytes in the basal layer. The degree of pigmentation is determined by an individual's skin type.

Abnormal photo-sensitivity to UVR occurs in a range of skin conditions, including chronic actinic dermatitis (CAD). In order to confirm the diagnosis of CAD photo-testing is carried out with a diffraction grating monochromator to determine MED. This painless test involves exposing skin on the back to a range of different doses of UV radiation and also to visible light. These tests usually reveal significant photo-sensitivity to one or more of the wavelengths of these types of light. This helps to establish the diagnosis and may also be useful when planning how best to protect the skin from the responsible wavelengths.

Phototesting is used to evaluate the skin's response to UVR and attempt to establish the spectrum of radiation that will cause adverse reactions or inhibit them. A phototesting session can determine a) the MED; b) abnormal responses to UVR and c) abnormal responses to visible light. Although phototesting guidelines have recently become available [2], the UV irradiation doses able to induce erythema in healthy individuals and standardised MED doses for testing have not been well established in the literature [118]. Therefore, physicians who undertake phototesting, may disagree about how to read and interpret the results. For practical purposes, the MED thresholds described by Fitzpatrick [90] are usually considered reference values for assessing an individual's MED according to phototype.

Photo-sensitivity is generally tested on skin sites that are not normally exposed to the sun and is measured 24 hours after irradiation, since UV erythema (particularly UVB) peaks within 24 hours of exposure. There is also variation of the normal threshold depending on skin type, with the lightest skin types (types I—III) generally having lower MED values reflecting higher sensitivity to UV radiation and

darker skin types having higher MED values and lower sensitivity as seen in Table 6.1. It should be noted that the MED of UVA is measured in joules while the MED of UVB is measured in millijoules. As UVA radiation is far less erythemogenic than UVB, the skin can absorb and sustain UVA radiation without erythema by orders of magnitude greater than UVB.

Table 6.1: Skin phototype and UV sensitivity [48].

| Skin type | UVB MED ($mJcm^{-2}$) | UVA MED ($Jcm^{-2}$) |
|---|---|---|
| I | 15-30 | 20-35 |
| II | 25-40 | 30-45 |
| III | 30-50 | 40-55 |
| IV | 45-60 | 50-80 |
| V | 60-90 | 70-100 |
| VI | 90-150 | >100 |

Monochromator photo-testing is essential for a diagnosis of CAD and other photosensitive disorders and it does this by establishing the MED at particular wavelengths. However, it does not directly predict how the patient will respond to broadband emission from a lamp, which contains a range of UV wavelengths. The question arises if a patient receives half a MED at one wavelength and another half at a different wavelength, do they combine to effectively deliver an erythemal dose? Conflicting results were published in the 1970s (Willis *et al.* 1972; Ying *et al.* 1974; Kaidbey and Kligman 1975) and there has been very little work done on this since [140, 290, 298].

Resolving this issue would help in understanding whether or not there are different mechanisms involved in eliciting erythema at different wavelengths. More practically, knowing how to combine sensitivity at different wavelengths will allow us to predict more accurately how a photosensitive patient will respond to exposure from a broadband source, which may contain a range of UV emissions. This is of importance because of the introduction of energy efficient lighting that has been shown to contain levels of UV radiation that may be damaging to photo-sensitive patients

[5, 6]. Since the introduction of a new generation of monochromators, we are now in a position to undertake this simple but crucial investigation into the effect of combining multiples of sub-erythemal doses at different UV wavelengths in patients with known photo-sensitivity as well as in healthy volunteers. The principal component of the skin analysis was to successfully differentiate between a single-exposure MED and a multiple exposure MED. In this study, we use a tristimulus colour analysis in addition to the human eye to analyse the data obtained from healthy volunteers and CAD patients to evaluate if a classification of a MED is more accurate than the human eye.

**Erythema**

UV induced erythema (redness) of the skin occurs upon exposure to the sun or artificial UV sources where a faint, transient redness may begin within minutes. For the most part, the erythema response of skin to UV radiation is a delayed onset. This delayed reaction may not appear for several hours after UV exposure, which gradually increases to reach a maximum at 12–24 hours after exposure, and then fades over several days. Erythema caused by UV radiation is mostly confined to the exposed region and demonstrates the blood vessel dilation and increased quantities of blood in the dermis.

The existence and degree of delayed erythema induced by exposure to UV radiation are dependent upon exposure dose. For a given region, the exposure dose equals the product of irradiance and exposure time. The erythema is relative to the radiant energy delivered per unit area of skin surface and not to the rate of delivery (irradiance) per se. Erythemal effects of UVA require a greater radiant exposure compared to shorter wavelengths.

After irradiating adjacent sites of skin with increasing increments of UV exposure doses, the skin is observed after 24 hours to find which sites become red as a result of exposure. The lowest exposure dose required to produce a just perceptible erythema is regarded as the threshold or breaking dose and it is this we use to define the MED.

Generally, it is the reciprocal of this value, determined at various wavelengths, that is plotted as erythema action spectrum [187]. Refer to Chapter 2 Figure 2.14 for different action spectra for different wavelengths. Here the erythemal effectiveness of 365nm is approximately 0.1% of that at 305nm.

Evaluation of redness induced by UV radiation is difficult to quantify; degrees of redness of the skin are generally estimated by subjective visual evaluations, which may differ from one observer to the next. Therefore, to determine the degree of redness we used a chromameter to take measurements in addition to visual assessments.

**Wavelength Photoaddition**

Apart from the induction of redness from a single exposure, UV erythema may be induced by the combination of multiple exposures. There are three possible ways by which suberythemal doses at different wavelengths may combine. Let MED($\lambda_1$) represent the MED at wavelength $\lambda_1$ and MED($\lambda_2$) be the MED at wavelength $\lambda_2$.

1. Linear addition - In this mode, if the skin was exposed to half MED at ($\lambda_1$) plus half the MED at ($\lambda_2$), this would produce a just perceptible erthema. This may be written as,

$$0.5\text{MED}(\lambda_1) + 0.5\text{MED}(\lambda_1) = \text{MED}(\lambda_1 + \lambda_2)$$

2. Photoaugmentation - This means that adding 0.5MED($\lambda_1$) to 0.5MED($\lambda_2$) produces a greater than just perceptible erythema, or,

$$0.5\text{MED}(\lambda_1) + 0.5\text{MED}(\lambda_1) > \text{MED}(\lambda_1 + \lambda_2)$$

3. Photoprotection or photorecovery - In this case the addition of 0.5MED($\lambda_1$) and 0.5MED($\lambda_2$) fails to produce a perceptible erythema, as shown,

$$0.5\text{MED}(\lambda_1) + 0.5\text{MED}(\lambda_1) < \text{MED}(\lambda_1 + \lambda_2)$$

Linear addition implies a single mechanism for erythema induction at $\lambda_1$ and $\lambda_2$. If this does not occur, then there must be different mechanisms at $\lambda_1$ and $\lambda_2$. In this present study we were interested in three wavelengths at sub erythemal doses. So in our multiple exposures the three sub MED exposure should yield a just perceptible MED

$$1/3\,\mathrm{MED}(\lambda_1) + 1/3\,\mathrm{MED}(\lambda_2) + 1/3\,\mathrm{MED}(\lambda_3) = \mathrm{MED}(\lambda_1 + \lambda_2 + \lambda_3)$$

. This time the photoaugmentation follows

$$1/3\,\mathrm{MED}(\lambda_1) + 1/3\,\mathrm{MED}(\lambda_2) + 1/3\,\mathrm{MED}(\lambda_3) > \mathrm{MED}(\lambda_1 + \lambda_2 + \lambda_3)$$

and similarly for photoprotection where

$$1/3\,\mathrm{MED}(\lambda_1) + 1/3\,\mathrm{MED}(\lambda_2) + 1/3\,\mathrm{MED}(\lambda_3) < \mathrm{MED}(\lambda_1 + \lambda_2 + \lambda_3)$$

.

While the sum of the sub MED exposures can cause the above cases, it is also possible that pre-irradiation of the site with a certain wavelength may influence the outcome. Photo-augmentation, in which UVA irradiation enhanced the subsequent response to UVB irradiation to a greater degree than expected from photoaddition, was demonstrated by Willis *et al.* [290]. The authors found that erythema responses to solar simulating radiation and sunlight were enhanced in skin pre-irradiated with long UVAI (365nm) radiation. When the sequence of exposures to solar simulator and UVA radiation were reversed similar intensification of the sunburn response was observed. However, photo-augmentation was not reproducible in experiments performed by Ying *et al.* [298] and Paul *et al.* [218]. Conversely, they demonstrated additive property of high dose of UVA to subclinical UVB erythema.

The concept of photoaddition was first proposed by Adams *et al.* in 1931 [9]. Sayre *et al.* revealed evidence of photoaddition phenomenon for UVC radiation. [244] This result was confirmed by Ying et al. who discovered that in threshold ranges, the erythemogenic properties of UVA and UVB were also linearly additive [298]. More recently, Diffey and Farr stated that there was a "lack of photorecovery of UV erythema in human skin" [72].

In a study to exhibit photorecovery phenomena to UV erythema (300nm) by longwave radiation , van der Leun and Stoop [276] observed that when 300nm irradiation was preceded by exposure $\lambda > 315$nm, the sunlight irradiated sites demonstrated an increased sensitivity to 300nm. The investigators believed that the initial irradiation of UVA could give an additive mechanism to the erythema produced at 300nm.

Wilis *et al.,* using clinical observations, assessed the responses of human skin to UVA, UVA + UVB and UVB alone [290]. Their findings indicated that UVA radiation had an augmentative effect on sunburn damage caused by UVB. In comparison to sites that were exposed to UVB alone, pre-irradiation of skin with UVA increased the redness that occurred from UVB. This response was interpreted by the authors as a synergistic effect between UVA and UVB.

### 6.1.1 Experimental Design

The minimal erythema dose (MED) was determined on the backs of 10 subjects at wavelengths of 305, 335 and 365nm using an irradiation monochromator. At each of the three central wavelengths, three determinations of the MED were carried out using full bandwidths at half maximum intensity of 5nm, 27nm and 27 nm at the respective wavelengths.

The design concept for the clinical trial involved splitting the MED into a third at 305nm(UVB), 335nm(UVAII) and 365nm (UVAI). By taking a third of the dose required for one MED at 305nm, 335nm and 365nm we investigate if the wavelengths are linearly additive, where the sum of the fractionated MED of UVB and UVA can

induce a just perceptible MED.

The order in which the UVR was irradiated was also investigated by using various combinations of the wavelengths. This was achieved by comparing two different sequence protocols:

Sequence I: UVB, UVAII, UVAI

Sequence II: UVAI, UVAII, UVB

The full sequence schematic is depicted in Figure 6.1 showing the five control sites and Sequences I and Sequence II.

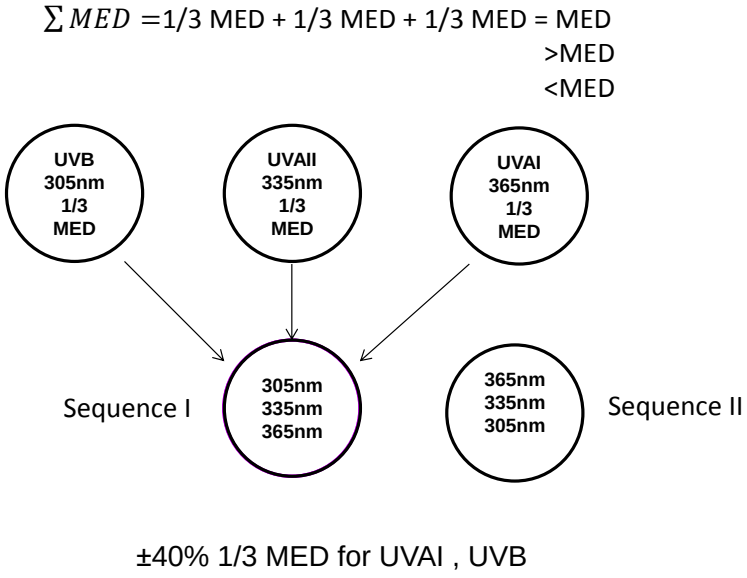


Figure 6.1: Multiple sub MED exposures.

In case the fractionated MED dose were below or above the threshold for inducing an erythema we examined the effect of increasing and decreasing the fractionated UVB and UVAI MED by ±40%. Here the MED is fractionated into one third

MED at the UVAI and UVB with ±40% combinations. However, the ±40% did not induce a significant different erythemal response. The next step was to raise the fractionated one third MED with ±90% in order to catch any erythema that might be just on the threshold of a response.

Five control sites were used in conjunction with the ±40% fractionated MEDs depicted as green circles in Figure 6.2. These included three 1/3 MEDs at each single wavelength 305nm, 335nm and 365nm known as Ctrls (a-e). In addition to this were two control sites for sequences I and II without the ±40% fractional dose UVB or UVAII known as Ctrl d) and e).

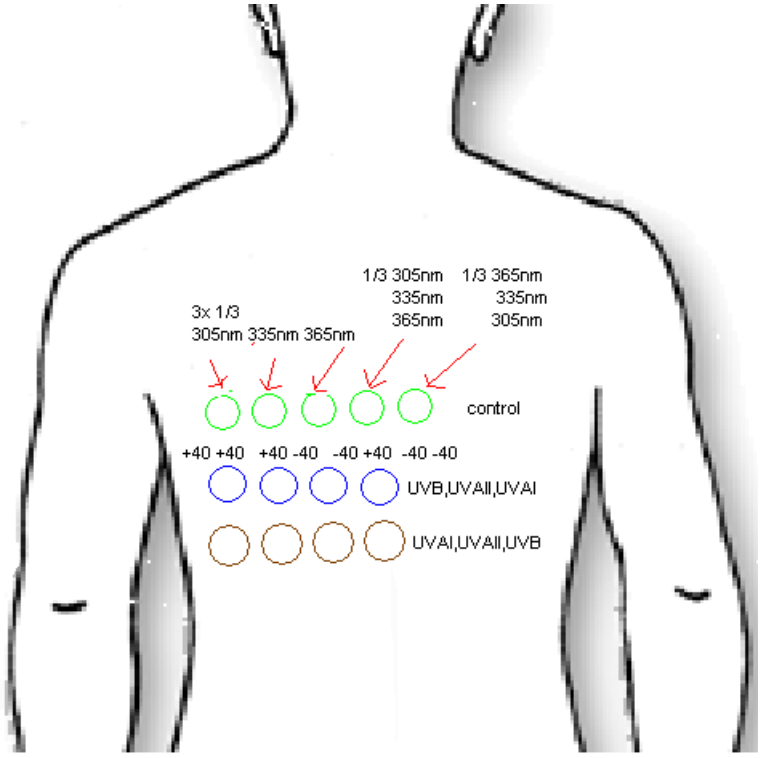


Figure 6.2: Schematic of the back with five control sites, Sequence I and Sequence II ±40%. Control sites are designated Ctrls (a-e) from left to right.

Finally there were four combinations of the fractional doses for UVB and UVAII for each sequence I (blue circles) and II (brown circles) depicted in Figure 6.2.
For Sequence I (blue circles) the fractional doses are as follows from left to right:

(a) UVB 1/3 MED +40 UVAII 1/3 MED UVAI 1/3 MED +40

(b) UVB 1/3 MED +40 UVAII 1/3 MED UVAI 1/3 MED -40

(c) UVB 1/3 MED -40 UVAII 1/3 MED UVAI 1/3 MED +40

(d) UVB 1/3 MED -40 UVAII 1/3 MED UVAI 1/3 MED -40

Brown circles followed the same pattern as above except the UVAI exposure was given first and the UVB last. The rationale behind this was to provide a greater or lesser MED and observe the biological reaction. Then which ever combination gave a response would give an indication of the mechanism.

Furthermore, several of the diseases that cause abnormal sensitivity to ultraviolet radiation are precipitated or worsened by 320 – 400nm radiation. People with such disorders may be sensitive to UVB or to UVA or to a wide spectrum of UV and visible light. For this reason, we also investigated patients with CAD.

### Chronic actinic dermatitis (CAD)

Chronic actinic dermatitis (CAD), previously known as actinic reticuloid, photosensitivity dermatitis, photosensitive eczema, and persistent light reaction, is an immunologically mediated photodermatosis characterised by pruritic eczematous lesions of areas exposed to the sun seen in Figure 6.3. Haxthausen first described this condition in 1933 in a patient with hypersensitivity to light after intravenous trypaflavine, a photosensitizing dye [120]. Actinic reticuloid and two milder forms of CAD, referred to as photosensitive eczema and photosensitivity dermatitis, were reported in 1974 [93].

Figure 6.3: CAD image of the posterior neck provided by Dr. Sally Ibbotston, PBU, Ninewells Hospital, University of Dundee, Dundee.

The term "chronic actinic dermatitis" or "CAD" was introduced by Hawk *et al.* in 1979 [119]. CAD is used to describe a particularly severe form of eczema in which an individual is abnormally sensitive to light. CAD is deemed chronic when the condition typically persists for a number of years. 'Actinic' means "caused by sun" and 'dermatitis' (which is another term for eczema) means itchy inflammation of the skin. The light doses are used to investigate the sensitivity of CAD patients in the Photobiology Unit at Ninewells Hospital are shown in Table 6.2.

CAD is an eczematous disorder associated with disproportionate UVB sensitivity, although abnormal UVA and visible light responses are also often seen. Phototesting

Table 6.2: Monochromator phototesting CAD patient doses

| **Waveband (nm)** | **Dose (mJ cm$^{-2}$)** | **Dose (mJ cm$^{-2}$)** | **Dose (mJ cm$^{-2}$)** | **Dose (mJ cm$^{-2}$)** | **Dose (mJ cm$^{-2}$)** |
|---|---|---|---|---|---|
| **305±5** | 3.9 | 8.2 | 18 | 39 | |
| **335±27** | 220 | 470 | 1000 | 2200 | 4700 |
| **365±27** | 1000 | 2200 | 4700 | 10000 | 22000 |

is carried out with a grating monochromator to determine MED. CAD predominatly occurs on sun-exposed areas such as the face, ears, scalp, 'V' shaped area of the neck and the chest, forearms and backs of hands. There can be sharp cut-off lines where covered areas meet sun-exposed skin. After some time, the skin becomes thickened, dry and scaly. These changes may persist throughout the winter months but tend to be more severe in the summer. In general CAD is more common in older males over the age of 50 years but it can occur in younger people with atopic dermatitis [57].

Phototesting is the key investigation, with broad UV waveband sensitivity occurring as a dermatitis rather than a sunburn response. Contact allergy recognition and avoidance, along with photo-protective measures, are helpful in most cases. Photochemotherapy, light sensitising drugs, psoralens, in combination with UVA(PUVA), and systemic immunosuppression may be required in those patients who fail to respond. In some cases, spontaneous resolution follows after a number of years.

### 6.1.2 Materials and Methods

Measurements were obtained from the posterior backs of 10 healthy volunteers and 3 CAD patients. Skin responses were graded approximately 24 hours after phototesting for severity of erythema and pigmentation using a pre-specified skin grading scale shown in Table 6.4 and chromameter L*a*b* parameters are described later in section 6.1.3. Visual grading was done by trained phototesting assessors according to standard working practices of the Ninewells Hospital Photobiology Unit. The backs of healthy volunteers and CAD patients were irradiated with varying doses of UVA and UVB to determine MED in each of the wavelengths 305nm, 335nm and

365nm. The subjects received overlapping suberythemal doses of UVA and UVB in each of the several sites.

**On day 1**, after informed consent was taken, skin on the subject's right or left side of the back was exposed to irradiation at the wavelengths and doses indicated in Table 6.3. Evidence of erythema was documented at 0, 5, 10, 15 and 30 minutes post irradiation. Skin responses were visually assessed according to the scale provided in Table 6.4 and approximate MEDs at each waveband determined.

Table 6.3: Monochromator Phototesting Healthy Volunteer Doses

| **Waveband (nm)** | **Dose (mJ cm$^{-2}$)** | **Dose (mJ cm$^{-2}$)** | **Dose (mJ cm$^{-2}$)** | **Dose (mJ cm$^{-2}$)** |
|---|---|---|---|---|
| **305±5** | 27 | 56 | 120 | |
| **335±27** | 3300 | 6800 | 15000 | 33000* |
| **365±27** | 15000 | 33000 | 68000 | |

* Only if skin type III

**On day 2**, the test site was examined for 24 hour delayed erythema and a more precise MED established with smaller step incremental doses. Erythema was visually assessed by the technicians and by chromameter readings.

**On day 3**, the precise MED from the delayed erythema response from day 2 was visually assessed. At this stage the fractionated MED testing can be implemented. Fractionated MED is where the dose to achieve 1 MED at a certain wavelength is divided by a third as seen in Figure 6.1. Therefore, the sum of the dose at three UV wavelengths will equal one MED. Further chromameter readings were taken to assess for erythema.

**On day 4**, the fractionated MED body-sites were assessed for erythema. Examination took approximately 1 hour and included photography and chromameter readings to quantify redness.

A chromameter (used for colourimetry) is a type of spectrophotometer which can be used for complex colour analysis with high precision and can accurately determine the spectral reflectance at each wavelength [13]. Several studies have reported the quantification of skin colour and pigmentation using a colourimeter

[14–16]. Different skin areas on the back of healthy adults were tested using the chromameter to quantify small skin colour changes due to erythema. Chromameter measurements detected increases in 'redness' with the a* parameter of the CIE L*a*b* system discussed later in section 6.1.3

**Study Subjects**

Ten healthy, adults, aged 20–50 years, with Fitzpatrick's skin type I, II, III or IV were recruited. Sun protected areas of the back were chosen for irradiation sites. Informed consent as well as complete medical histories were obtained. None of the subjects had any history of drug hypersensitivity or abnormal reaction to sunlight. They had not taken any drugs for 4 weeks and had avoided sun exposure on their backs for 3 months prior to the study.

Visual evaluation of erythema was conducted by a panel of expert assessors on a 0–4 standardised grading response scale listed in Table 6.4 .

Table 6.4: Grading of skin responses.

| Observation | Score |
|---|---|
| No evidence of any skin reaction | 0 |
| Faint but definite erythema filling the majority of the test site (i.e. the MED) | 1 |
| Definite, marked erythema | 2 |
| Erythema with evidence of oedema | 3 |
| Erythema, oedema and blistering | 4 |
| Query result, i.e. uncertain result | ? |
| Brown pigment | B |
| Flare | F |
| Petechia | G |
| Urticaria | U |

### Radiation source and dosimetry

The equipment used in phototesting comprises of a Bentham (TMS300) monochromator and Bentham (IL450E) 450W xenon lamp with a rectifier power supply (IREM Ex-30 G/1) suitable for the operation of high power arc lamps. The system also includes an integrating sphere (Bentham 9938), optical radiation meter (Bentham ORM400) and Liquid Light Guide (8 mm diameter, 2 m length, FOP-UVL-2-d8)(Figure 6.4). The monochromator has the ability to split light into its constituent wavelengths. Individual wavelengths can be selected and irradiated directly onto the surface of the back for varying time from 3 seconds to 15 minutes. This procedure is painless.

Figure 6.4: Phototesting with monochromator and light guide.

### Correlation of Chromameter with Expert Assessment

As an aside, an investigation was conducted to check if there was a correlation between expert grading of erythema with the instrument. Two chromameter readings were obtained: the first on the non-irradiated site (background) and the second on post irradiation (erythema). The difference after subtracting the background skin

measurements, the UV irradiated site values were subtracted from the a* value of the untreated site to obtain $\Delta$a* value (see Table 6.5). Visual scoring of skin erythema, as graded 1 to 4, based on a standardised scale, was done by a panel of trained observers. The visual grading of skin erythema is generally considered the difference between baseline skin colour and increase in redness as observed by the eye. The subjective visual assessment of skin phototypes according to Fitzpatrick et al. combines the intensity in melanisation and the erythemal response to sun exposure [89]. Due to this subjective nature of skin evaluation we consider a chromameter to quantify skin colour.

### 6.1.3 Chromameter

Skin colour measurements were made with a spectrophotometer (CM-700d, Konica Minolta Sensing, Inc., Osaka, Japan) as seen in Figure 6.5. The spectral reflectance on the device was set for standard illuminant D65 and recorded at 10 nm intervals from 400 to 740 nm under the visual field of 2° for a standard observer. The device is handheld and the aperture of the removable probes have diameters ranging from 3 mm to 9 mm. All readings were taken with light pressure applied to the skin to avoid blanching.

Three-dimensional colour coordinates, i.e., L* (lightness), a* (red-green chromaticity index), b* (yellow-blue chromaticity index) in the CIELAB colour space, were determined for each sample. The spectral reflectance curves and three-dimensional CIELAB colour coordinates for different skin types and erythema were obtained. We selected a numerical aperture size of 3 mm to measure the irradiated region on the skin. The measurement using the spectrophotometer was performed 3 times, and the mean values for each site were used in this study. The chromameter is calibrated to CIE 1976 L*a*b* colour system using a white plate before each measurement.

The a* values represent red–green ratio (red shift, a* >0). Since skin redness is primarily determined by the presence of hemoglobin and melanin, erythema can be assessed using the redness parameter a* [85,279]. As erythema begins to appear, the

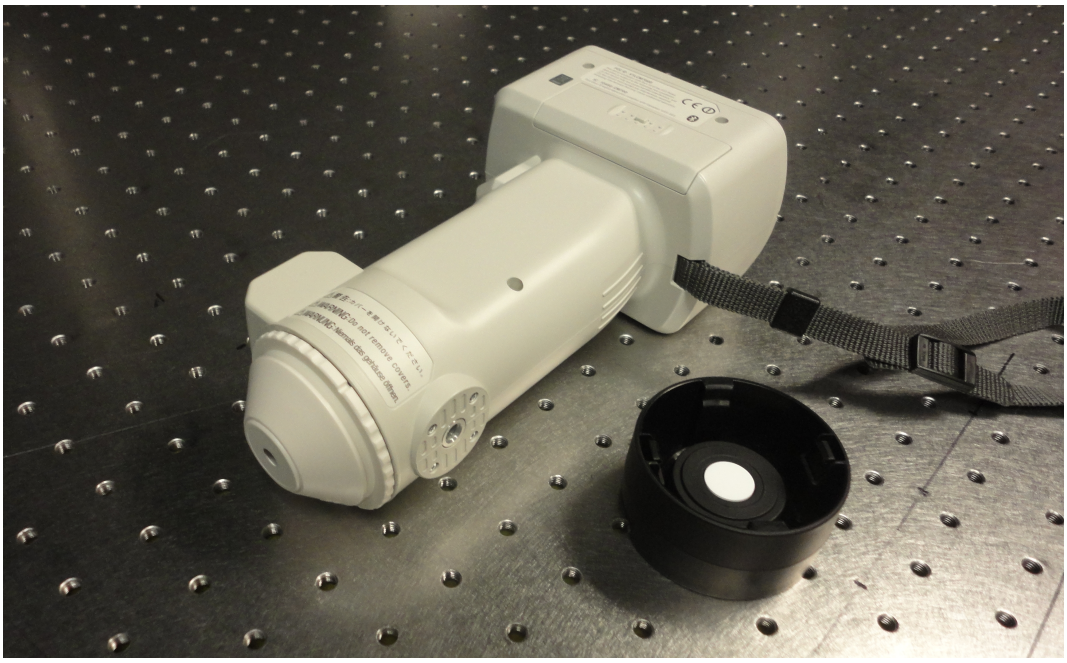

Figure 6.5: Spectrophotometer (CM-700d) with calibration plate.

a* value becomes more positive. The MED threshold for colourimetry was chosen according to COLIPA recommendations as an increase of the redness parameter $\Delta a^* = 2.5$ [88].

One of the advantages of using the CIELAB uniform colour space in expressing the colour of the object is that the colour difference between two objects can be expressed by a simple parameter, $\Delta E^*$ The value is the distance between two points, each expressed in terms of L*, a*, b*, in the CIELAB uniform colour space, as shown in Figure 6.6. The colour difference parameter $\Delta E^*$ - value is then calculated by the following expression:

$$\Delta E^* = [(\Delta L^*)^2 + (\Delta a^*)^2 + (\Delta b^*)^2]^{1/2} \tag{6.1}$$

where

$$L^* = L_1 - L_2$$

$$a^* = a_1 - a_2$$

$$b^* = b_1 - b_2$$

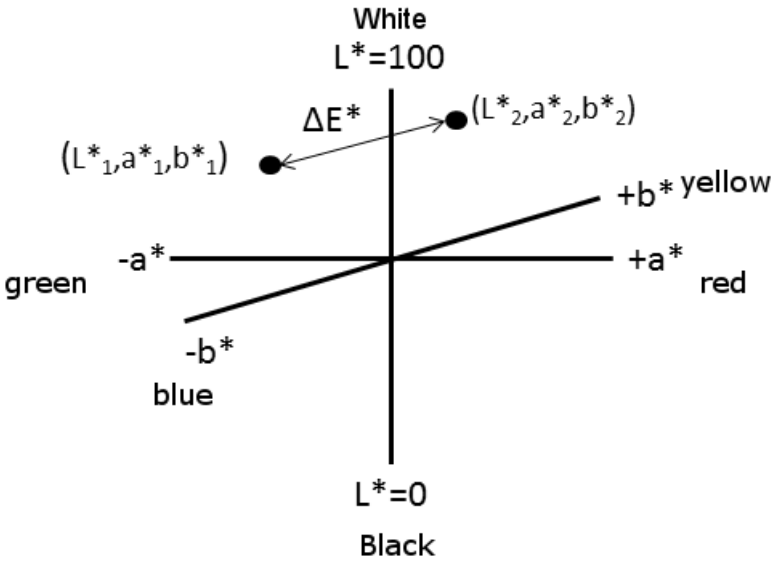


Figure 6.6: Colourimetric representation of colour space CIELAB.

The larger the $\Delta E^*$ value, the larger the colour difference becomes. It is known that a $\Delta E^*$ of 1.0 is just discernible by the human eye. The ranges indicated the degree of difference as: 1.0 to 3.0 for visible difference, 3.0 to 6.0 for appreciable difference and 6.0 to 12.0 for much difference [46]. The L* and a* readings in colourimetry are well suited to quantify erythema [19, 247]. The L* value decreases when erythema develops, indicating some skin darkening but to a relatively smaller extent than the increase of a*.

For the MED, the $\Delta E^*$, which is the colour difference of the normal skin and the phototested area, was within the range of 1.0 – 4.0 shown in Figure 6.7 and this showed a visible difference and could not be accepted as a same colour by the spectrophotometer for ten of the subjects. For the MED, among the 10 healthy subjects , the $\Delta E^*$ of 5 subjects was within the range of 1.0 – 3.0, which could be accepted as a difference of colours, and 5 subjects were within the range of 3.0 – 6.0, which showed a distinct colour difference.

We know there is an erythema induced for these readings established on day 2 for phototesting. However, the visual assessment scoring for the control sites and the sequences did not correspond with the chromameter readings. In fact all the $\Delta E^*$ values gave values >1 when some of the naked eye assessments indicated

no erythema. Thus, the chromameter measurements could not be used in MED quantification and the visual grading ranking was used.

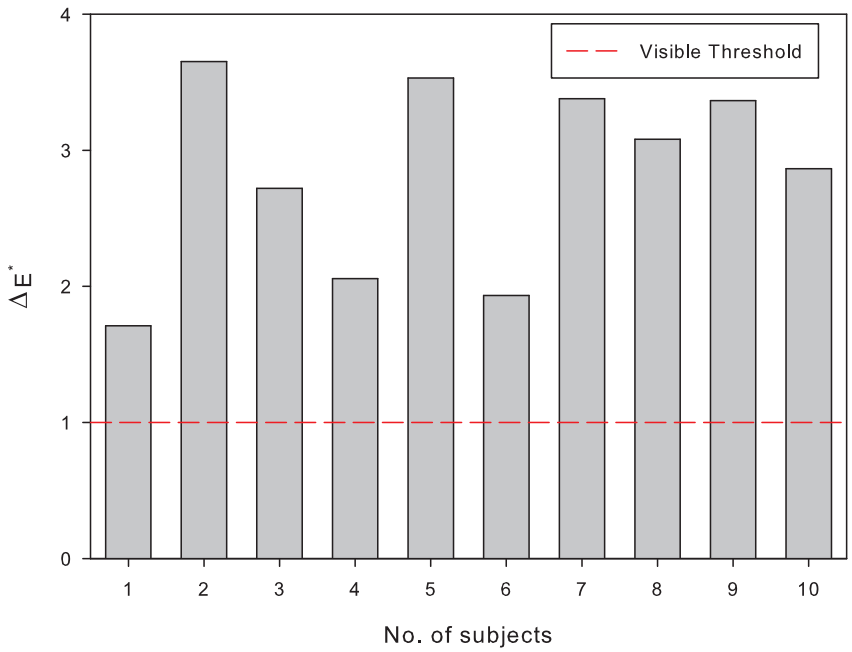


Figure 6.7: $\Delta E^*$ for each healthy subject red dashed line indicates threshold for visible difference.

**Reflectance**

For a turbid medium such as human skin, the diffuse reflectance, R($\lambda$), determines the apparent optical density, OD, of the medium [130]. Tissue chromophores such as melanin content can be determined from the reflectance spectra in a model first proposed by Kollias *et al.* whereby the slope of the optical density (OD) versus wavelength in the range 620 – 720 nm can determine the melanin epidermal melanin content [151]. This model was improved by Jacques et al. demonstrating any choice of wavelength in the 600 – 900 nm range can be used to calculate the composition of melanin [131]. The OD for turbid medium is expressed in Equation 6.2.

$$OD\left(\lambda\right) = -log_e\left(R\left(\lambda\right)\right) \tag{6.2}$$

Owing to the strong absorption of melanin in the UV spectral range the melanin score (MS) may be defined as a slope of the in vivo reflectance spectrum ,which correlates with melanin content [28]. The skin reflectance spectra, R($\lambda$), for all ten healthy volunteers were acquired with spectrophotometer (CM-700d). The spectra for different skin types are displayed in Figure 6.8a. Figure 6.9 illustrates the analysis technique whereby the OD at the wavelengths $\lambda_1 = 620$nm and $\lambda_2 = 670$nm are used to acquire a slope in order to determine the melanin score. The MS is proportional to the melanin content of the pigmented epidermis and is calculated with the following equation:

$$MS = \frac{OD(\lambda_1) - OD(\lambda_2)}{\lambda_2 - \lambda_1} \tag{6.3}$$

Figure 6.8 displays the reflectance for different pigmentation levels from the spectrophotometer for wavelengths from 400 to 700nm and the calculated OD from Equation 6.2.

Figure 6.9 shows three OD spectra for a) high, b) medium and c) low pigmented skin types. We can see an example of the slope technique for the high pigmented spectrum which gives a MS value of $1.8 \times 10^{-3}$ from Equation 6.3. The MS value was

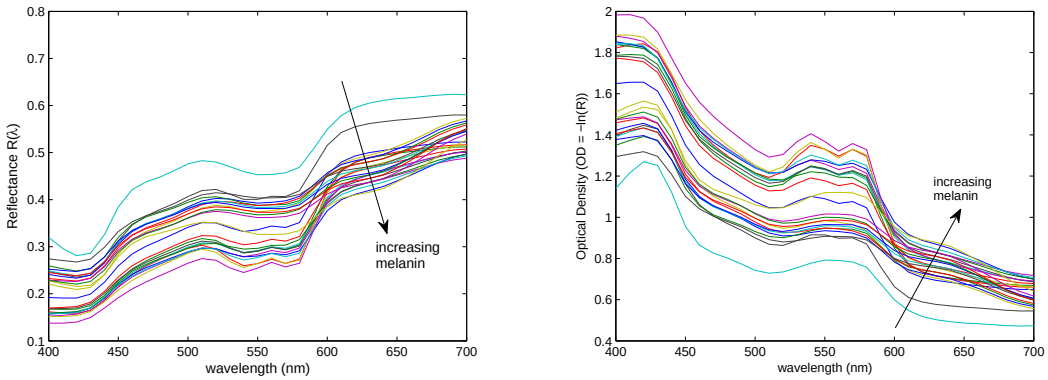


(a) Spectrophotometer reflectance. (b) OD for different skin types.

Figure 6.8: Melanin characterisation.

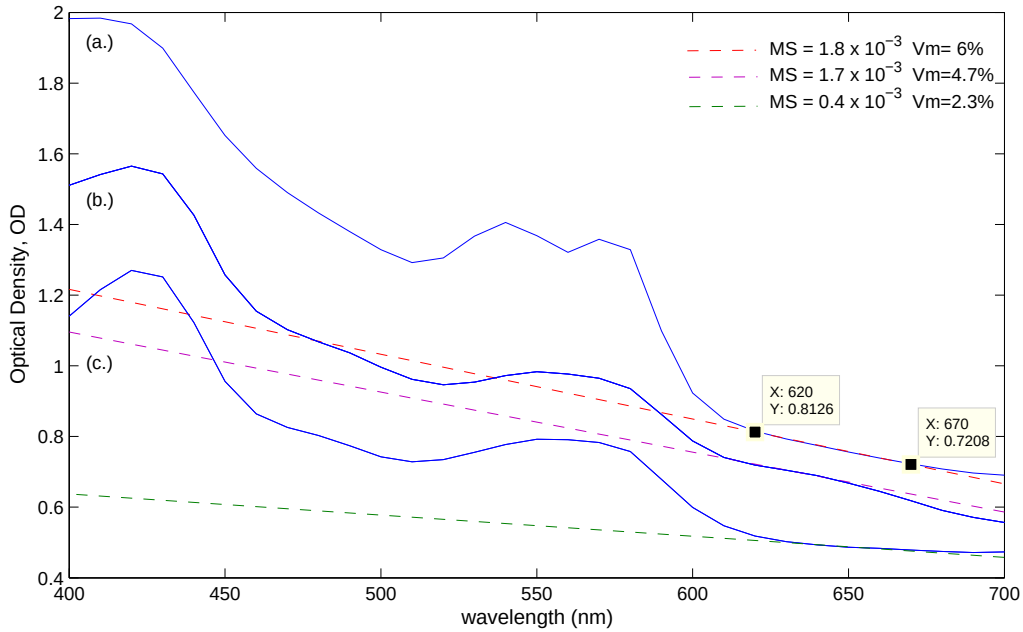


Figure 6.9: Optical density, OD $= -ln(R(\lambda))$. The MS and corresponding melanin volume fraction (Vm) from look up tables [130].

used in the look up tables from Jacques [130] this translates to a melanosome volume fraction of Vm = 6%. This volume fraction would correspond to a relatively high pigmented skin type III. Investigating the spectrum (c.) in Figure. 6.9 MS=$0.4 \times 10^{-3}$ which corresponds to a low pigmented skin type I with Vm=2.3%. The latter is similar to the Vm used in the MCRT simulations described in Chapter 5.

### 6.1.4 Statistical Analysis

Results from the volunteers and patients were compiled using the statistical package SPSS (IBM SPSS V.20.,Chicago, Illinois, USA). In order to investigate correlation, the chromameter "redness" readings for erythema were compared to visual gradings done by eye. The readings were completed fully blinded, whereby the visual assessor was concealed from the device readings so there would be no bias in the results. The difficulty was comparing a yes/no MED visual assessment and the device reading. A rank correlation for ordinal numbers was required to allow for "ties" in case there was agreement between the device and the naked eye gradings. The statistical test used was a non-parametric rank correlation, more specifically tau-b correlation coefficient. This allowed a test for significance if $p<0.05$.

The p-value of 0.495 indicate there was no significant relationships between the visual degree of colour Vs. chromameter readings since $p>0.05$. The lack of correlation between the two methods has led us to rely on the visual assessment rather than the chromameter. The PBU has carried out visual assessment of erythema for many years and has been subject to regular audits. Thus, we can consider it more reliable than the chromameter.

Visual observations are often graded on an ordinal (non linear) scale, as seen in Table 6.4. Since this data is not a continuous numeric form, non-parametric analysis is usually performed. The choice of statistical analysis for significance between the visual erythema MED rating and the control sites visual ratings including the sequences was done using the Friedman test. This choice of test has been the statistical test for visual assessment [19, 148]. The Friedman test is similar to repeated measures Analysis of variance (ANOVA) that can be performed on ordinal (ranked) data.

A non-parametric test is required when distribution is not normal. Visual erythema grading scores for the 13 sites one each subject were ranked for the Friedman test, with one been the least (assigned to lowest visual score) and three (assigned to the highest grading) thus making rankings ordinal. Since the instrumentation did

not offer a good grading for skin assessment it was decide to use the visual grading readings to compare and established MED to the five control sites, the Sequence I and Sequence II protocols. It was then possible to conducted a Friedman repeated measures analysis of variance on ranks.

The null hypothesis was that there is no difference between the background and the MED control groups or sequences. In Appendix A the ranks of each row are calculated and the total rank of each column in each rank is returned. This is the method for calculating the mean rank and is confirmed by the Sigmaplot output in Appendix B. The three skin tests are put into blocks: Block 1: the controls, Block 2: sequence I and Block 3: sequence II. The Friedman test for Block 1 returns a Chi-square value of 22.69 which is greater than the critical value of 11.07 for five degrees of freedom with $\alpha = 0.05$. In this case the null hypothesis is rejected i.e. there is a statistically significant difference amongst the groups. However, there are 5 irradiation sites. We would like to know which of these sites are significantly different from the MED and the controls. So the next step was to employ a post-hoc test to compare pairwise background Vs. MED controls. The differences in the mean values among the treatment groups are greater than would be expected by chance; there is a statistically significant difference ($p = 0.001$). To isolate the group or groups that differ from each other a pairwise comparison test was performed. The Friedman test can itself be used as a post-hoc test when just two groups are involved. The results of the multiple pairwise comparison tests are displayed in Tables 6.5–6.10.

### 6.1.5 Results

**Healthy MED - MED 40**

When various incremental fractions of UVAI and UVB were used, erythema resulted only when the sum of the MEDs for UVAI, UVAII and UVB was 1 or greater. Thus, disagreement exists as to whether UVA radiation augments or simply adds to the erythema produced by UVB alone. The skin types of all the subjects were categorised by an expert assessor and the MED values for all three wavelengths were ascertained from phototesting described above. The chromameter was used to measure the average background readings, another method to investigate the accuracy of the chromameter was to calculate $\Delta a*$ for each of the readings. However, six of the 10 subjects had a negative $\Delta a*$ indicating that the background reading was actually higher than the MED reading. The remaining four subjects had a higher MED reading but the $\Delta a*$ did not give a difference greater than 2.5 which is deemed minimum for erythema. Table 6.5 represents the Fitzpatrick skin type for all ten healthy subjects with MED doses and L*a*b* readings and erythemal difference reading for "redness" $\Delta a*$.

Table 6.5: MED, L*a*b* and $\Delta$a* values for healthy volunteers posterior back.

| Subject no. | Fitzpatrick skin type | MED(mJ cm$^{-2}$) 305±5 | 335±27 | 365±27 (nm) | Avg. background L* | a* | b* | Erythemal difference $\Delta a*$ |
|---|---|---|---|---|---|---|---|---|
| 1 | II | 68 | 18000 | 27000 | 65.84 | 6.89 | 13.95 | -0.34 |
| 3 | I | 39 | 8200 | 18000 | 69.60 | 7.24 | 14.64 | -3.09 |
| 4 | II | 68 | 1200 | 22000 | 70.38 | 2.99 | 13.00 | 0.67 |
| 6 | II | 100 | 1500 | 39000 | 65.70 | 7.34 | 15.45 | 0.76 |
| 7 | II | 100 | 6800 | 18000 | 64.04 | 9.11 | 15.20 | -3.38 |
| 9 | III | 56 | 1500 | 33000 | 66.74 | 6.60 | 11.98 | -0.86 |
| 10 | III | 56 | 10000 | 22000 | 67.64 | 5.35 | 16.09 | 0.13 |
| 11 | III | 39 | 12000 | 27000 | 67.73 | 6.07 | 19.99 | -1.12 |
| 12 | II | 82 | 6800 | 33000 | 67.59 | 5.10 | 15.44 | -1.37 |
| 13 | II | 47 | 6800 | 18000 | 70.94 | 4.45 | 12.29 | 0.39 |

The results of the post-hoc pairwaise Friedman test is represented in Table 6.6 with the p-value for significance for the background reading Vs. the five multi expo-

sure sub erythemal control sites for ±40% 1/3 MED described previously in Figure 6.2.

Table 6.6: Background unexposed site versus control groups (Friedman Two-Way Analysis).

| Comparison | p-value |
|---|---|
| Background Vs. Ctrl. a | .317 |
| Background Vs. Ctrl. b | .003* |
| Background Vs. Ctrl. c | .008* |
| Background Vs. Ctrl. d | .014* |
| Background Vs. Ctrl. e | .046* |

* Statistically significant difference ($p < 0.05$).

When we investigate the sequences of ±40% 1/3MED we notice a significant difference between background and control sites (Ctrls b-e). However, there was no significance for Ctrl a) This seems idiosyncratic as one would expect the more energetic UVB 305nm to induce an erythemal response. However, in our controls we did not notice such a response.

The Friedman test was passed for both sequence groups with statistics in Appendix C. Thus, allowing for pairwise comparisons. Table 6.7 shows that the fractionated doses at $+40-40\%$ and $-40-40\%$ for Sequence I have no significance difference with p-values of 0.083, greater than 0.05. The pre-irradiation of UVB at +40% would suggest a photo-recovery mechanism occurring. While one would expect no difference at $-40-40\%$ as the one third fractionated doses for UVB and UVAI both are below the MED dose for 305nm and 365nm.

Again for sequence II there was no significant difference at the lower $-40-40\%$. Conversely, this time round we notice significance for Sequence II with $+40-40\%$ in comparison to background site. So the UVAI first did enhance the post irradiation of the UVB irradiation to produce erythema. This is interesting in that it might offer an augmentative effect to provide synergy. Table 6.7 indicates the two different sequences and the percentage of one third MED dose.

The next stage was to investigate if there was a significant difference in the visual

Table 6.7: Background non-exposed site versus Sequences I and II ±40% 1/3Med (Friedman Two-Way Analysis).

| | Comparison | p-value |
|---|---|---|
| Sequence I | Background *Vs.* $+40+40\%$ | .008* |
| | Background Vs. $+40-40\%$ | .083 |
| | Background Vs. $-40+40\%$ | .025* |
| | Background Vs. $-40-40\%$ | .083 |
| Sequence II | Background *Vs.* $+40+40\%$ | .003* |
| | Background Vs. $+40-40\%$ | .005* |
| | Background Vs. $-40+40\%$ | .025* |
| | Background Vs. $-40-40\%$ | .157 |

* Statistically significant difference ($p < 0.05$).

scoring for Sequences I and Sequences II. The Friedman test was passed for both sequence groups with statistics in Appendix C so a pairwise test was conducted.

The results for sequence I ±40% 1/3 Med indicate there is a significant difference at $+40+40\%$ and $-40+40\%$. The later sub erythemal dose combination points towards an augmentative mechanism. Conversely, there is no significance for the $+40-40\%$ which may seem counter intuitive considering the energetic UVB has the higher fractional dose compared to UVA. However, the dose is given as multiples or sub-multiples of MEDs. Therefore, one should expect the same fraction of a MED at any wavelength to produce the same effect. For sequence II all the combinations except $-40-40\%$ show a significant difference. Both sequences for $-40-40\%$ show no significance which is expected since both UVB and UVAI have a fractional less than the fractional 1/3 MED.

The results here are interesting with Sequence I $+40-40\%$ which might suggest post irradiation of UVA offers photorecovery. However, it was inconclusive whether irradiating the site with 305nm first offered a synergistic effect or if the UVAI 365nm had the same influence. However, a significant $p<0.05$ is also noted at $-40-40\%$ for Sequence II which suggests that there could be equally an augmentative effect. These results seem paradoxically different. A more probable explanation is that the $-40-40\%$ fractionated doses are just on the cusp on producing a MED. Therefore,

in response to these results we redesigned our experiment to use Sequences I and II ±90% 1/3 Med. The rationale was that we were not catching the MED for the fractioned MED sequences. The new MED levels are explored section 6.1.6.

**CAD Results**

During the study only 4 of the 10 CAD patients were recruited. However, one of these patients was dropped from the study as they did not meet the requirements stipulated. Table 6.8 represents the three CAD patients readings for $-40-40\%$ MEDs corresponding skin type and chromameter readings.

Table 6.8: Skin type, MED, L*a*b* and $\Delta$ a* values for CAD patients posterior back.

| Subject no. | Fitzpatrick skin type | MED(mJ cm$^{-2}$) 305±5 | 335±27 | 365±27 (nm) | Avg. background L* a* b* | Erythemal difference $\Delta a*$ |
|---|---|---|---|---|---|---|
| 1 | I | 12 | 680 | 3300 | 71.62 2.32 14.95 | -1.89 |
| 2 | I | 5.6 | 1500 | 6800 | 66.29 4.99 13.42 | -0.55 |
| 3 | III | 3.9 | 680 | 4700 | 65.58 5.54 14.68 | 0.23 |

Unfortunately, due to the time frame and low sample number valid statistics could not be performed on this data. Further investigation is warranted to achieve a higher sample group.

### 6.1.6 MED 90

In the final series of experiments the fractional dose for UVB and UVAI are changed from ±40% 1/3 MED to ±90% 1/3 MED with rationale that we produce a MED for border line fractional doses. Figure 6.10 demonstrates a good responder for a skin type II healthy subject under the new fractional dose regime. The controls show a good erythemal response including both Sequence I and II.

The Friedman test for the background and the control sites returns a Chi-square value of 17.51 which is greater than 11.07 for 5 degrees of freedom (dof) seen in Appendix D. Therefore we reject the null hypothesis as there is a significant difference between the groups with a p-value of 0.04.

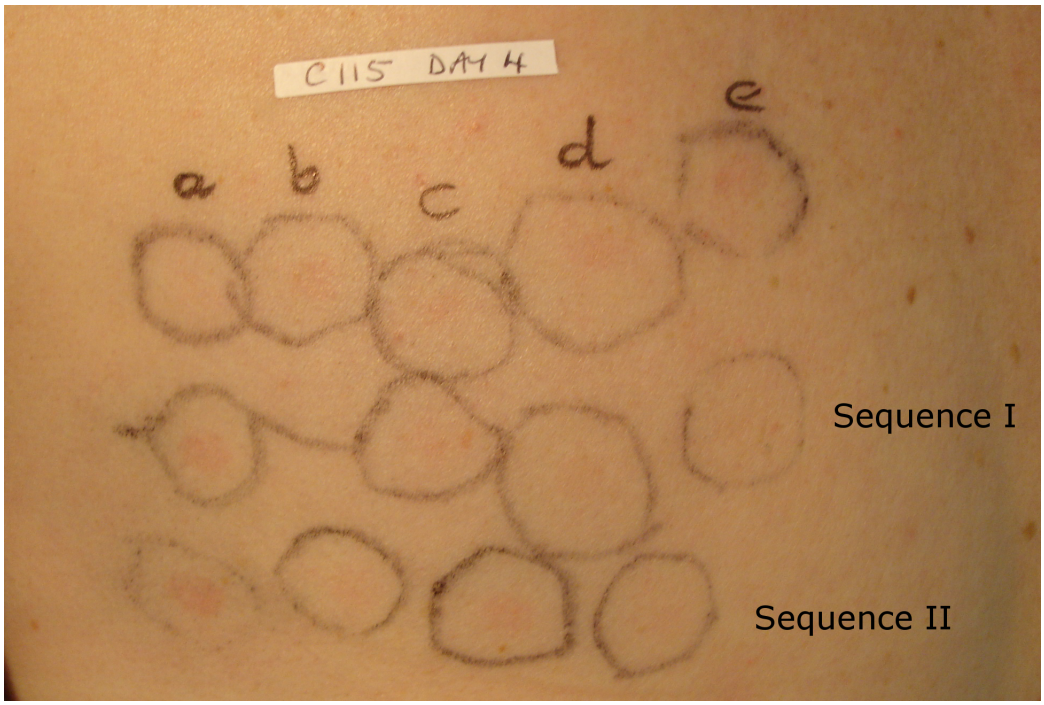


Figure 6.10: Example of day 4 multi sub-erythemal exposures for ctrls (a-e), Sequence I and Sequence II.

Investigating Sequence I and II ±90% 1/3 MED we reject the null hypothesis as obtained Chi-square values of 26.128 and 28.359 (refer to Appendix E) respectively, which is greater than the larger critical value (9.48) for 4 dof. Therefore a pairwise test was implemented between the background non-exposed site and the control MED group. This resulted in all control sites been significantly different.

Table 6.9 shows p-value for significance for the background unexposed site Vs.

the five control MED sites ±90% 1/3 MED. This time round all the control sites produced an MED according to the visual assessment scoring. This suggests a purely photo linear addition.

Table 6.9: Background unexposed site versus control groups (Friedman Two-Way Analysis).

| Comparison | p-value |
|---|---|
| Background Vs. Ctrl. a | .025* |
| Background Vs. Ctrl. b | .014* |
| Background Vs. Ctrl. c | .008* |
| Background Vs. Ctrl. d | .014* |
| Background Vs. Ctrl. e | .005* |

* Statistically significant difference (p <0.05).

Again we wanted to investigate the various sequences with ±90% 1/3 MED. For sequence I all combinations showed a significant difference except for the sequence I at $-90-90\%$ which is expected as the fractionated dose at 305nm and 365nm are both below the one third MED dose. This is the same case for sequence II with $-90-90\%$ been the only combination not to give a significant difference with p-value 0.317 greater than 0.05. The fact that these two combinations do not result in MED suggests no photoaugmentation mechanism occurs.

Table 6.10: MED versus Sequences I and II ±90% 1/3MED (Friedman Two-Way Analysis).

| | Comparison | p-value |
|---|---|---|
| Sequence I | Background *Vs.* $+90+90\%$ | 0.002* |
| | Background *Vs.* $+90-90\%$ | 0.014* |
| | Background *Vs.* $-90+90\%$ | 0.008* |
| | Background *Vs.* $-90-90\%$ | 0.083 |
| Sequence II | Background *Vs.* $+90+90\%$ | 0.002* |
| | Background *Vs.* $+90-90\%$ | 0.008* |
| | Background *Vs.* $-90+90\%$ | 0.025* |
| | Background *Vs.* $-90-90\%$ | 0.317 |

* Statistically significant difference (p <0.05).

**Discussion and Conclusion**

UVR is sometimes used as a treatment for various common skin conditions, including psoriasis, acne, and eczema. The dosage of UV light is prescribed according to an individual's skin sensitivity. Human skin varies in its sensitivity to UV radiation because of varying degrees of skin pigmentation, thickness, and other factors. Thus, to establish the proper dosage of UV light to administer to a patient, the patient's MED was determined, which is generally understood as the amount of UV radiation that will produce minimal erythema (sunburn or redness caused by engorgement of capillaries) of an individual's skin following an UV exposure. The effects of repeated sub-erythemal UVR exposure on human skin have been insufficiently investigated. Fractions of the predetermined MED were used in various combinations to show superimposed sub-erythemal exposures of UVA and UVB could be added linearly.

The purpose of this study was to determine the MED in normal volunteers and CAD patients following irradiation at wavelengths 305nm, 335nm and 320nm, using full bandwidths at half maximum intensity 5nm, 27nm and 27nm at each wavelength respectively. Then we compared the effectiveness of different wavelength combinations assuming linear additivity or photo addition.

Figures 6.1 and 6.3 summarise the two sequences used in this investigation. Sequence I involved irradiation with UVB first and the second with UVAI first, while UVAII, second super imposed irradiated in the sequence, remained constant at just 1/3 of the fractional dose. An erythemal response was the biological endpoint for the fractionated MED doses and sequence combinations. The order of the sequences for each individual was generated by a random number (1-100) in a Matlab program where if number $< 50$ Sequence I was irradiated first or if if number $> 50$ Sequence II was irritated. The visual assessor was not involved in the phototesting and did not know the sequence order maintaining a blind study.

Once the Friedman test revealed there was a significant difference among the groups, a pairwise test was implemented using the Friedman two way statistics to test if there was a difference between the background non-exposed site and the

individual sub erythemal multi exposed sites.

In conclusion, the spectrophotometer as a colourimeter tool did not offer a quantitative assessment for subtle biological changes. Although Westerhof *et al.* [287] reported that the a* value reflects the perceptive erythema or MED measured by the optical method, the a* values measured in MED sites did not show any remarkable pattern in this study. In addition, $\Delta E^*$ values were all >1 even for irradiated sites where the visual assessment score was 0 using the grading system in Table 6.4.

Therefore, all MEDs were determined by the naked eye. Various sequence combinations were developed to investigate the photobiological phenomena of multiple fractionated MEDs to induce an erythemal reaction. The observed MEDs in each subject at each central wavelength and bandwidth are given in Table 6.5. We can see the corresponding L*a*b* readings for each skin type and the $\Delta a*$ for erythema response. It must be noted that for many of these readings the difference between background and irradiated MED site resulted in a negative value as many times the a* for the background was higher than after exposure. All the $\Delta a* < 2.5$ criteria to quantify as an increase in erythema.

Referring to Tables 6.7 and 6.10 the $+40 + 40\%$ and $+90 + 90\%$ sites all gave a significant increase in redness, which is unsurprising and does not help in the understanding the question of - photoaddition. Likewise, the $-40 - 40\%$ and $-90 - 90\%$ sites failed to reveal redness and, again, does not improve our knowledge of photoaddition mechanisms.

However, with one exception, there was a significant increase in redness where a percentage increase of the fractional MED at one wavelength was balanced by an equal decrease in percentage for the fractional MED at another wavelength. The exception was $+40 - 40\%$, but since there was a significant erythema at $+90 - 90\%$, it is likely that this was an aberrant result.

In summation, this pilot study implies that UVB, UVAII and UVAI are linearly additive. In other words, there was no evidence to support either photoaugmentation or photoprotection. Furthermore the order of which the wavelengths are irradiated

is inconsequential to the ensuing reaction. We recognise there is considerable variability in the results but the conclusion is that UV exposure is linearly additive between wavelengths 305 nm and 365 nm. This provides support for the practice of considering exposure to a broadband source as being comparable to the summation of response at each individual wavelength.

While the MED was ranked as a just perceptible erythema perhaps a well defined demarcated MED would be of better consideration if the study was repeated. Since the measurements involved such subtle changes of the skin a well defined MED could be also more quantifiable by the spectrophotometer device. The lack of CAD data was a problem for performing statistics with n=3 which stopped any comparison with mechanisms for sub-erythemal with healthy subjects. This low sample number and interesting results from the healthy subjects warrants further investigation with a greater population sample.

Some of the difficulties incurred in this study were problems in interpreting the erythema on day 4 of phototesting due to pressure points from bra-straps, noised "blotchy" skin areas or an overheated subject.

# Chapter 7

# Concluding Remarks

## 7.1 Summary

UVR is the main known environmental risk factor for skin cancer. Exposure to high levels of UV is known to have consequences for human health including erythema, DNA damage and skin cancer (BCC, SCC and melanoma).

Few studies have estimated the output from artificial tannings units and no data existed in England prior to this work. The initial objective of the thesis was to measure and collate the UV emissions from 200 sunbeds across the UK including boroughs of London. The final number of measured sunbeds exceeded this number reaching 402 making this the largest comprehensive study worldwide [267].

A diode array spectrometer was used to acquire the data. This was the obvious choice for field measurements as it offered fast acquisition times which was important for short sunbed sessions. The small compact nature of the device also offered good portability which was necessary when moving quickly between sunbed premises. However, calibration is paramount for this device to offer accurate results. The spectrophotometer was calibrated in the photophysics lab with a reference source that is traceable to the NPL. An inherent problem with spectroradiometers is that they suffer from high levels of stray light, especially at shorter wavelenghts. However, stray light can be removed with careful mathematical corrections [52] ensuring correct responsivity of the instrument. In this study a stray light correction method

used wavelength cut-off filters described in Chapter 2.

One of the aims of the study requested by CRUK and Westminster was to compare the output levels to the European compliance levels which states sunbeds should not exceed the 0.3 $Wm^{-2}$ erythemal weighted irradiance level described in Table 2.1. The erythemal weighted irradiance level describes the ability of a particular dose of UVR to induce erythema and serves as an indicator for adverse effect of the sunbed. The weighted irradiance is calculated by weighting the sunbed's emission spectrum with a biologically effective action spectrum. The findings showed that 90% of sunbeds in the UK are over the compliance level [267]. An average erythema-effective irradiance of 0.56 $Wm^{-2}$ was determined for sunbeds. This corresponds to a UV index of 22.4, which is significantly higher than the UV index of 8.5 of the high summer sun at noon at intermediate latitudes [107].

While the erythemal action spectrum was used to compare the compliance levels, another action spectrum called SCUP-h was used to investigate the potential carcinogenic effect of sunbeds. The SCUP-h action spectrum indicates the relative effectiveness for induction of nonmelanoma skin cancer [62]. Its merit is in facilitating a quantitative comparison between artificial tanning units and sunlight. This action spectrum was also applied to the solar spectrum from Thessaloniki to give a relative comparison between sun and sunbeds. In the present study, the mean SCUP-h irradiance was 2.3 times that of Mediterranean sunlight.

A recent study by Public Health England confirmed the results in a similar study on sunbed emissions where 85% of the 197 sunbeds were indeed over the compliance limit [146]. This bolsters confidence in the accuracy of the calibration methodology and in field measuring technique.

**Squamous Cell Carcinoma**

Chapter 3 presented a mathematical model that predicts the increased risk of SCC with sunbed use. There is persuasive evidence both of experimental and epidemiological nature that the sun can cause SCC, BCC and melanoma skin cancer. As

SCC is directly related to UV exposure it was possible to develop a model to include plausible sunbed scenarios including the exposure doses calculated from empirical data. This is the first time a model has included sunbed use to predict increased risk of SCC. The data presented here provides a dose-response relationship between sunbed use and the risk of SCC. The model was based on a power law relationship based on cumulative lifetime dose and advanced age. The model considered sunbed use of a young adult beginning in their 20s and period of use for 5, 10 and 15 years. Other model scenarios could have been use but these we considered the most relevant. There was also quite a variation in the sunbed output which translated into a variation of times when a sunbed session exposure time was applied. Again not every scenario was modeled but the 5th, 50th and 95th percentile was used to give a flavour of the range. The sunbed time was set for 12 mins and day to day dose 166 SED. The Relative Cumulative Incidence (RCI) of SCCs for sunbed user to non-sunbed user for a baseline day-to-day dose 166 SED, 10.5 days holiday and additional sunbed dose based on a 12 min session 45 times per year (equivalent to 6 min 90 sessions or 9 min 60 sessions) was found to be 90% increase for median sunbed dose at 55 years of age and 180% increase for the top 95th percentile sunbed output.

**Optical Properties and Monte Carlo Radiative Transfer**

Accurate understanding of the optical properties of human skin layer is vital for modelling of light propagation in skin turbid media [12, 277]. The radiative transfer theory has served as a framework for modelling light propagation and distribution described fully in Chapter 5. The tissue model is only as accurate as the optical properties entered into the Monte Carlo Radiative Transfer (MCRT) code. Thus, it is important to have accurate data for the various layers and light absorbing chromophores. The optical properties were derived from published literature but challenge was in deciphering which data were more reliable. Furthermore, much of this published data was for optical properties in the visible range and it proved even

more difficult to derive data for the UV wavelengths.

The main chromophores involved in skin tissue are melanin and haemoglobin. In order to derive the melanin levels in the epidermis the concentrations were estimated from literature and personal correspondence. The final melanin contents volume fraction Vm= 2.55% represented a skin type I individual. This number was later confirmed by specrophotometer reflectance readings and conversion to a melanin score which could be used in a look-up table, the result of which was Vm= 2.3% which was a good approximation of the melanosome volume fraction used to calculate the melanin optical properties used in the MCRT simulations.

**Quantification of DNA Damage**

The main objective of the MCRT was to estimate the amount of photons absorbed by the DNA. The DNA optical properties were established from first principles with the molar absorption for oligonucleotide. Comparing the DNA adsorbed photon yield for the solar and sunbed spectra allows us to establish a comparable value for CPD formation. While we only consider the UVA component as generating CPDs it is a valid argument as the increasing genotoxic evidence of UVA radiation emerge. While the mechanism required to transfer energy of UVA to DNA directly is yet unidentified there are studies showing CPD formation. Some argue that the damage is an indirect process. However, this notion seems to downplay the fact that absorbance of UVA radiation, albeit small, is not insignificant [255], and exposure in sunbeds involve high radiation doses. Quantification of CPD frequency from UVR is important to understanding DNA damage and the aetiology of photo-carcinogenesis.

The results confirm that subgroups of fair-skinned individuals are particularly 'at risk'. By understanding which patterns of exposure to natural and artificial sources of ultraviolet radiation are most detrimental and which subgroups of the population are most 'at risk' when exposed, one may be able to design more precise models by using detailed phenotypic, sunbed and sun exposure data.

In DNA a cyclobutane pyrimidine dimer (CPD) is formed by linkage of two

adjacent pyrimidines and can occur after UV irradiation. The induction of the various CPD lesions is wavelength dependent. Formation follows photon absorption. Most photoproducts are induced efficiently at the absorption maximum of DNA, i.e. 260 nm, but the UVB wavelength range is still very effective in this respect. Generally, cells possess effective mechanisms to remove damage from their DNA. In mammalian cells NER is the most important mechanism for the removal of these lesions from the genome [98].

The biological effects of UV exposure of the skin are manifold. In many of these, mainly UVB-induced effects, CPDs have been shown to play important roles. The research on this subject has made strong progress in demonstrating that UVA also plays a role in CPD formation. UV can also indirectly cause damage to DNA. Indeed, the long UVAI and UVAII are only very weakly absorbed by the DNA. On the other hand, they excite cellular chromophores which, in turn, generate ROS [272]. Examples of ROS are singlet oxygen, hydrogen peroxide and hydrogen radical.

Few studies have analysed specifically the use of sunbeds as a function of skin type and DNA damage. In 1992 the IARC stated "There is sufficient evidence in humans for carcinogenicity of solar radiation. Solar radiation causes cutaneous malignant melanoma and non-melanotic skin cancer" [14]. If we know that the DNA chromophore is damaged by UVR and sunbeds contain a higher irradiance for this UV region of spectrum it suggests that artificial tanning units have a greater carcinogenic potential.

An increase in noninherited (somatic) mutations has been documented in aged cells and tissues of both humans and mice, and presumably relates to cumulative lifetime exposure to exogenous DNA damaging agents such as UVR. Somatic mutation theory explains how DNA damage can lead to the malignant transformation of cells. Thus it elucidates the connection between UV genotoxic agents and cancers.

Somatic mutagenesis theory, developed by Thilly [264], and improved by Holmquist and Gao [123], attempts to predict the probability that damage generated by a mutagen causes a mutation. This probability is theoretical and difficult, if not im-

possible, to implement. It is dependent on the frequency of the damage sustained by the mutagen, the speed by which the cell repairs the damage and the possibility that this damage becomes a mutation after the replication of DNA (mutagenic potential). High frequency of damage to a particular nucleotide, a speed of slow repair and a mutagenic potential of damage are ideal conditions for forming mutation. This probability is also dependent on the fact that this mutation can lead to tumourigenicity.

In fact, only a very small portion of our genomic DNA codes for genes, and only a small portion of these genes are important in the maintenance of cell integrity. The transfer must occur at the level of a gene that, when mutated, contributes to the neoplastic development. Fundamentally sunbeds are a carcinogenic mutagen and risk is enhanced with usage. Carcinogenesis risk is based on individual genetic susceptibility. However this increases with enhanced exposure to photon hits. The following sequence of events leads to skin cancer:

DNA absorbed photons $\rightarrow$ CPD kbp$^{-1}$ lesions $\rightarrow$ tumourgenesis $\rightarrow$ photo-carcinoma

## 7.2 Future Work

The Monte Carlo program could be further refined and extended. For instance the absorbed photons in the DNA could be extended to included ROS and generation of singlet oxygen species, possibly together with 6-4 photoproducts and CPDs. While we can simulate the number of CPD lesions formed a step further would be find the quantum yield for number of CPDs that lead to tumourgenesis. While not every absorbed photon yields a lesion one possible refinement would be to adopt the "double hit" theory where a skin cell requires at least two solar events in order to emerge and become skin cancer [36]. It would be possible to implement this model by tracking the location where the photon is absorbed in the DNA and if two photons are absorbed in the same location then a mutation is formed in the genome. The MCRT could be further refined by having the melanin and DNA

diploid inter-dispersed in the epidermis instead of a mono-layer.

Collection of large datasets from case–control, families and twin studies with detailed phenotypic and sunbed exposure data combined with genotyping may help in the future in dissecting the relative contribution of genes and environment in the causation of melanoma. The increase in sun exposure and sunbed use in Caucasian populations over the last 20 years may also have a significant effect on the melanoma risk in the years to come, so the true impact of sunbed exposure is, as yet, uncertain.

Possible refinements could be the addition of more time reduction techniques, or more efficient programming, by improving algorithms and writing time critical parts of the program in machine code. Future work would involve adding an extra layer to account for degradation of sebum layer as we age, consider distribution of melanin through out the epidermis for skin types IV and greater. Another advancement would involve the ROS species for UVA generation of singlet oxygen generation similar to work done in photodynamic therapy Monte Carlo modelling [274].

While the mathematical model for SCC considers period of sunbed use the risk does not continue after cessation of sunbed use. However, this would not be the full picture as there would be a lag time of tumour induction of UV exposure. This could be possibly added to the SCC model to include the lag times. Another improvement would be to consider the sensitivity of different body sites and possible cancer risk weighting for different skin types. In this work we consider the sensitivity to be equal for all the body-sites. However, normally unexposed unpigmented areas could have a higher susceptibility to SCC.

The multiple sub-erythemal exposure clinical study could be redesigned to quantify an MED as fully demarcated MED helping to better quantify the chromameter readings.

The scope of this study covers a broad range from direct radiometric measurements, epidemiology, MCRT modelling and clinical work. The main underlying question addressed is the carcinogenic potential artificial tanning units possess.

## 7.3 Conclusion

In conclusion, the work presented in this thesis has demonstrated the potential photo-carcinogenic impact of artificial tanning units on the skin. The initial findings on compliance levels have helped inform Westminster on sunbed dangers from which laws have been imposed. However, much more has to be done to govern the industry. This could be by introducing nationwide licensing or outright ban.

This thesis with its complementary publications has strived to inform the public of the dangers of sunbeds. This is achieved by increasing the knowledge and understanding of the mechanisms involved with artificial UV on skin through mathematical and MCRT modelling in addition to a clinical study. Firstly the SCC model has demonstrated the increased like-hood of developing NMSC by mid 50s. While the MCRT has revealed the UV penetration depths into the basal and the number of absorbed photons. Lastly, the MCRT model has estimated the potential CPD formation from sunbeds. UVA, previously, considered to be innocuous to humans, may actually play a greater role in the induction of skin cancer. This thesis presents a basic model which offers a tentative approach to quantify DNA damage. One has to appreciate the level of complexities involved in human pathways to photoprotect the skin from UVR [205]. Skin type I-II fair-skinned people require three to five times less UVR to induce erythema than do those with moderately pigmented skin skin type III-IV, and up to 30 times less than darkly pigmented people skin type V-VI [214]. However, the MCRT simulations reveal that there is not a great deal of difference in the number of absorbed of photons by DNA in basal layer (epidermis 100 $\mu$m) which suggests it is the genetic makeup of the system that handles the UV damage from CPDs which is more efficient in some individuals.

Melanin also plays a protective role in the development of basal and squamous cell carcinomas of the skin. This is seen in the consistent negative association between these effects and skin pigmentation, although the precise mechanisms of protection are not known. It was demonstrated that melano-compromised skin type I had a higher degree of DNA photon absorption. In fact skin type I had on

average approximately 35% more absorbed photons at the basal layer than higher skin type III. There is still a high number of photons reaching DNA layer for skin type III. While pigmentation of an individual governs the amount of photo-shielding for the DNA basal layer, susceptibility to photo-carcinoma is also dependent on a individual's genetic ability to repair DNA damage. The work here suggests that that melanin may play a further role more than just photo-protection and may be involved in the genetic ability to repair.

In Chapter 6 we demonstrated that multiple sub-erythemal exposures are photoadditive giving an erythemal biological response for an individual's MED. The MED can vary from person to person depending on skin type. Young et al. suggests that DNA is a major chromophore for erythema in the 280–340 nm region [302].

One of the main motivations for individual use of sunbeds is for appearance (i.e. to look good) and general well-being, followed by "relaxation", the pleasant feeling of light and warmth, and the intention to get a "pre-holiday tan". People can get addicted to using sunbeds and the term tanorexic has emerged in recent years to describe such excessive behaviour [202].

There is no doubt of the biological consequences of UV exposure and deleterious effect it can have on humans at a cellular level. Sunbeds represent an additional source of UVR which can increase the UV burden on the cellular DNA in the epidermis. The incidence of NMSC continues to rise each year and the use of sunbeds is adding to these incidence rates. While SCC occurs more frequently in older people mainly due to the amount of UV exposure over a lifetime, young people are also at risk of developing SCC, especially those who expose themselves to artificial tanning sources such as sunbeds. As this is an unnecessary and avoidable risk, the data presented here strongly supports public health campaigns aiming to significantly reduce sunbed exposure.

Increasing the awareness surrounding sunbed hazards has improved in recent years with media campaigns. However, much work has to be done to inform the public of their susceptibility to skin cancer from these artificial tanning units. If

this has had one outcome, with its media presence, to make an individual consider twice before using what is essentially a “cancer tube” then we would deem this work a success.

# Appendix A

# Ranking Stats

| Background | | Crtl A | | Ctrl B | | Ctrl C | | Ctrl D | | Ctrl E | |
|---|---|---|---|---|---|---|---|---|---|---|---|
| Rated | Ranked | Rated | Ranked | Rated | Ranked | Rated | Ranked | Rated | Ranked | Rated | Ranked |
| 1 | 2.5 | 1 | 2.5 | 2 | 5.5 | 2 | 5.5 | 1 | 2.5 | 1 | 2.5 |
| 1 | 3.5 | 1 | 3.5 | 1 | 3.5 | 1 | 3.5 | 1 | 3.5 | 1 | 3.5 |
| 1 | 2 | 1 | 2 | 2 | 4 | 1 | 2 | 3 | 5.5 | 3 | 5.5 |
| 1 | 1.5 | 1 | 1.5 | 2 | 4.5 | 2 | 4.5 | 2 | 4.5 | 2 | 4.5 |
| 1 | 2 | 1 | 2 | 2 | 5 | 2 | 5 | 2 | 5 | 1 | 2 |
| 1 | 2 | 2 | 5 | 2 | 5 | 2 | 5 | 1 | 2 | 1 | 2 |
| 1 | 1.5 | 1 | 1.5 | 2 | 4.5 | 2 | 4.5 | 2 | 4.5 | 2 | 4.5 |
| 1 | 2.5 | 1 | 2.5 | 2 | 5.5 | 2 | 5.5 | 1 | 2.5 | 1 | 2.5 |
| 1 | 2 | 1 | 2 | 2 | 5 | 2 | 5 | 2 | 5 | 1 | 2 |
| 1 | 2 | 1 | 2 | 2 | 5 | 1 | 2 | 2 | 5 | 2 | 5 |
| **Rank total:** | 21.5 | | 24.5 | | 47.5 | | 42.5 | | 40 | | 34 |
| **Rank mean:** | 2.15 | | 2.45 | | 4.75 | | 4.25 | | 4 | | 3.4 |

Figure A.1: Example of Ranking for Control Group MED Healthy Volunteers.

# Appendix B

# Friedman Statistics

**Descriptive Statistics**

| | N | Mean | Std. Deviation | Minimum | Maximum |
|---|---|---|---|---|---|
| Background | 10 | 1.00 | .000 | 1 | 1 |
| ctrlA | 10 | 1.10 | .316 | 1 | 2 |
| ctrlB | 10 | 1.90 | .316 | 1 | 2 |
| ctrlC | 10 | 1.70 | .483 | 1 | 2 |
| ctrlD | 10 | 1.70 | .675 | 1 | 3 |
| ctrlE | 10 | 1.50 | .707 | 1 | 3 |

**Ranks**

| | Mean Rank |
|---|---|
| Background | 2.15 |
| ctrlA | 2.45 |
| ctrlB | 4.75 |
| ctrlC | 4.25 |
| ctrlD | 4.00 |
| ctrlE | 3.40 |

**Test Statistics[a]**

| | |
|---|---|
| N | 10 |
| Chi-Square | 22.692 |
| df | 5 |
| Asymp. Sig. | .000 |

a. Friedman Test

Figure B.1: SPSS Freidman test, Chi-Square=22.68.

# Appendix C

# Post-hoc Friedman Statistics

Sequence I

**Descriptive Statistics**

| | N | Mean | Std. Deviation | Minimum | Maximum |
|---|---|---|---|---|---|
| Background | 10 | 1.00 | .000 | 1 | 1 |
| SeqIa | 10 | 1.90 | .738 | 1 | 3 |
| SeqIb | 10 | 1.30 | .483 | 1 | 2 |
| SeqIc | 10 | 1.60 | .699 | 1 | 3 |
| SeqId | 10 | 1.30 | .483 | 1 | 2 |

**Ranks**

| | Mean Rank |
|---|---|
| Background | 2.10 |
| SeqIa | 3.90 |
| SeqIb | 2.75 |
| SeqIc | 3.40 |
| SeqId | 2.85 |

**Test Statistics[a]**

| | |
|---|---|
| N | 10 |
| Chi-Square | 11.656 |
| df | 4 |
| Asymp. Sig. | .020 |

a. Friedman Test

Sequence II

**Descriptive Statistics**

| | N | Mean | Std. Deviation | Minimum | Maximum |
|---|---|---|---|---|---|
| Background | 10 | 1.00 | .000 | 1 | 1 |
| SeqIIa | 10 | 2.10 | .568 | 1 | 3 |
| SeqIIb | 10 | 1.90 | .568 | 1 | 3 |
| SeqIIc | 10 | 1.60 | .699 | 1 | 3 |
| SeqIId | 10 | 1.20 | .422 | 1 | 2 |

**Ranks**

| | Mean Rank |
|---|---|
| Background | 1.80 |
| SeqIIa | 4.10 |
| SeqIIb | 3.75 |
| SeqIIc | 3.05 |
| SeqIId | 2.30 |

**Test Statistics[a]**

| | |
|---|---|
| N | 10 |
| Chi-Square | 22.626 |
| df | 4 |
| Asymp. Sig. | .000 |

a. Friedman Test

Figure C.1: Sequences I and II for MED fractional sub-erythema dose ±40%.

# Appendix D

# Friedman Statistics

**Descriptive Statistics**

| | N | Mean | Std. Deviation | Minimum | Maximum |
|---|---|---|---|---|---|
| Background | 10 | 1.00 | .000 | 1 | 1 |
| ctrlA | 10 | 1.60 | .699 | 1 | 3 |
| ctrlB | 10 | 1.80 | .789 | 1 | 3 |
| ctrlC | 10 | 2.00 | .816 | 1 | 3 |
| ctrlD | 10 | 1.90 | .876 | 1 | 3 |
| ctrlE | 10 | 2.10 | .738 | 1 | 3 |

**Ranks**

| | Mean Rank |
|---|---|
| Background | 1.90 |
| ctrlA | 3.05 |
| ctrlB | 3.60 |
| ctrlC | 4.15 |
| ctrlD | 3.85 |
| ctrlE | 4.45 |

**Test Statistics[a]**

| | |
|---|---|
| N | 10 |
| Chi-Square | 17.510 |
| df | 5 |
| Asymp. Sig. | .004 |

a. Friedman Test

Figure D.1: SPSS Friedman Test Controls 90, Chi-Square=17.51.

# Appendix E

# Post-hoc Friedman Statistics

Sequence I

**Descriptive Statistics**

| | N | Mean | Std. Deviation | Minimum | Maximum |
|---|---|---|---|---|---|
| Background | 10 | 1.00 | .000 | 1 | 1 |
| SeqIa | 10 | 2.60 | .516 | 2 | 3 |
| SeqIb | 10 | 1.60 | .516 | 1 | 2 |
| SeqIc | 10 | 1.80 | .632 | 1 | 3 |
| SeqId | 10 | 1.30 | .483 | 1 | 2 |

**Ranks**

| | Mean Rank |
|---|---|
| Background | 1.70 |
| SeqIa | 4.70 |
| SeqIb | 2.95 |
| SeqIc | 3.30 |
| SeqId | 2.35 |

**Test Statistics[a]**

| | |
|---|---|
| N | 10 |
| Chi-Square | 26.128 |
| df | 4 |
| Asymp. Sig. | .000 |

a. Friedman Test

Sequence II

**Descriptive Statistics**

| | N | Mean | Std. Deviation | Minimum | Maximum |
|---|---|---|---|---|---|
| Background | 10 | 1.00 | .000 | 1 | 1 |
| SeqIIa | 10 | 2.70 | .483 | 2 | 3 |
| SeqIIb | 10 | 2.00 | .816 | 1 | 3 |
| SeqIIc | 10 | 1.80 | .919 | 1 | 3 |
| SeqIId | 10 | 1.10 | .316 | 1 | 2 |

**Ranks**

| | Mean Rank |
|---|---|
| Background | 1.85 |
| SeqIIa | 4.55 |
| SeqIIb | 3.55 |
| SeqIIc | 3.10 |
| SeqIId | 1.95 |

**Test Statistics[a]**

| | |
|---|---|
| N | 10 |
| Chi-Square | 28.359 |
| df | 4 |
| Asymp. Sig. | .000 |

a. Friedman Test

Figure E.1: Sequences I and II for MED fractional sub-erythema dose ±90%.

# Appendix F

# Sunbed and Lamp Details

Table F.1: London Borough of Barnet

| Type | Type | Lamp | Watt | Effective UVB | Effective UVA | Total Erythemal Weighting | SCUP-H |
|---|---|---|---|---|---|---|---|
| Sunquest Aurora | V | Heraeus MagicSun 20/160R | 160 | 0.56 | 0.26 | 0.82 | 1.45 |
| Megasun Ultrapower 6800 | H | Heraeus Magicsun 20/160R | 160 | 0.65 | 0.37 | 1.02 | 1.74 |
| | face | | 400 | 0.13 | 0.20 | 0.33 | 0.58 |
| UWE P90 | HP | Heraeus MagicSun 20/160R | | 0.37 | 0.19 | 0.55 | 0.98 |
| | | XTT | 600 | 0.14 | 0.16 | 0.30 | 0.55 |
| | | Face XTT | 1000 | 0.12 | 0.16 | 0.28 | 0.51 |
| Tansun Symphony | V | Sun Extreme B 250W | 250 | 0.57 | 0.26 | 0.83 | 1.44 |
| Tansun Symphony | V | Sun Extreme B 160-225W | 225 | 0.65 | 0.29 | 0.94 | 1.66 |
| Ergoline Affinity 660 Dynamic | H | Ergoline Dynamic Power SR | 100-200 | 0.58 | 0.29 | 0.88 | 1.52 |
| | face | | 520 | 0.10 | 0.09 | 0.19 | 0.33 |
| Ergoline Lounge | V | Ergoline SR VXL | 180 | 0.47 | 0.22 | 0.69 | 1.21 |
| Topaz | V | Sunquest SQR | 180/200 | 0.74 | 0.33 | 1.07 | 1.97 |
| Solec UVB R (German) | V | Solec UVB-R | 160 | 0.28 | 0.14 | 0.41 | 0.71 |
| GardaSun Sunshine 7000 | V | Sunfit XL3 | 180 | 0.09 | 0.15 | 0.24 | 0.39 |
| Hex Cabin | V | Cosmolux VHR | 160 | 0.30 | 0.18 | 0.48 | 0.80 |
| Ergoline Classic 300 | H | NewColors 23/100R | 100 | 0.44 | 0.19 | 0.63 | 1.13 |
| | face | | 400 | 0.10 | 0.14 | 0.24 | 0.40 |
| Tansun VT2000 | V | Blue 2.2 /160W RXXL longlife (German) | | 0.17 | 0.10 | 0.27 | 0.45 |
| UltraSun Tower | V | Sunfit XXl Pro | 200 | 0.25 | 0.14 | 0.40 | 0.72 |
| Sontegra | H | New Technology Energy TX SR | 160 | 0.48 | 0.15 | 0.63 | 1.10 |
| | face | | 400 | 0.10 | 0.16 | 0.26 | 0.43 |
| TanCab | V | Philips Cleo Swift XPT TL 200W-R | 200 | 0.39 | 0.18 | 0.57 | 0.97 |
| TanCab | V | Philips Cleo Swift XPT TL 200W-R | 200 | 0.35 | 0.16 | 0.51 | 0.87 |
| TanCab | V | Philips Cleo Swift XPT TL 200W-R | 200 | 0.55 | 0.23 | 0.78 | 1.34 |
| Megasun Ultrapower 6800 by KBL | H | Megasun Super R | 160 | 0.23 | 0.16 | 0.39 | 0.64 |
| | Face | | 400 | 0.16 | 0.17 | 0.33 | 0.59 |
| Ergoline Classic Turbo Power 500 | H | High Power 160w RM | | 0.32 | 0.27 | 0.58 | 0.94 |
| | face | Ultra VIT 2.3 | 500 | 0.08 | 0.22 | 0.30 | 0.40 |
| | shoulder | | 25 | 0.36 | 0.18 | 0.54 | 0.93 |
| Ergo SunLounge | V | Ergo turbo power | 160 | 0.26 | 0.17 | 0.44 | 0.72 |
| Topaz | V | Platinum Max 240 | 180/240 | 0.58 | 0.24 | 0.82 | 1.51 |
| Topaz | V | Sunquest SQR | 180/200 | 0.38 | 0.20 | 0.58 | 1.00 |
| Sunvision V180XXl | V | New TechnologyIndependence Xtreme | 200 | 0.26 | 0.11 | 0.37 | 0.68 |
| MegaSun UltraPower 4000 | H | Sun-Xtreme B 160W-225W | 225 | 0.77 | 0.29 | 1.06 | 1.98 |
| | face | | 400 | 0.18 | 0.16 | 0.34 | 0.60 |
| UWE ibed | | Cosmedico | 180 | 0.19 | 0.12 | 0.30 | 0.52 |
| | face | Herasus Swing$^{TM}$ Powerspot | 250 | 0.22 | 0.15 | 0.37 | 0.73 |
| MegaSun by KBL | V | T230 MegaSun Pure Energy Reflector | 160 | 0.47 | 0.21 | 0.68 | 1.21 |
| UltraSun Power Tower | V | Sunfit Pro. XL + | 180 | 0.26 | 0.14 | 0.40 | 0.69 |
| Ergoline Avantgarde 600 | H | Fusion Power 1800XX(160R 2.6) | 180 | 0.51 | 0.20 | 0.71 | 1.32 |
| | face | Ultra VIT 2.3 | 500 | 0.16 | 0.36 | 0.52 | 0.78 |
| | shoulder | Discover UVA/UVB 2.0 Longlife | 25 | 0.18 | 0.08 | 0.26 | 0.46 |
| MegaSun by KBL | V | Fusion Power | 200 | 0.59 | 0.26 | 0.85 | 1.54 |
| Tansun Vitesse | V | Sun Extreme B | 160-225 | 0.63 | 0.29 | 0.92 | 1.61 |
| Ergoline Affinity 660 Dynamic | H | Ergoline E2 | 80-200 | 0.08 | 0.13 | 0.21 | 0.31 |
| | Face | | 500 | 0.03 | 0.10 | 0.12 | 0.18 |
| | shoulder | | 25 | 0.09 | 0.09 | 0.17 | 0.29 |
| Sun Angel S52 | H | Sonnen Angel | 80-200 | 0.02 | 0.08 | 0.10 | 0.18 |
| | face | Sonnen Angel type -B | 420 | 0.02 | 0.10 | 0.12 | 0.19 |
| UltraSun Alison V600 | V | Sunvision | 225 | 0.41 | 0.18 | 0.60 | 1.09 |
| Sunquest Aurora | V | Sunquest SQR | 200 | 0.54 | 0.26 | 0.80 | 1.39 |
| Sunquest Aurora | V | Sunquest SQR | 200 | 0.60 | 0.27 | 0.87 | 1.57 |
| GardaSun Sunshine 7000 | V | Sunfit XXl Pro | 180 | 0.29 | 0.14 | 0.43 | 0.80 |

## Table F.2: London Borough of Bexley

| Type | Type | Lamp | Watt | Effective UVB | Effective UVA | Total Erythemal Weighting | SCUP-H |
|---|---|---|---|---|---|---|---|
| UWE TuttiFrutti 41 UPP | H | New Technology | 180 | 0.21 | 0.11 | 0.32 | 0.57 |
| MegaSun 4000 UltraPower by KBL | V | Fusion Power | 180 | 0.34 | 0.17 | 0.52 | 0.95 |
| | face | | 400 | 0.15 | 0.15 | 0.29 | 0.55 |
| Ergoline Excellence 800 Turbo | H | Herasus Magicsun | 160 | 0.41 | 0.21 | 0.62 | 0.82 |
| | face | VIT 2.4 | 520 | 0.11 | 0.10 | 0.21 | 0.37 |
| | shoulder | | 25 | 0.25 | 0.11 | 0.36 | 0.62 |
| Tansun Symphony | V | Cosmostar X-tra Intensiv | 200 | 0.27 | 0.15 | 0.42 | 0.70 |
| Solton X-50 Turbo | V | Herasus NewColors 160R/23 | 160 | 0.26 | 0.12 | 0.38 | 0.68 |
| | face | | 400 | 0.18 | 0.15 | 0.33 | 0.63 |
| ErgolineEvolution 600 Turbo | H | Ergoline | 160 | 0.26 | 0.22 | 0.48 | 0.78 |
| | face | ultra VIT 2.4 | 520 | 0.20 | 0.21 | 0.41 | 0.74 |
| | shoulder | Ergoline SD | 25 | 0.26 | 0.11 | 0.36 | 0.62 |
| Ergoline Unknown | V | Maylight XL 180W-R High Intensiv | 180 | 0.19 | 0.15 | 0.33 | 0.56 |
| Sunquest Aurora | V | Sunquest SQR 180/200 | 180 | 0.47 | 0.22 | 0.69 | 1.21 |
| Sunquest Unknown | H | Sunquest SQR160 | 160 | 0.32 | 0.17 | 0.49 | 0.84 |
| Sunquest Aurora | H | Sunquest SQR 200/225 | 225 | 0.41 | 0.21 | 0.62 | 1.08 |
| Sunquest Aurora | H | Sunquest SQR 200/225 | 225 | 0.49 | 0.25 | 0.74 | 1.30 |
| Sunquest Zenith | H | Sunquest SQR 180/200 | 180 | 0.39 | 0.15 | 0.54 | 0.99 |
| Sunquest Aurora | V | Sunquest SQR 180/200 | 200 | 0.57 | 0.23 | 0.80 | 1.48 |
| Sunquest Aurora | V | Sunquest SQR 180/200 | 200 | 0.55 | 0.22 | 0.77 | 1.43 |
| Ergoline Classic 500 | H | Powerlight Inferno | 200 | 0.52 | 0.23 | 0.75 | 1.40 |
| | face | Ultra VIT 2.3 | 500 | 0.08 | 0.26 | 0.34 | 0.45 |
| | shoulder | Solarium | 25 | 0.32 | 0.15 | 0.47 | 0.80 |
| Soltron M55 Reflex | H | Cosmosun 28R | 200 | 0.52 | 0.19 | 0.72 | 1.34 |
| | face | PSR | 460 | 0.17 | 0.16 | 0.33 | 0.62 |
| | shoulder | Soltor Solarium P | 25 | 0.29 | 0.13 | 0.42 | 0.71 |
| Tansun Vitesse | V | Cosmedico 160-200W | 160-200 | 0.45 | 0.20 | 0.65 | 1.13 |
| Tansun Vitesse | V | Cosmedico 160-200W | 160-200 | 0.46 | 0.20 | 0.66 | 1.15 |
| Luxura X5 by Harpo | H | New Tech. Independent B. Extreme B | 160 | 0.54 | 0.22 | 0.76 | 1.42 |
| | face | Maxlight HPA | 400 | 0.09 | 0.21 | 0.30 | 0.48 |
| Tansun | V | Cosmedico Cosmolux | 160 | 0.27 | 0.15 | 0.43 | 0.70 |
| Tansun | V | Cosmedico Cosmolux | 160 | 0.40 | 0.21 | 0.61 | 1.04 |
| Luxura X7 by Harpo | H | New Technology Independent SR200 | 200 | 0.55 | 0.26 | 0.81 | 1.45 |
| | face | Maxlight HPA | 400 | 0.16 | 0.19 | 0.36 | 0.62 |
| Sunquest Aurora | V | Sunstream 200W 0.3W/m$\hat{2}$ | 200 | 0.14 | 0.19 | 0.33 | 0.50 |
| Sunvision by Alisun V200XXl | V | Unknown | 180 | 0.24 | 0.15 | 0.39 | 0.66 |
| Sunquest Aurora | V | Sunquest SQR 200/225 | 225 | 0.45 | 0.23 | 0.68 | 1.15 |
| Sunquest Aurora | V | Sunquest SQR 200/225 | 225 | 0.46 | 0.24 | 0.70 | 1.19 |
| Sunquest Aurora | V | Bellarium 180/225W X'treme R Max | 180 | 0.36 | 0.19 | 0.55 | 0.92 |
| Sunquest Aurora | V | Bellarium 180/225W X'treme R Max | 180 | 0.41 | 0.21 | 0.63 | 1.05 |
| Sunquest Zenith | H | Sunquest SQR160 | 160 | 0.37 | 0.22 | 0.58 | 1.00 |
| Sunquest Aurora | V | Tan 365 250W R Extreme | 250 | 0.70 | 0.28 | 0.98 | 1.85 |
| Sunquest Aurora | V | Tan 365 250W R Extreme | 250 | 0.70 | 0.27 | 0.97 | 1.82 |
| Sunquest Zenith | H | Sun-Xtreme B 160-225W Max | 225 | 0.48 | 0.17 | 0.65 | 1.01 |
| Sunquest Eclipse | V | Sun C-Xtreme Vit D | 225 | 0.50 | 0.16 | 0.66 | 1.28 |

## Table F.3: London Borough of Bromley

| Type | Type | Lamp | Watt | Effective UVB | Effective UVA | Total Erythemal Weighting | SCUP-H |
|---|---|---|---|---|---|---|---|
| UltraSun Solarwind 5000 | H | Sun-Xtreme B 160-225W Max | 225 | 0.39 | 0.18 | 0.57 | 1.03 |
| Sunquest Aurora | V | Sunquest SQR 180/200 | 200 | 0.40 | 0.24 | 0.64 | 1.07 |
| Ergoline Excellence 800 turbo | H | Heraeus | 160 | 0.31 | 0.13 | 0.44 | 0.81 |
| | face | Ultra VIT 2.4 | 520 | 0.18 | 0.13 | 0.30 | 0.59 |
| Ergoline Advantage 400 | H | Ergo 160 SR XXL Magic Power | 160 | 0.55 | 0.22 | 0.77 | 1.45 |
| | face | Ultra VIT 2.3 | 400 | 0.10 | 0.28 | 0.38 | 0.55 |
| | shoulder | Heraeus | 25 | 0.14 | 0.07 | 0.20 | 0.36 |
| Ergoline 800 iq intelligent power-climatron | H | Ergo 160 SR XXL Magic Power | 160 | 0.45 | 0.19 | 0.64 | 1.20 |
| | face | Ultra VIT 2.3 | 400 | 0.20 | 0.12 | 0.32 | 0.65 |
| Ergo 500 Classic | H | Sun Extreme B 160-225W | 225 | 0.31 | 0.15 | 0.47 | 0.81 |
| | face | ultra vit 2.3 | 400 | 0.05 | 0.14 | 0.19 | 0.29 |
| | shoulder | Ergo SD | 25 | 0.16 | 0.07 | 0.23 | 0.39 |
| Ergo 600 Classic | H | Fusion Power 180XX 160R 2.6 | 180 | 0.43 | 0.16 | 0.59 | 1.11 |
| | face | ultra vit 2.3 | 400 | 0.11 | 0.21 | 0.32 | 0.50 |
| | shoulder | Philips Cleo | 25 | 0.06 | 0.04 | 0.11 | 0.18 |
| Sunquest Aurora | V | Fusion Power 200XXX CCt | 200 | 0.49 | 0.19 | 0.68 | 1.26 |
| Sunquest Zenith | H | Sunquest SQR 225W | 225 | 0.38 | 0.18 | 0.56 | 0.96 |
| Sunquest Aurora | V | Sunquest SQR 225W | 225 | 0.56 | 0.27 | 0.84 | 1.45 |
| Topaz | V | Sunquest SQR 225W | 225 | 0.63 | 0.29 | 0.92 | 1.59 |
| Tansun Symphony | V | Titan 200W | 200 | 0.25 | 0.13 | 0.38 | 0.64 |
| Tansun Symphony | V | Titan 200W | 200 | 0.28 | 0.15 | 0.43 | 0.74 |
| Ergoline Advantage 600 | H | Ergo XXL 160SR Magic Power | 160 | 0.62 | 0.25 | 0.87 | 1.65 |
| | face | Ultra Vit 2.3 | 400 | 0.13 | 0.26 | 0.38 | 0.57 |
| | shoulder | Ergo SD | 25 | 0.17 | 0.09 | 0.26 | 0.48 |
| Sunquest Aurora | V | Ergoline 200W Magic Plus 2.4 R | 200 | 0.65 | 0.30 | 0.95 | 1.70 |
| Ergoline Advantage 600 | H | Bodysoft 364b Rss Reflector S | 160 | 0.23 | 0.14 | 0.37 | 0.63 |
| | face | ultra vit 2.3 | 400 | 0.04 | 0.10 | 0.15 | 0.21 |
| | shoulder | Ergoline SD 254 | 25 | 0.09 | 0.05 | 0.14 | 0.55 |
| Ergoline Excellence 700 | H | Ergoline 160XXl R Magic Power | 160 | 0.65 | 0.24 | 0.89 | 1.67 |
| | face | Ultra VIT 2.4 | 520 | 0.19 | 0.30 | 0.50 | 1.63 |
| | shoulder | Ergoline SD | 25 | 0.21 | 0.11 | 0.33 | 0.61 |
| Ergoline Advantgarde 600 | H | Ergo XXl 160SR Magic Power | 160 | 0.65 | 0.27 | 0.93 | 1.72 |
| | face | Ultra VIT 2.3 | 400 | 0.11 | 0.31 | 0.41 | 0.54 |
| | shoulder | Ergoline SD | 25 | 0.18 | 0.09 | 0.27 | 1.72 |
| Ergoline Excellence 700 | H | Ergoline 160XXl R Magic Power | 160 | 0.71 | 0.28 | 0.99 | 1.86 |
| | face | Ultra VIT 2.3 | 400 | 0.12 | 0.31 | 0.43 | 0.62 |
| | shoulder | Ergoline SD | 25 | 0.24 | 0.14 | 0.39 | 0.72 |
| Ergoline Excellence 800 | H | Ergoline 160XXl R Magic Power | 160 | 0.69 | 0.30 | 0.99 | 1.84 |
| | face | Ultra VIT 2.4 | 520 | 0.16 | 0.26 | 0.43 | 0.69 |
| | shoulder | Ergoline SD | 25 | 0.38 | 0.17 | 0.55 | 0.94 |

## Table F.4: London Borough of Islington

| Type | Type | Lamp | Watt | Effective UVB | Effective UVA | Total Erythemal Weighting | SCUP-H |
|---|---|---|---|---|---|---|---|
| UVScan | V | New Technology Independence B | 160 | 0.54 | 0.22 | 0.76 | 1.43 |
| Garda Sunshine 7000 | V | Sunfit XL3 R180W Pro | 180 | 0.11 | 0.11 | 0.21 | 0.35 |
| UltraSun i7 | V | Sunfit XL3 R180W Pro | 180 | 0.12 | 0.13 | 0.25 | 0.41 |
| Sunquest | H | Sunquest SQR | 160 | 0.34 | 0.18 | 0.52 | 0.90 |
| Sunquest | V | Sunstream | 200 | 0.06 | 0.41 | 0.47 | 0.77 |
| Sunquest | V | Sunstream | 200 | 0.05 | 0.44 | 0.49 | 0.76 |
| Ergoline Classic 500 | H | Ergoline XXl 160SR Magic Power | 160 | 0.69 | 0.26 | 0.95 | 1.81 |
| face | | Ultra VIT 2.3 | 500 | 0.08 | 0.20 | 0.27 | 0.39 |
| shoulder | | Ergoline SD Power | 25 | 0.15 | 0.10 | 0.25 | 0.46 |
| Ergoline | V | Tan 365 | 225 | 0.62 | 0.22 | 0.83 | 1.60 |
| Ergoline | V | Tan 365 | 225 | 0.56 | 0.19 | 0.75 | 1.43 |
| Luxura by Harpo V7 | V | V7 48 XL Intensiv | 180 | 0.38 | 0.19 | 0.58 | 1.03 |
| Soltron M55 Wave Turbo | H | Ergoline XXl 160SR Magic Power | 160 | 0.57 | 0.23 | 0.80 | 1.49 |
| face | | Soltron | 500 | 0.17 | 0.11 | 0.28 | 0.54 |
| shoulder | | soltron | 25 | 0.34 | 0.15 | 0.49 | 0.85 |
| Soltron M55 Wave Turbo | H | Ergoline XXl 160SR Magic Power | 160 | 0.53 | 0.25 | 0.79 | 1.44 |
| face | | Soltron | 500 | 0.12 | 0.10 | 0.22 | 0.42 |
| shoulder | | soltron | 25 | 0.37 | 0.16 | 0.53 | 0.93 |
| Ergoline Sunlounge | V | Ergoline PurePower | 180 | 0.24 | 0.16 | 0.40 | 0.66 |
| Ergoline Advantage 400 TurboPower | H | Ergo | 160 | 0.13 | 0.15 | 0.28 | 0.43 |
| face | | Ultra Vit 2.4 | 520 | 0.20 | 0.16 | 0.35 | 0.67 |
| Ergoline Sunlounge | V | Cosmedico Cosmofit | 180 | 0.13 | 0.16 | 0.29 | 0.45 |
| Ergoline Sunlounge | V | Ergoline Max Tan V Turbo Power | 180 | 0.25 | 0.15 | 0.39 | 0.65 |
| Sunvision V180XXl | V | Fusion Power 180 R | 180 | 0.21 | 0.12 | 0.33 | 0.59 |
| Sunquest | H | Sunquest SQR 180/200W | 200 | 0.36 | 0.18 | 0.53 | 0.92 |
| Sunquest | H | Sunquest SQR 180/200W | 200 | 0.50 | 0.21 | 0.71 | 1.31 |
| UltraSun Power Tower i8 | V | Sunfit XXL3 | 200 | 0.11 | 0.14 | 0.25 | 0.41 |
| Ergoline 500 | H | Ergoline XXL 160SR Magic Power | 160 | 0.70 | 0.33 | 1.03 | 1.90 |
| face | | ultra VIT 2.3 | 500 | 0.11 | 0.25 | 0.36 | 0.50 |
| shoulder | | Ergoline SD | 25 | 0.45 | 0.21 | 0.66 | 1.15 |
| Ergoline 500 | H | Bermuda Gold Supernova 160W SR+ | 160 | 0.37 | 0.22 | 0.59 | 1.02 |
| face | | ultra VIT 2.3 | 500 | 0.08 | 0.24 | 0.31 | 0.46 |
| shoulder | | Ergoline SD | 25 | 0.30 | 0.15 | 0.45 | 0.85 |
| Megasun Ultra Power 4000 by KBL | H | Discover UVA/UVB Longlife 2.4 160W | 160 | 0.76 | 0.27 | 1.03 | 1.97 |
| face | | | 400 | 0.19 | 0.20 | 0.39 | 0.70 |
| Garda Sunshine 8000 | V | Sunfit 180 XL Pro | 180 | 0.33 | 0.20 | 0.53 | 0.91 |
| Ultrasun 3500 | H | Cosmedico Cosmolux 120W XT 1.9M | 120 | 0.24 | 0.13 | 0.37 | 0.63 |
| Ergoline 500 | H | B'Xtreme Powerlight 160-200W | 200 | 0.53 | 0.28 | 0.81 | 1.40 |
| face | | Ultra VIT 2.3 | 500 | 0.11 | 0.36 | 0.47 | 0.68 |
| shoulder | | Heraeus | 25 | 0.11 | 0.06 | 0.17 | 0.28 |
| Sunvision by Alisun v200XXl X-Classic | V | Fusion Power 200W | 200 | 0.37 | 0.17 | 0.54 | 0.98 |
| Sunvision by Alisun 500XXl | H | Fusion Power 200W | 200 | 0.35 | 0.17 | 0.52 | 0.93 |
| face | | | 500 | 0.09 | 0.15 | 0.24 | 0.39 |
| Gardasun | V | Sunfit XL Pro | 180 | 0.24 | 0.12 | 0.36 | 0.66 |
| Gardasun | V | Sunfit XL Pro | 180 | 0.27 | 0.13 | 0.40 | 0.73 |
| Sun Angel S52 | H | Sonnen Angel 80-200W type N | 80-200 | 0.08 | 0.14 | 0.22 | 0.37 |
| face | | Sonnen Angel type -B | 420 | 0.02 | 0.14 | 0.17 | 0.26 |
| Sunvision by Alisun | V | Fusion Power 250R 2.6 1.9XX | 250 | 0.32 | 0.15 | 0.47 | 0.87 |
| Sunquest Aurora | V | Sunquest SQR 180/200W | 200 | 0.29 | 0.18 | 0.47 | 0.80 |
| Sunquest Aurora | V | Sunquest SQR 180/200W | 200 | 0.42 | 0.23 | 0.65 | 1.12 |

## Table F.5: London Borough of Newham

| Type | Type | Lmp | Watt | Effective UVB | Effective UVA | Total Erythemal Weighting | SCUP-H |
|---|---|---|---|---|---|---|---|
| Ergroline Soltron X50 turbo | H | Pure Sylvina | 160 | 0.36 | 0.15 | 0.51 | 0.95 |
| | face | | 400 | 0.19 | 0.14 | 0.33 | 0.64 |
| Ultrasun Power Tower | V | Cosmedico Cosmolux | 220 | 0.29 | 0.15 | 0.44 | 0.75 |
| Tansun Symphony | V | Philips TL 225W Max-R Cleo Cage Advantage XPT | 225 | 0.68 | 0.21 | 0.89 | 1.75 |
| Tansun Symphony | V | Pure Power Sylvina | 200 | 0.46 | 0.17 | 0.63 | 1.17 |
| Ergoline 600 | H | Tan 365 160-225W R Extreme | 200 | 0.38 | 0.13 | 0.51 | 0.98 |
| | face | Ultra VIT 2.3 | 500 | 0.06 | 0.12 | 0.18 | 0.27 |
| | | Heraeus | 25 | 0.14 | 0.07 | 0.21 | 0.36 |
| UWE XTT | H | UWE Breeze Tec Funatic Newcolors | 160 | 0.34 | 0.13 | 0.47 | 0.86 |
| | face | | 400 | 0.10 | 0.10 | 0.20 | 0.35 |
| Tan Cabin Unknown | V | UVA Speed HRR-S | 200 | 0.37 | 0.17 | 0.54 | 0.96 |
| Harpo Lumina 3603 | H | New Technology Independent Extreme | 200 | 0.38 | 0.21 | 0.59 | 1.03 |
| | face | | 400 | 0.03 | 0.08 | 0.12 | 0.18 |
| Malibu Tanning Sola | V | New Technology Independent Extreme | 200 | 0.50 | 0.27 | 0.77 | 1.35 |
| Tansun Viva | V | Power Max High Intensiv | 200 | 0.24 | 0.13 | 0.38 | 0.65 |
| Garda Sunshine 7000 | V | Sunfit XL | 180 | 0.19 | 0.10 | 0.29 | 0.53 |
| Topaz by Sunquest | V | Discover 225-250W | 225 | 0.64 | 0.27 | 0.91 | 1.68 |
| Topaz by Sunquest | V | Discover 225-250W | 225 | 0.52 | 0.22 | 0.74 | 1.38 |
| Megasun Space 2000 by KBL | V | New Technology | 200 | 0.63 | 0.31 | 0.94 | 1.66 |
| Megasun Space 2000 by KBL | V | New Technology | 200 | 0.67 | 0.32 | 0.99 | 1.76 |
| Sunvision V200XXL by Alisun | V | New Technology | 200 | 0.47 | 0.21 | 0.69 | 1.28 |
| Sunvision V200XXL by Alisun | V | New Technology | 200 | 0.49 | 0.22 | 0.71 | 1.32 |
| Contour Suntan Express | V | UHP-R | 200 | 0.22 | 0.15 | 0.37 | 0.63 |
| Q-Med High Performance Q50-180 | V | Ergoline 200W R | 200 | 0.58 | 0.29 | 0.87 | 1.54 |
| Soltron Charming Cherry L-65 Dynamic Power AVS. | H | Ergoline SR 100-200W | 200 | 0.51 | 0.23 | 0.75 | 1.34 |
| | face | | 500 | 0.17 | 0.23 | 0.40 | 0.67 |

# Table F.6: London Borough of Sutton

| Type | Type | Lamp | Watt | Effective UVB | Effective UVA | Total Erythemal Weighting | SCUP-H |
|---|---|---|---|---|---|---|---|
| UVAscan | V | Turbo Power TVR200 FR2MT12 , ERGOLINE | 180 | 0.38 | 0.17 | 0.56 | 1.01 |
| Ergoline 600 Avantgarde | H | Ergo XXL 160 SR Magic Power | 160 | 0.53 | 0.20 | 0.73 | 1.37 |
| | face | Ultra VIT 2.3 | 500 | 0.12 | 0.29 | 0.41 | 0.58 |
| | shoulder | Ergo SD | 25 | 0.13 | 0.06 | 0.19 | 0.33 |
| Ergoline 600 Avantgarde | H | Cosmedico Cosmolux | 160 | 0.31 | 0.16 | 0.47 | 0.79 |
| | face | ultra VIT 2.3 | 500 | 0.10 | 0.33 | 0.43 | 0.59 |
| | shoulder | Cosmedico | 25 | 0.09 | 0.04 | 0.13 | 0.22 |
| Ergoline 800 Excellence | H | Cosmedico Cosmolux | 160 | 0.28 | 0.14 | 0.43 | 0.72 |
| | face | Ultra VIT 2.4 | 520 | 0.11 | 0.23 | 0.34 | 0.55 |
| | shoulder | Ergoline SD | 25 | 0.16 | 0.08 | 0.24 | 0.40 |
| Tansun Symphony | | unknown | 180 | 0.39 | 0.20 | 0.59 | 1.01 |
| Ergoline Lounge | H | Ergoline SR VXL 180W | 180 | 0.33 | 0.15 | 0.48 | 0.84 |
| Ergoline Excellence 700 | H | Ergoline SR 100-200W Dynamic Power | 100-200 | 0.35 | 0.19 | 0.54 | 0.95 |
| | face | Ulta VIT 2.4 | 520 | 0.12 | 0.19 | 0.31 | 0.51 |
| Tansun Viva | V | Powermax 200 High Intensiv | 200 | 0.34 | 0.17 | 0.51 | 0.89 |
| Ultrasun Power Tower 8000 | V | Sunfit Pro 200W XXl | 200 | 0.29 | 0.15 | 0.45 | 0.81 |
| Ultrasun Sunrise 3500 | H | Sunfit Pro XL+ | 120 | 0.24 | 0.12 | 0.36 | 0.63 |
| GardaSun Sunshine 7000 | V | Sunfit Pro XL3 | 180 | 0.08 | 0.12 | 0.20 | 0.32 |
| SolArt by ACN system | H | New Technology Extreme B | 160 | 0.47 | 0.19 | 0.67 | 1.25 |
| | face | | 400 | 0.10 | 0.13 | 0.23 | 0.39 |
| | | New Technology TX SR | 25 | 0.12 | 0.06 | 0.17 | 0.29 |
| Ergoline Soltron X50 Turbo Plus | H | Philips TL 225W Cleo Active XPT | 225 | 0.52 | 0.18 | 0.69 | 1.32 |
| | face | | 400 | 0.21 | 0.15 | 0.36 | 0.70 |
| Tansun Aurora | V | C-Xtreme Duet Plus 180-220W | 220 | 0.42 | 0.17 | 0.59 | 1.00 |
| Tansun Aurora | V | Philips 250-R XPT/TS | 250 | 0.65 | 0.22 | 0.87 | 1.65 |
| Tansun Aurora | V | Power Max Hi Intensiv 200W | 200 | 0.38 | 0.17 | 0.55 | 1.01 |
| Sunvision V200XXL by Alisun | V | Cosmedico Cosmostar 200-225W | 225 | 0.50 | 0.25 | 0.75 | 1.28 |
| Harpo Lumina 3603 | H | Philips Cleo Swift TL160W-R | 160 | 0.34 | 0.17 | 0.51 | 0.87 |
| | face | | 400 | 0.04 | 0.09 | 0.14 | 0.21 |
| Ergoline Excellence 800 | H | Pure Power Sylvania PPB 160W 2.5 RLL | 160 | 0.47 | 0.20 | 0.67 | 1.26 |
| | face | Ultra VIT 2.4 | 520 | 0.31 | 0.33 | 0.65 | 1.18 |
| | shoulder | Pure Bronze | 25 | 0.31 | 0.14 | 0.45 | 0.77 |
| Ergoline 500 | H | Pure Power Sylvania PPB 160W 2.5 RLL | 160 | 0.42 | 0.17 | 0.59 | 1.12 |
| | face | Ultra VIT 2.4 | 520 | 0.11 | 0.35 | 0.46 | 0.64 |
| | shoulder | Pure Bronze | 25 | 0.41 | 0.19 | 0.59 | 1.02 |
| Ergoline 600 Avantgarde | H | Pure Power Sylvania PPB 160W 2.5 RLL | 160 | 0.45 | 0.18 | 0.63 | 1.19 |
| | face | Ultra VIT 2.3 | 500 | 0.11 | 0.33 | 0.44 | 0.59 |
| | shoulder | Pure Bronze | 25 | 0.17 | 0.08 | 0.25 | 0.43 |
| Ergoline 300 | H | Cosmedico Gold Arium SR 100W | 100 | 0.19 | 0.12 | 0.31 | 0.57 |
| | face | | 400 | 0.04 | 0.06 | 0.10 | 0.16 |
| Ergoline 500 | H | Pure Power Sylvania PPB 160W 3.32LL; Bermuda Gold Supernova 160W SR Plus | 160 | 0.42 | 0.16 | 0.58 | 1.13 |
| | face | ultra VIT 2.3 | 500 | 0.06 | 0.21 | 0.26 | 0.36 |
| | shoulder | MA10500 | ? | 0.04 | 0.03 | 0.07 | 0.12 |

# Table F.7: North Tyneside  Newcastle Upon Tyne

| Type | Type | Lamp | Watt | Effective UVB | Effective UVA | Total Erythemal Weighting | SCUP-H |
|---|---|---|---|---|---|---|---|
| Tansun Serenity 3040 SRL | H | Powerplus Hi Intensity Longlife | 225 | 0.57 | 0.31 | 0.88 | 1.58 |
| Tansun Symphony | V | Cosmedcio Cosmolux VHR 180-200 | 200 | 0.37 | 0.20 | 0.57 | 0.95 |
| Tansun Symphony | V | Cosmedcio Cosmolux VHR 180-200 | 200 | 0.33 | 0.19 | 0.52 | 0.86 |
| Tansun Symphony | V | Cosmedcio Cosmolux VHR 180-200 | 200 | 0.39 | 0.21 | 0.59 | 0.98 |
| Unknown Tanning Booth | V | Powerlight Inferno 11R | 160 | 0.34 | 0.18 | 0.52 | 0.88 |
| Unknown Tanning Booth | V | Powerlight Inferno 11R | 160 | 0.37 | 0.19 | 0.56 | 0.94 |
| Ultra Tan Booth | V | Cosmedcio Cosmolux 180-200 | 200 | 0.36 | 0.24 | 0.60 | 0.98 |
| Ultra Tan Booth | V | Cosmedcio Cosmolux 180-200 | 200 | 0.46 | 0.28 | 0.74 | 1.24 |
| Ultra Tan Booth | V | Philips Cleo 200W-R | 200 | 0.38 | 0.21 | 0.59 | 1.00 |
| Sunvision by Alisun 400 series XXl | H | Fusion Power 200R 2.3 200xx | 200 | 0.61 | 0.22 | 0.83 | 1.58 |
| Sunvision by Alisun V200 series XXl | V | Fusion Power 200R 2.3 200xx | 200 | 0.55 | 0.24 | 0.79 | 1.46 |
| Sunvision by Alisun V200 series XXl | V | Fusion Power 200R 2.3 200xx | 200 | 0.57 | 0.25 | 0.81 | 1.52 |
| Tansun VT2000 | V | SFX UV Extreme Performance Duo | 225 | 0.77 | 0.26 | 1.03 | 1.90 |
| Unknown Tanning Booth | V | Epcot C T T-R /Philips 160WR | 160 | 0.44 | 0.20 | 0.64 | 1.16 |
| Unknown Tanning Booth | V | Epcot C T T-R/Platinum | 160 | 0.43 | 0.19 | 0.62 | 1.10 |
| Ultrasun Sunburst 400 | H | Sunfit Pro. VX3 180W/ Sunfit Pro. XXlL 200W | 180 | 0.14 | 0.14 | 0.28 | 0.46 |
| Ergoline Classic 450 | H | Platinum 200W | 200 | 0.38 | 0.19 | 0.58 | 1.02 |
|  | F | ULTRA VIT 2.3 | 400 | 0.04 | 0.15 | 0.20 | 0.28 |
| Harpo Lumina 3603 | H | Cosmedico Cosmolux | 160 | 0.35 | 0.17 | 0.52 | 0.94 |
|  | F | Harpo Halide | 400 | 0.14 | 0.18 | 0.32 | 0.55 |
| Unknown Tanning Booth | V | Exteme B. Xtreme R 250W | 250 | 0.63 | 0.22 | 0.85 | 1.54 |
| Unknown Tanning Booth | V | Exteme B. Xtreme R 250W | 250 | 0.57 | 0.24 | 0.81 | 1.39 |
| Unknown Tanning Booth | V | Exteme B. Xtreme R 250W | 250 | 0.45 | 0.18 | 0.63 | 1.10 |
| Sunvision by Alisun V180 series XXl | V | Cosmolux VHR 200 W ; Philips Cleo Swift XPT TL 200WR (Dutch) | 200 | 0.45 | 0.24 | 0.69 | 1.18 |
| Elegence Pro Sunbed | H | Sunquest SQR 225W/ Bellarium X'treme 225W | 225 | 0.41 | 0.21 | 0.62 | 1.08 |
| Sunquest | V | Sunquest SQR 225W | 225 | 0.64 | 0.28 | 0.93 | 1.62 |
| Sunquest | V | Sunquest SQR 225W | 225 | 0.65 | 0.29 | 0.94 | 1.68 |
| Unknown Tanning Booth | V | Philips 250 R XPT/TS | 250 | 1.06 | 0.37 | 1.43 | 2.70 |
| Unknown Tanning Booth | V | Cosmedico Cosmolux 200-225W | 225 | 0.45 | 0.21 | 0.66 | 1.13 |
| Delta Luxura 500 Intensiv. | V | Fusion Power Trio XXX 180/250 | 250 | 0.49 | 0.21 | 0.70 | 1.29 |
| Delta Luxura 500 Intensiv. | V | Fusion Power Trio XXX 180/251 | 250 | 0.54 | 0.23 | 0.76 | 1.42 |
| Delta Luxura 500 Intensiv. | V | Fusion Power Trio XXX 180/252 | 250 | 0.55 | 0.23 | 0.79 | 1.46 |
| UVA Scan VL8: Suntube | V | Cosmedico Cosmolux VHR 160W + SunJunkie Supreme 15W | 160 | 0.28 | 0.16 | 0.43 | 0.73 |
| Sunquest Aurora | V | Cosmedcio Cosmolux VHR 180-200 | 200 | 0.44 | 0.26 | 0.70 | 1.17 |
| Sunquest Aurora | V | Cosmedcio Cosmolux VHR 180-200 | 200 | 0.45 | 0.25 | 0.70 | 1.17 |
| Sunquest Aurora | V | Cosmedcio Cosmolux VHR 180-200 | 200 | 0.48 | 0.26 | 0.73 | 1.22 |
| Sunquest Zenith | H | Powerlight Inferno II R + Beauty Sun S (Wolf System) 25W | 160 | 0.41 | 0.19 | 0.60 | 1.03 |
| SuperShuttle VHR | H | Philips 160 W Sunlamp Solarium Super Pro. Hightech | 160 | 0.26 | 0.14 | 0.40 | 0.68 |
| EPCOT Carousle Revolution | V | Platimun Max 200 | 160 | 0.48 | 0.22 | 0.70 | 1.26 |
| EPCOT Carousle Revolution | V | Platimun Max 200 | 200 | 0.55 | 0.23 | 0.77 | 1.39 |
| EPCOT Carousle Revolution | V | Platimun Max 200 | 200 | 0.51 | 0.22 | 0.73 | 1.32 |
| EPCOT Carousle Revolution | V | Platimun Max 200 | 200 | 0.56 | 0.22 | 0.78 | 1.40 |
| EPCOT Carousle Revolution | V | Platimun Max 200 | 200 | 0.49 | 0.21 | 0.70 | 1.28 |
| EPCOT | H | EPCOT Revolution | 160 | 0.50 | 0.22 | 0.72 | 1.32 |
| EPCOT | H | EPCOT Revolution | 160 | 0.58 | 0.21 | 0.79 | 1.45 |
| Tansun Serenity 3040 XXL | H | Cosmedico Cosmolux 200VHR | 200 | 0.53 | 0.24 | 0.77 | 1.38 |
| BodyTan | V | Cosmedico Cosmolux 200VHR | 200 | 0.39 | 0.21 | 0.60 | 0.99 |
| BodyTan | V | Cosmedico Cosmolux 200VHR | 200 | 0.36 | 0.19 | 0.54 | 0.90 |
| BodyTan | V | Cosmedico Cosmolux 200VHR | 200 | 0.38 | 0.21 | 0.59 | 0.99 |
| BodyTan | V | Cosmedico Cosmolux 200VHR | 200 | 0.34 | 0.19 | 0.54 | 0.89 |
| BodyTan | V | Cosmedico Cosmolux 200VHR | 200 | 0.42 | 0.22 | 0.63 | 1.05 |
| Sontegra Tri Tan | H | Tan 365 R Extreme | 250 | 0.66 | 0.25 | 0.91 | 1.70 |
| Sonte Raysun | H | Tan 365 R Extreme | 250 | 0.69 | 0.23 | 0.92 | 1.77 |
|  | V | Cosmosun 28R | 225 | 0.78 | 0.36 | 1.14 | 2.00 |
|  | V | Tan 365 R Extreme | 225 | 0.81 | 0.25 | 1.06 | 2.08 |
| Unknown Tanning Booth | V | Tan 365 R Extreme | 225 | 0.87 | 0.29 | 1.16 | 2.25 |
| Ergoline avantgarde 600 UTP | H | Heraeus 160R | 160 | 0.68 | 0.32 | 1.00 | 1.82 |
|  | F | Ultra VIT 2.4 | 520 | 0.17 | 0.42 | 0.59 | 0.85 |
| Sontegra | H | Cosmolux | 160 | 0.21 | 0.21 | 0.41 | 0.72 |
|  | F | sontegra | 300 | 0.19 | 0.13 | 0.32 | 0.36 |
| Unknown Tanning Booth | V | Heraeus MagicSun | 200 | 0.81 | 0.30 | 1.11 | 2.14 |
| Sun Vitale 400 Series | H | Titan | 180 | 0.62 | 0.35 | 0.97 | 1.62 |
| Unknown Tanning Booth | V | Titan Stamina | 235 | 0.55 | 0.33 | 0.88 | 1.51 |
| Unknown Tanning Booth | V | Titan Stamina | 235 | 0.81 | 0.34 | 1.15 | 2.00 |
| Ergoline 300 Superpower | H | Titan Stamina VHR | 160 | 0.60 | 0.25 | 0.85 | 1.47 |
|  | F | Ultra VIT 2.3 | 300 | 0.09 | 0.08 | 0.17 | 0.26 |
| Tansun Serenity | H | Wolff Bellarium B' Xtreme R 250W | 250 | 0.52 | 0.30 | 0.82 | 1.39 |
| Tansun Serenity | H | Wolff Bellarium B' Xtreme R 250W | 225 | 0.38 | 0.21 | 0.58 | 1.00 |
| Tansun Desire | V | Wolff Bellarium B' Xtreme R 250W | 250 | 1.06 | 0.35 | 1.41 | 2.72 |
| Tansun Symphony | V | Cosmedico Cosmolux 225W | 225 | 0.53 | 0.29 | 0.82 | 1.39 |
| Tansun Symphony | V | Cosmedico Cosmolux 225W | 225 | 0.56 | 0.29 | 0.86 | 1.45 |
| Tansun Symphony | V | Cosmedico Cosmolux 225W | 225 | 0.55 | 0.28 | 0.83 | 1.41 |
| Tansun Symphony | V | Cosmedico Cosmolux 225W | 225 | 0.50 | 0.26 | 0.75 | 1.27 |
| Tansun Symphony | V | Cosmedico Cosmolux 225W | 225 | 0.49 | 0.25 | 0.75 | 1.26 |
| Tansun Symphony | V | Cosmedico Cosmolux 225W | 225 | 0.50 | 0.25 | 0.75 | 1.27 |
| Tansun Desire | V | Wolff Bellarium B' Xtreme R 250W | 225 | 0.50 | 0.24 | 0.74 | 1.24 |
| Tansun Vitesse | V | Wolff Bellarium B' Xtreme R 250W | 250 | 0.98 | 0.26 | 1.25 | 2.46 |
| Tansun Vitesse | V | Wolff Bellarium B' Xtreme R 250W | 250 | 0.75 | 0.25 | 1.00 | 1.93 |
| Tansun Vitesse | V | Wolff Bellarium B' Xtreme R 250W | 250 | 0.71 | 0.24 | 0.95 | 1.84 |

# Table F.8: Nottinghamshire  Derbyshire

| Manufacturer | Type | Lamp | Watt | Effective UVB | Effective UVA | Total Erythemal Weighting | SCUP-H |
|---|---|---|---|---|---|---|---|
| Tansun Symphony | V | Pure Power | 250 | 0.404 | 0.147 | 0.551 | 1.05 |
| Tansun Symphony | V | Cosmedico | 225 | 0.36 | 0.22 | 0.58 | 0.968 |
| Tansun Symphony | V | Pure Power 2.3 R | 200 | 0.444 | 0.203 | 0.647 | 1.176 |
| Tansun Symphony | V | Cosmedico | 225 | 0.341 | 0.214 | 0.555 | 0.924 |
| Sol 50 | V | Intersun/Philips 160W ; Bodysoft 220VR | 220 | 0.348 | 0.173 | 0.52 | 0.923 |
| Tansun Symphony | V | Cosmedico Cosmolux | 200 | 0.434 | 0.226 | 0.66 | 1.118 |
| Ergoline 600 Avantgarde | H | Cosmedico | 160 | 0.421 | 0.162 | 0.583 | 1.066 |
| | face | Ultra Vit 2.3 | 400 | 0.13 | 0.417 | 0.547 | 0.81 |
| | shoulder | Philips | 25 | 0.078 | 0.05 | 0.128 | 0.232 |
| Unknown Booth | V | Wolff Bellarium B' Xtreme | 250 | 0.427 | 0.19 | 0.617 | 1.064 |
| Unknown Booth | V | Wolff Bellarium B' Xtreme | 250 | 0.376 | 0.166 | 0.542 | 0.938 |
| Tansun VT2000 | V | Intersun | 160 | 0.425 | 0.151 | 0.575 | 1.005 |
| Ergoline 600 Avantgarde | H | Fusion Power 180XX /160R , BX'Treme 160-200W Powerlight | 180 | 0.461 | 0.232 | 0.693 | 1.26 |
| | face | Ultra Vit 2.3 | 400 | 0.06 | 0.254 | 0.314 | 0.464 |
| | shoulder | Discover | 25 | 0.155 | 0.096 | 0.251 | 0.438 |
| Ergoline 600 Avantgarde | H | Bronze PBO 160W 2.5R, Powerlight Inferno 11R (Wolf system), Heraesus Magic 25 160W | 160 | 0.352 | 0.17 | 0.522 | 0.96 |
| | face | Ultra Vit 2.3 | 520 | 0.087 | 0.336 | 0.423 | 0.575 |
| | shoulder | Ergo SD | 25 | | | | |
| Unknown Booth | V | New Technology Perfect LUX | 200 | 0.321 | 0.137 | 0.458 | 0.823 |
| Unknown Booth | V | Light Tech Combi r 180W Intensiv | 180 | 0.354 | 0.196 | 0.55 | 0.944 |
| Zenith by Sunquest | H | Sunquest SQR | 250 | 0.677 | 0.177 | 0.854 | 1.661 |
| Zenith by Sunquest | H | Wolff Bellarium B' Xtreme | 225 | 0.497 | 0.259 | 0.756 | 1.308 |
| Aurora SE by Sunquest | V | Cosmolux 180-200W | 180 | 0.483 | 0.233 | 0.716 | 1.228 |
| Aurora SE by Sunquest | V | Cosmolux 180-200W | 180 | 0.544 | 0.258 | 0.802 | 1.379 |
| Smart tech: UVA Intensiv X6 | HP | High Pressure Metal Halide E400 | 400 | 0.271 | 0.142 | 0.412 | 0.814 |
| Tansun Symphony | V | Wolff Bellarium B' Xtreme | 250 | 0.439 | 0.17 | 0.609 | 1.061 |
| Sontegra Limited Edition | H | Solarium XLR 160W/ Sontegra 225W | 225 | 0.751 | 0.287 | 1.037 | 1.928 |
| | face | sontegra | 400 | 0.137 | 0.081 | 0.218 | 0.414 |
| Tansun Symphony 250 Extreme | V | Sun-Xtreme Plus Mx 250W | 250 | 0.704 | 0.255 | 0.959 | 1.795 |
| Tansun Symphony 250 Extreme | V | Sun-Xtreme Plus Mx 250W | 250 | 0.826 | 0.278 | 1.104 | 2.102 |
| Ergoline Advantage 400 turbo power | H | Cosmedico Cosmofit | 160 | 0.135 | 0.199 | 0.334 | 0.5 |
| | face | Ultra VIT 2.4 | 520 | 0.125 | 0.189 | 0.314 | 0.533 |
| Ergoline Lounge | V | Cosmedico Cosmosun 28R 200-240W | 200 | 0.558 | 0.214 | 0.772 | 1.425 |
| Eclipse LE by Sunquest | V | Sunquest SQR 200W | 200 | 0.461 | 0.233 | 0.694 | 1.221 |
| Tansun VT2000 | V | Power Max 160W Intensiv XLL | 160 | 0.47 | 0.171 | 0.64 | 1.191 |
| Tansun Symphony | V | Wolff Bellarium B' Xtreme | 225 | 0.346 | 0.184 | 0.53 | 0.887 |
| Tansun Symphony | V | Wolff Bellarium B' Xtreme | 225 | 0.386 | 0.221 | 0.607 | 1.008 |
| Tansun Symphony | V | Wolff Bellarium B' Xtreme | 225 | 0.337 | 0.203 | 0.54 | 0.903 |
| Ergoline 300 Classic | H | Bermuda Star Gold R | 100 | 0.132 | 0.139 | 0.271 | 0.427 |
| | face | VIT 2.3 | 400 | 0.072 | 0.143 | 0.214 | 0.34 |
| Tansun Symphony | V | Pure Power PPB 200W RII | 200 | 0.384 | 0.165 | 0.549 | 0.996 |
| Zenith by Sunquest | H | Heraeus New Colors Speedster | 160 | 0.331 | 0.15 | 0.481 | 0.891 |
| Eclipse by Sunquest | V | Fusion Power 200 XXX | 200 | 0.502 | 0.21 | 0.712 | 1.309 |
| Sontegra | H | Cosmolux VHO | 160 | 0.271 | 0.134 | 0.405 | 0.682 |
| Ergoline 450 Classic | H | Fusion Power 180xx 160R 26 | 180 | 0.484 | 0.214 | 0.698 | 1.3 |
| | face | Ultra VIT 2.3 | 400 | 0.104 | 0.324 | 0.428 | 0.589 |
| Eclipse by Sunquest | V | Pure Power PPB 160W 2.5 RII | 160 | 0.54 | 0.195 | 0.736 | 1.388 |
| Tansun Symphony | V | Cosmedico Cosmostar 180R | 180 | 0.448 | 0.21 | 0.659 | 1.133 |
| Tansun Symphony | V | Cosmedico Cosmostar 180R | 180 | 0.467 | 0.221 | 0.688 | 1.183 |
| Unknown Sunbed | H | Cosmedico Cosmostar 180R | 180 | 0.423 | 0.199 | 0.622 | 1.063 |
| Eclipse by Sunquest | V | Pure Power PPB 200W 2.3 RII | 200 | 0.429 | 0.213 | 0.642 | 1.155 |
| Eclipse by Sunquest | V | Pure Power PPB 200W 2.3 RII | 200 | 0.39 | 0.193 | 0.582 | 1.045 |
| Sunrise 8000 by Gardasun | V | Sunfit XXL3 200W | 200 | 0.098 | 0.137 | 0.235 | 0.386 |
| Elcipse by Sunquest | V | Independence New technology | 160 | 0.469 | 0.202 | 0.671 | 1.228 |
| Ergoline Prestige 990 Dynamic Power | H | Ergo Extreme SR 100-200W | 80-200 | 0.537 | 0.234 | 0.771 | 1.423 |
| | face | VIT 2.4 | 520 | 0.256 | 0.285 | 0.542 | 0.972 |
| | shoulder | Ergo HD | 240 | 0.475 | 0.499 | 0.974 | 1.75 |
| Bodywave Q-med | V | Bermuda Gold Supernova 200 | 180 | 0.499 | 0.285 | 0.784 | 1.346 |
| Sunvision V200XXL by Alisun | V | Cosmosun 28 R | 225 | 0.191 | 0.119 | 0.31 | 0.52 |
| Elcipse LE by Sunquest | V | Cosmedico Cosmolux | 200 | 0.388 | 0.146 | 0.535 | 0.996 |
| Elcipse LE by Sunquest | V | Heraeus | 180 | 0.348 | 0.144 | 0.493 | 0.897 |
| Sunvision 466 by Alisun | H | Cosmedico Cosmolux | 160 | 0.404 | 0.155 | 0.559 | 1.087 |
| | face | Alisun | 400 | 0.04 | 0.105 | 0.145 | 0.229 |
| Tansun Serenity 3036 XXL | H | Cosmedico Cosmolux | 180 | 0.285 | 0.16 | 0.446 | 0.75 |
| Tansun Symphony | V | Power Max 200 | 200 | 0.286 | 0.144 | 0.43 | 0.749 |
| Tansun Symphony | V | Cosmedico Cosmolux | 180 | 0.257 | 0.133 | 0.39 | 0.682 |
| Tansun Symphony | V | Pure Power Sylvania PPB 250W 3.3Rll | 250 | 0.609 | 0.22 | 0.828 | 1.601 |
| Sunrise 7000 by Gardasun | V | Cosmolux VHR | 160 | 0.179 | 0.114 | 0.293 | 0.484 |

Table F.9: Cheltenham, Coleford  Newton Abbot

| Manufacturer | Type | Lamp | Watt | Effective UVB | Effective UVA | Total Erythemal Weighting | SCUP-h |
|---|---|---|---|---|---|---|---|
| GardaSun Sunrise 7000 | V | Sunfit VRXT Pro. | 160 | 0.425 | 0.201 | 0.626 | 1.067 |
| GardaSun Power Tower | V | Sunfit XXL Pro. | 180 | 0.362 | 0.202 | 0.564 | 0.976 |
| Ergoline Excellence 700 | H | Bodysoft | 180 | 0.13 | 0.134 | 0.264 | 0.43 |
| | face | Ultra VIT 2.4 | 520 | 0.106 | 0.103 | 0.208 | 0.384 |
| | shoulder | bodysoft | 25 | 0.146 | 0.072 | 0.217 | 0.377 |
| Ergoline Excellence 700 | H | Bodysoft | 180 | 0.146 | 0.204 | 0.35 | 0.525 |
| MegaSun by KBL T200, Pure Energy CPL with VibraNano | V | unknown | 180 | 0.09 | 0.121 | 0.211 | 0.337 |
| Ergoline Excellence 700 | H | Bodysoft | 180 | 0.137 | 0.147 | 0.284 | 0.464 |
| | face | Ultra VIT 2.4 | 520 | 0.134 | 0.197 | 0.332 | 0.549 |
| | shoulder | Bodysoft | 25 | 0.157 | 0.071 | 0.229 | 0.397 |
| Ergoline Classic 600 Turbo | H | Body Soft CE 410B LongLife 140-160W 13% Max 0.5 Reflector | 140 | 0.12 | 0.135 | 0.255 | 0.413 |
| | face | Ultra VIT 2.4 | 520 | 0.154 | 0.202 | 0.356 | 0.642 |
| | shoulder | Bodysoft | 25 | 0.141 | 0.07 | 0.211 | 0.369 |
| Ergoline Excellence 700 | H | Bodysoft | 180 | 0.147 | 0.152 | 0.298 | 0.485 |
| | H | Ultra VIT 2.4 | 520 | 0.141 | 0.149 | 0.29 | 0.525 |
| | shoulder | Bodysoft | 25 | 0.161 | 0.079 | 0.24 | 0.413 |
| Ergoline Excellence 700 | H | Bodysoft | 180 | 0.15 | 0.155 | 0.305 | 0.494 |
| | face | Ultra VIT 2.4 | 520 | 0.075 | 0.092 | 0.167 | 0.295 |
| | shoulder | Bodysoft | 25 | 0.155 | 0.074 | 0.229 | 0.397 |
| Ergoline Classic 600 Turbo | H | BodySoft 140-160W 13%Max 0.5 Reflector | 140 | 0.14 | 0.111 | 0.251 | 0.359 |
| Sunquest Aurora | V | Cosmedcio VHR 200 | 200 | 0.59 | 0.319 | 0.909 | 1.536 |
| Sunquest Aurora | V | Cosmedcio VHR 200 | 200 | 0.583 | 0.31 | 0.893 | 1.506 |
| Sunquest Aurora | V | Cosmedcio VHR 200 | 200 | 0.634 | 0.344 | 0.978 | 1.647 |
| Zenith by Sunquest | H | Cosmedcio VHR 200 | 200 | 0.475 | 0.301 | 0.776 | 1.302 |
| Ergoline Lounge | V | Cosmosun 28R | 180 | 0.679 | 0.238 | 0.917 | 1.773 |
| Ergoline Lounge | V | Cosmosun 28R | 180 | 0.613 | 0.259 | 0.872 | 1.589 |
| Club Tan by UWE | H | New Technology/ Discover UVA /UVB 2.4 Longlife | 100 | 0.437 | 0.194 | 0.631 | 1.132 |
| SolArt50 by ACN Systems | H | New Technology Independence B SR Plus | 160 | 0.58 | 0.333 | 0.914 | 1.598 |
| Starflight by UWE | H | New Technology | 100 | 0.218 | 0.136 | 0.354 | 0.603 |
| Starflight by UWE | H | New Technology | 100 | 0.27 | 0.128 | 0.398 | 0.696 |
| GardaSun | V | Sunfit XXL Pro. | 200 | 0.228 | 0.104 | 0.332 | 0.617 |
| Sunquest | V | Cosmedico Cosmolux | 200 | 0.277 | 0.177 | 0.455 | 0.743 |
| GardaSun Power Tower | V | Sunfit XXL Pro. | 200 | 0.236 | 0.117 | 0.353 | 0.651 |
| Eclipse by Sunquest | V | B.Xtreme R | 180 | 0.23 | 0.217 | 0.448 | 0.708 |
| Eclipse by Sunquest | V | C-xtreme Duet plus | 225 | 0.558 | 0.225 | 0.783 | 1.353 |
| Eclipse by Sunquest | V | Sunquest SQR 200W | 200 | 0.485 | 0.216 | 0.701 | 1.247 |
| Ultrasun Sunburst 4000 | H | Sunfit Pro. VX3 | 160 | 0.179 | 0.149 | 0.328 | 0.546 |
| Sunvision by Alisun V180 series XXl | V | Cosmedico Cosmolux | 180 | 0.29 | 0.185 | 0.474 | 0.778 |
| Crouzet Solarium | V | Solarium Super Profi R 160 W / Philips Swift XPT 160W-R | 160 | 0.28 | 0.132 | 0.413 | 0.737 |
| Eclipse by Sunquest | V | Cosmolux | 200 | 0.522 | 0.239 | 0.761 | 1.32 |
| Sunvision by Alisun V180 series XXl | V | Cosmolux Reflector | 180 | 0.444 | 0.21 | 0.654 | 1.183 |
| Eclipse by Sunquest | V | Cosmedico Cosmosun 28R | 160 | 0.483 | 0.194 | 0.677 | 1.239 |
| Ergoline Esprit 700 | H | Ergoline Trend R E6 80-200W | 160 | 0.183 | 0.281 | 0.464 | 0.689 |
| | face | Ultra VIT 2.4 | 520 | 0.148 | 0.213 | 0.361 | 0.661 |
| Ergoline Excellence 700 | H | Bodysoft 410B G3 Longlife 140-160W 13 % Max 0,5 Reflector | 160 | 0.158 | 0.167 | 0.326 | 0.531 |
| | shoulder | Bodysoft | 25 | 0.175 | 0.082 | 0.256 | 0.442 |
| | face | Ultra VIT 2.4 | 520 | 0.19 | 0.242 | 0.432 | 0.779 |
| MegaSun by KBL T200, Pure Energy CPL with VibraNano | V | Unknown | 180 | 0.096 | 0.109 | 0.205 | 0.33 |
| Sunvision by Alisun 500 Series | H | Sunvision XTR 200S 120W ; Cosmolux VLR 2M 120W | 120 | 0.321 | 0.155 | 0.476 | 0.831 |
| Sunvision V200 XXL by Alisun | V | Cosmolux VHR +Cosmolux UVA plus 15W + Philips Cleo 15W SR | 160 | 0.218 | 0.143 | 0.361 | 0.596 |
| Sunshine 7000 by GardaSun | V | Sunfit Pro XL3 | 180 | 0.107 | 0.144 | 0.252 | 0.419 |
| Sunvision Vcompact XL by Alisun | V | Sunvision XTR 190 Intensiv | 120 | 0.153 | 0.082 | 0.235 | 0.414 |
| Unknown Tanning Booth | V | New Technology | 200 | 0.826 | 0.348 | 1.174 | 2.204 |
| Unknown Tanning Booth | V | New Technology | 200 | 0.756 | 0.305 | 1.061 | 2.005 |
| Unknown Tanning Booth | V | New Technology | 200 | 0.736 | 0.31 | 1.047 | 1.969 |
| Tansun Symphony | V | LightTech II R-UVA 180W XLL intensiv | 180 | 0.152 | 0.128 | 0.28 | 0.46 |
| Sunvision V200 XXL by Alisun | V | Fusion | 200 | 0.506 | 0.258 | 0.764 | 1.359 |
| Tansun Symphony | V | PowerMax | 200 | 0.379 | 0.185 | 0.564 | 0.995 |

# Bibliography

[1] European Commission, Preliminary opinion on biological effects of ultraviolet radiation relevant to health with particular reference to sun beds for cosmetic purposes. http://ec.europa.eu/health/scientific_committees/consultations/public_consultations/sccp_cons_03_en.htm. Accessed: 16-05-2015.

[2] European dermatology guideline for the photodermatoses. http://www.euroderm.org/images/stories/guidelines/ guideline phototesting.pdf. Accessed: 11-05-2015.

[3] International Commission on Illumination 17-1245 spherical irradiance. http://eilv.cie.co.at/termlist. Accessed: 06-05-2015.

[4] Ocean optics maya technical manual. http://www.oceanoptics.com/technical/maya.pdf. Accessed: 26-04-2015.

[5] Office for National Statistics(ONS), Travel trends. http://www.ons.gov.uk/ons/rel/ott/travel-trends/2013/rpt-travel-trends–2013l. Accessed: 12-10-2014.

[6] Royal Society of Chemistry, fighting skin cancer with prodrugs. http://www.rsc.org/education/eic/issues/2007May/FightingSkinCancer WithProdrugs.asp. Accessed: 23-04-2015.

[7] Incidence of squamous cell carcinoma in the United Kingdom. *Celtic National Cancer Data Repository, report TP140213.* (2014).

[8] 60335-2-27:2010, B. S. I. E. Household and similar electrical appliances, safety, particular requirements for appliances for skin exposure to ultraviolet and infrared radiation. *London: BSI* (2010).

[9] Adams, E. Erythema due to Ultraviolet radiation. *JOSA 21*, 4 (1931), 207.

[10] Ahmed, F. E., and Setlow, R. Saturation of DNA repair in mammalian cells. *Photochemistry and photobiology 29*, 5 (1979), 983–989.

[11] Alexander, H., Miller, and DL. Determining skin thickness with pulsed ultra sound. *Journal of Investigative Dermatology 72*, 1 (1979), 17–19.

[12] Anderson, R. R., and Parrish, J. A. The optics of human skin. *Journal of Investigative Dermatology 77*, 1 (1981), 13–19.

[13] Armstrong, B., and Kricker, A. How much melanoma is caused by sun exposure?. *Melanoma research 3*, 6 (1993), 395–402.

[14] Armstrong, B. K. How sun exposure causes skin cancer: an epidemiological perspective. In *Prevention of skin cancer*. Springer, 2004, pp. 89–116.

[15] Armstrong, B. K., and Kricker, A. Cutaneous melanoma. *Cancer surveys 19* (1993), 219–240.

[16] Augustsson, A., Stierner, U., Rosdahl, I., and Suurkula, M. Regional distribution of melanocytic naevi in relation to sun exposure, and site-specific counts predicting total number of naevi. *Acta Derm. Venereol. 72*, 2 (1992), 123–127.

[17] Autier, P., Doré, J.-F., Lejeune, F., Koelmel, K. F., Geffeler, O., Hille, P., Cesarini, J.-P., Lienard, D., Liabeuf, A., Joarlette, M., et al. Cutaneous malignant melanoma and exposure to sunlamps or sunbeds: An eortc multicenter case-control study in belgium, france and germany. *International journal of cancer 58*, 6 (1994), 809–813.

[18] Azizi, E., Lusky, A., Kushelevsky, A., and Schewach-Millet, M. Skin type, hair color, and freckles are predictors of decreased minimal erythema ultraviolet radiation dose. *Journal of the American Academy of Dermatology 19*, 1 (1988), 32–38.

[19] Babulak, S. W., Rhein, L. D., Scala, D. D., and Simion, F. A. Quantitation of erythema in a soap chamber test using the minolta chroma (reflectance) meter: Comparison of. *J. Soc. Cosmet. Chem 37* (1986), 475–479.

[20] Bais, A., Gardiner, B., Slaper, H., Blumthaler, M., Bernhard, G., McKenzie, R., Webb, A., Seckmeyer, G., Kjeldstad, B., Koskela, T., et al. Suspen intercomparison of Ultraviolet spectroradiometers. *Journal of Geophysical Research: Atmospheres (1984–2012) 106*, D12 (2001), 12509–12525.

[21] Baldea, I., Mocan, T., and Cosgarea, R. The role of Ultraviolet radiation and tyrosine stimulated melanogenesis in the induction of oxidative stress alterations in fair skin melanocytes. *Exp Oncol 31*, 4 (2009), 200–8.

[22] Banyasz, A., Douki, T., Improta, R., Gustavsson, T., Onidas, D., Vaya, I., Perron, M., and Markovitsi, D. Electronic excited states responsible for dimer formation upon UV absorption directly by thymine strands: Joint experimental and theoretical study. *Journal of the American Chemical Society 134*, 36 (2012), 14834–14845.

[23] Banyasz, A., Vayá, I., Changenet-Barret, P., Gustavsson, T., Douki, T., and Markovitsi, D. Base pairing enhances fluorescence and favors cyclobutane dimer formation induced upon absorption of UVA radiation by DNA. *Journal of the American Chemical Society 133*, 14 (2011), 5163–5165.

[24] Barr, E. S. The infrared pioneers—ii. macedonio melloni. *Infrared physics 2*, 2 (1962), 67–74.

[25] Bashkatov, A. N., Genina, E. A., and Tuchin, V. V. Optical properties of skin, subcutaneous, and muscle tissues: a review. *Journal of Innovative Optical Health Sciences 4*, 01 (2011), 9–38.

[26] Bataille, V., Winnett, A., Sasieni, P., Bishop, J. N., and Cuzick, J. Exposure to the sun and sunbeds and the risk of cutaneous melanoma in the uk: a case–control study. *European Journal of Cancer 40*, 3 (2004), 429–435.

[27] Bird, R. E., and Hulstrom, R. L. Simplified clear sky model for direct and diffuse insolation on horizontal surfaces. Tech. rep., Solar Energy Research Inst., Golden, CO (USA), 1981.

[28] Bjerring, P., and Andersen, P. Skin reflectance spectrophotometry. *Photo-dermatology 4*, 3 (1987), 167–171.

[29] Black, H., Forbes, P., Cleaver, J., Ananthaswamy, H., Ullrich, S., Tyrrell, R., et al. Photocarcinogenesis: an overview. *Journal of Photochemistry and Photobiology B: Biology 40*, 1 (1997), 29–47.

[30] Blum, H. F. Ultraviolet radiation and skin cancer: In mice and men*. *Photochemistry and photobiology 24*, 3 (1976), 249–254.

[31] Bock, C., Diehl, K., Litaker, D., Breitbart, E. W., Greinert, R., and Schneider, S. Sunbed use in Germany: trends, user histories and

factors associated with cessation and readiness to change. *Br. J. Dermatol. 169*, 2 (Aug 2013), 441–449.

[32] Boniol, M., Autier, P., Boyle, P., Gandini, S., et al. Cutaneous melanoma attributable to sunbed use: systematic review and meta-analysis. *Bmj 345* (2012).

[33] Botev, I. A new conception of bouguer-lambert-beer's law. *Fresenius' Zeitschrift für analytische Chemie 297*, 5 (1979), 419–419.

[34] Bowker, K., and Longford, A. Ultra-violet radiation hazards from the use of solaria. *Human Exposure to Ultraviolet Radiation: Risk and Regulations (Edited by Passhier, WF and BFM Bosnjakovic)* (1987), 365–369.

[35] Boyle, P., Dore, J.-F., Autier, P., and Ringborg, U. Cancer of the skin: a forgotten problem in europe. *Annals of oncology 15*, 1 (2004), 5–6.

[36] Brash, D. E. Sunlight and the onset of skin cancer. *Trends in genetics 13*, 10 (1997), 410–414.

[37] Brenner, M., and Hearing, V. J. The protective role of melanin against UV damage in human skin†. *Photochemistry and photobiology 84*, 3 (2008), 539–549.

[38] Breuninger, H., Brantsch, K., Eigentler, T., and Häfner, H.-M. Comparison and evaluation of the current staging of cutaneous carcinomas. *JDDG: Journal der Deutschen Dermatologischen Gesellschaft 10*, 8 (2012), 579–586.

[39] Bruls, W. A., and Van Der Leun, J. C. Forward scattering properties of human epidermal layers. *Photochemistry and photobiology 40*, 2 (1984), 231–242.

[40] Bruyneel-Raap, F., Dorsey, S. B., and Guin, J. D. The tanning salon: an area survey of equipment, procedures, and practices. *Journal of the American Academy of Dermatology 18*, 5 (1988), 1030–1038.

[41] Buchvarov, I., Wang, Q., Raytchev, M., Trifonov, A., and Fiebig, T. Electronic energy delocalization and dissipation in single-and double-stranded DNA. *Proceedings of the National Academy of Sciences 104*, 12 (2007), 4794–4797.

[42] Cadet, J., Berger, M., Douki, T., Morin, B., Raoul, S., Ravanat, J., and Spinelli, S. Effects of UV and visible radiation on DNA-final base damage. *Biological chemistry 378*, 11 (1997), 1275–1286.

[43] Cavaluzzi, M. J., and Borer, P. N. Revised UV extinction coefficients for nucleoside-5-monophosphates and unpaired DNA and RNA. *Nucleic acids research 32*, 1 (2004), e13–e13.

[44] Chandrasekhar, S. *Radiative Transfer*. Dover Books on Intermediate and Advanced Mathematics. Dover Publications, 1960.

[45] Cheong, W.-F., Prahl, S. A., Welch, A. J., et al. A review of the optical properties of biological tissues. *IEEE journal of quantum electronics 26*, 12 (1990), 2166–2185.

[46] Choi, K.-W., Kim, K.-H., and Kim, Y.-H. Comparative study of the gross interpretation of phototesting and objective measurement with using a spectrophotometer for patients with psoriasis and vitiligo treated with narrow-band UVB. *Annals of dermatology 21*, 2 (2009), 136–141.

[47] Clingen, P. H., Arlett, C. F., Roza, L., Mori, T., Nikaido, O., and Green, M. H. Induction of cyclobutane pyrimidine dimers, pyrimidine (6-4) pyrimidone photoproducts, and dewar valence isomers by natural sunlight in normal human mononuclear cells. *Cancer research 55*, 11 (1995), 2245–2248.

[48] Cockerell, C., and Calame, A. *Cutaneous Manifestations of HIV Disease*. CRC Press, 2012.

[49] Coelho, S. G., Zmudzka, B. Z., Yin, L., Miller, S. A., Yamaguchi, Y., Tadokoro, T., Hearing, V. J., and Beer, J. Z. Non-invasive diffuse reflectance measurements of cutaneous melanin content can predict human sensitivity to ultraviolet radiation. *Experimental dermatology 22*, 4 (2013), 266–271.

[50] Cohen, J. L. Actinic keratosis treatment as a key component of preventive strategies for nonmelanoma skin cancer. *The Journal of clinical and aesthetic dermatology 3*, 6 (2010), 39.

[51] Colantonio, S., Bracken, M. B., and Beecker, J. The association of indoor tanning and melanoma in adults: systematic review and meta-analysis. *Journal of the American Academy of Dermatology 70*, 5 (2014), 847–857.

[52] Coleman, A., Sarkany, R., and Walker, S. Clinical ultraviolet dosimetry with a ccd monochromator array spectroradiometer. *Physics in medicine and biology 53*, 18 (2008), 5239.

[53] Cosman, B., Heddle, S. B., and Crikelair, G. V. The increasing incidence of melanoma. *Plastic and reconstructive surgery 57*, 1 (1976), 50–56.

[54] Costin, G.-E., and Hearing, V. J. Human skin pigmentation: melanocytes modulate skin color in response to stress. *The FASEB Journal 21*, 4 (2007), 976–994.

[55] Darvin, M., Gersonde, I., Albrecht, H., Gonchukov, S., Sterry, W., and Lademann, J. Determination of beta carotene and lycopene concentrations in human skin using resonance raman spectroscopy. *Laser Phys 15*, 2 (2005), 295–299.

[56] Davidson, M. W. Pioneers in optics: Alexandre edmond becquerel and william henry bragg. *Microscopy Today 19*, 04 (2011), 42–44.

[57] Dawe, R. S., and Ferguson, J. Diagnosis and treatment of chronic actinic dermatitis. *Dermatologic therapy 16*, 1 (2003), 45–51.

[58] De Gruijl, F. Health effects from solar UV radiation. *Radiation Protection Dosimetry 72*, 3-4 (1997), 177–196.

[59] De Gruijl, F., and Van der Leun, J. Estimate of the wavelength dependency of ultraviolet carcinogenesis in humans and its relevance to the risk assessment of a stratospheric ozone depletion. *Health Physics 67*, 4 (1994), 319–325.

[60] de Gruijl, F. R. Photocarcinogenesis: UVA vs. UVB radiation. *Skin pharmacology and applied skin physiology 15*, 5 (2001), 316–320.

[61] de Gruijl, F. R., and Forbes, P. D. UV-induced skin cancer in a hairless mouse model. *Bioessays 17*, 7 (1995), 651–660.

[62] de Gruijl, F. R., Sterenborg, H. J., Forbes, P. D., Davies, R. E., Cole, C., Kelfkens, G., van Weelden, H., Slaper, H., and van der Leun, J. C. Wavelength dependence of skin cancer induction by ultraviolet irradiation of albino hairless mice. *Cancer research 53*, 1 (1993), 53–60.

[63] de Gruijl, F. R., and van der Leun, J. C. Development of skin tumors in hairless mice after discontinuation of Ultraviolet irradiation. *Cancer Res. 51*, 3 (Feb 1991), 979–984.

[64] De Gruijl, F. R., Van Der Meer, J. B., and Van Der Leun, J. C. Dose-time dependency of tumor formation by chronic UV exposure. *Photochem. Photobiol. 37*, 1 (Jan 1983), 53–62.

[65] de l'Éclairage, C. I. Methods of characterizing the performance of radiometers and photometers. *Publication CIE 53* (1982).

[66] de Vries, E., and Coebergh, J.-W. W. Melanoma incidence has risen in europe. *BMJ: British Medical Journal 331*, 7518 (2005), 698.

[67] Del Bino, S., Sok, J., Bessac, E., and Bernerd, F. Relationship between skin response to Ultraviolet exposure and skin color type. *Pigment cell research 19*, 6 (2006), 606–614.

[68] Diffey, B. A mathematical model for Ultraviolet optics in skin. *Physics in medicine and biology 28*, 6 (1983), 647.

[69] Diffey, B. Analysis of the risk of skin cancer from sunlight and solaria in subjects living in northern europe. *Photo-dermatology 4*, 3 (1987), 118–126.

[70] Diffey, B. Human exposure to Ultraviolet radiation. In *Seminars in dermatology* (1990), vol. 9, pp. 2–10.

[71] Diffey, B. A quantitative estimate of melanoma mortality from Ultraviolet a sunbed use in the uk. *British Journal of dermatology 149*, 3 (2003), 578–581.

[72] Diffey, B., and Farr, P. Lack of photorecovery of Ultraviolet erythema in human skin. *Photo-dermatology 2*, 2 (1985), 115.

[73] Diffey, B., and Farr, P. Tanning with UVB or UVA: an appraisal of risks. *Journal of Photochemistry and Photobiology B: Biology 8*, 2 (1991), 219.

[74] Diffey, B. L. Cosmetic tanning and human skin cancer. *Skin cancer: mechanisms and human relevance. Boca Raton, FL: CRC Press, Inc* (1995), 31–8.

[75] Diffey, B. L. Sources and measurement of Ultraviolet radiation. *Methods 28*, 1 (2002), 4–13.

[76] d'Ischia, M., Wakamatsu, K., Napolitano, A., Briganti, S., Garcia-Borron, J.-C., Kovacs, D., Meredith, P., Pezzella, A., Picardo, M., Sarna, T., et al. Melanins and melanogenesis: methods, standards, protocols. *Pigment cell & melanoma research 26*, 5 (2013), 616–633.

[77] Donnelly, J. F., and Massa, N. M. *Light: Introduction to Optics and Photonics*. Lulu. com, 2010.

[78] Doré, J.-F., and Chignol, M.-C. Tanning salons and skin cancer. *Photochemical & Photobiological Sciences 11*, 1 (2012), 30–37.

[79] Douki, T., Reynaud-Angelin, A., Cadet, J., and Sage, E. Bipyrimidine photoproducts rather than oxidative lesions are the main type of DNA damage involved in the genotoxic effect of solar UVA radiation. *Biochemistry 42*, 30 (2003), 9221–9226.

[80] Dubin, N., Moseson, M., and Pasternack, B. S. Sun exposure and malignant melanoma among susceptible individuals. *Environmental health perspectives 81* (1989), 139.

[81] El Ghissassi, F., Baan, R., Straif, K., Grosse, Y., Secretan, B., Bouvard, V., Benbrahim-Tallaa, L., Guha, N., Freeman, C., Galichet, L., et al. A review of human carcinogens—part d: radiation. *The lancet oncology 10*, 8 (2009), 751–752.

[82] Elliott, F., Suppa, M., Chan, M., Leake, S., Karpavicius, B., Haynes, S., Barrett, J. H., Bishop, D. T., and Newton-Bishop, J. A. Relationship between sunbed use and melanoma risk in a large case-control study in the united kingdom. *International Journal of Cancer 130*, 12 (2012), 3011–3013.

[83] English, D. R., Armstrong, B. K., Kricker, A., Winter, M. G., Heenan, P. J., and Randell, P. L. Case-control study of sun exposure and squamous cell carcinoma of the skin. *International journal of cancer 77*, 3 (1998), 347–353.

[84] Epstein, J. H. Photocarcinogenesis, skin cancer, and aging. *Journal of the American Academy of Dermatology 9*, 4 (1983), 487–502.

[85] Farr, P., and Diffey, B. Quantitative studies on cutaneous erythema induced by ultraviolet radiation. *British Journal of Dermatology 111*, 6 (1984), 673–682.

[86] Fawcett, D. W. *An atlas of fine structure: The cell; Its organelles and inclusions*. Saunders, 1967.

[87] Fears, T. R., Scotto, J., and Schneiderman, M. A. Mathematical models of age and ultraviolet effects on the incidence of skin cancer among whites in the United States. *Am. J. Epidemiol. 105*, 5 (May 1977), 420–427.

[88] Ferguson, J., Brown, M., Alert, D., Bielfeldt, S., Brown, J., Chardon, A., Hourseau, C., Mazilier, C., Cuthbert, J., D'Arcy-Burt, K., et al. Collaborative development of a sun protection factor test method: a proposed european standard. colipa task force 'sun protection

measurement', europe. *International journal of cosmetic science 18*, 5 (1996), 203–218.

[89] Fitzpatrick, T., Pathak, M., Harber, L., Seiji, M., and Kukita, A. Sunlight and man, normal and abnormal photobiological responses. *Sunlight and man: normal and abnormal photobiological responses* (1974).

[90] Fitzpatrick, T. B. The validity and practicality of sun-reactive skin types i through vi. *Archives of Dermatology 124*, 6 (1988), 869–871.

[91] for Research on Cancer, I. A. *Exposure to artificial UV radiation and skin cancer*, vol. 1. World Health Organization, 2006.

[92] for Research on Cancer, I. A., et al. Working group on artificial ultraviolet (uv) light and skin cancer. the association of use of sunbeds with cutaneous malignant melanoma and other skin cancer: A systematic review. *Int J Cancer 120*, 5 (2007), 1116–22.

[93] FRAIN-BELL, W., Lakshmipathi, T., Rogers, J., and WILLOCK, J. The syndrome of chronic photosensitivity dermatitis and actinic reticuloid. *British Journal of Dermatology 91*, 6 (1974), 617–634.

[94] Franceschi, S., Levi, F., Randimbison, L., and La Vecchia, C. Site distribution of different types of skin cancer: new aetiological clues. *International Journal of Cancer 67*, 1 (1996), 24–28.

[95] Freeman, S. E., Gange, R. W., Sutherland, J. C., Matzinger, E. A., and Sutherland, B. M. Production of pyrimidine dimers in DNA of human skin exposed in situ to UVA radiation. *Journal of investigative dermatology 88*, 4 (1987), 430–433.

[96] Freeman, S. E., Hacham, H., Gange, R., Maytum, D., Sutherland, J., and Sutherland, B. Wavelength dependence of pyrimidine dimer formation in DNA of human skin irradiated in situ with ultraviolet light. *Proceedings of the National Academy of Sciences 86*, 14 (1989), 5605–5609.

[97] Frercks, J., Weber, H., and Wiesenfeldt, G. Reception and discovery: the nature of johann wilhelm ritter's invisible rays. *Studies in History and Philosophy of Science Part A 40*, 2 (2009), 143–156.

[98] Friedberg, E., Barbis, D., Chenevert, J., Fleer, R., Kalainov, D., Naumovski, L., Nicolet, C., Robinson, G., Schultz, R., Weiss, W., et al. Molecular approaches to the study of nucleotide excision repair

in eukaryotes. In *Mechanisms of DNA Damage and Repair*. Springer, 1986, pp. 311–318.

[99] Friedberg, E. C. DNA damage and repair. *Nature 421*, 6921 (2003), 436–440.

[100] Gaigalas, A., Wang, L., He, H.-J., and DeRose, P. Procedures for wavelength calibration and spectral response correction of ccd array spectrometers. *Journal of Research of the National Institute of Standards and Technology 114*, 4 (2009), 215–228.

[101] Gallagher, R. P., Hill, G. B., Bajdik, C. D., Fincham, S., Coldman, A. J., McLean, D. I., and Threlfall, W. J. Sunlight exposure, pigmentary factors, and risk of nonmelanocytic skin cancer: I. basal cell carcinoma. *Archives of Dermatology 131*, 2 (1995), 157–163.

[102] Gallagher, R. P., Ma, B., McLean, D. I., Yang, C. P., Ho, V., Carruthers, J. A., and Warshawski, L. M. Trends in basal cell carcinoma, squamous cell carcinoma, and melanoma of the skin from 1973 through 1987. *Journal of the American Academy of Dermatology 23*, 3 (1990), 413–421.

[103] Gallagher, R. P., Spinelli, J. J., and Lee, T. K. Tanning beds, sunlamps, and risk of cutaneous malignant melanoma. *Cancer Epidemiology Biomarkers & Prevention 14*, 3 (2005), 562–566.

[104] Gallus, S., Naldi, L., Carli, P., and La Vecchia, C. Nevus count on specific anatomic sites as a predictor of total body count: a survey of 3,406 children from Italy. *Am. J. Epidemiol. 166*, 4 (Aug 2007), 472–478.

[105] Gandjbakhche, A. H. Diffuse optical imaging and spectroscopy, in vivo. *Comptes Rendus de l'Académie des Sciences-Series IV-Physics 2*, 8 (2001), 1073–1089.

[106] Gange, R. W., Blackett, A. D., Matzinger, E. A., Sutherland, B. M., and Kochevar, I. E. Comparative protection efficiency of UVA-and UVB-induced tans against erythema and formation of endonuclease-sensitive sites in DNA by UVB in human skin. *Journal of investigative dermatology 85*, 4 (1985), 362–364.

[107] Gerber, B., Mathys, P., Moser, M., Bressoud, D., and Braun-Fahrländer, C. Ultraviolet emission spectra of sunbeds. *Photochemistry and photobiology 76*, 6 (2002), 664–668.

[108] Gibson, P., and Diffey, B. Techniques for spectroradiometry and broadband radiometry. *Radiation Measurement in Photobiology* (1989), 71–84.

[109] Gies, H., Roy, C., and Elliott, G. Artificial suntanning: spectral irradiance and hazard evaluation of ultraviolet sources. *Health Physics 50*, 6 (1986), 691–703.

[110] Green, A., Autier, P., Boniol, M., Boyle, P., Dore, J.-F., Gandini, S., Newton-Bishop, J., Secretan, B., Walter, S. J., Weinstock, M. A., et al. The association of use of sunbeds with cutaneous malignant melanoma and other skin cancers: a systematic review. *International Journal of Cancer 120*, 5 (2007), 1116–1122.

[111] Green, A., Autier, P., Boniol, M., Boyle, P., Dore, J.-F., Gandini, S., Newton-Bishop, J., Secretan, B., Walter, S. J., Weinstock, M. A., et al. The association of use of sunbeds with cutaneous malignant melanoma and other skin cancers: a systematic review. *International Journal of Cancer 120*, 5 (2007), 1116–1122.

[112] Green, A., and Trichopoulos, D. Skin cancer. *Textbook of cancer epidemiology*, Ed. 2 (2008), 378–402.

[113] Halder, R. M., and Bridgeman-Shah, S. Skin cancer in african americans. *Cancer 75*, S2 (1995), 667–673.

[114] Hall, A. On an experimental determination of pi. *Messeng. Math 2* (1873), 113–114.

[115] Hanson, K. M., and Simon, J. D. Photochemistry of urocanic acid: Evidence that urocanic acid should be used with caution in cosmetic formulations. *Journal of the Society of Cosmetic Chemists 48*, 3 (1997), 151–157.

[116] Hanson, K. M., and Simon, J. D. Epidermal trans-urocanic acid and the UV-A-induced photoaging of the skin. *Proceedings of the National Academy of Sciences 95*, 18 (1998), 10576–10578.

[117] Harm, W. Biological effects of ultraviolet radiation.

[118] Harrison, G. I., and Young, A. R. Ultraviolet radiation-induced erythema in human skin. *Methods 28*, 1 (2002), 14–19.

[119] Hawk, J. Chronic actinic dermatitis: an idiopathic syndrome including actinic reticuloid and photosensitive eczema. *Br J Dermatol 101*, 17 (1979), 24.

[120] Haxthausen, H. Infra-red photography of subcutaneous veins. *British Journal of Dermatology 45*, 12 (1933), 506–511.

[121] Hemminki, K., Zhang, H., and Czene, K. Familial and attributable risks in cutaneous melanoma: effects of proband and age. *Journal of investigative dermatology 120*, 2 (2003), 217–223.

[122] Holick, M. F., Chen, T. C., Lu, Z., and Sauter, E. Vitamin d and skin physiology: Ad-lightful story. *Journal of Bone and Mineral Research 22*, S2 (2007), V28–V33.

[123] Holmquist, G. P., and Gao, S. Somatic mutation theory, DNA repair rates, and the molecular epidemiology of p53 mutations. *Mutation Research/Reviews in Mutation Research 386*, 1 (1997), 69–101.

[124] Huffman, D. Absorption and scattering of light by small particles. *Printed in the United States of America* (1983).

[125] Ishimaru, A. Theory and application of wave propagation and scattering in random media. *Proceedings of the IEEE 65*, 7 (1977), 1030–1061.

[126] Ishimaru, A. Wave propagation and scattering in random media. volume i-single scattering and transport theory. *Research supported by the US Air Force, NSF, and NIH. New York, Academic Press, Inc., 1978. 267 p. 1* (1978).

[127] Jacques, P. S. L. Melanosome volume fraction, personal communication, January 29 2015.

[128] Jacques, S. L. Origins of tissue optical properties in the UVA, visible, and nir regions. *OSA TOPS on advances in optical imaging and photon migration 2* (1996), 364–369.

[129] Jacques, S. L. Skin optics. *Oregon Medical Laser Center News 1998*, 1 (1998), 1–9.

[130] Jacques, S. L. Quick analysis of optical spectra to quantify epidermal melanin and papillary dermal blood content of skin. *Journal of Biophotonics 8*, 3 (2014).

[131] Jacques, S. L. Quick analysis of optical spectra to quantify epidermal melanin and papillary dermal blood content of skin. *Journal of biophotonics 9999* (2014).

[132] Jacques, S. L., Alter, C., and Prahl, S. A. Angular dependence of hene laser light scattering by human dermis. *Lasers Life Sci 1*, 4 (1987), 309–333.

[133] Jacques, S. L., Joseph, R., and Gofstein, G. How photobleaching affects dosimetry and fluorescence monitoring of pdt in turbid media. In *OE/LASE'93: Optics, Electro-Optics, & Laser Applications in Science& Engineering* (1993), International Society for Optics and Photonics, pp. 168–179.

[134] Jensen, U. B., Lowell, S., and Watt, F. M. The spatial relationship between stem cells and their progeny in the basal layer of human epidermis: a new view based on whole-mount labelling and lineage analysis. *Development 126*, 11 (1999), 2409–2418.

[135] Jiang, Y., Rabbi, M., Kim, M., Ke, C., Lee, W., Clark, R. L., Mieczkowski, P. A., and Marszalek, P. E. UVA generates pyrimidine dimers in DNA directly. *Biophysical journal 96*, 3 (2009), 1151–1158.

[136] Jimbow, K., Reszka, K., Schmitz, S., Salopek, T., and Thomas, P. Distribution of eu-and pheomelanins in human skin and melanocytic tumors, and their photoprotective vs. phototoxic properties. *Melanin: Its role in human photoprotection* (1995), 155–175.

[137] Joerger, A., and Fersht, A. Structure–function–rescue: the diverse nature of common p53 cancer mutants. *Oncogene 26*, 15 (2007), 2226–2242.

[138] Johnson, B. Formation of thymine containing dimers in skin exposed to ultraviolet radiation. *Bulletin du cancer 65*, 3 (1977), 283–297.

[139] Jones, D. T. Incidence of squamous cell carcinoma in the united kingdom personal communication. Personal communication, Feb. 2 2014. Senior Cancer Analyst, Knowledge and Intelligence Team (South West)Public Health England.

[140] Kaidbey, K. H., and Kligman, A. M. Further studies of photoaugmentation in humans: phototoxic reactions. *Journal of Investigative Dermatology 65*, 5 (1975), 472–475.

[141] Karagas, M. R., Stannard, V. A., Mott, L. A., Slattery, M. J., Spencer, S. K., and Weinstock, M. A. Use of tanning devices and risk of basal cell and squamous cell skin cancers. *Journal of the National Cancer Institute 94*, 3 (2002), 224–226.

[142] Karagas, M. R., Stannard, V. A., Mott, L. A., Slattery, M. J., Spencer, S. K., and Weinstock, M. A. Use of tanning devices and risk of basal cell and squamous cell skin cancers. *Journal of the National Cancer Institute 94*, 3 (2002), 224–226.

[143] Karsten, A. E., and Smit, J. E. Modeling and verification of melanin concentration on human skin type. *Photochemistry and photobiology 88*, 2 (2012), 469–474.

[144] Keijzer, M., Jacques, S. L., Prahl, S. A., and Welch, A. J. Light distributions in artery tissue: Monte carlo simulations for finite-diameter laser beams. *Lasers in surgery and medicine 9*, 2 (1989), 148–154.

[145] Kennedy, C., ter Huurne, J., Berkhout, M., Gruis, N., Bastiaens, M., Bergman, W., Willemze, R., and Bavinck, J. N. B. Melanocortin 1 receptor (mc1r) gene variants are associated with an increased risk for cutaneous melanoma which is largely independent of skin type and hair color. *Journal of Investigative Dermatology 117*, 2 (2001), 294–300.

[146] Khazova, M., O'Hagan, J. B., and Robertson, S. Survey of UV emissions from sunbeds in the uk. *Photochemistry and photobiology* (2015).

[147] Kielbassa, C., Roza, L., and Epe, B. Wavelength dependence of oxidative DNA damage induced by UV and visible light. *Carcinogenesis 18*, 4 (1997), 811–816.

[148] Klaus Peter Wilhelm, Hongbo Zhai, H. I. M. *Dermatotoxicology,Eighth Edition*. Informa Healthcare, London, 2012.

[149] Kobayashi, N., Nakagawa, A., Muramatsu, T., Yamashina, Y., Shirai, T., Hashimoto, M. W., Ishigaki, Y., Ohnishi, T., and Mori, T. Supranuclear melanin caps reduce ultraviolet induced DNA photoproducts in human epidermis. *Journal of investigative dermatology 110*, 5 (1998), 806–810.

[150] Koller, L. R. *Ultraviolet radiation*. Wiley New York, 1965.

[151] Kollias, N., and Baqer, A. Spectroscopic characteristics of human melanin in vivo. *Journal of investigative dermatology 85*, 1 (1985), 38–42.

[152] Konishi, E., and Yoshizawa, Y. Estimation of depth of basal cell layer of skin for radiation protection. *Radiation protection dosimetry 11*, 1 (1985), 29–33.

[153] Kraemer, K. H., Lee, M.-M., Andrews, A. D., and Lambert, W. C. The role of sunlight and DNA repair in melanoma and nonmelanoma skin cancer: the xeroderma pigmentosum paradigm. *Archives of Dermatology 130*, 8 (1994), 1018–1021.

[154] Kricker, A., Armstrong, B. K., and English, D. R. Sun exposure and non-melanocytic skin cancer. *Cancer Causes & Control 5*, 4 (1994), 367–392.

[155] Kricker, A., Armstrong, B. K., English, D. R., and Heenan, P. J. Does intermittent sun exposure cause basal cell carcinoma? a case-control study in western australia. *International Journal of Cancer 60*, 4 (1995), 489–494.

[156] Krishnaswamy, A., and Baranoski, G. V. A study on skin optics. *Natural Phenomena Simulation Group, School of Computer Science, University of Waterloo, Canada, Technical Report 1* (2004), 1–17.

[157] Kubelka, P., and Munk, F. A contribution to the optics of pigments. *Z. Tech. Phys 12* (1931), 593–599.

[158] Kuluncsics, Z., Perdiz, D., Brulay, E., Muel, B., and Sage, E. Wavelength dependence of ultraviolet-induced DNA damage distribution: involvement of direct or indirect mechanisms and possible artefacts. *Journal of Photochemistry and Photobiology B: Biology 49*, 1 (1999), 71–80.

[159] Kvam, E., and Tyrrell, R. M. Induction of oxidative DNA base damage in human skin cells by UV and near visible radiation. *Carcinogenesis 18*, 12 (1997), 2379–2384.

[160] Kvam, E., and Tyrrell, R. M. The role of melanin in the induction of oxidative DNA base damage by ultraviolet a irradiation of DNA or melanoma cells. *Journal of investigative dermatology 113*, 2 (1999), 209–213.

[161] Lancaster, H. Some geographical aspects of the mortality from melanoma in europeans. *The Medical Journal of Australia 43*, 26 (1956), 1082–1087.

[162] Lazovich, D., Vogel, R. I., Berwick, M., Weinstock, M. A., Anderson, K. E., and Warshaw, E. M. Indoor tanning and risk of melanoma: a case-control study in a highly exposed population. *Cancer Epidemiology Biomarkers & Prevention 19*, 6 (2010), 1557–1568.

[163] Lechler, T., and Fuchs, E. Asymmetric cell divisions promote stratification and differentiation of mammalian skin. *Nature 437*, 7056 (2005), 275–280.

[164] Lee, J. The current rapid increase in incidence and mortality from malignant melanoma in developed societies. *Pigment cell 2* (1976), 414–420.

[165] Leiter, U., and Garbe, C. Epidemiology of melanoma and nonmelanoma skin cancer—the role of sunlight. In *Sunlight, vitamin D and skin cancer*. Springer, 2008, pp. 89–103.

[166] Levine, J. A., Sorace, M., Spencer, J., and Siegel, D. M. The indoor UV tanning industry: a review of skin cancer risk, health benefit claims, and regulation. *Journal of the American Academy of Dermatology 53*, 6 (2005), 1038–1044.

[167] Ley, R. D. Ultraviolet radiation A-induced precursors of cutaneous melanoma in Monodelphis domestica. *Cancer research 57*, 17 (1997), 3682–3684.

[168] Ley, R. D., Peak, M. J., and Lyon, L. L. Induction of pyrimidine dimers in epidermal DNA of hairless mice by UVB: an action spectrum. *Journal of Investigative Dermatology 80*, 3 (1983), 188–191.

[169] Li, L., Ng, C. S.-L., Mastorakis, N., Croitoru, A., Balas, V., Son, E., and Mladenov, V. A, physically-based human skin reflection model. In *WSEAS International Conference. Proceedings. Mathematics and Computers in Science and Engineering* (2009), no. 10, World Scientific and Engineering Academy and Society.

[170] Lim, J. L., and Stern, R. S. High levels of ultraviolet b exposure increase the risk of non-melanoma skin cancer in psoralen and ultraviolet a-treated patients. *Journal of investigative dermatology 124*, 3 (2005), 505–513.

[171] Lin, J. Y., and Fisher, D. E. Melanocyte biology and skin pigmentation. *Nature 445*, 7130 (2007), 843–850.

[172] Lodish H, Berk A, M. P. K. C. K. M. S. M. Z. S. D. J. *Molecular cell biology*, vol. 5. WH Freeman New York, 2004.

[173] Mackie, R., Freudenberger, T., and Aitchison, T. Personal risk-factor chart for cutaneous melanoma. *The Lancet 334*, 8661 (1989), 487–490.

[174] Magnus, K. Incidence of malignant melanoma of the skin in norway, 1955–1970. variations in time and space and solar radiation. *Cancer 32*, 5 (1973), 1275–1286.

[175] Magnus, K. The nordic profile of skin cancer incidence. a comparative epidemiological study of the three main types of skin cancer. *International journal of cancer 47*, 1 (1991), 12–19.

[176] Marchesini, R., Bertoni, A., Andreola, S., Melloni, E., and Sichirollo, A. Extinction and absorption coefficients and scattering phase functions of human tissues in vitro. *Applied Optics 28*, 12 (1989), 2318–2324.

[177] Maresca, V., Flori, E., Briganti, S., Camera, E., Cario-André, M., Taïeb, A., and Picardo, M. UVA-induced modification of catalase charge properties in the epidermis is correlated with the skin phototype. *Journal of Investigative Dermatology 126*, 1 (2006), 182–190.

[178] Marieb, E. Human anatomy and physiology. 1995, redwood city.

[179] Marnett, L. J. Oxyradicals and DNA damage. *Carcinogenesis 21*, 3 (2000), 361–370.

[180] Marrot, L., and Meunier, J.-R. Skin DNA photodamage and its biological consequences. *Journal of the American Academy of Dermatology 58*, 5 (2008), S139–S148.

[181] Mathys, P., Moser, M., Bressoud, D., Gerber, B., and Braun-Fahrländer, C. [behavior of sunbed users in switzerland]. *Sozial-und Praventivmedizin 47*, 5 (2001), 318–329.

[182] MATLAB. *version 7.13 (R2011b)*. The MathWorks Inc., Natick, Massachusetts, 2011.

[183] Matsunaga, T., Hieda, K., and Nikaido, O. Wavelength dependent formation of thymine dimers and (6-4) photoproducts in DNA by monochromatic ultraviolet light ranging from 150 to 365 nm. *Photochemistry and photobiology 54*, 3 (1991), 403–410.

[184] McGinley, J., Martin, C., and MacKie, R. Sunbeds in current use in scotland: a survey of their output and patterns of use. *British Journal of Dermatology 139*, 3 (1998), 428–438.

[185] McKinlay, A., and Diffey, B. A reference action spectrum for ultraviolet induced erythema in human skin. *CIE j 6*, 1 (1987), 17–22.

[186] Mead, M. N. Benefits of sunlight: a bright spot for human health. *Environmental health perspectives 116*, 4 (2008), A160.

[187] Meanwell, E., and Diffey, B. Reciprocity of ultraviolet erythema in human skin. *Photo-dermatology 6*, 3 (1989), 146.

[188] Meglinsky, I., and Matcher, S. Modelling the sampling volume for skin blood oxygenation measurements. *Medical and Biological Engineering and Computing 39*, 1 (2001), 44–50.

[189] Meinhardt, M., Krebs, R., Anders, A., Heinrich, U., and Tronnier, H. Absorption spectra of human skin in vivo in the ultraviolet wavelength range measured by optoacoustics. *Photochemistry and photobiology 85*, 1 (2009), 70–77.

[190] Melnikova, V. O., and Ananthaswamy, H. N. Cellular and molecular events leading to the development of skin cancer. *Mutation Research/Fundamental and Molecular Mechanisms of Mutagenesis 571*, 1 (2005), 91–106.

[191] Menon, I., and Haberman, H. Mechanisms of action of melanins. *British Journal of Dermatology 97*, 1 (1977), 109–112.

[192] Meredith, P., and Sarna, T. The physical and chemical properties of eumelanin. *Pigment Cell Research 19*, 6 (2006), 572–594.

[193] Metropolis, N., and Ulam, S. The monte carlo method. *Journal of the American statistical association 44*, 247 (1949), 335–341.

[194] Mette, M., et al. UVA1 is skin deep: molecular and clinical implications. *Photochemical & Photobiological Sciences 12*, 1 (2013), 95–103.

[195] Moan, J., and Dahlback, A. Ultraviolet radiation and skin cancer: epidemiological data from scandinavia. In *Environmental UV Photobiology*. Springer, 1993, pp. 255–293.

[196] Moan, J., Dahlback, A., and Setlow, R. Epidemiological support for an hypothesis for melanoma induction indicating a role for UVA radiation. *Photochemistry and photobiology 70*, 2 (1999), 243–247.

[197] Modest, M. F. *Radiative heat transfer*. Academic press, 2013.

[198] Mohlenhoff, B., Romeo, M., Diem, M., and Wood, B. R. Mie-type scattering and non-beer-lambert absorption behavior of human cells in infrared microspectroscopy. *Biophysical journal 88*, 5 (2005), 3635–3640.

[199] Moseley, H. *Non-ionising radiation*. Hilger, 1988.

[200] Moseley, H., Davidson, M., and Ferguson, J. A hazard assessment of artificial tanning units. *Photodermatology, photoimmunology & photomedicine 14*, 2 (1998), 79–87.

[201] Moseley, H., Davidson, M., and Ferguson, J. Sunbeds and the need to know. *The British journal of dermatology 141*, 3 (1999), 589–590.

[202] Mosher, C. E., and Danoff-Burg, S. Addiction to indoor tanning: relation to anxiety, depression, and substance use. *Archives of Dermatology 146*, 4 (2010), 412–417.

[203] Mouret, S., Baudouin, C., Charveron, M., Favier, A., Cadet, J., and Douki, T. Cyclobutane pyrimidine dimers are predominant DNA lesions in whole human skin exposed to UVA radiation. *Proceedings of the National Academy of Sciences 103*, 37 (2006), 13765–13770.

[204] Mouret, S., Philippe, C., Gracia-Chantegrel, J., Banyasz, A., Karpati, S., Markovitsi, D., and Douki, T. UVA-induced cyclobutane pyrimidine dimers in DNA: a direct photochemical mechanism? *Organic & biomolecular chemistry 8*, 7 (2010), 1706–1711.

[205] Natarajan, V. T., Ganju, P., Ramkumar, A., Grover, R., and Gokhale, R. S. Multifaceted pathways protect human skin from UV radiation. *Nature chemical biology 10*, 7 (2014), 542–551.

[206] Network, N. C. I. The Importance of Skin Cancer Registration - NCIN Data Briefing, July 6 2014. URL http://www.ncin.org.uk/publications/databriefings/skincancerregistration.

[207] Nielsen, K. P., Zhao, L., Stamnes, J. J., Stamnes, K., and Moan, J. The importance of the depth distribution of melanin in skin for DNA protection and other photobiological processes. *Journal of Photochemistry and Photobiology B: Biology 82*, 3 (2006), 194–198.

[208] Nilsen, L. T. N., Aalerud, T. N., Hannevik, M., and Veierød, M. B. UVB and UVA irradiances from indoor tanning devices. *Photochemical & Photobiological Sciences 10*, 7 (2011), 1129–1136.

[209] Nilsen, L. T. N., Hannevik, M., Aalerud, T. N., Johnsen, B., Friberg, E. G., and Veierød, M. B. Trends in UV irradiance of tanning devices in norway: 1983–2005. *Photochemistry and photobiology 84*, 5 (2008), 1100–1108.

[210] NRPB. Health effects from ultraviolet radiation. Documents of the NRPB, 2002. Report of an Advisory Group on Non-ionising Radiation.

[211] Oliver, H., Ferguson, J., and Moseley, H. Quantitative risk assessment of sunbeds: impact of new high power lamps. *British Journal of Dermatology 157*, 2 (2007), 350–356.

[212] Ortonne, J.-P. Photoprotective properties of skin melanin. *British Journal of Dermatology 146*, s61 (2002), 7–10.

[213] Parkin, D., Mesher, D., and Sasieni, P. 13. cancers attributable to solar (ultraviolet) radiation exposure in the uk in 2010. *British journal of cancer 105* (2011), S66–S69.

[214] Parrish, J. A., Jaenicke, K. F., and Anderson, R. Erythema and melanogenesis action spectra of normal human skin. *Photochemistry and Photobiology 36*, 2 (1982), 187–191.

[215] Pathak, M. A., Jimbow, K., Szabo, G., and Fitzpatrick, T. B. Sunlight and melanin pigmentation. In *Photochemical and photobiological reviews*. Springer, 1976, pp. 211–239.

[216] Patterson, M. S., Wilson, B. C., and Wyman, D. R. The propagation of optical radiation in tissue i. models of radiation transport and their application. *Lasers in Medical Science 6*, 2 (1991), 155–168.

[217] Patwardhan, S. V., Dhawan, A. P., and Relue, P. A. Monte carlo simulation of light-tissue interaction: three-dimensional simulation for trans-illumination-based imaging of skin lesions. *Biomedical Engineering, IEEE Transactions on 52*, 7 (2005), 1227–1236.

[218] Paul, B. S., and Parrish, J. A. The interaction of UVA and UVB in the production of threshold erythema. *Journal of Investigative Dermatology 78*, 5 (1982), 371–374.

[219] Pawsey, S., Magnus, I., Ramsay, C., Benson, P., and Giannelli, F. Clinical, genetic and DNA repair studies on a consecutive series of patients with xeroderma pigmentosum. *QJM 48*, 2 (1979), 179–210.

[220] Payne, P. A. Measurement of properties and function of skin. *Clinical Physics and Physiological Measurement 12*, 2 (1991), 105.

[221] Petersen, B., Thieden, E., Philipsen, P., Heydenreich, J., Wulf, H., and Young, A. Determinants of personal ultraviolet-radiation exposure

doses on a sun holiday. *British Journal of Dermatology 168*, 5 (2013), 1073–1079.

[222] Pick, T., and Howden, R. Gray's anatomy, descriptive and surgical, 1977.

[223] Pillai, S., Oresajo, C., and Hayward, J. Ultraviolet radiation and skin aging: roles of reactive oxygen species, inflammation and protease activation, and strategies for prevention of inflammation-induced matrix degradation–a review. *International journal of cosmetic science 27*, 1 (2005), 17–34.

[224] Prahl, S. Optical absorption of hemoglobin. *Oregon Medical Laser Center, http://omlc.org/spectra/hemoglobin/index.html (accessed Nov 16, 2014)* (1999).

[225] Prahl, S. A., Keijzer, M., Jacques, S. L., and Welch, A. A monte carlo model of light propagation in tissue. *Dosimetry of laser radiation in medicine and biology 5* (1989), 102–111.

[226] Prahl, S. A., van Gemert, M. J., and Welch, A. J. Determining the optical properties of turbid media by using the adding–doubling method. *Applied optics 32*, 4 (1993), 559–568.

[227] Profio, A., and Doiron, D. Transport of light in tissue in photodynamic therapy. *Photochemistry and photobiology 46*, 5 (1987), 591–599.

[228] Pye, S., and Martin, C. A study of the directional response of ultraviolet radiometers: I. practical evaluation and implications for Ultraviolet measurement standards. *Physics in medicine and biology 45*, 9 (2000), 2701.

[229] Quevedo, W. C., and Smith, J. A. Studies on radiation-induced tanning of skin. *Annals of the New York Academy of Sciences 100*, 1 (1963), 364–389.

[230] Reichmann, M., Rice, S., Thomas, C., and Doty, P. A further examination of the molecular weight and size of desoxypentose nucleic acid. *Journal of the American Chemical Society 76*, 11 (1954), 3047–3053.

[231] Richards-Kortum, R., and Sevick-Muraca, E. Quantitative optical spectroscopy for tissue diagnosis. *Annual review of physical chemistry 47*, 1 (1996), 555–606.

[232] Riley, P. Melanin. *The international journal of biochemistry & cell biology 29*, 11 (1997), 1235–1239.

[233] Rivers, J., Norris, P., Murphy, G., Chu, A., Midgley, G., Morris, J., Morris, R., Young, A., and Hawk, J. UVA sunbeds: tanning, photoprotection, acute adverse effects and immunological changes. *British journal of dermatology 120*, 6 (1989), 767–777.

[234] Rochette, P. J., Therrien, J.-P., Drouin, R., Perdiz, D., Bastien, N., Drobetsky, E. A., and Sage, E. UVA-induced cyclobutane pyrimidine dimers form predominantly at thymine–thymine dipyrimidines and correlate with the mutation spectrum in rodent cells. *Nucleic acids research 31*, 11 (2003), 2786–2794.

[235] Rosenstein, B. S., and Setlow, R. Photoreactivation of icr 2a frog cells after exposure to monochromatic ultraviolet radiation in the 252–313 nm range. *Photochemistry and photobiology 32*, 3 (1980), 361–366.

[236] Rosso, S., Zanetti, R., Martinez, C., Tormo, M., Schraub, S., Sancho-Garnier, H., Franceschi, S., Gafa, L., Perea, E., Navarro, C., et al. The multicentre south european study 'helios'. ii: Different sun exposure patterns in the aetiology of basal cell and squamous cell carcinomas of the skin. *British journal of cancer 73*, 11 (1996), 1447.

[237] Rouabhia, M., Drouin, R., Rhainds, M., and Claveau, J. Assessment of human skin damage following exposure to harmful agents, June 25 2002. US Patent 6,410,333.

[238] Rowe, D. E., Carroll, R. J., and Day Jr, C. L. Prognostic factors for local recurrence, metastasis, and survival rates in squamous cell carcinoma of the skin, ear, and lip: implications for treatment modality selection. *Journal of the American Academy of Dermatology 26*, 6 (1992), 976–990.

[239] Rünger, T. M., and Kappes, U. P. Mechanisms of mutation formation with long-wave ultraviolet light (uva). *Photodermatology, photoimmunology & photomedicine 24*, 1 (2008), 2–10.

[240] Rupert, C. S. Dosimetric concepts in photobiologyn. *Photochemistry and photobiology 20*, 3 (1974), 203–212.

[241] Saidi, I. S., Jacques, S. L., and Tittel, F. K. Mie and rayleigh modeling of visible-light scattering in neonatal skin. *Applied optics 34*, 31 (1995), 7410–7418.

[242] Salasche, S. J. Epidemiology of actinic keratoses and squamous cell carcinoma. *Journal of the American Academy of Dermatology 42*, 1 (2000), S4–S7.

[243] SALOPEK, T. G., YAMADA, K., ITO, S., AND JIMBOW, K. Dysplastic melanocytic nevi contain high levels of pheomelanin: quantitative comparison of pheomelanin/eumelanin levels between normal skin, common nevi, and dysplastic nevi. *Pigment cell research 4*, 4 (1991), 172–179.

[244] SAYRE, R. M., OLSON, R. L., AND EVERETT, M. A. Quantitative studies on erythema1. *Journal of Investigative Dermatology 46*, 3 (1966), 240–244.

[245] SCHARFFETTER-KOCHANEK, K., WLASCHEK, M., BRENNEISEN, P., SCHAUEN, M., BLAUDSCHUN, R., AND WENK, J. UV-induced reactive oxygen species in photocarcinogenesis and photoaging. *Biological chemistry 378*, 11 (1997), 1247–1258.

[246] SCOTT, M. C., WAKAMATSU, K., ITO, S., KADEKARO, A. L., KOBAYASHI, N., GRODEN, J., KAVANAGH, R., TAKAKUWA, T., VIRADOR, V., HEARING, V. J., ET AL. Human melanocortin 1 receptor variants, receptor function and melanocyte response to UV radiation. *Journal of cell science 115*, 11 (2002), 2349–2355.

[247] SERUP, J., AND AGNER, T. Colorimetric quantification of erythema—a comparison of two colorimeters (lange micro color and minolta chroma meter cr-200) with a clinical scoring scheme and laser-doppler flowmetry. *Clinical and experimental dermatology 15*, 4 (1990), 267–272.

[248] SETLOW, R. B. The wavelengths in sunlight effective in producing skin cancer: a theoretical analysis. *Proceedings of the National Academy of Sciences 71*, 9 (1974), 3363–3366.

[249] SLAVIN, W. Stray light in ultraviolet, visible, and near-infrared spectrophotometry. *Analytical Chemistry 35*, 4 (1963), 561–566.

[250] SPENCER, J. M., AND AMONETTE, R. A. Indoor tanning: risks, benefits, and future trends. *Journal of the American Academy of Dermatology 33*, 2 (1995), 288–298.

[251] STEEL, B. Skin cancer-an overview for dentists. *British dental journal 216*, 10 (2014), 575–581.

[252] STELIAROVA-FOUCHER, E., O'CALLAGHAN, M., FERLAY, J., MASUYER, E., ROSSO, S., FORMAN, D., BRAY, F., AND COMBER, H. The european cancer observatory: A new data resource. *European Journal of Cancer* (2014).

[253] Strickland, P. T., and Rosenthal, F. S. Association of nonmelanoma skin cancer and actinic keratosis with cumulative solar ultraviolet exposure in maryland watermen. *Cancer 65*, 2811-2817 (1990), 3L.

[254] Subbaraman, R., and Kang, T. T. Qualitative studies on quartz filters used in ultraviolet sterilization system. In *The 15th International Conference on Biomedical Engineering* (2014), Springer, pp. 407–410.

[255] Sutherland, J. C., and Griffin, K. P. Absorption spectrum of DNA for wavelengths greater than 300 nm. *Radiation research 86*, 3 (1981), 399–410.

[256] Talreja, P. S., Kasting, G. B., Kleene, N. K., Pickens, W. L., and Wang, T.-F. Visualization of the lipid barrier and measurement of lipid pathlength in human stratum corneum. *Aaps Pharmsci 3*, 2 (2001), 48–56.

[257] Tarrant, A. Basic principles of light measurement. *Radiation measurement in photobiology. Academic Press, London* (1989), 1–21.

[258] Taylor, H. R., West, S. K., Rosenthal, F. S., Muñoz, B., Newland, H. S., Abbey, H., and Emmett, E. A. Effect of ultraviolet radiation on cataract formation. *New England Journal of Medicine 319*, 22 (1988), 1429–1433.

[259] Taylor, S. C. Skin of color: biology, structure, function, and implications for dermatologic disease. *Journal of the American Academy of Dermatology 46*, 2 (2002), S41–S62.

[260] Therrien, J.-P., Rouabhia, M., Drobetsky, E. A., and Drouin, R. The multilayered organization of engineered human skin does not influence the formation of sunlight-induced cyclobutane pyrimidine dimers in cellular DNA. *Cancer research 59*, 2 (1999), 285–289.

[261] Thieden, E., Agren, M. S., and Wulf, H. C. The wrist is a reliable body site for personal dosimetry of ultraviolet radiation. *Photodermatol Photoimmunol Photomed 16*, 2 (Apr 2000), 57–61.

[262] Thieden, E., Philipsen, P. A., Heydenreich, J., and Wulf, H. C. UV radiation exposure related to age, sex, occupation, and sun behavior based on time-stamped personal dosimeter readings. *Arch Dermatol 140*, 2 (Feb 2004), 197–203.

[263] Thieden, E., Philipsen, P. A., Sandby-M?ller, J., Heydenreich, J., and Wulf, H. C. Proportion of lifetime UV dose received by children,

teenagers and adults based on time-stamped personal dosimetry. *J. Invest. Dermatol. 123*, 6 (Dec 2004), 1147–1150.

[264] Thilly, W. G. Analysis of chemically induced mutation in single cell populations. In *Induced Mutagenesis*. Springer, 1983, pp. 337–378.

[265] Thompson, L. H. Nucleotide excision repair. In *DNA damage and repair*. Springer, 1998, pp. 335–393.

[266] Thomson, C. S., Woolnough, S., Wickenden, M., Hiom, S., Twelves, C. J., et al. Sunbed use in children aged 11-17 in england: face to face quota sampling surveys in the national prevalence study and six cities study. *BMJ 340* (2010).

[267] Tierney, P., Ferguson, J., Ibbotson, S., Dawe, R., Eadie, E., and Moseley, H. Nine out of 10 sunbeds in England emit ultraviolet radiation levels that exceed current safety limits. *Br. J. Dermatol. 168*, 3 (Mar 2013), 602–608.

[268] Tobi, S. E., Gilbert, M., Paul, N., and McMillan, T. J. The green tea polyphenol, epigallocatechin-3-gallate, protects against the oxidative cellular and genotoxic damage of UVA radiation. *International journal of cancer 102*, 5 (2002), 439–444.

[269] Tornaletti, S., and Pfeifer, G. P. UV damage and repair mechanisms in mammalian cells. *Bioessays 18*, 3 (1996), 221–228.

[270] Tseng, S.-H., Bargo, P., Durkin, A., and Kollias, N. Chromophore concentrations, absorption and scattering properties of human skin in-vivo. *Optics express 17*, 17 (2009), 14599–14617.

[271] Tuchin, V. *Tissue optics: light scattering methods and instruments for medical diagnosis*.

[272] Tyrrell, R., and Keyse, S. New trends in photobiology the interaction of UVA radiation with cultured cells. *Journal of Photochemistry and Photobiology B: Biology 4*, 4 (1990), 349–361.

[273] Urbach, F. Biologic effects of ultraviolet radiation. *Pergamon Press, New York* (1969).

[274] Valentine, R. M., Brown, C. T. A., Moseley, H., Ibbotson, S., and Wood, K. Monte carlo modeling of in vivo protoporphyrin ix fluorescence

and singlet oxygen production during photodynamic therapy for patients presenting with superficial basal cell carcinomas. *Journal of biomedical optics 16*, 4 (2011), 048002–048002.

[275] Van de Hulst, H. Multiple light scattering: Tables. *Formulas, and Applications (Academic, New York, 1980) 1* (1980), 477–492.

[276] Van der Leun, J., and Stoop, T. Photorecovery of Ultraviolet erythema, the biologic effects of ultraviolet radiation (with emphasis on the skin) 1969 edited by f urbach. *The Biologic Effects of Ultraviolet Radiation* (1969), 251–254.

[277] Van Gemert, M., Jacques, S. L., Sterenborg, H., and Star, W. Skin optics. *Biomedical Engineering, IEEE Transactions on 36*, 12 (1989), 1146–1154.

[278] Verkruysse, W., Lucassen, G. W., de Boer, J. F., Smithies, D. J., Nelson, J. S., and van Gemert, M. J. Modelling light distributions of homogeneous versus discrete absorbers in light irradiated turbid media. *Physics in medicine and biology 42*, 1 (1997), 51.

[279] Wagner, J. K., Jovel, C., Norton, H. L., Parra, E. J., and Shriver, M. D. Comparing quantitative measures of erythema, pigmentation and skin response using reflectometry. *Pigment cell research 15*, 5 (2002), 379–384.

[280] Walter, S. D., Marrett, L. D., From, L., Hertzman, C., Shannon, H. S., and Roy, P. The association of cutaneous malignant melanoma with the use of sunbeds and sunlamps. *American journal of epidemiology 131*, 2 (1990), 232–243.

[281] Watson, J. D., and Stent, G. S. *Double helix*. Simon and Schuster, 1998.

[282] Wehner, M. R., Chren, M.-M., Nameth, D., Choudhry, A., Gaskins, M., Nead, K. T., Boscardin, W. J., and Linos, E. International prevalence of indoor tanning: a systematic review and meta-analysis. *JAMA dermatology 150*, 4 (2014), 390–400.

[283] Wehner, M. R., Shive, M. L., Chren, M.-M., Han, J., Qureshi, A. A., and Linos, E. Indoor tanning and non-melanoma skin cancer: systematic review and meta-analysis. *BMJ: British Medical Journal 345* (2012).

[284] Wenczl, E., Van der Schans, G. P., Roza, L., Kolb, R. M., Timmerman, A. J., Smit, N., Pavel, S., and Schothorst, A. A. (pheo) melanin

photosensitizes UVA-induced DNA damage in cultured human melanocytes. *The Journal of investigative dermatology 111*, 4 (1998), 678–682.

[285] Wester, U. Measurements of solar UVA, UVB and of Ozone: Estimates of population UV doses. *Radiation protection dosimetry 91*, 1-3 (2000), 115–118.

[286] Westerdahl, J., Ingvar, C., Måsbäck, A., Jonsson, N., and Olsson, H. Risk of cutaneous malignant melanoma in relation to use of sunbeds: further evidence for uv-a carcinogenicity. *British Journal of Cancer 82*, 9 (2000), 1593.

[287] Westerhof, W., Van Hasselt, B., and Kammeijer, A. Quantification of UV-induced erythema with a portable computer controlled chromameter. *Photo-dermatology 3*, 5 (1986), 310–314.

[288] Whiteman, D. C., Whiteman, C. A., and Green, A. C. Childhood sun exposure as a risk factor for melanoma: a systematic review of epidemiologic studies. *Cancer Causes & Control 12*, 1 (2001), 69–82.

[289] Whitmore, S. E., Morison, W. L., Potten, C. S., et al. Tanning salon exposure and molecular alterations. *Journal of the American Academy of Dermatology 44*, 5 (2001), 775–780.

[290] Willis, I., Kligman, A., and Epstein, J. Effects of long ultraviolet rays on human skin: Photoprotective or photoaugmentative? *Journal of Investigative Dermatology 59*, 6 (1972), 416–420.

[291] Wilson, B., and Adam, G. A monte carlo model for the absorption and flux distributions of light in tissue. *Medical Physics 10*, 6 (1983), 824–830.

[292] Wilson, B. C., and Jacques, S. L. Optical reflectance and transmittance of tissues: principles and applications. *Quantum Electronics, IEEE Journal of 26*, 12 (1990), 2186–2199.

[293] Wlaschek, M., Tantcheva-Poór, I., Naderi, L., Ma, W., Schneider, L. A., Razi-Wolf, Z., Schüller, J., and Scharffetter-Kochanek, K. Solar UV irradiation and dermal photoaging. *Journal of Photochemistry and Photobiology B: Biology 63*, 1 (2001), 41–51.

[294] Wood, K., Bjorkman, J., Whitney, B., and Code, A. The effect of multiple scattering on the polarization from axisymmetric circumstellar envelopes. ii. thomson scattering in the presence of absorptive opacity sources. *The Astrophysical Journal 461* (1996), 847.

[295] Wood, K., Bjorkman, J., Whitney, B. A., and Code, A. D. The effect of multiple scattering on the polarization from axisymmetric circumstellar envelopes. i. pure thomson scattering envelopes. *The Astrophysical Journal 461* (1996), 828.

[296] Woollons, A., Clingen, P., Price, M., Farlett, C., and Green, M. Induction of mutagenic DNA damage in human fibroblasts after exposure to artificial tanning lamps. *British Journal of Dermatology 137*, 5 (1997), 687–692.

[297] Yamaguchi, Y., Takahashi, K., Zmudzka, B. Z., Kornhauser, A., Miller, S. A., Tadokoro, T., Berens, W., Beer, J. Z., and Hearing, V. J. Human skin responses to UV radiation: pigment in the upper epidermis protects against DNA damage in the lower epidermis and facilitates apoptosis. *The FASEB journal 20*, 9 (2006), 1486–1488.

[298] Ying, C. Y., Parrish, J. A., and Pathak, M. Additive erythemogenic effects of middle-(280–320 nm) and long-(320–400 nm) wave ultraviolet light. *Journal of Investigative Dermatology 63*, 3 (1974), 273–278.

[299] Yoon, J.-H., Lee, C.-S., O'Connor, T. R., Yasui, A., and Pfeifer, G. P. The DNA damage spectrum produced by simulated sunlight. *Journal of molecular biology 299*, 3 (2000), 681–693.

[300] Young, A. R. Chromophores in human skin. *Physics in Medicine and Biology 42*, 5 (1997), 789.

[301] Young, A. R. Tanning devices–fast track to skin cancer? *Pigment Cell Research 17*, 1 (2004), 2–9.

[302] Young, A. R., Chadwick, C. A., Harrison, G. I., Nikaido, O., Ramsden, J., and Potten, C. S. The similarity of action spectra for thymine dimers in human epidermis and erythema suggests that DNA is the chromophore for erythema. *Journal of investigative dermatology 111*, 6 (1998), 982–988.

[303] Zastrow, L., Groth, N., Klein, F., Kockott, D., Lademann, J., and Ferrero, L. [UV, visible and infrared light. which wavelengths produce oxidative stress in human skin?]. *Der Hautarzt; Zeitschrift fur Dermatologie, Venerologie, und verwandte Gebiete 60*, 4 (2009), 310–317.

[304] Zastrow, L., Groth, N., Klein, F., Kockott, D., Lademann, J., Renneberg, R., and Ferrero, L. The missing link–light-induced (280-

1,600 nm) free radical formation in human skin. *Skin pharmacology and physiology 22*, 1 (2009), 31–44.

[305] Zhang, M., Qureshi, A. A., Geller, A. C., Frazier, L., Hunter, D. J., and Han, J. Use of tanning beds and incidence of skin cancer. *Journal of Clinical Oncology 30*, 14 (2012), 1588–1593.